ACCCS 2023

Anniversary Workshop in Commemoration of the

1999 Chi-Chi and 2022 Chihshang Earthquakes

EDITED BY

Chung-Che Chou 周中哲
Chiun-Lin Wu 吳俊霖
Hung-Hao Hsieh 謝宏灝
Chih-Wei Chang 張志偉

PROCEEDINGS

NCREE

NARLabs National Applied Research Laboratories
National Center for Research on Earthquake Engineering

9.25 MON — 9.27 WED 2023
Taipei, Taiwan

Contents

Hosts and Co-hosts

Hosts

- **National Center for Research on Earthquake Engineering, NARLabs (NCREE, NARLabs)**
  (財團法人國家實驗研究院國家地震工程研究中心)

Co-hosts

- **Chinese Taiwan Society for Earthquake Engineering (CTSEE)**
  (中華民國地震工程學會)

- **Chinese Society of Structural Engineering (CSSE)**
  (中華民國結構工程學會)

- **Chinese Institute of Civil and Hydraulic Engineering (CICHE)**
  (中國土木水利工程學會)

- **Taiwan Earthquake Research Center (TEC)**
  (台灣地震科學中心)

Committee

Workshop Chair

Prof. Chung-Che Chou
Director General of National Center for Research on Earthquake Engineering
President of Chinese Taiwan Society for Earthquake Engineering

Advisory Committee

Prof. Kuo-Chun Chang
National Taiwan University

Prof. Hsuan-Teh Hu
National Cheng Kung University

Prof. Cheng-Chih Chen
National Yang Ming Chiao Tung University

Prof. Shyh-Jiann Hwang
National Taiwan University

Prof. Jeng-Tzong Chen
National Taiwan Ocean University

Prof. Chi-Chang Lin
Chaoyang University of Technology

Prof. Tung-Yang Chen
National Cheng Kung University

Prof. Chin-Hsiung Loh
National Taiwan University

Prof. Lap-Loi Chung
National Taiwan University

Prof. Chang-Yu Ou
National Taiwan University of Science and Technology

Director Sun-Lin Chung
Institute of Earth Sciences, Academia Sinica

Prof. Keh-Chyuan Tsai
National Taiwan University

Prof. Louis Ge
National Taiwan University

Chairman Sheng-Bao Tseng
Sinotech Engineering Consultants, Inc.

Agenda

<table>
<tr><th colspan="4">Day 1 (Monday, Sep. 25th, 2023)</th></tr>
<tr><td>08:00~09:00</td><td colspan="3">Registration</td></tr>
<tr><td>09:00~09:30</td><td>Opening Ceremony</td><td colspan="2">Opening Welcome Remarks
Chung-Che Chou, Director General
Chair of ACCCS
National Center for Research on Earthquake Engineering

Distinguished Guest's Remarks
Chih-Peng Li, Director General
Department of Engineering and Technologies, NSTC

Meng-Fan Luo, Director General
Department of Natural Sciences and Sustainable Development, NSTC

Jianye Ching, Convener
Civil & Hydraulic Engineering Program

Bou-Wen Lin, Vice President
National Applied Research Laboratories</td></tr>
<tr><td>09:30~10:05</td><td rowspan="2">Presentation Session 1

Moderator
Prof.
Chin-Hsiung Loh</td><td>Prof.
Chung-Che Chou</td><td>Shaking Table Tests of a Three-Story Dual Frame with Moderately Ductile Steel Columns and All-Steel SBRBs under the 2022 Chihshang Earthquake</td></tr>
<tr><td>10:05~10:40</td><td>Prof.
Masayoshi Nakashima</td><td>Utilities of Monitoring for Advancing Seismic Design – A Japanese Experience from past Earthquakes</td></tr>
<tr><td>10:40~11:00</td><td colspan="3">Coffee Break</td></tr>
<tr><td>11:00~11:35</td><td rowspan="2">Presentation Session 2

Moderator
Prof.
Keh-Chyuan Tsai</td><td>Prof.
James M. Ricles</td><td>Advances and Application of Real-Time Hybrid Simulation Towards Creating Seismically Resilient Structural Systems</td></tr>
<tr><td>11:35~12:10</td><td>Prof.
Chia-Ming Uang</td><td>Recent Development of Local Buckling Requirements in AISC Seismic Provisions</td></tr>
<tr><td>12:10~13:30</td><td colspan="3">Lunch Break</td></tr>
<tr><td>13:30~14:05</td><td rowspan="3">Presentation Session 3

Moderator
Prof.
Kuo-Liang Wen</td><td>Prof.
Norman Abrahamson</td><td>Non-Ergodic Ground-Motion Models Based on a Combined Set of Empirical Ground-Motion Data, 3-D Simulations, and Macro-Seismic Intensity Data</td></tr>
<tr><td>14:05~14:40</td><td>Dr.
Brian Chiou</td><td>Principal Surface Displacement of Strike-Slip Earthquakes</td></tr>
<tr><td>14:40~15:15</td><td>Prof.
Domniki Asimaki</td><td>GEER-NCREE Reconnaissance of the 2022 M_W 6.9 Chihshang, Taiwan Earthquake Sequence</td></tr>
<tr><td>15:15~15:35</td><td colspan="3">Coffee Break</td></tr>
<tr><td>15:35~16:10</td><td rowspan="3">Presentation Session 4

Moderator
Prof.
Jianye Ching</td><td>Prof.
Kenneth H. Stokoe</td><td>Recent Advances in Evaluating the Linear and Nonlinear Dynamic Properties of Rock Subjected to Earthquake Shaking</td></tr>
<tr><td>16:10~16:45</td><td>Prof.
Adrian Rodriguez-Marek</td><td>Epistemic Uncertainty in Site Response for Site-Specific PSHA</td></tr>
<tr><td>16:45~17:20</td><td>Prof.
Chi-Chin Tsai</td><td>Geotechnical Insights: Lessons Learned from the 2022 M_L 6.8 Chihshang Earthquake, Taiwan</td></tr>
</table>

Day 2 (Tuesday, Sep. 26th, 2023)			
09:00~09:35	Presentation Session 5 Moderator Prof. Chung-Chan Hung	Prof. Jack P. Moehle	Design of Thick Foundation Mats with Special Attention on Shear Strength
09:35~10:10		Prof. Hanbin Ge	Advances in Seismic Resilience Improvement for Urban Aboveground and Underground Structures
10:10~10:30	Coffee Break		
10:30~10:55	Presentation Session 6 Moderator Prof. Ta-Peng Chang	Prof. Tony Yang	Performance-Based Earthquake Engineering from Theory to Implementation to the Future
10:55~11:20		Prof. Carlos Ventura	Understanding Ground Motions and their Relation to Structural Damage
11:20~11:45		Prof. Murat Saatcioglu	Innovative Solutions for Seismic Retrofit of Non-Ductile Construction
11:45~12:10		Dr. Chung-Pi Luan	Introduction to the Policy of Net-Zero Building Among the Net-Zero Transition
12:10~13:20	Lunch Break		
13:20~13:45	Presentation Session 7 Moderator Prof. Tzu-Kang Lin	Dr. Trevor Nightingale	Key Issues in Decarbonizing the Built Environment
13:45~14:10		Prof. Sheryl Staub-French	A Review of Digital Transformation Efforts and Initiatives in Canada's Built Asset Industry
14:10~14:35		Prof. David Lau	New Shake Table Testing Facility for Structures and Non-structural Components
14:35~15:05	Coffee Break		
15:05~15:40	Presentation Session 8 Moderator Prof. Kuo-Chun Chang	Prof. Andres Winston Oreta	Integration of Technology in Earthquake Engineering Education: A Pathway to Enhancing Learning and Preparedness
15:40~16:15		Prof. Yi-Lung Mo	Where Do We Stand on Metamaterial-Based Seismic Design of Engineering Structures
16:15~16:50		Prof. Andrew S. Whittaker	Seismic Isolation of Advanced Reactors - A Pathway to Standardization and to Climate Targets
16:50~17:25		Dr. Daan Liang	Enabling and Accelerating Community-Based Innovation in Disaster Resilience – A US Perspective

Day 3 (Wednesday, Sep. 27th, 2023)			
09:00~09:35	Presentation Session 9 Moderator Prof. Chien-Kuo Chiu	Prof. Shyh-Jiann Hwang	Seismic Retrofitting Programs of RC Buildings after the 1999 Chi-Chi Earthquake in Taiwan
09:35~10:10		Prof. Takuya Nagae	System-Level and Component-Level Verification by Seismic-Response Building Tests Towards PBEE
10:10~10:30	Coffee Break		
10:30~11:05	Presentation Session 10 Moderator Prof. Lyan-Ywan Lu	Prof. Gilberto Mosqueda	Hybrid Simulation of Steel Moment Frame Structures with Column Shortening
11:05~11:40		Prof. Tracy Becker	Multi-Degree of Freedom Hybrid Testing with Model Updating of an Isolated Bridge
11:40~12:00	Closing Ceremony		

PROCEEDINGS

DAY 1

Proceedings: Day 1

Day 1 (Monday, Sep. 25th, 2023)				
09:30~10:05	Presentation Session 1	Prof. Chung-Che Chou	Shaking Table Tests of a Three-Story Dual Frame with Moderately Ductile Steel Columns and All-Steel SBRBs under the 2022 Chihshang Earthquake	page 7
10:05~10:40		Prof. Masayoshi Nakashima	Utilities of Monitoring for Advancing Seismic Design – A Japanese Experience from past Earthquakes	page 15
11:00~11:35	Presentation Session 2	Prof. James M. Ricles	Advances and Application of Real-Time Hybrid Simulation Towards Creating Seismically Resilient Structural Systems	page 20
11:35~12:10		Prof. Chia-Ming Uang	Recent Development of Local Buckling Requirements in AISC Seismic Provisions	page 29
13:30~14:05	Presentation Session 3	Prof. Norman Abrahamson	Non-Ergodic Ground-Motion Models Based on a Combined Set of Empirical Ground-Motion Data, 3-D Simulations, and Macro-Seismic Intensity Data	page 35
14:05~14:40		Dr. Brian Chiou	Principal Surface Displacement of Strike-Slip Earthquakes	page 42
14:40~15:15		Prof. Domniki Asimaki	GEER-NCREE Reconnaissance of the 2022 M_W 6.9 Chihshang, Taiwan Earthquake Sequence	page 49
15:35~16:10	Presentation Session 4	Prof. Kenneth H. Stokoe	Recent Advances in Evaluating the Linear and Nonlinear Dynamic Properties of Rock Subjected to Earthquake Shaking	page 56
16:10~16:45		Prof. Adrian Rodriguez-Marek	Epistemic Uncertainty in Site Response for Site-Specific PSHA	page 63
16:45~17:20		Prof. Chi-Chin Tsai	Geotechnical Insights: Lessons Learned from the 2022 M_L 6.8 Chihshang Earthquake, Taiwan	page 69

Day1 (Monday, Sep. 25th, 2023) 09:30~10:05

Shaking Table Tests of a Three-Story Dual Frame with Moderately Ductile Steel Columns and All-Steel SBRBs under the 2022 Chihshang Earthquake

Chung-Che Chou

Professor, Dept. of Civil Engineering, National Taiwan University, Taiwan, and Director, National Center for Research on Earthquake Engineering (NCREE), Taiwan

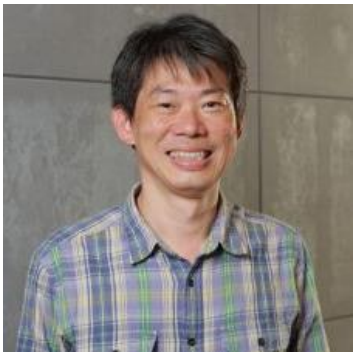

Chung-Che Chou is a Director of National Center for Research on Earthquake Engineering, Professor of Civil Engineering of National Taiwan University, and President of Chinese Taiwan Society for Earthquake Engineering. He obtained his Bachelor degree and Master degree both from National Taiwan University and Ph.D. degree from the University of California, San Diego (UCSD) in 2001. He then worked at UCSD as an Assistant Project Scientist for the New San Francisco-Oakland Bay Bridge project (2001-2003) and the National Chiao Tung University as Associate Professor, before joining the National Taiwan University in 2008. He then served as an Associate Dean of College of Engineering, National Taiwan University from 2017-2021, being a director of NCREE in 2021. Dr. Chou's main research areas include steel structure, composite structure, earthquake-resisting design, and large-scale structural testing. His work has been focused on the steel moment connection, post-tensioned connection, and seismic-resisting brace, such as the self-centering brace and sandwiched buckling-restrained brace (SBRB). He also developed a FRP-wrapped corrugated tube to simplify the fabrication of a ribbed interface between concrete and FRP, and investigated steel column response under high axial load associated with seismic lateral load in subassemblage test, hybrid simulation, and shake table test.

SHAKE TABLE TESTS OF A THREE-STORY DUAL FRAME WITH MODERATELY DUCTILE STEEL COLUMNS AND ALL-STEEL SBRBS UNDER THE 2022 CHIHSHANG EARTHQUAKE

Chung-Che Chou[1], Huang-Zuo Lin[2], Alvaro Córdova[3], Jian-Ming Chen[4], Yen-Hsun Chou[5], Shu-Hsien Chao[6], Shih-Ho Chao[7], Georgios Tsampras[8], Chia-Ming Uang[9], Hsin-Yang Chung[10], Chin-Hsiung Loh[11], Hsuan-Teh Hu[12]

[1]Professor (Corresponding Author), Dept. of Civil Engineering, National Taiwan University, Taiwan, cechou@ntu.edu.tw
Director, National Center for Research on Earthquake Engineering (NCREE), Taiwan
[2]Graduate Student Researcher, Dept. of Civil Engineering, National Taiwan University, Taiwan, *r10521239@ntu.edu.tw*
[3]Ph.D. Student Researcher, Dept. of Civil Engineering, National Taiwan University, Taiwan, *alvarojose.cordova@acestsolutions.com*
[4]Graduate Student Researcher, Dept. of Civil Engineering, National Taiwan University, Taiwan, *r10521242@ntu.edu.tw*
[5]Graduate Student Researcher, Dept. of Civil Engineering, National Cheng Kung University, Taiwan, *danielchou0305@gmail.com*
[6] Researcher, National Center for Research on Earthquake Engineering (NCREE), Taiwan, *shchao@narlabs.org.tw*
[7]Professor, Dept. of Civil Engineering, University of Texas, Arlington, USA, *shchao@uta.edu*
[8]Assistant Professor, Dept. of Structural Engineering, University of California, San Diego, USA, gtsampras@eng.ucsd.edu
[9]Professor, Dept. of Structural Engineering, University of California, San Diego, USA, cmu@ucsd.edu
[10]Associate Professor, Dept. of Civil Engineering, National Cheng Kung University, Taiwan, hychung@mail.ncku.edu.tw
[11]Professor, Dept. of Civil Engineering, National Taiwan University, Taiwan, lohc0220@ntu.edu.tw
[12]Professor, Dept. of Civil Engineering, National Cheng Kung University, Taiwan, hthu@mail.ncku.edu.tw

ABSTRACT

AISC 341-22 (2022) is conservative on the width-thickness requirement for steel built-up box columns, particularly in the buckling-restrained braced frame (BRBF). This study was aimed to assess the seismic performance of moderately ductile built-up box columns in a 3-story steel dual frame system, which had a 4-m special moment frame (SMF) bay and a 3-m BRBF bay. The effect of slab sliding on the floor acceleration reduction was also studied. Two test phases were conducted on the frame specimen: (1) the slab can slide relative the frame specimen in phase 1, and (2) a nearly-rigid connection between the slab and frame specimen is adopted for investigating the column and all-steel BRB response in phase 2. A near-fault motion, recorded in the September 18th, 2022 Chishang Earthquake, was used as an input motion. In phase 1, the slab sliding was effective in reducing the floor acceleration up to 25% compared to a rigid slab frame system. In phase 2, the maximum interstory drift angle of the frame was 0.045 rad without local buckling at the column base, and the maximum core strain of the first-story BRB was 2.5%. Post-earthquake tests were conducted on the first-story BRB, removed from the frame specimen after all shake table tests, showing high-mode buckling of the core plate near both ends of the restraining member.

Keywords: Sandwiched buckling restrained brace, moderately ductile built-up box column, sliding slab, shake table test, 2022 Chishang Earthquake

INTRODUCTION

A full-scale shake table collapse test of a four-story steel SMF with hollow structural section (HSS) columns under earthquake excitations was ever conducted at the E-defense facility in Japan (Suita et al. 2008, Lignos et al. 2013). The collapse test showed a side-sway first-story collapse mechanism, but the width-thickness (*b/t*) ratio of the HSS column is 31.3, exceeding the design limit for moderately ductile box columns in AISC 341-16 (2016). In AISC 341-22 (2022), as compared to the previous version AISC 341-16, the requirement for the width-thickness ratio (*b/t*) of built-up box columns becomes more stringent than that used in Japan. Additionally, the column section requirement in the BRBF has been transitioned from originally being use of moderately ductile to highly ductile members. The requirement can maintain good seismic performance of the built-up box column without strength degradation at high axial load and high lateral drift level (i.e., 0.04 rad drift) when compared to that of the steel I-shaped deep columns (Chou and Chen 2020, Lin and Chou 2022, Chou et al. 2022, Chou et al. 2023a). To study the seismic performance of moderately ductile built-up box columns, the system behavior of a BRBF was assessed by conducting quasi-static tests and hybrid simulations with a full-scale cruciform

subassemblage at NCREE (Wang et al. 2023). This study was aimed to conduct shake table tests on a full-scale, three-story steel dual frame that was designed using only the moderately ductile built-up box members in AISC 341 (2022) and all-steel sandwiched buckling-restrained braces (SBRB). Moreover, an attention has also been paid to reduce seismic force to an earthquake-resisting frame so that less design force or lighter structural members can be adopted in design (Tsampras and Sause 2022). This work also explores the potential of a new system by using a sliding slab to mitigate seismic force demand on the seismic-resisting frame.

STEEL DUAL FRAME SPECIMEN

The specimen is a full-scale, three-story steel frame with precast concrete slabs, designed based on a site condition on stiff soil and 3.5 km from a Xinhua fault in Tainan, Taiwan. The lateral force resisting system (LFRS) is a two-dimensional, two-bay dual frame system that consists of a special moment frame (SMF) and a buckling-restrained braced frame (BRBF). The gravity force resisting system (GFRS) is positioned at the perimeter of the dual frame with pin at the column base and the beam-to-column connection, not designed for lateral earthquake resistance. Figure 1(a) and (b) show the plan and elevation views, with the LFRS (the center frame Line B) positioned along the shaking direction (north-south direction). The LFRS is designed with a SMF in the north bay and a BRBF in the south bay. The total height of the specimen is 9000 mm with each floor height of 3000 mm. A total weight of each floor was 333 kN for the second and third floors and 335 kN for the roof.

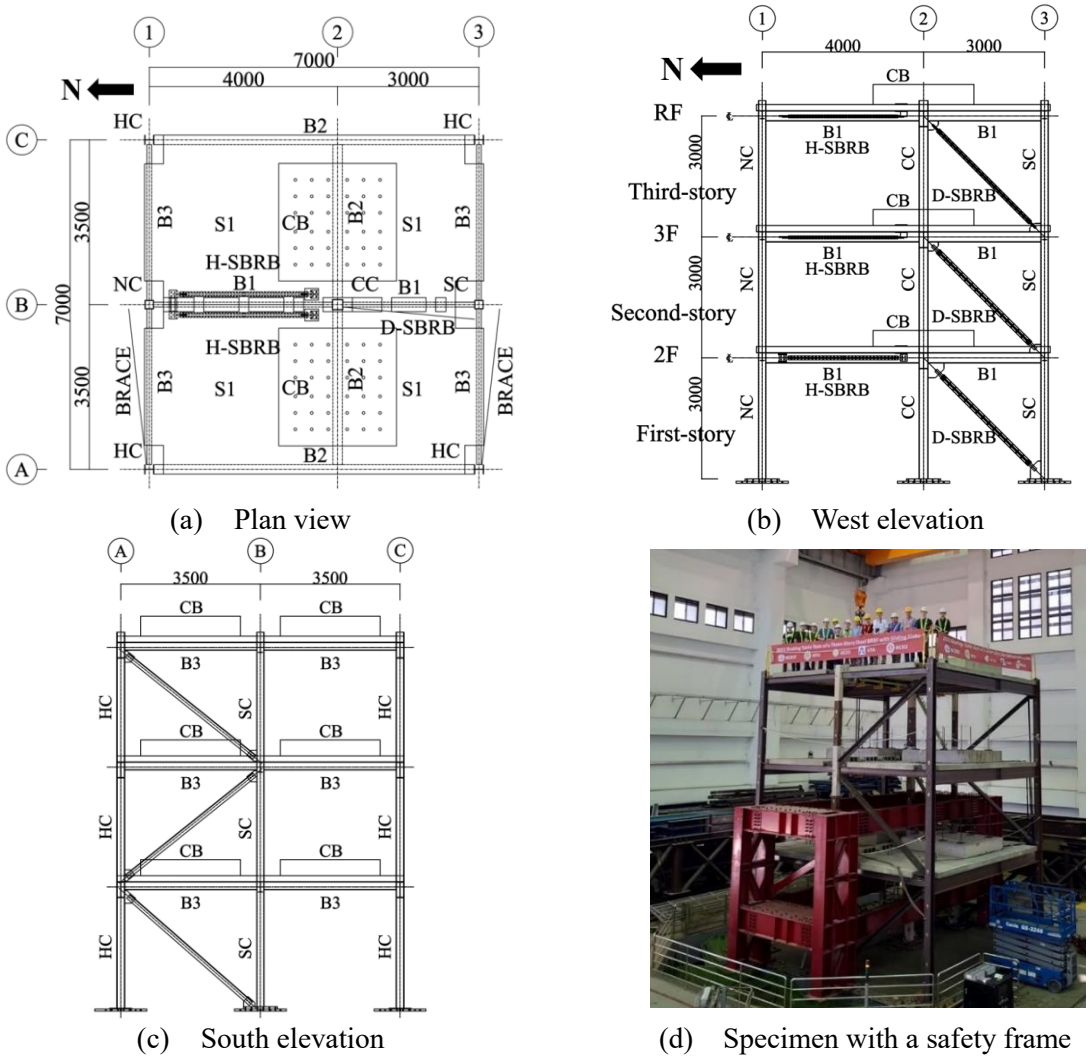

(a) Plan view (b) West elevation

(c) South elevation (d) Specimen with a safety frame

Figure 1 Test specimen (unit: mm)

Table 1 lists the column and beam sections. SN490B steel with a nominal yield stress of F_y= 325 MPa was specified for all square built-up box columns, wide-flange columns, built-up I-shaped beams, and all-steel sandwiched buckling-restrained braces (SBRBs). The north column (NC), center column

(CC), and south column (SC) have a width-thickness ratio (b/t) of 21.1, 20.5, and 21.1, respectively. These b/t values do not meet the highly ductile requirement for built-up box column sections (λ_{hd}=12.2), but meet the moderately ductile column requirement (λ_{md}=22.2) in Table D1.1, AISC 341-22 (2022):

$$\lambda_{md} = 1.0\sqrt{\frac{E}{R_y F_y}} \quad (1)$$

The all-steel sandwiched buckling-restrained brace (SBRB) was used in the BRBF bay for lateral earthquake resistance. The SBRB consisted of a steel core and a pair of bolted restraining members, with no concrete filling in the restraining member. The design of SBRBs followed a procedure outlined by Chou and Chen (2010). The SBRBs in the first and second stories had a core plate of 75×12 mm with a channel 75×45×6 mm and face plate 180×12 mm, and the SBRBs on the third story had a core plate of 50×8 mm with a channel 50×35×6 mm and face plate 155×12 mm. All SBRBs were connected to the frame by using a dual-gusset-plate configuration (Chou et al. 2012, Pham and Chou 2020).

Two Test Phases

Shake table test was conducted in two phases: 7 tests in phase 1 and 10 tests in phase 2. In phase 1, two horizontally placed SBRBs, named by H-SBRB in this work, were connected between the slab and beam at each floor in the SMF bay [Figure 1(b)]. Two H-SBRBs per floor were considered to provide energy dissipation when the slab moved relative to the beam. Teflon pads with 1 mm thick were placed between all interface of the precast slab and the beam to minimize friction. In phase 2, all H-SBRBs were replaced by structural T-members with high stiffness and strength to simulate a rigid connection between the slab and beam. The test instrument included 262 strain gauges, 47 displacement transducers, 28 accelerometers, and 16 linear variable differential transformers (LVDTs). A motion-capture system with 221 sensors was used to record the slab, frame, and SBRB displacement.

GROUND MOTION FOR SHAKE TABLE TEST

The test was conducted at the Tainan laboratory, NCREE, under a unidirectional shake table test in the North-South direction. The table size is 8 m by 8 m with a payload capacity of 2000 kN. The selected ground motion with PGA=0.43 g was obtained from the September 18th, 2022, Chishang earthquake, recorded at the EYUL-EW station which is about 1.4 km from a collapsed three-story RC building in Yuli township [Figure 2(a)], Hualien. The Chihshang earthquake sequence induced a series of ground ruptures and caused one fatality, 170 injuries, two collapsed buildings and two collapsed bridges, and partially damaged hundreds of buildings and several bridges across or along the faults (Chou et al. 2023b, Lin et al. 2023). The measured acceleration time history was baseline-corrected, and high-pass filtered to remove the residual displacement as the table input motion to avoid the dislocation of the shake table after each test. Obtained at the base of the shake table, a scale factor of 0.07-1.4 was used for 7 tests in phase 1, and 0.07-2.44 for 10 tests in phase 2. Figure 2(b) and (c) show the response spectra for these 17 tests with the design basis earthquake (DBE) and maximum considered earthquake (MCE) levels in Taiwan.

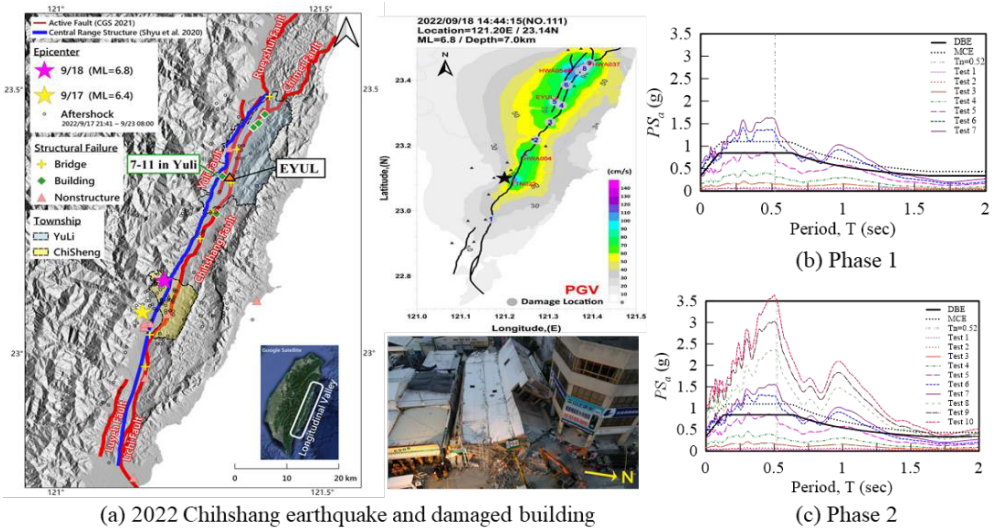

(a) 2022 Chihshang earthquake and damaged building

(b) Phase 1

(c) Phase 2

Figure 2 Chihshang earthquake motion and response spectra from EYUL record

Table 1 Column and beam sections

Element	Location		Section (mm)
Column	LFRS (1st~3rd story)	North	Box185×185×8
		Center	Box 225×225×10
		South	Box185×185×8
Beam	GLRS (1st~3rd story)		H 200×200×8×12
	LFRS (2F~RF)		H 257×102×6×9
	GLRS (2F~RF)		H 200×100×5.5×8
			H 400×200×8×13

OVERALL FRAME RESPONSE

Figure 3(a) and (b) show the roof drift history in phases 1 and 2. In phase 1 tests, the beam and column remained elastic; only H-SBRB and D-SBRB yielded. A reverse motion was applied to the specimen in test 6 after the specimen completed test 5 at the DBE level with a residual roof drift of 0.00011 rad. The maximum roof drift angle of the frame was -0.013 rad with a residual drift of -0.0031 rad in test 6. To limit residual drift, the original motion was applied to the specimen in test 7 (1.4MCE level) with a maximum roof drift angle of 0.0156 rad and small residual drift, allowing that HBRBs could be disassembled from the frame specimen and structural T-members could be installed to the frame specimen for conducting phase 2 tests.

For comparison purposes, the same motion with the same test sequence in phase 1 was conducted on the frame specimen in phase 2; a slightly lower maximum acceleration measured from the shake table was observed in tests 6 and 7 in phase 2 than phase 1. Figure 4(a) shows maximum interstory drift angle in phases 1 and 2; the third floor has a maximum interstory drift angle of 0.045 rad. Figure 4(b) shows the slab acceleration normalized by the table base acceleration in test 7. It shows a significant slab acceleration reduction at all floors in phase 1, such as 25% reduction at the roof even when the phase 1 test has a larger PGA than the phase 2 test (0.62g versus 0.56g). Moreover, a method that can be used to estimate residual drifts of the dual frame in the pulse type motion from the measured acceleration at each floor is detailed in Huang et al. (2023).

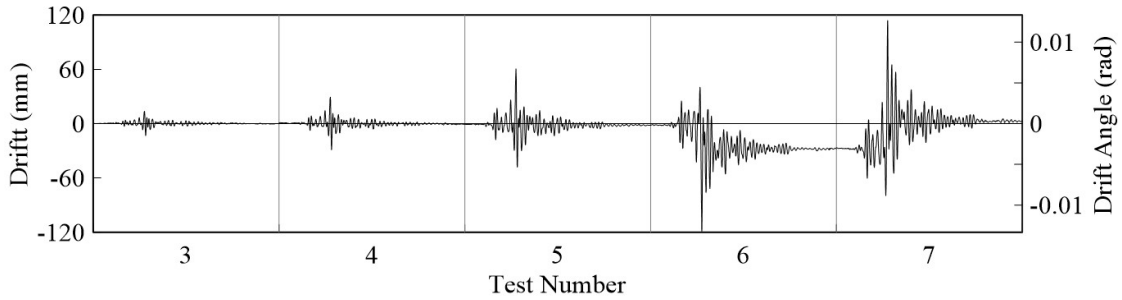

(a) Phase 1

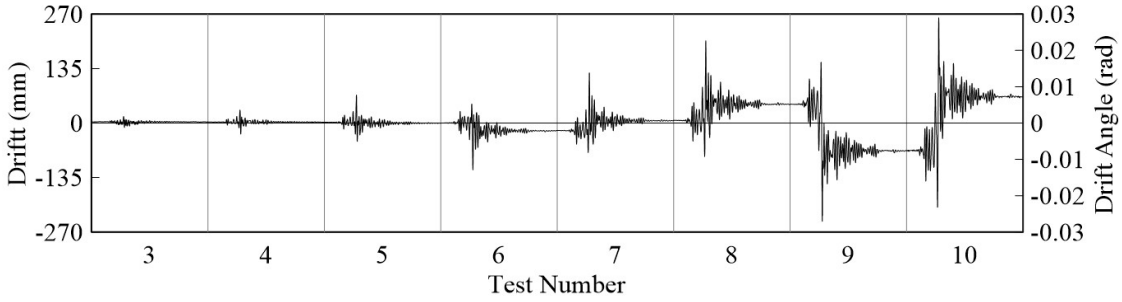

(b) Phase 2

Figure 3 Roof drift response

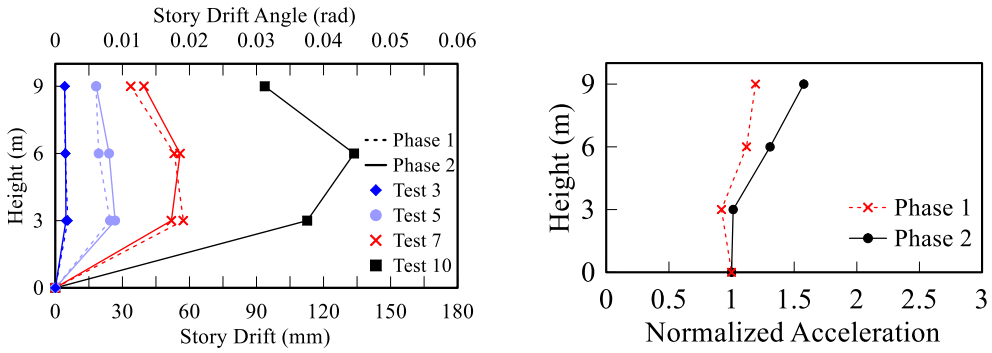

(a) Interstory drift (b) Acceleration reduction (Test 7)

Figure 4 Maximum interstory drift and acceleration reduction

MODERATELY DUCTILE BOX COLUMN RESPONSE

In phase 2, the H-SBRB at each floor was replaced by a structural T-member to simulate a nearly-rigid connection between the slab and the beam so that a steel dual system with moderately ductile box columns in the BRBF can be examined in the shaking table test. No sign of column yielding was observed up to test 5 at DBE level. Slight yielding lines as shown by whitewash flaking were observed at the bottom and top ends of the first-story center column in test 6 (1.2MCE level in Figure 2), as well as the second and third floor beam flanges in the SMF bay. From tests 7 to 10, yielding propagated in the center column ends at three floors; no yielding was observed in the north and south columns. Significant yielding was also observed in the second and third floor beams within the RBS in the SMF bay, as well as in the gusset plate and the beam outside the gusset connection in the BRBF bay. No sign of local buckling was observed in the beam, gusset plate, or SBRB after test 10 (2.4MCE level). Figure 5 shows the observation of the center column, gusset-to-SBRB connection, and RBS after test 10 in phase 2; significant yielding was observed at the column base without any sign of local buckling.

The center column moment exceeded the plastic moment M_{pc} in tests 9 and 10 [Figure 6(a)], which caused the column to move from -0.018 to 0.038 rad with a residual drift angle of 0.012 rad. The earthquake intensity that represents a seismic event of 2.4 times the MCE level resulted in a first-story peak interstory drift of 0.038 rad and the second-story drift of 0.045 rad. The box columns performed well without strength degradation although they only met the requirement for moderately ductile members in AISC 341-22, rather than that for highly ductile members. The maximum base shear is 750 kN, about 3.2 times the design base shear (237 kN) in Figure 6(d). If the first yield displacement of the frame specimen is Δ_s=29.8 mm in test 4 [Figure 6(d)], the displacement amplification factor, C_d, is 11 (=328.9/29.8) in test 10, exceeding a recommended value of 5.5 in ASCE-7 (2022).

D-SBRB RESPONSE

The first-story D-SBRBs yielded in test 5 with a maximum core strain of 0.41%, exceeding the yield strain of 0.16%. The axial strain increased to 1.12% in test 7; the brace response in phases 1 and 2 was similar. The axial strain increased to 2.51% in test 10, phase 2 [Figure 6(b)]. The cumulative plastic ductility (CPD) of D-SBRB was 217 at the first floor, 176 at the second floor and 112 at the third-floor in 17 shake table tests. The test results verify the satisfactory performance of all-steel SBRBs under a strong shaking with a pulse moving to one direction with a maximum inter-story drift to 0.045 rad.

The first-story D-SBRB was removed from the frame specimen and positioned to a 5000 kN uni-axial testing machine. Two tests were conducted on the brace. First, the D-SBRB was tested using a recorded displacement history from displacement transducers in test 10. The hysteretic response of the single D-SBRB component is close to that obtained from the shake table test, as shown in Figure 6(b), validating the data processing for the story shear and column moment in the shake table tests. The second phase test of the brace component was performed to a core strain of 2.5% using the AISC 341-22 standard loading protocol (reversed cyclic loading). The high-mode buckling of the core plate was observed after removing bolts from the restraining member of the SBRB. The high mode buckling of the core plate started from stiffener ends of the SBRB [Figure 6(c)], and extended 560 mm towards the core plate center. No high mode buckling was observed in the center portion of the core plate or the restraining member. The total CPD of the D-SBRB increased to 526 from 217 after all tests.

Figure 5 Column base, SBRB connection, and RBS after all tests

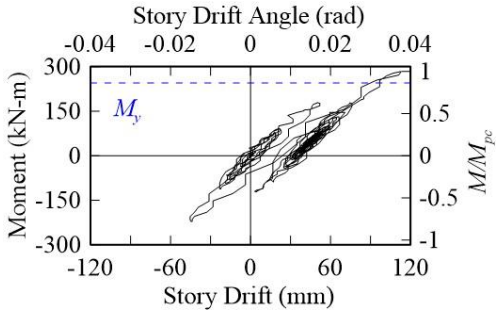

(a) Center column base (Test 10)

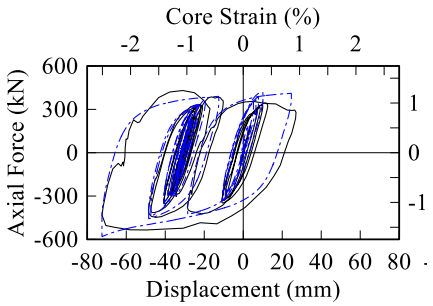

(b) First-story SBRB (Test 10)

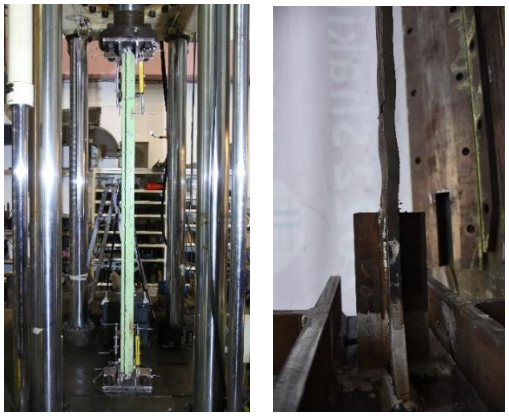

(c) SBRB component test

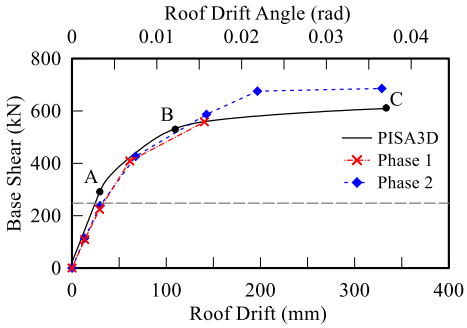

(d) Test versus pushover analysis

Figure 6 Column and SBRB responses in tests

CONCLUSIONS

This work was aimed to evaluate the seismic performance of a full-scale, 3-story steel dual frame that has a 4-m span SMF and a 3-m span BRBF in shake table tests. The built-up box columns with *b/t* values of 20-21 were used in the frame specimen to meet only the moderately ductile column requirement (λ_{md}=22.2) in AISC 341-22 (2022). Dynamic tests were conducted using an 8m×8m shake table at NCREE under a Yuli scaled motion from the EYUL station, recorded in the 2022 Chihshang earthquake that occurred in Taitung, eastern Taiwan with M_L 6.8. The measured motion with a peak ground acceleration (PGA) was 0.43 g, its intensity close to the design basis earthquake (DBE) level. In addition to examine the rationality of the AISC 341 revision on the BRBF, the other objective is to reduce seismic force to the lateral force resisting system (LFRS) by adopting a sliding mechanism for the slab.

In phase 1 test using a sliding slab mechanism, the H-SBRB in the roof showed yielding, resulting in floor acceleration reduction by 25% when compared to that in phase 2 test using nearly rigid slab-to-beam connectors. In phase 2 tests, the maximum interstory drifts were 0.038 rad at the first floor, 0.045 rad at the second floor, and 0.031 rad at the third floor. The center column developed the plastic moment M_{pc} when the column moved from -0.018 to 0.038 rad with a residual drift angle of 0.012 rad. No strength degradation or local buckling was observed near the column base at 2.4MCE level, which is about 3.2 times the design base shear (=237 kN) in this dual frame system. Large *b/t* values (i.e., 20-21) that exceed the highly ductile box column requirement (λ_{hd} =12.2) in AISC 341-22 (2022) still provide

satisfactory performance for first-story columns at large drifts (i.e., 0.038 rad). Therefore, the moderately ductile limit for *b/t* ratio (λ_{md}=22.2) can be applied to the dual frame with both SMF and BRBF in high seismic areas. Moreover, the all-steel SBRB with no concrete filling in the restraining member perform well in all shake table tests and post-earthquake tests, with a cumulative plastic ductility of 526.

ACKNOWLEDGMENTS

This work was funded by the National Science and Technology Council under the project number MOST 111-2625-M-002-006, Taiwan and the 2022 Innovative Project of the National Applied Research Laboratories.

REFERENCES

AISC (2016), *Seismic provisions for structural steel buildings*, ANSI/AISC 341-16, American Institute of Steel Construction, Chicago, Illinois.

AISC (2022), *Seismic provisions for structural steel buildings*, ANSI/AISC 341-22, American Institute of Steel Construction, Chicago, Illinois.

ASCE/SEI 7-22. *Minimum design loads and associated criteria for buildings and other structures*. American Society of Civil Engineers. 2022

Chou, C. C., Chen, S. Y. (2010). Subassemblage tests and finite element analyses of sandwiched buckling-restrained braces. *Engineering Structures*, 32, 2108-2121.

Chou, C. C., Liu, J. H., Pham D. H. (2012). Steel buckling-restrained braced frames with single and dual corner gusset connections: seismic tests and analyses. *Earthquake Engineering & Structural Dynamics,* 7(41): 1137-1156.

Chou, C. C., Chen, G. W. (2020). Lateral cyclic testing and backbone curve development of high-strength steel built-up box columns under axial compression. *Engineering Structures* 223, 111147

Chou, C. C., Lai, Y. C., Xiong, H. C., Lin, T. H., Uang, C. M., Mosqueda G., Ozkula, G., El-Tawil, S., McCormick, J. P. (2022). Effect of boundary condition on the cyclic response of I-shaped steel columns: two-story subassemblage versus isolated column tests. *Earthquake Engineering & Structural Dynamics*, DOI: 10.1002/eqe.3730.

Chou, C. C., Xiong, H. C., Kumar, A., Lai, Y. C., Uang, C. M. (2023a). Effects of section compactness and SCWB condition on moment redistribution and plastic hinging in SMF built-up box columns. *J. Structural Engineering,* ASCE, 149(11): 04023144

Chou, C. C., Wu, C. L., Chao, J. F., Yao, G. C. (2023b). Reconnaissance report on seismic damage caused by the 2022 Guanshan and Chihshang earthquake sequence, Taiwan. *Report NCREE-23-007*, National Center for Research on Earthquake Engineering, Taipei, Taiwan.

Huang, Y. T., Loh, C. H., Chou, C. C. (2023). Estimation of the seismically induced residual drift of structures. *J. Earthquake Engineering,* https://doi.org/10.1080/13632469.2023.2236227

Lignos, D. G., Hikino, T., Matsuoka, Y., Nakashima, M. (2013). Collapse assessment of steel moment frames based on E-Defense full-scale shake table collapse tests. *J. Structural Engineering,* ASCE, 139(1), 120-132.

Lin, T. H., Chou, C. C. (2022). High-strength steel deep H-shaped and box columns under proposed near-fault and post-earthquake loadings. *Thin-Walled Structures*, 172, 108892.

Lin, C. M., Chang, Y. W., Chou, C. C., Jhuang, S. J., Lee, Z. K., Wu, C. L., Chao, S. H., Huang, J. Y., Yang, H. C., Chang, C. Y., Mosqueda, G., Hung, C. C. (2023). Reconnaissance of the 2022 Guanshan and Chihshang earthquakes in eastern Taiwan. *Earthquake Spectra*, EQE-23-0031 (under re-review).

Pham, D. H., Chou, C. C. (2020). Strong-axis instability of sandwiched buckling restrained braces in a steel two-story X-BRBF: seismic tests and finite element analyses. *Thin-Walled Structures*, 157, 107011

Tsampras, G., Sause, R. (2022). Force-based design method for force-limiting deformable connections in earthquake-resistant buildings. *J. Structural Engineering*, ASCE, 148(10), 04022150.

Suita, K., Yamada, S., Tada, M., Kasai, K., Matsuoka, Y., Sato, E. (2008). Results of recent E-defense tests on full-scale steel buildings: part 1—collapse experiments on 4-story moment frames. *Structures Congress 2008: Crossing Borders*.

Wang, K. J., Chou, C. C., Huang, C. W., Shen, H. K., Sepulveda, C., Mosqueda G., Uang, C. M. (2023). Hybrid simulation of a steel dual system with buckling-induced first-story column shortening: a mixed control mode approach. *Earthquake Engineering & Structural Dynamics***.** DOI: 10.1002/eqe.3944

Day1 (Monday, Sep. 25th, 2023) 10:05~10:40

Utilities of Monitoring for Advancing Seismic Design – A Japanese Experience from past Earthquakes

Masayoshi Nakashima

President, Kobori Research Complex Inc., Tokyo, Japan, and Professor Emeritus, Kyoto University, Japan

Masayoshi Nakashima has been engaged in the education and research of structural engineering at Kyoto University, Japan, for many decades.

His research fields include seismic analysis and design of steel building structures and large-scale experimental techniques for simulating earthquake responses. He supervised over 120 graduate students, post-docs, and visiting researchers. He and his students have published about four hundred technical papers, nearly two hundred and fifty in archived journals. He has earned various research awards from such activities, including the ASCE Moisseiff Award, the ASCE Howard Award, the AISC Special Achievement Award, and the EERI Housner Medal, among others.

Nakashima also served/serves for the management of academic organizations, which includes the Director of the Disaster Prevention Research Institute of Kyoto University, the Director of E-Defense, the facility equipped with the world's largest shaking table, the President of the Architectural Institute of Japan, and the President of International Association for Earthquake Engineering. He also serves as the Executive Editor of the Journal of Earthquake Engineering and Structural Dynamics (EESD).

Because of his long-term contribution to the structural and earthquake engineering community, Nakashima has been bestowed a Member of the Engineering Academy of Japan, an International Member of the National Academy of Engineering of the United States, a Corresponding Member of the Mexican Academy of Engineering, and a Corresponding Member of the Slovenian Academy of Arts and Science.

Nakashima retired from Kyoto University in 2017, and since then, he has worked as President of Kobori Research Complex and Chief Technical Counselor of Kajima Corporation.

UTILITIES OF MONITORING FOR ADVANCING SEISMIC DESIGN – A JAPANESE EXPERIENCE FROM PAST EARTHQUAKES

Masayoshi Nakashima[1] and Yu Fukutomi [2]
1. President, Kobori Research Complex Inc., Tokyo, Japan, and Professor Emeritus, Kyoto University, Japan
2. Research Engineer, Kobori Research Complex Inc., Tokyo, Japan
Email: nakashima@archi.kyoto-u.ac.jp, fukutomi@kobori-rc.com

ABSTRACT

Japan is a very earthquake-prone country and has been equipped with various sensor networks and monitoring systems to detect and measure the shaking of lands and the response of various built facilities. The data collected have been used to advance research and practice on seismology and earthquake engineering and promote practice on immediate damage detection and earthquake early warning. This article briefly introduces an overview on the current status of Japanese monitoring, followed by discussions, based on the quarter-century experience, on how those monitored data have been transferred to and utilized for advancing earthquake engineering.

Keywords: 1995 Kobe Earthquake, seismograph networks, monitoring for built facilities, seismic hazard maps, performance-based seismic design, nonstructural elements

INTRODUCTION

Japan is earthquake-prone, and earthquake disaster mitigation has been one of the most serious national problems for centuries. The 1995 Kobe earthquake caused severe damage to the modern city of Kobe and its vicinities, and it revealed various issues that would impede a safer life and society. Out of many, two challenges recognized as lessons of the 1995 Kobe earthquake (AIJ, 2000) are: 1) the need for detailed data on the shaking of lands and the response of built facilities, and 2) the need for prompt responses immediately after a disastrous event to minimize the growth of damage. The public and private sectors responded to those needs and began and continue monitoring our lands and built facilities.

First, the progress and current situation of such monitoring is introduced. Then, the influences of the data obtained by such monitoring on the assessment and evolution of seismic design practices are touched upon. Three episodes are presented, one on seismic hazard assessment, another on performance-based design, and the last on nonstructural elements' behavior.

PARTIAL SUMMARY OF EARTHQUAKE-RELATED MONITORING IN JAPAN

Monitoring of Land

The history of Japan reveals that it cannot escape large earthquakes and according loss of lives and businesses. Even after the turn of the century, more than 150 earthquakes involved human injuries/deaths (JMA, 2023). The Nankai Trough, located alongside Japan, is known to rupture periodically with an interval of about one to one-half century, and historical documents revealed the ruptures caused severe damage to both humans and properties. Following the pattern of rupture occurrences, the next large rupture along the Nankai Trough is expected to occur about 70 to 80% of the chance for the coming 30 years (Cabinet Office of Japan, 2023). The magnitude of damage in the next Nankai Trough rupture could be more than ten times in the death toll and direct property loss than the 2011 Tohoku earthquake. Furthermore, Japan has many active faults throughout the country, adding threats of severe land shaking.

The history of deployment of strong motion accelerographs was long in Japan. Before the 1995 Kobe earthquake, however, systematic and organizational efforts to deploy such accelerographs and record and store the data in a unified manner remained limited. Having recognized the importance of

monitoring land shaking, the Government of Japan launched national programs immediately after the 1995 Kobe and deployed various types of sensors to monitor the shaking of land surfaces and underneath. The sensor networks developed by the national programs have continued to be maintained and upgraded until now. By this writing, over 4,000 such sensors have been deployed throughout Japan, combining those operated by the public and private sectors.

Monitoring of Utilities and Mechanical Systems

Monitoring of land shaking, including new installation, maintenance, and replacement, has been led exclusively by the Central Government of Japan, with the belief that the Government shall provide its people with the basics to maintain their safety, security, and welfare. However, when it comes to monitoring of built facilities such as utilities, public transport, manufacturing factories, and private buildings, the Government does not offer any financial support. Such monitoring is being implemented on the basis of "market," and proprietors of respective facilities and buildings are in charge of necessary expenditures.

The Tokai Japan Railway (JR), a railway firm operating the Japanese fast train system dubbed "Shinkansen," developed a system in the 1980s in which fast trains would reduce the speed and stop safely before primary shaking. In 1992, the system, dubbed UrEDAS (Urgent Earthquake Detection and Alarm System), began its operation and has been used successfully for the past three decades. Since the start of the operation, the system has been expanded to all fast train systems and upgraded by combining it with the JMA's EEW. The JR took care of the entire expenditure associated with the system.

Monitoring of Buildings

The history of building monitoring in Japan is long. Until recently, however, the installation of sensors in buildings remained limited, and its use was primarily for calibrating building responses against the predicted response. The attitude changed after experiencing the 2011 Tohoku earthquake. About 5.15 million people in the Tokyo metropolitan region had trouble returning to their homes after the quake, which created a severe problem throughout the Tokyo metropolitan region. The Tokyo Metropolitan Government (2013) enforced an ordinance in 2013 that, for safety, people should remain in their buildings when possible rather than leaving them. Building owners, particularly those who manage many buildings and are keen on business continuity planning (BCP), have come to respond to the ordinance. This new trend differs from the movement we saw for land monitoring in that the installation of building monitoring is driven almost primarily by business and market forces rather than by public expenditure. Before the 2011 Tohoku earthquake, the number of instrumented buildings in Japan was in the range of 150. Since the market-based instruments began, the number of monitored buildings increased dramatically, now (as of 2023) in a range of 1,000, among which over 80% are regarded as private-owned and private-operated.

Among the market-based building monitoring systems deployed in Japan, a monitoring system named q-NAVIGATOR (or q-NAVI in short), started for installation in 2015, has the largest share, with 530 buildings equipped with q-NAVI, as presented by Kanda *et al.* (2011). The system consists of a few 3D sensors installed in some stories along the height and wired to the PC installed in the building's maintenance room, the PC for collecting the sensor data and assessing the maximum story drifts and floor accelerations, and the screen to show the results, with "safe", caution," and "danger." The PC is further connected via the Internet to a cloud system, from which the building owners and managers can receive the necessary data within a short period, say 2 to 5 minutes.

UTILITIES OF MONITORING FOR ADVANCMENT IN SEISMIC DESIGN

Design Seismic Loads

In response to the severe damage disclosed in the 1995 Kobe earthquake, the Government of Japan established the Headquarters for Earthquake Research Promotion (HERP) of Japan. The institution's

primary mission is to develop and regularly update Japan's earthquake hazard maps. The hazard maps can serve as a benchmark to evaluate and modify the design seismic loads stipulated in the seismic design code. However, in the past two decades, the design seismic loads remained unchanged despite a few large earthquakes in some parts of Japan, such as the 2011 Tohoku and 2016 Kumamoto earthquakes.

Differences in the estimated magnitude of strong shaking are significant among the regions in Japan. When looking into the hazard maps, the difference is by several times between the largest and smallest strong motions. However, the corresponding difference in the design seismic loads is only 20%. Furthermore, discrepancies were disclosed in many cases between the level of recorded shaking, say, PGA and PGV, and the degree of actual structural damage observed in the recorded region. Such observations naturally discouraged the motivation to change (increase) the design seismic loads. Public sentiment also plays an essential role in determining the design seismic loads. Japan exercises a centralized operation system at the time of disastrous events, and the public sector covers most post-disaster recovery supports. The general public also values "equality" for such post-disaster recovery supports. Those bring cautiousness in the revision of relevant codes and specifications. The full detail of this argument is presented in Suzuki *et al.* (2023).

Performance-based Seismic Design

Japanese seismic design enforces two levels of design seismic load, i.e., Level 1 for serviceability and Level 2 for safety. Level 2 corresponds to about 1 g in terms of the pseudo acceleration spectrum. For Level 2, the designed building shall stay safe, but damage to the structural and nonstructural members and elements is permitted in design. For the past quarter century, the land sensors deployed around Japan recorded many ground motions that were more significant than what has been stipulated in the Japanese seismic design code. Still, the actual damage to major structural elements and even the damage to nonstructural elements remained minimal, ensuring life and business continuities. Many reasons have been speculated, for instance, the soil-foundation-structure interaction by which the effective input to the superstructure could decrease notably and the contribution of nonstructural elements to the actual strength of the building. With the increase in building monitoring, we have learned that structural performance has been significantly enhanced in recent years. The structure remains nearly elastic even in the Level 2 design seismic load, particularly for large and tall buildings where performance-based design (involving response history analysis) is employed. Details about the performance-based design and analysis of tall buildings designed by the Japanese seismic codes are presented in Hori *et al.* (2022) and Kolozvari *et al.* (2022).

Characterization of Damage to Nonstructural Elements

Another notable benefit of building monitoring is characterizing the damage to nonstructural elements. After damaging earthquakes, we found various types of damage to nonstructural elements, and such surveillance has given us valuable information for assessing the nonstructural damage. However, what we saw from the surveillance was only the final state of damage and cannot give us any clue for the magnitude of responses, i.e., the maximum interstory drifts and/or the maximum floor accelerations that the damaged elements had sustained. We can assess such response magnitudes once the building is equipped with sensors. We can develop “fragility curves” for nonstructural elements with the magnitude and damage level combined.

There is a good example presented by Kanda *et al*. (2021), in which various nonstructural elements (exterior walls, window glasses, interior walls, doors, ceilings, furniture, and expansion joints) were surveyed in detail for 27 buildings shaken during the 2018 Osaka earthquake. Observed were only for 27 buildings, but the numbers of nonstructural elements, for instance, the number of ceilings, were very many when counted for each room as a ceiling unit. Considering the inherent nonuniformity and variability of nonstructural elements, particularly in their connection details, “approximate” but “many” sample data are exceptionally suited for developing “fragility curves.” This benefit of building monitoring can never be underestimated.

CONCLUSIONS

This article presented two issues related to monitoring land shakings and responses of built facilities. First, the current status of such monitoring in Japan was summarized, followed by discussions on how such observed data have influenced the seismic design practice. Three relevant episodes were presented. One is the interaction of seismic hazard assessment with design seismic loads. It was observed that compared to the regional differences in the magnitude of shakings (estimated) by the seismic hazard assessment, the differences in the magnitude of design seismic loads are significantly more minor. Another is the differences between the expected performance in design and the actual performance observed in real earthquakes. In not a few cases, the actual performance was significantly superior to the expected performance. The last is the benefit of building monitoring to characterize the behavior and performance of nonstructural elements. The maximum inter-story drifts and maximum floor accelerations obtained by monitoring can significantly help us establish fragility curves for major nonstructural elements.

ACKNOWLEDGMENTS

The authors are grateful to the following individuals for their input and advice in the writing of this article: K. Kanda, A. Kusaka, H. Hasegawa, A. Suzuki of Kobori Research Complex Inc.

REFERENCES

AIJ (1995). Preliminary Reconnaissance Report of the 1995 Hyogoken-Nanbu Earthquake, edited by Nakashima, M. and Bruneau, M., The Architectural Institute of Japan (AIJ), Tokyo, Japan, 216pp.

AIJ (2000). Reconnaissance Report of the Hanshin-Awaji Earthquake Disaster, Summary Volume. the Architectural Institute of Japan (AIJ), Tokyo, Japan. ISBN978-4-8189-2021-7 (in Japanese).

Cabinet Office of Japan (2023): https://www.bousai.go.jp/jishin/nankai/index.html (About assessment of damage by next Nankai Trough earthquake, in Japanese).

Hori, Y., Suzuki, Y., Kolozvari, K., Johansson, O., Naeim, F., Nakashima, M. (2022). "A comparative study of seismic analysis, design, and collapse safety margins of tall buildings in the United States and Japan, Part I: performance-based analysis and design." Earthquake Spectra. 38(3), 2297-2318. Doi.10.1177/87552930221076528.

JMA (2023). https://www.data.jma.go.jp/eqev/data/higai/higai1996-new.html (About recent large earthquakes in Japan, in Japanese).

Kanda K., Nakashima M., Suzuki Y., Ogasawara S. (2021). "q-NAVI: a case of market-based implementation of structural health monitoring in Japan." Earthquake Spectra. 37(1),160-179.

Kolozvari, K., Hori, Y., Yasumoto, H., Suzuki, Y., Nakashima, M., Naeim, F. (2022). "A comparative study of seismic analysis, design, and collapse safety margins of tall buildings in the United States and Japan: Part II: comparison of seismic capacity and collapse safety margin." Earthquake Spectra. 38(3), 2319-2335. Doi.1177/87552930221076534.

Suzuki, A., Kusaka, A., Nakashima M. (2023). "Japanese attitudes toward risk control in seismic design in light of observation, prediction, and actual performance of building structures." Earthquake Engineering and Structural Dynamics. Doi: 10.1002/eqe.3853.

Tokyo Metropolitan Government (2013). https://www.bousai.metro.tokyo.lg.jp/_res/projects/default_project/_page_/001/000/939/english_02.pdf (About an ordinance on building safety check and according actions, in Japanese).

Day1 (Monday, Sep. 25th, 2023) 11:00~11:35

Advances and Application of Real-Time Hybrid Simulation Towards Creating Seismically Resilient Structural Systems

James M. Ricles

Bruce G. Johnston Professor of Structural Engineering, Lehigh University, Bethlehem, Pennsylvania, U.S.

Dr. James M. Ricles is the Bruce G. Johnston Professor of Structural Engineering and a faculty member of the Department of Civil and Environmental Engineering at Lehigh University. He is also the director of the Real-Time Multidirectional Facility for Seismic Performance Simulation of Large-Scale Structural Systems, a National Science Foundation (NSF)-supported Natural Hazards Engineering Research Infrastructure (NHERI) Equipment Facility located at Lehigh University. He received his B.S. and M.S. degrees from the University of Texas, Austin in Architectural and Civil Engineering, respectively, and Ph.D. degree from the University of California, Berkeley. His current research interests include: (1) the behavior of structural steel connections, members, and systems under extreme loading conditions, including seismic, fire, wind, and blast loading; (2) performance-based design of resilient structural systems for extreme loading conditions; (3) development of resilient civil infrastructure concepts using innovative structural systems, including passive and semi-active controlled devices for reduction of damage from natural-hazards; (4) offshore wind turbine structures subject to aeroelastic, hydrodynamic, and mechanical loading effects; (5) resiliency of coastal civil infrastructure; and, (6) large-scale multi-directional real-time hybrid simulation of structural systems subject to dynamic loading conditions. As the Director of the Lehigh NHERI Experimental Facility, Professor Ricles has been leading the development in large-scale multi-directional real-time hybrid simulation, a technique that enables the development and experimental validation of performance-based engineered resilient structural system concepts that mitigate the effects of natural hazards. Professor Ricles is the Editor-in-Chief for the Engineering Structures Journal published by Elsevier and a member of the Advisory Editorial Board for the Journal of Earthquake Engineering and Structural Dynamics published by Wiley. He is a registered professional engineer in the State of California, active in working with industry to disseminate and promote concepts for structural resiliency, and serves on

several technical committees associated with structural engineering code development. He has supervised or co-supervised 33 completed Ph.D. students and 35 completed M.S. students, and published over 563 research articles, including 170 publications in peer-reviewed journals and 13 book chapters. Professor Ricles has received numerous research awards, including the American Institute of Construction Special Achievement Award (AISC) for his research related to seismically resilient steel structures, including moment resisting connections and self-centering frames. Other noteworthy awards also include the Lehigh University Bruce G. Johnston Endowed Chair, American Society of Civil Engineers Raymond C. Reese Research Prize, the National Science Foundation Presidential Young Investigator Award, the NASA Research Fellowship Award, and the Lincoln Arc Welding Foundation Chairman's Award for Outstanding Achievement in Arc Welded Design.

ADVANCES AND APPLICATION OF REAL-TIME HYBRID SIMULATION TOWARDS CREATING SEISMICALLY RESILIENT STRUCTURAL SYSTEMS

James M. Ricles[1], Richard Sause[2], Chinmoy Kolay[3], Yunbyeong Chae[4], and Baiping Dong[5]
1. Bruce G. Johnston Professor of Structural Engineering, Lehigh University, Bethlehem, Pennsylvania, U.S.
2. Joseph T. Stuart Professor of Structural Engineering, Lehigh University, Bethlehem, Pennsylvania, U.S.
3. Assistant Professor, IIT Kanpur, Kanpur, India
4. Associate Professor, Seoul National University, Seoul, Korea
5. Research Professor, Tongji University, Shanghai, CHN
Email: jmr5@lehigh.edu, rs0c@lehigh.edu, ckolay@iitk.ac.in, ybchae@snu.ac.kr, baipingdong@gmail.com

ABSTRACT

Recent earthquakes in many parts of the world have resulted in damage to civil infrastructure, resulting in fatalities and economic loss. This experience has led to stake holders demanding a more resilient infrastructure and the mitigation of earthquake hazards to minimize their impact on society. Researchers have developed concepts for structural systems to promote resilient performance. Real-time hybrid simulation (RTHS) provides an experimental technique to meet the need to validate these concepts. RTHS enables a complete structural system, including the soil and foundation to be considered in a simulation, interaction effects and rate dependency in component and system response to be considered, and, realistic demand imposed onto the system for prescribed hazard levels. The concept of RTHS and developments achieved at the Lehigh NHERI Experimental Facility is presented that have advanced RTHS to enable accurate large-scale, multidirectional simulations involving multi-natural hazards to be readily performed. In addition to presenting the background of RTHS, the role that hybrid simulation has played in enabling a deeper understanding of the seismic behavior of a structural system with nonlinear viscous dampers is illustrated. This illustration consists of a steel frame building outfitted with nonlinear viscous dampers.

Keywords: Real-time hybrid simulation, earthquake engineering, resiliency, steel structures, large-scale testing, nonlinear viscous dampers

INTRODUCTION

Real-time hybrid simulation (RTHS) offers an experimental technique to meet the need to validate new concepts, while overcoming computational modelling burdens. In a hybrid simulation, components of a system that lack accurate computational models are physically modelled in the laboratory as experimental substructures, and are kinematically linked to an analytical substructure. The remaining part of the system not included in the experimental substructure, and for which accurate computational models exists, are part of the analytical substructure. RTHS enables a complete structural system to be considered in a simulation, accounting for rate dependency and interaction effects in components and the soil-foundation-structural system under dynamic load conditions. During a RTHS realistic demand can be prescribed and imposed onto the system for various hazard levels.

REAL-TIME HYBRID SIMULATION BACKGROUND

The discretization of a structural system into analytical and experimental substructures for performing a RTHS is shown in Figure 1. As mentioned above, components of the system for which analytical models exist are modelled numerically and reside in the analytical substructure while the remaining components are modelled physically in the laboratory as the experimental substructure. The mass and inherent viscous damping of the structural system are included in the analytical substructure.

The displacement compatibility between analytical and experimental substructures are enforced through

their common degrees of freedom (DOF) in real time to capture the rate dependency of the experimental substructure and interaction with the complete structural system. The equations of motion at time step *i+1* are shown below in Equation (1), and include the following terms: inertia ($\boldsymbol{M}\ddot{\boldsymbol{X}}_{i+1}$), inherent viscous damping ($\boldsymbol{C}\dot{\boldsymbol{X}}_{i+1}$), the restoring forces $\boldsymbol{R}^a{}_{i+1}$ and $\boldsymbol{R}^e{}_{i+1}$ of the analytical and experimental substructures, respectively, and the applied load $\boldsymbol{F}_{i+1}$. The equations are numerically integrated to obtain displacements, velocities, and accelerations at each time step. These results are then used to compute the inertia, inherent viscous damping, and the restoring forces $\boldsymbol{R}^a{}_{i+1}$ of the analytical substructure. Simultaneously, the displacements associated with the experimental substructure (called the target displacements) are imposed onto this substructure, and the restoring forces $\boldsymbol{R}^e{}_{i+1}$ are measured. With $\boldsymbol{R}^a{}_{i+1}$ and $\boldsymbol{R}^e{}_{i+1}$ known, the integration process is then completed and repeated for the next time step. See Kolay & Ricles 2014, Kolay et al. 2015, Dong et al. 2015, Kolay & Ricles 2019, Kolay et al. 2020 for further details.

$$\boldsymbol{M}\ddot{\boldsymbol{X}}_{i+1} + \boldsymbol{C}\dot{\boldsymbol{X}}_{i+1} + \boldsymbol{R}^a{}_{i+1} + \boldsymbol{R}^e{}_{i+1} = \boldsymbol{F}_{i+1} \tag{1}$$

There are several challenges in performing a RTHS. These include: (1) integrating the equations of motion in real-time to determine the target displacements $\boldsymbol{x}^t$ for the system; (2) performing the state-determination process in real-time to obtain the restoring forces $\boldsymbol{R}^a{}_{i+1}$, where often nonlinear computational models of the analytical substructure are required; and (3) accurate real-time control of the servo-hydraulic actuators to impose command displacements where the target displacements $\boldsymbol{x}^t$ are achieved and precise values of $\boldsymbol{R}^e{}_{i+1}$ are obtained. These challenges are discussed further below and solutions to overcome the barriers that they pose are presented.

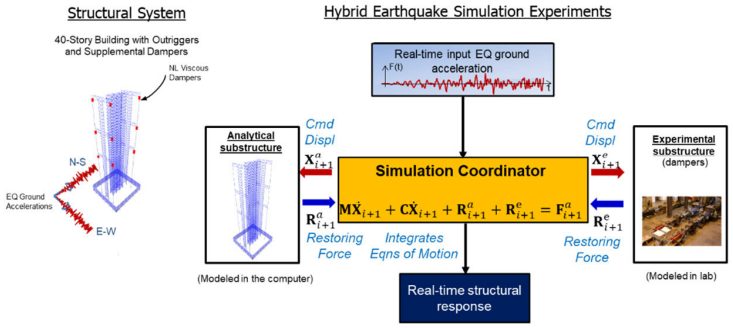

Figure 1. Conceptual framework of a real-time hybrid simulation of a tall building with nonlinear viscous dampers.

Integration of the Equations of Motion

Kolay and Ricles (2014, 2016) proposed a family of model-based second-order accurate explicit algorithms with controllable numerical energy dissipation. The algorithms include the KR- α Method and Modified KR- α (MKR- α) Method (Kolay et al. 2015, Kolay and Ricles 2019). Kolay and Ricles showed that the methods are unconditionally stable for linear elastic and stiffness softening type nonlinear response. The following equations describe the methods' algorithm for a nonlinear multi-degree of freedom (MDOF) system at time step *i+1*:

$$\dot{\boldsymbol{X}}_{i+1} = \dot{\boldsymbol{X}}_i + \Delta t\boldsymbol{\alpha_1}\ddot{\boldsymbol{X}}_i \tag{2}$$

$$\boldsymbol{X}_{i+1} = \boldsymbol{X}_i + \Delta t\dot{\boldsymbol{X}}_i + \Delta t^2\boldsymbol{\alpha_2}\ddot{\boldsymbol{X}}_i \tag{3}$$

$$\boldsymbol{M}\hat{\ddot{\boldsymbol{X}}}_{i+1} + \boldsymbol{C}\dot{\boldsymbol{X}}_{i+1-\alpha_f} + \boldsymbol{R}_{i+1-\alpha_f} = \boldsymbol{F}_{i+1-\alpha_f} \tag{4}$$

In Equations (2) and (3) Δt is the time step, and $\boldsymbol{X}_i$, $\dot{\boldsymbol{X}}_i$, and $\ddot{\boldsymbol{X}}_i$ are the vectors of displacement, velocity and acceleration, respectively, at time step *i.* Equation (4) is the weighted equations of motion (Kolay and Ricles, 2019), where

$$\hat{\ddot{\boldsymbol{X}}}_{i+1} = (\boldsymbol{I} - \boldsymbol{\alpha_3})\ddot{\boldsymbol{X}}_{i+1} + \boldsymbol{\alpha_3}\ddot{\boldsymbol{X}}_i \tag{5}$$

$\boldsymbol{\alpha_1}$, $\boldsymbol{\alpha_2}$, and $\boldsymbol{\alpha_3}$ in the above are matrices of model-based integration parameters (see Kolay et al. 2015, Kolay and Ricles 2019). Part of the restoring forces in a RTHS is measured from the physical experimental substructure ($\boldsymbol{R}^e_{i+1}$) and added to the analytical substructure restoring forces($\boldsymbol{R}^a_{i+1}$). Thus, $\boldsymbol{R}_{i+1-\alpha_f}$ appearing in Equation (4) can be rewritten as

$$\boldsymbol{R}_{i+1-\alpha_f} = (1 - \alpha_f)(\boldsymbol{R}^a_{i+1} + \boldsymbol{R}^e_{i+1}) + \alpha_f(\boldsymbol{R}^a_i + \boldsymbol{R}^e_i) \tag{6}$$

The parameter α_f is related to the high-frequency spectral radius ρ_∞ by:

$$\alpha_f = \frac{\rho_\infty}{\rho_\infty + 1} \tag{7}$$

The high-frequency spectral radius ρ_∞ prescribes the amount of dissipation assigned to the algorithm, as shown in Figure 2. Complete details about the KR- α Method and MKR- α Method can be found in Kolay et al. (2015) and Kolay and Ricles (2019).

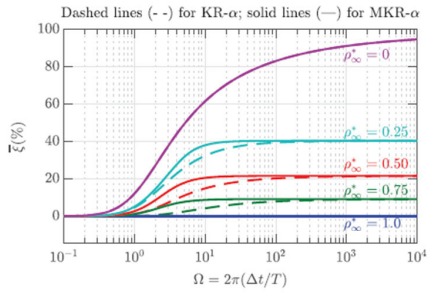

Figure 2. KR- α and MKR- α methods: equivalent damping ratio $\bar{\xi}$ as a function of frequency Ω for selected values of ρ^*_∞ ranging from 0 to 1.0 (from Kolay and Ricles (2019)).

Explicit-based State Determination

The integration of the equations of motion requires the determination of the restoring forces. . For the analytical substructure, the determination of the restoring forces $\boldsymbol{R}^a_{i+1}$ is obtained by subjecting the deformations associated with $\boldsymbol{X}_{i+1}$ and $\dot{\boldsymbol{X}}_{i+1}$to the computational model that represents the analytical substructure. The state determination process must be completed within the time step Δt to avoid accruing a delay that can lead to a numerical instability. Hence the state-determination process associated with the analytical substructure computational elements must be fast and accurate. Therefore, the state determination process must be deterministic, and allow only a fixed number of iterations. To avoid non-deterministic iterations, Kolay and Ricles (2017) formulated an explicit force-based beam-column element for conducting RTHS that involve nonlinear analytical substructure response. The element formulation includes a fixed number of iterations at the element level to satisfy element local equilibrium by reducing unbalanced internal member forces at the element's integration points and the associated element deformations. Any residual unbalanced section deformations are carried over and eliminated in subsequently time steps.

The accuracy of the formulation was assessed by Kolay and Ricles (2017) by modelling a highly nonlinear reinforced concrete MRF and subjecting it to multi-directional ground motions. The response of a beam in the model was studied which had extensive nonlinear response throughout the element that included reinforcement yielding, in addition to cracking, spalling, and crushing of the concrete. The moment-curvature hysteretic response of a section of the modelled beam is shown in Figure 3 where extensive nonlinear response is evident. The results based on the explicit formulation (identified by CO = Yes) are compared to the results from OpenSees (2017), referred to herein as *Reference*, where the latter is obtained using an implicit element formulation and the implicit average acceleration integration algorithm. Exceptional agreement between the two is seen in Figure 3(a), indicating that the element

residual section forces and deformations are small at the end of the state determination process, and therefor the results are accurate. Included in Figure 3(a) are results based on using the explicit formulation without carrying forward residual unbalanced section deformations (identified as CO = No). Divergence from the correct solution is evident. Shown in Figure 3(b) is the energy increment *EI* at the end of the state determination of each time step . The quantity *EI* represents the energy caused by unbalanced loads and unbalanced deformations throughout the element. The results for the case where the residual unbalanced section deformations are carried forward has an *EI* that is five orders of magnitude smaller compared to the case when the residual unbalanced section deformations are not carried forward. It is desirable to have *EI* as small as possible, for it is associated with energy that has been injected into the system that should not exist and will cause the solution to diverge, as shown in Figure 3(a). Further details about the formulation are found in by Kolay and Ricles (2017).

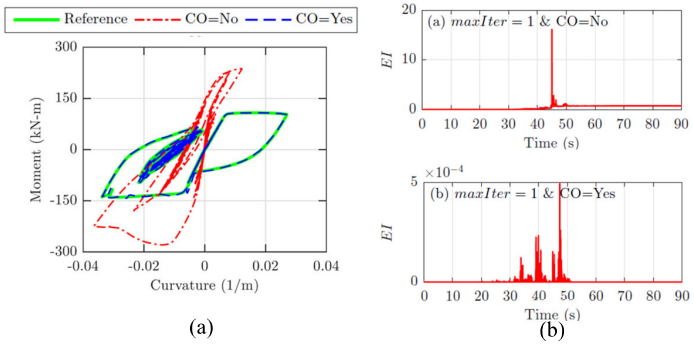

(a) (b)

Figure 3. (a) Section moment-curvature response at south end of roof beam from numerical simulations of an RC MRF with a fixed number of element iterations = 1, with and without carryover (CO); and, (b) associated energy increment (EI) at the end of each time step's element state determination.

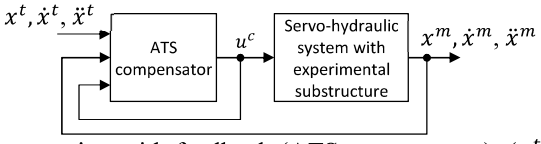

Figure 4. Actuator delay compensation with feedback (ATS compensator); $(x^t, \dot{x}^t, \ddot{x}^t)$: actuator target displacement, velocity, and acceleration; u^c : compensated actuator input displacement command, $(x^m, \dot{x}^m, \ddot{x}^m)$: actuator measured displacement, velocity, and acceleration.

Servo-hydraulic Actuator Control

The determination of the restoring forces $\boldsymbol{R}_{i+1}^e$ of the experimental substructure of a RTHS are obtained by subjecting targeted deformations x^t to the test setup associated with $\boldsymbol{X}_{i+1}$ and $\dot{\boldsymbol{X}}_{i+1}$ and then measuring the forces required to impose these deformations. These deformations need to be imposed accurately, with minimal amplitude error and delay between the measured deformations x^m and the targeted deformations x^t, otherwise the consequence is that the wrong $\boldsymbol{R}_{i+1}^e$ are measured and incorrect RTHS results are obtained. Hydraulic actuators are typically used in a RTHS to impose displacements to the experimental substructure. The inherent nonlinearity of an actuator as well as any nonlinear response of the experimental substructure can result in an amplitude-dependent behavior of the servo-hydraulic system, making it challenging to accurately control an actuator. Accurate actuator control is one of the critical issues to achieve a successful RTHS because it affects the accuracy and stability of the simulation. An adaptive delay compensation method was developed by the author and his colleagues (Chae et al. 2013). The method is based on the time series relationship of the input and output displacements of the combined servo-hydraulic and experimental substructure systems. The method is referred to as the adaptive time series (ATS) compensator. The ATS compensator updates the coefficients of the relationship between the actuator compensated target displacement command u^c and target deformations x^t, velocities $\dot{x}^t$, and accelerations $\ddot{x}^t$at each time step of a RTHS using regression analysis. The system identification procedure does not involve a user-defined adaptive gain, which is

one of the advantages the ATS compensator has over other adaptive compensation methods.

The procedure to minimize actuator delay and amplitude error that is presented in this paper is shown conceptually in Figure 4, where a compensated displacement command u^c is sent to the actuator to attempt to have x^m match x^t. A 2nd order system is presented herein for the calculation of the compensated input actuator displacement, whereby:

$$u_k^c = a_{0k}x_k^t + a_{1k}\dot{x}_k^t + a_{2k}\ddot{x}_k^t \tag{8}$$

In Equation (8) x_k^t, $\dot{x}_k^t$ and $\ddot{x}_k^t$ are the actuator target displacement, velocity and acceleration, respectively, at time step k. a_{0k}, a_{1k}, and a_{2k} are the adaptive coefficients at time step k, and are related to the compensated amplitude error A_k and time delay τ_k, where:

$$A_k \cong \frac{1}{a_{0k}}, \quad \tau_k \cong \frac{a_{1k}}{a_{0k}} \tag{9a,b}$$

The coefficients are determined by performing a regression analysis of an objective function associated with a 1-second window of data preceding the current time step k, where

$$\mathbf{A} = \left(\mathbf{X_m}^T\mathbf{X_m}\right)^{-1}\mathbf{X_m}^T\mathbf{U_c} \tag{10}$$

In Equation (10) $\mathbf{A}$, $\mathbf{X_m}$, and $\mathbf{U_c}$ are equal to the vectors of adaptive coefficients, measured motions (displacements, velocities, and accelerations) of the actuator, and the actuator compensated actuator signals from the preceding 1-second window of data, respectively (Chae et al. 2013.)

APPLICATION TO DEVELOPING SEISMIC RESILIENT STEEL BUILDINGS

Braced Frame Systems with Nonlinear Viscous Dampers

Dong et al. (2016) used RTHS to perform a large-scale experimental study of the seismic performance of a multistory steel frame building structure with nonlinear viscous dampers. The purpose of the study was to investigate the behavior of building systems with nonlinear viscous dampers when subjected to strong ground motions. Items of interests included the interaction of the dampers with the lateral load resisting system, the effectiveness of the dampers in reducing seismic structural damage, and whether the design base shear of the system can be reduced when the dampers are used to control drift. Load rate dependent nonlinear viscous dampers were used in the study, and therefore it was necessary to perform a hybrid simulation in real-time. The RTHS involved the complete building system. A test structure with a full base shear design strength (D100V) and test structures with reduced (75% and 60%) base shear design strengths (D75V and D60V) were studied using ensembles of ground motions with 14 and 19 records scaled to the DBE and MCE hazard level, respectively.

The prototype building is shown in Figures 5(a) and (b). Due to symmetry, and considering unidirectional ground motions, the test structure consisted of one MRF and one braced frame (DBF) with dampers, along with the gravity load system and seismic tributary mass of the MRF and DBF. The MRFs, gravity system, and mass were part of the analytical substructure and the remaining DBF modeled via the experimental substructure (Figure 5(c)). The RTHS used a time step Δt = 3/1024 seconds and ρ_∞ = 0.866.

The story drift ratio time histories from the DBE level RTHS using the 1999 Hector Mine HECTOR-11625090 record for the D100V, D75V, and D60V structures are shown in Figures 6(a)-(c). Negligible residual story drifts are seen at the end of the simulations, indicating that even the test structures with reduced strength designs exhibited a nearly elastic response under the DBE. Figures 6(d)-(f) show the story drift ratio time histories from the MCE level RTHS using the 1999 Chi-Chi earthquake TCU055-N record. The story drift ratio time histories for the D100V and D75V structures are almost zero at the end of the simulations, but residual story drifts are seen at the end of the simulation for the D60V structure. The second story has a slightly larger drift ratio than the first and third stories for each structure.

The mean of the residual drift ratios for the ground motion ensembles from the RTHS ranged from 0.0001 (3rd story, D100V) to 0.0006 (2nd story, D60V) for the DBE and 0.0006 (1st, 2nd, and 3rd stories, D100V) to 0.002 (1st, 2nd, and 3rd stories, D60V) for the MCE.

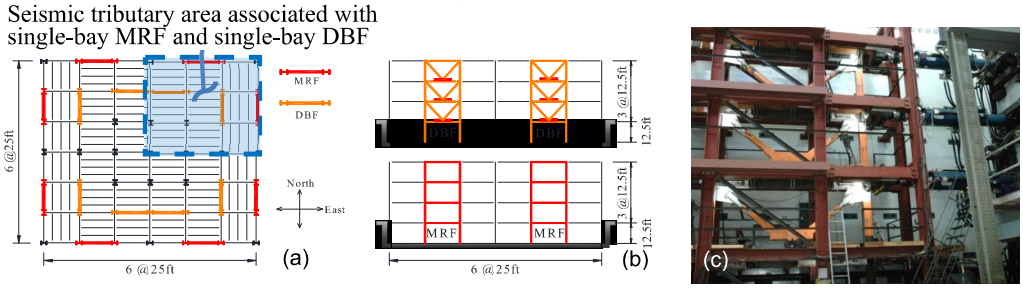

Figure 5. Prototype building (a) plan view, (b) section view, and (c) photograph of SC-MRF experimental substructure, (from Dong et al. 2016); note: 1 m = 3.28 ft.

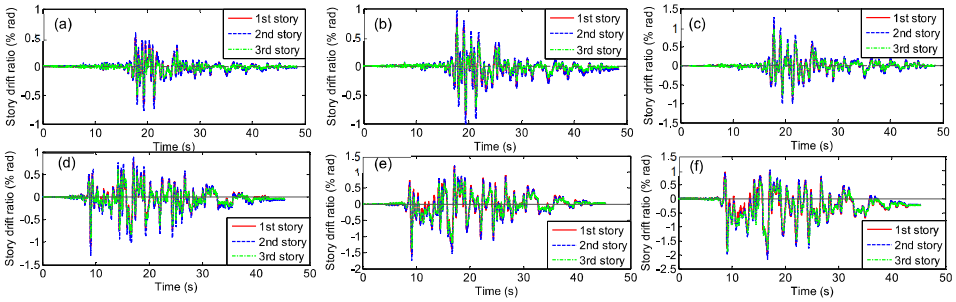

Figure 6. Story drift ratio time histories from DBE level RTHS using Hector Mine HECTOR-11625090 record: (a) D100V; (b) D75V; and (c) D60V; and MCE level RTHS using Chi-Chi TCU055-N record: (d) D100V; (e) D75V; and (f) D60V (from Dong et al. 2016).

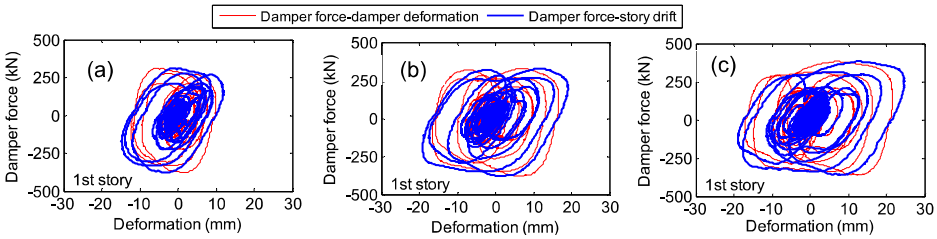

Figure 7. Damper force-deformation response from DBE level RTHS with HECTOR-11625090 record level: (a) D100V; (b) D75V; and (c) D60V, (after Dong et al. 2016).

The effects of elastic flexibility in the damper force path of the test structure (i.e., including the connections, braces, beams, and columns of the DBF), designed and constructed under practical conditions, were observed in the RTHS results as shown in Figure 7. The figure shows that the story drifts are larger than the damper deformations and the damper force–story drift hysteresis loops are inclined relative to the damper force–damper deformation hysteresis loops. This elastic flexibility is associated with the force path from the dampers to the seismic mass DOF, including the connections, braces, beams, and columns of the DBF. This elastic flexibility causes the viscous damper forces to be partially in phase with the story drifts (i.e., when the story drifts are at their peak values, the damper forces are large). This in-phase behavior of the damper forces with story drifts results in a combined axial force and bending moment response in the DBF columns with large axial forces at the times of peak bending moments. Such combinations of axial forces and bending moments should be considered in the design of the columns of frames with nonlinear viscous dampers. This in-phase damper force behavior also results in significant contributions of damper forces to the total story shear forces of the test structure at the times of peak story drifts, and as a result, this in-phase damper force behavior stiffened the test structures and reduced the story drift response.

SUMMARY AND CONCLUSIONS

This paper presented the concept of RTHS and developments achieved at the NHERI Lehigh Experimental Facility that have advanced RTHS to enable readily accurate large-scale, earthquake simulations to be performed. Advancements include the development of dissipative explicit direct integration algorithms that are unconditionally stable and well suited for RTHS with nonlinear geometric and material nonlinearities, an explicit force-based fiber element formulation that is ideal for the real-time state determination of nonlinear analytical substructures, and adaptive control to enable precise real-time control of servo-hydraulic actuators in test setups of a RTHS experimental substructure. The use of RTHS is shown to enable steel frame buildings to have their design base shear reduced further than existing current U.S. codes recommend, while still achieving satisfactory behavior. In addition, it was shown that there exists an in-phase behavior of the damper forces with the frame, which should be accounted for in the design of braced frames with dampers.

ACKNOWLEDGMENTS

The research and testing presented herein were performed at the Lehigh NHERI Experimental Facility, whose operation has been supported by grants from the National Science Foundation (NSF) under Cooperative Agreement No. CMS-0402490 and Cooperative Agreement No. CMMI-1520765. The research was supported by NSF under Award No. CMS-0936610 in the George E. Brown, Jr. Network for Earthquake Engineering Simulation Research (NEESR) program, and Award No. CMS-0402490 for the George E. Brown, Jr. Network for Earthquake Engineering Simulation (NEES) consortium operations. Support was also provided by the Pennsylvania Department of Community and Economic Development through the Pennsylvania Infrastructure Technology Alliance. The opinions expressed in this paper are those of the authors and do not necessarily reflect the views of the sponsors.

REFERENCES

Chae, Y., Kazemibidokhti, K., and J. Ricles, (2013). "Adaptive Time Series Compensator for Delay Compensation of Servo-Hydraulic Actuator Systems for Real-Time Hybrid Simulation," *Earthquake Engineering and Structural Dynamics*, **42**(11):1697–1715.

Dong, B., Sause, R., and J. Ricles (2015)."Accurate Real-Time Hybrid Earthquake Simulations on Large-Scale MDOF Steel Structure with Nonlinear Viscous Dampers." *Earthquake Engineering and Structural Dynamics*, **44**(12):2035–2055.

Dong, B., Sause, R., and J. Ricles (2016). "Seismic Response and Performance of Steel MRF Building with Nonlinear Viscous Dampers Under DBE and MCE," *Journal of Structural Engineering*, **142**(6).

Kolay, C., and J. Ricles (2014). "Development of a Family of Unconditionally Stable Explicit Direct Integration Algorithms with Controllable Numerical Energy Dissipation," *Earthquake Engineering and Structural Dynamics*, **43**(9):1361–1380.

Kolay, C., Ricles, J., Marullo, T., Mahvashmohammadi, A., and R. Sause, (2015). "Implementation and Application of the Unconditionally Stable Explicit Parametrically Dissipative KR-α Method for Real-Time Hybrid Simulation," *Earthquake Engineering and Structural Dynamics*, **44**(5):735-755.

Kolay, C., and J. Ricles (2016). "Assessment of Explicit and Semi-Explicit Classes of Model-Based Algorithms for Direct Integration in Structural Dynamics," *International Journal for Numerical Methods in Engineering*, **107**:49-73.

Kolay, C. and J. Ricles (2017). "Force-Based Frame Element Implementation for Real-Time Hybrid Simulation Using Explicit Direct Integration Algorithms." *Journal of Structural Engineering*. **144**(2).

Kolay, C. and J. Ricles (2019). "Improved Explicit Integration Algorithms for Structural Dynamic Analysis with Unconditional Stability and Controllable Numerical Dissipation." *Journal of Earthquake Engineering*; **23**(5):771-792.

Kolay, C., Al-Subaihawi, S., Marullo, T., Ricles, J. and S. Quiel, (2020). "Multi-hazard real-time hybrid simulation of a tall building with damped outriggers." *Intl Jrnl of Lifecycle Performance Engineering*, **4**(1/2/3):103–132.

OpenSees (2017). Pacific Earthquake Engineering Research Center, University of California, Berkeley, CA.

Day1 (Monday, Sep. 25th, 2023) 11:35~12:10

Recent Development of Local Buckling Requirements in AISC Seismic Provisions

Chia-Ming Uang

Professor, University of California, San Diego

Professor Uang's research is in the seismic design, rehabilitation, and testing of large-scale steel structures, including buildings and bridges. He studies seismic code design issues and actively participates in code committees to ensure that structures perform well and withstand forces during earthquakes. Uang has served in a variety of capacities in professional engineering societies. He is a member of the Committee on Specifications, Committee of Research, and Connection Prequalification Review Panel for the American Institute of Steel Construction (AISC). Uang received three research awards from American Society of Civil Engineers: Raymond C. Reese Research Prize in 2001 as well as Moisseiff Award in 2004 and 2014. AISC awarded him a Special Achievement Award in 2007 for his contributions in research and service to the steel industry. Uang is coauthor of two textbooks on structural analysis and structural steel design and three book chapters.

RECENT DEVELOPMENT OF LOCAL BUCKLING REQUIREMENTS IN AISC SEISMIC PROVISIONS

Chia-Ming Uang[1]
1. Distinguished Professor, Dept. of Structural Engineering, University of California, San Diego, CA, USA
Email: cuang@ucsd.edu

ABSTRACT

For seismic design of steel structures, designated structural members that are expected to dissipate energy through plastic hinging in the form of axial, flexural, or shear action need to be designed and detailed to provide ductile response by controlling, not eliminating, buckling. At the section level, building codes usually specify limiting width-thickness (b/t) limits such that excessive local buckling that leads to a significant degradation of strength can be avoided. In this paper, history of the development of local buckling limits in the AISC Seismic Provisions that lead to the latest (2022) edition is presented. Concerns that were raised from this code cycle and ongoing efforts to address these issues for the next (2027) edition are discussed.

Keywords: seismic design, steel structures, local buckling, AISC Seismic Provisions

INTRODUCTION

AISC 341 provides requirements based on the ductility and capacity design principles. For structural components designated to experience inelastic action, detailing requirements are specified. One important aspect is the control of local instability, which aims to delay, but not prevent, the onset of local buckling when these structural components are strained way beyond the yield strain. These requirements also aim to reduce the rate of strength degradation and the potential for fracture due to low-cycle fatigue.

Two types of limiting width-to-thickness ratios (b/t or h/t) are specified in AISC 341-22 (AISC 2022). For members that are expected to experience "significant" inelastic deformation, a Highly Ductile limit, λ_{hd}, is required. When only "limited" inelastic deformation is required, these members only need to meet the Moderately Ductile limit, λ_{md}. For examples, limiting values for two popular systems are provided below. For Special Moment Frames (SMF), significant flexural yielding is expected in the beam ends and the base of the columns. Therefore, sections of both beams and columns are to meet the highly ductile limits. But only moderately ductile limits are required for beams and columns of Intermediate Moment Frames (IMF). Similarly, diagonal braces in a Special Concentrically Braced Frame (SCBF) need to meet the Highly Ductile requirement, but braces in an Ordinary Concentrically Braced (OCBF) Frame only need to be Moderately Ductile.

In the following, several major changes made to AISC 341-22, concerns that were raised during this code cycle, and ongoing efforts to resolve these issues for the next (2027) edition are presented.

FORMAT OF WIDTH-TO-THICKNESS LIMITS

The width-to-thickness limits are a function of the yield stress of the steel materials. When the Seismic Provisions were first published in 1990, these limits were expressed in the form as follows:

$$\left(\frac{b}{t}\right)_{\text{limit}} = \frac{C_1}{\sqrt{F_y}} \tag{1}$$

where F_y is the specified minimum yield stress. This form was then re-written as the following by introducing the elastic Young's modulus, E, while the values of these limiting ratios remained unchanged:

$$\left(\frac{b}{t}\right)_{\text{limit}} = \frac{C_2}{\sqrt{F_y/E}} \quad (2)$$

The format was changed again in the 2016 edition such that the R_y factor, which represents the ratio between the expected yield stress and the specified minimum yield stress, F_y, was introduced while the values of these limits still remained practically unchanged from the previous editions:

$$\left(\frac{b}{t}\right)_{\text{limit}} = \frac{C_3}{\sqrt{(R_y F_y)/E}} \quad (3)$$

In doing so, a value of R_y needed to be assumed as a compromise. Taking λ_{hd} for flange local buckling of I-shaped beams and columns for example, the value of C_2 (= 0.30) was increased to 0.32 by assuming $R_y = 1.1$, which corresponded to that for A992 steel; this steel grade is commonly used for I-shaped members in the US. Next consider the HSS section for diagonal braces of SCBF. The value of C_2 was 0.55 in AISC 341-10. The correspond C_3 value in AISC 341-16 was increased to a larger extent to 0.65 because $R_y = 1.4$ was assumed to reflect the fact that A500 Gr. B steel was common for construction at the time. This would unnecessarily penalize other similar sections grouped in the same category as the HSS section, e.g., built-up box shapes with a steel grade having a lower R_y value (e.g., 1.1) when used as diagonal members in an SCBF.

In developing AISC 341-22, it was realized that researchers would traditionally use the measured yield stress in recommending width-to-thickness limits in the literature (Schafer et al. 2022). However, code committees would then adopt the recommendation by keeping the numerator C_1 (or C_2) while rename the actual yield stress as the specified minimum yield stress, i.e., in a form like Eq. (2), for the 2010 and previous editions of AISC 341. Realizing that F_y in Eq. (2) is already the actual yield stress as reported in the literature, the procedure that was used to convert Eq. (2) in the 2010 edition to the 2016 edition was incorrect. This was corrected in the 2022 edition, i.e., the format of Eq. (3) is used, but the coefficient C_2 used in the 2010 edition is retained.

With this decision, λ_{hd} for HSS diagonal braces would have been significantly impacted due to the high values of R_y for the commonly used steel grade of A500 for HSS members in the US. Citing insufficient test data to justify the proposed change, the code committee was then decided to retain the value of C_2 as C_3 for AISC 341-22 before further research is conducted. Led by researchers at the University of Washington, AISC is currently sponsoring research projects to address this issue for the next edition.

SPLIT OF LIMITING WIDTH-TO-THICKNESS RATIO TABLE

AISC 341 summarizes all the limiting width-to-thickness ratios in Table D1.1. As the number of cases covered in the table expanded over the past three decades and with an attempt to make the table concise, it at times was not only less user-friendly but also created issues. One notable problem is related to the HSS member design. Up to the 2016 edition, the limiting width-to-thickness ratios for HSS members are the same no matter whether these members are used as diagonal braces in an SCBF or beams and columns in an SMF. As a results, the same limiting ratios that were originally intended for SCBF diagonals also apply to SMF beams and columns. Partly motivated by this issue, Table D1.1 has been split into two sub-tables in AISC 341-22. Specifically, Table D1.1(a) is for "Compression Elements–Diagonal Braces" and Table D1.1(b) is for "Compression Elements–All Members Diagonal Braces."

With this split, it is possible to fine-tune the limiting ratios of HSS members for moment frames in parallel with the University of Washington's research on HSS braces. Since it is judged that the current limits would severely penalize the design and construction of SMF with HSS members, AISC is sponsoring a joint research project in the US in partnership with NCREE in Taiwan (led by Profs. C.C. Chou and T.U. Wu). In the US, eight jumbo HSS columns have been fabricated for testing at the University of California, San Diego, and finite element simulation is to be conducted at the University of Michigan (led by Prof. J. McCormick). One test was conducted so far. The specimen size was HSS 16×16×5/8 with a length of 18 ft. The b/t ratio was 24.5, which exceeded λ_{hd} (=11.6) by a very large

Figure 1. Cyclic response of an HSS 16×16×5/8 column

margin. Based on the preliminary test result shown in Figure 1, it is expected that the limiting width-to-thickness ratios will be relaxed in AISC 341-27.

AISC 341 has been specifying the same limiting width-to-thickness ratios for both the HSS and built-up box sections. Parallel to the HSS column study in the US, researchers at NCREE will focus on built-up columns, the type of columns widely used for building construction in Taiwan.

I-SHAPED COLUMNS

Aside from the two changes (b/t limiting format change and split of Table D1.1), the most significant change made to AISC 341-22 is the λ_{hd} and λ_{md} limits for the web of I-shaped columns. This change was based on a research project sponsored by National Institute of Standards and Technology (NIST). A total of 44 deep columns were tested at the University of California, San Diego to address the concerns of buckling because deep column sections tend to have a much higher h/t_w ratio and a smaller r_y. Testing showed that this type of columns is indeed vulnerable to interactive flange-web local buckling, sometimes combined with lateral-torsional buckling (Chansuk et al. 2021). The deformation capacity is also sensitive to the axial force level as shown in Figure 2. Based on results from both experimental testing finite element simulation, alternate λ_{hd} and λ_{md} limits developed by Ozkula et al. (2021) have been adopted in AISC 341-22. Figure 3 shows a comparison of the limiting ratios between the 2016 and 2022 editions of AISC 341.

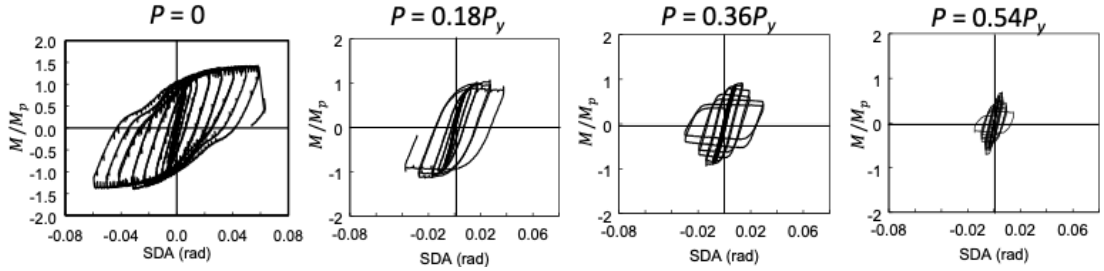

Figure 2. Effect of axial compression force level on cyclic response of W24×131 columns

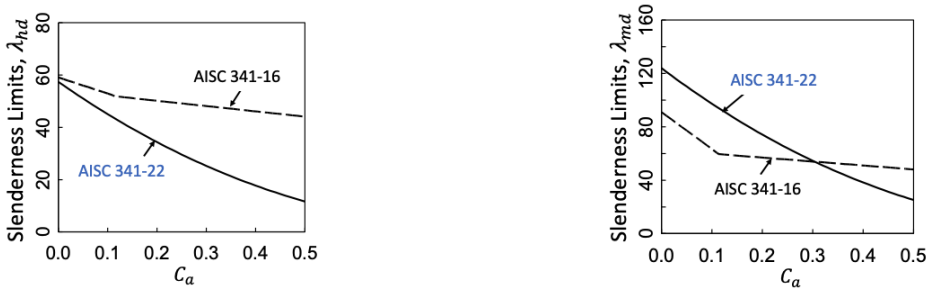

(a) Highly ductile limit (b) Moderately ductile limit

Figure 3. Comparison of I-shaped column web h/t_w limiting ratios

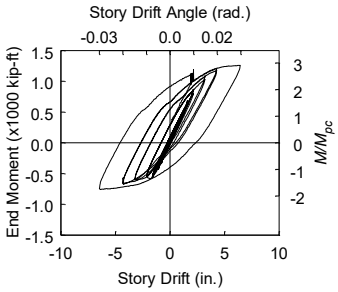

(a) Cyclic response

(b) Member end

(c) Weld fracture

Figure 4. Cyclic behavior of W14×132 column under alternating axial load

BRACED FRAME I-SHAPED COLUMNS

Applying the newly developed λ_{hd} and λ_{md} limits for braced frame columns is too conservative for two reasons. First of all, shallow sections (e.g., W12 and W14) with stocky web are usually used in braced frames. Secondly, these columns are subjected to cyclic axial load with alternating compression and tension due to overturning of the braced frame. Since these issues were not the main focus of the NIST research program, the code committee in developing AISC 341-22 decided to retain the same limits as in the 2016 edition but with the coefficients restored to the 2010 edition as explained previously.

To address braced frame column issues, AISC has initiated a research program with a goal to develop recommendations for AISC 341-27. Six shallow columns (W12 and W14) have been planned for testing at University of California, San Diego, with finite element simulation to be conducted at the University of Wisconsin, Platteville (led by Prof. G. Ozkula). Two columns under alternating axial load with cyclic drifts have been tested so far. Figure 4 shows the observed performance of a W14×132 column under alternating axial load, with the normalized axial load, $C_a(=\frac{P_u}{R_y P_y})$, ranging from 0.8 in compression and 0.2 in tension. Unlike those under constant axial compression in the NIST program, this column showed very little buckling, nor with strength degradation. Testing was ended due to overload and fracture of the CJP groove welds connecting the column to the end plates.

SUMMARY AND CONCLUSIONS

Local buckling control plays an important role for providing sufficient deformation capacity in seismic steel design. This paper provides a brief summary of important changes that have been made in the 2022 edition of AISC 341. Reasons for these changes, concerns that were raised, and ongoing AISC efforts to resolve these issues for the next (2017) edition of AISC 341 are presented.

ACKNOWLEDGMENTS

The author would like to acknowledge American Institute of Steel Construction, Steel Tube Institute, and Schuff Steel for sponsoring the steel column testing programs at UCSD. Professors G. Ozkula, G. Mosqueda, and C.S. Contreras assisted in the testing program.

REFERENCES

AISC. (2022). Seismic provisions for structural steel buildings, *ANSI/AISC 341-22*, American Institute of Steel Construction Chicago, IL.

Chansuk, P., G. Ozkula, C.-M. Uang, and J.L. Harris III (2021). "Seismic Behavior and Design of Deep, Slender Wide-Flange Structural Steel Beam-Columns," NIST Technical Note 2169, National Institute of Standards and Technology, Gaithersburg, MD.

Ozkula, G., C.-M. Uang, and J.L. Harris (2021). "Development of Enhanced Seismic Compactness Requirements for Webs in Wide-Flange Steel Columns," Journal of Structural Engineering, ASCE, **147**(7).

Schafer, B.W., L., Geschwindner, T., Sabol, C.-M. Uang. (2022). “Review of Local Buckling Width-to-Thickness Limits,” *Engineering Journal*, AISC, **59**(1), pp. 65-84.

Day1 (Monday, Sep. 25th, 2023) 13:30~14:05

Non-Ergodic Ground-Motion Models Based on a Combined Set of Empirical Ground-Motion Data, 3-D Simulations, and Macro-Seismic Intensity Data

Norman Abrahamson

Adjunct Professor,
Department of Civil and Environmental Engineering,
University of California, Berkeley, USA

Dr. Abrahamson is an internationally known expert in seismic hazard and risk analyses with 35 years of experience in the practical application of engineering seismology to the development of deterministic and probabilistic seismic criteria for engineering design and evaluations of seismic risk. He has been involved in developing or reviewing design ground motions for hundreds of projects around the world, including nuclear power plants, water dams, tailings dams, bridges, nuclear waste repositories, water and gas pipelines, rail lines, ports, airports, landfills, hospitals, electric substations, tunnels, and high-rise buildings.

Dr. Abrahamson received a PhD in geophysics from UC Berkeley in 1981. He has received a number of awards and honors: in 2001 he received the California Alumni Association Excellence in Achievement Award; in 2006, we was selected as the 2006 EERI/SSA Joyner Lecture; in 2009, he was selected as the EERI Distinguished Lecturer; in 2012, he received the SSA, EERI, and COSMOS Bruce Bolt Medal; in 2018, he was elected to the U.S. National Academy of Engineering; in 2019, he was elected as an Honorary Member of Structural Engineers Association of Northern California.

NON-ERGODIC GROUND-MOTION MODELS BASED ON A COMBINED SET OF EMPIRICAL GROUND-MOTION DATA, 3-D SIMULATIONS, AND MACRO-SEISMIC INTENSITY DATA

Norman Abrahamson[1] and Chih-Hsuan Sung[2]

1. Adjunct Professor, Department of Civil and Environmental Engineering, University of California, Berkeley, USA
2. Research Engineer, Department of Civil and Environmental Engineering, University of California, Berkeley, USA

Email: abrahamson@berkeley.edu, karensung@berkeley.edu

ABSTRACT

Three sources of data can be used to constrain non-ergodic path terms in California: recorded ground motions from seismic stations, simulated ground motions for 3-D crustal structure, and macroseismic intensity data. The three data types provide complementary information for the path effects: the recorded ground motions provide broadband constraints, but they have limited spatial coverage; the 3-D simulations provide dense spatial coverage, but the 3-D path effects are only constrained for long periods (T>1 sec); the intensity data also provides dense spatial coverage, but there can be large uncertainties in converting intensity data to ground motion values. The non-ergodic behavior is captured through the approach of Sung et al. (2023) which quantifies the anisotropic path effects due to the 3-D velocity structure using the varying coefficient model in an iterative process. There is a strong correlation between the path terms for observed ground motions at short periods and the path terms for intensity data, indicating that the non-ergodic path behavior from the intensity data can provide useful constraints for path terms for non-ergodic GMMs. 3-D simulations can be used to contain the median non-ergodic path effects for long-period ground motion, but the epistemic uncertainty in the path effects due to the uncertainty in the 3-D velocity structure has not been estimated.

Keywords: non-ergodic ground-motion models, path effects, intensity data, 3-D simulations

INTRODUCTION

Over the last decade, there has been a move from using global average ground-motion models (GMMs) in probabilistic seismic hazard (PSHA) to using non-ergodic GMMs that account for the systematic and repeatable effects for a specific source-path combination. The non-ergodic GMMs include source, path, and site terms. The development of non-ergodic path terms requires source/site-specific data. There are three types of data that can be used to constrain non-ergodic path effects: recorded ground-motions from seismic stations, simulated ground motions using 3-D velocity structures, and macroseismic intensity data. These data sets have strengths and weaknesses for constraining non-ergodic path terms.

The recorded ground motions provide constraints on the path terms for both low and high frequencies, but the spatial density of the recordings is limited. In some regions with dense seismic instrumentation, the seismic stations are a few km apart, but in many regions in the western US, the spacing between seismic stations is 10-50 km. The 3-D simulations can be computed at dense spatial sampling (REF), but they only constrain the path effects at low frequencies because the 3-D velocity model is only constrained at long wavelengths corresponding to periods greater than 1 sec. The intensity data is available at dense spatial sampling, but there is the issue of the uncertainty in the relation between intensity and ground motion. The correlation of the path effects for intensity is best correlated with the path effects for short-period ground motion.

In this paper, we summarize how recorded ground motions and 3- D simulations have been used in previous studies to develop non-ergodic GMMs and show that the intensity data provides useful information for constraining non-ergodic path effects for short-period ground motions despite the large uncertainties associated with intensity data and ground motions.

NON-ERGODIC GMMS

Most current non-ergodic GMMs are developed using recorded ground motions. For example, Lavrentiadis, G. and N. Abrahamson (2023) developed a non-ergodic GMM for California sites, source, and path effects using only recorded ground motions. In regions with sparse data, the epistemic uncertainty in the non-ergodic terms becomes large. To reduce the uncertainty of the non-ergodic terms, additional spatial sampling of the paths is needed. This can be from additional ground-motion data from small-magnitude earthquakes or from simulated ground motions from 3-D velocity structures.

Non-ergodic GMMs are beginning to be developed using 3-D simulations. For example, Sung and Abrahamson (2022) developed a non-ergodic GMM for Cascadia using 3-D simulations for M9 earthquakes. With 3-D simulations for a single scenario, the path and site effects are not separable, so the non-ergodic term is the combined path and site effect. If the set of 3-D simulations includes multiple scenarios at different locations, then the path effects can be separated from the site effects. Sung et al. (2023) developed a methodology to use the large set of CyberShake simulations with multiple scenarios that sampled a wide range of ray paths to incorporate the non-ergodic path effects of the 3-D velocity structure into a reference ergodic GMM for long spectral periods.

Intensity data provides dense spatial sampling of path effects, but these data have not yet been used to develop non-ergodic GMMs. One approach is to convert the intensity data into ground-motion estimates using ground-motion-intensity conversion equations (GMICE) such as Worden et al. (2012). Gallahue and Abrahamson (2023) found that there can be a large bias in the estimated ground motion (PGA or PGV) if standard GMICE are used. To address this bias, new GMICE need to be developed.

As an alternative to using GMICE to convert intensity data to ground-motion data, the residuals of intensity-prediction equations (IPE) can be computed and correlated with the residuals of a GMM. This avoids the bias in the ground motions from using the GMICE. We used the Atkinson et al. (2014) IPE to estimate the intensity residuals. These residuals are then used with the non-ergodic methodology described in the following section to evaluate the correlation of path effects from intensity data and the path effects from PGA.

METHODOLOGY

The non-ergodic path effects are estimated using the approach of Sung et al. (2023) which quantifies the anisotropic path effects due to the 3-D velocity structure using the varying coefficient model in an iterative process. The within-event residuals are computed for each data set. The within-site residuals are computed by first removing the non-ergodic site term from the within-even residual. Using the within-site residuals, the path terms are estimated for one site at a time with the spatial correlation based on the separation distance between earthquakes. Next, the model results of step 1 are used to estimate the median and epistemic uncertainty of the non-ergodic path terms for a specific source location for all site locations. This leads to a model that can be applied to any source location and any site location. This methodology is applied to the recorded ground-motion data, the 3-D simulations, and the intensity data.

As an example of non-ergodic terms based on 3-D simulations, the non-ergodic path terms for the spectral acceleration at T=3 sec for a site in the Los Angeles region is shown in Figure 1. For this site, the path terms can lead to an increase of about a factor of 7 (0.7 LN units) or a decrease of about a factor of 1.5 (0.4 LN units). The change in the distance scaling in three directions is shown in the lower frame of Figure 1.

CORRELATION OF PATH TERMS

The non-ergodic path terms from the intensity data are compared to the non-ergodic path terms from the recorded ground motions. The spatial sampling of the two data sets for an M5.4 event is shown in Figure 2. The intensity data has a much denser spatial sampling than the ground-motion data. The maps of the path terms for this event show similar overall spatial patterns between the intensity path effects and the ln(PGA) path effects. Because the intensity data has much denser spatial sampling, the epistemic uncertainty in the path terms is much smaller for the intensity data than for the ground-motion data as shown in the right-hand frame of Figure 2.

The correlations of the path terms are shown in Figure 3 for different azimuth bins. For this earthquake, the correlation coefficients are about 0.8 for three azimuths and lower for the other three azimuths. For the 0-60 azimuth, the correlation coefficient is low (0.08). Overall, there is a significant correlation between the path effects for intensity data and PGA. We also evaluated the correlation of the path terms for spectral acceleration at T=3 sec with the intensity path terms. The correlation is much lower for the long-period ground motion, indicating that the intensity data will be most useful for constraining the short-period path effects.

CONCLUSIONS

To constrain non-ergodic path effects, all sources of data should be used including recorded ground motions, 3-D simulations, and macroseismic intensity data. Although the relation between intensity and ground motion has a large uncertainty, the dense spatial sampling of the intensity data makes it a valuable data set for constraining non-ergodic path effects at short spectral periods. The dense spatial sampling of simulated ground motions based on 3-D velocity models provides constraints on the non-ergodic path effects at long spectral periods. Results from 3-D simulations and compiled intensity data are key data sets for estimating non-ergodic path terms in regions with limited seismic station coverage.

ACKNOWLEDGMENTS

The DYFI intensity data set was compiled by Mike Hearns and Eric Thompson at the U.S. Geological Survey.

REFERENCES

Atkinson, G. M., C. B. Worden, and D. J. Wald (2014). "Intensity prediction equations for North America, *Bulletin of the Seismological Society of America* **104(6)**, 3084-3093.

Gallahue, M. and N. Abrahamson (2023). “New Methodology for Unbiased Ground-Motion Intensity Conversion Equations (GMICE)", *Bulletin of the Seismological Society of America*, **113(3)**, 1133-1151.

Lavrentiadis, G. and N. Abrahamson (2023). “A non-ergodic spectral acceleration ground motion model for California developed with random vibration theory", April 2023**,** *Bulletin of Earthquake Engineering*, online edition.

Sung, C-H., and N. Abrahamson (2022). “A partially nonergodic ground-motion model for Cascadia interface earthquakes", *Bulletin of the Seismological Society of America*, **112(5)**, 2520-2541.

Sung, C-H., N. Abrahamson, and M. Lacour (2023). "A Methodology for Including Path Effects Due to 3-D Velocity Structure in Non-Ergodic Ground-Motion Models", *Bulletin of the Seismological Society of America*, June 2023, online

Worden, C., M. Gerstenberger, D. Rhoades, and D. Wald (2012). Probabilistic relationships between ground-motion parameters and modified Mercalli intensity in California, *Bulletin of the Seismological Society of America*, **102(1)**, 204-221.

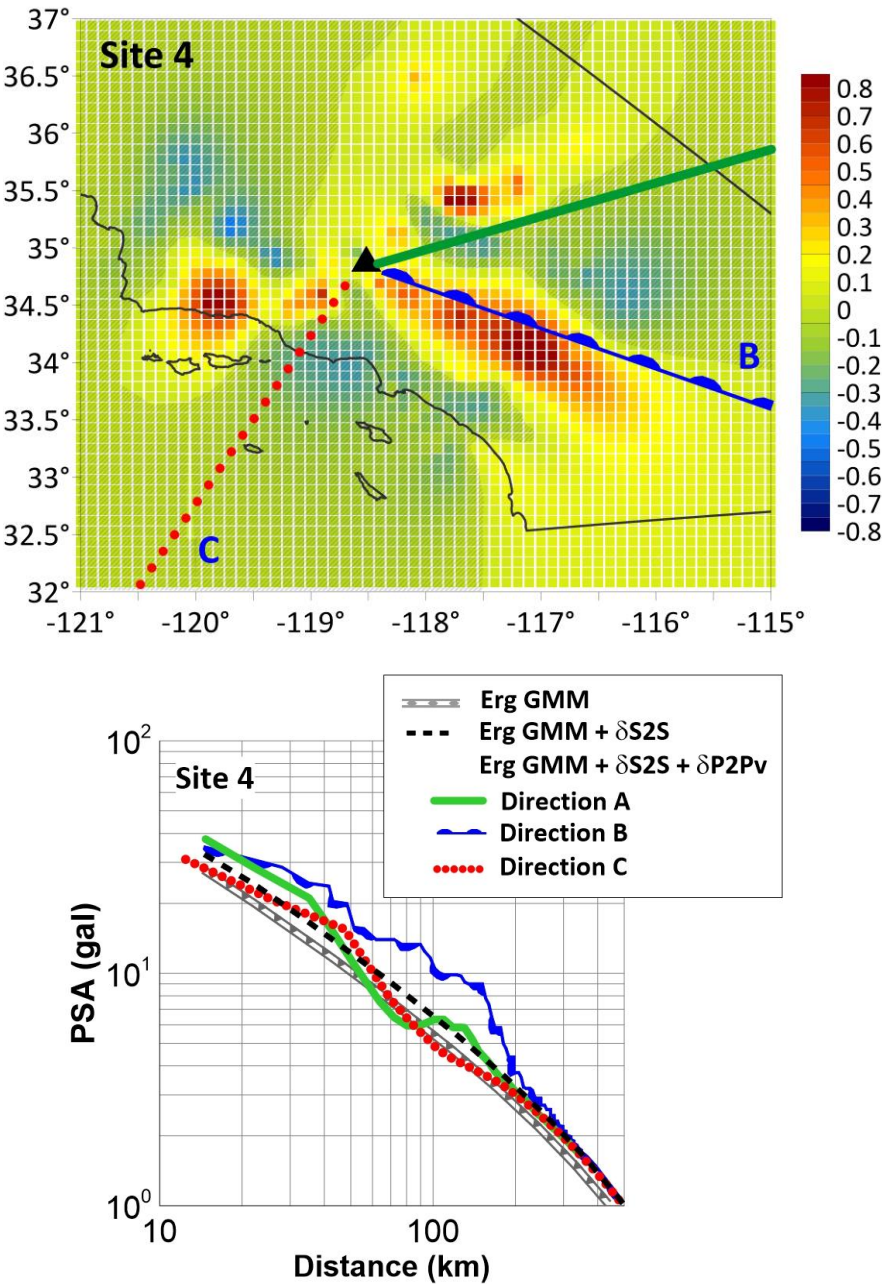

Figure 1. Example of non-ergodic path effects for T=3 sec using 3-D simulations. The site location is shown by the triangle. The mapped values are for different source locations. The color scale is in natural units. The distance scaling along three directions is shown in the lower frame. (From Sung et al., 2023).

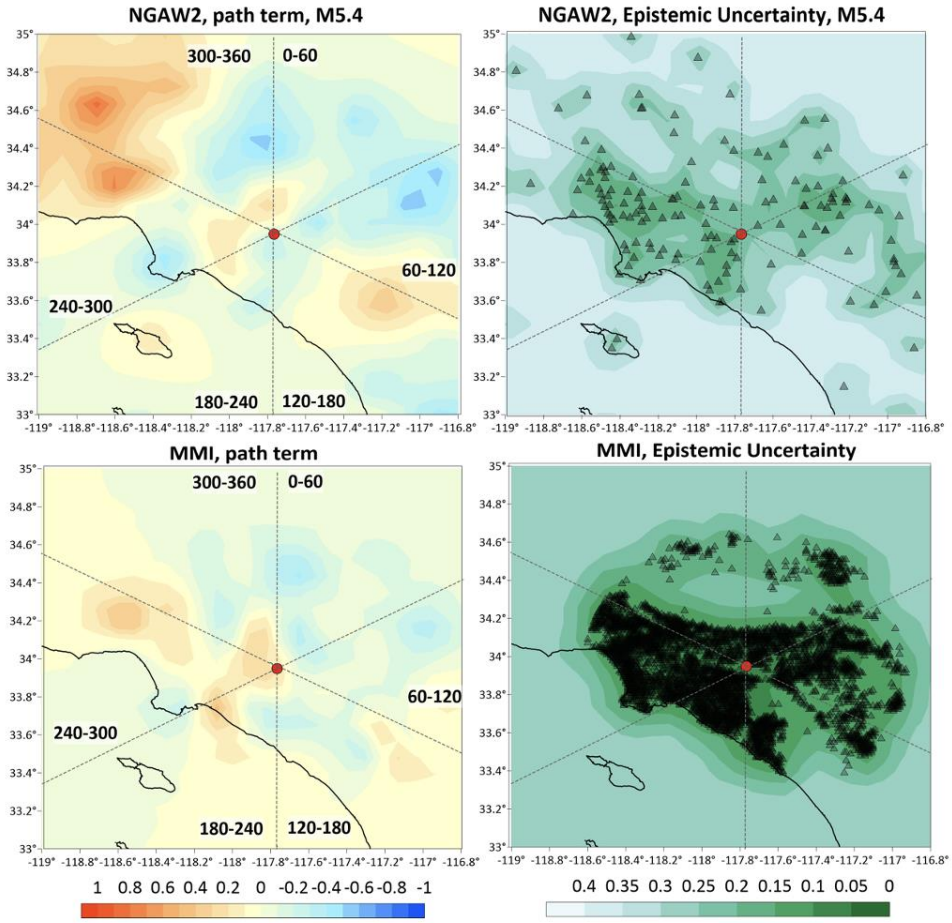

Figure 2. Example of non-ergodic path effects for ln(PGA) using recorded ground motion data in the NGA-W2 data set and for MMI using the Did-you-feel-it intensity data (MMI). The triangles on the left-hand frames show the locations of the seismic stations (top) and the intensity observations (bottom). The color scale is in natural log units.

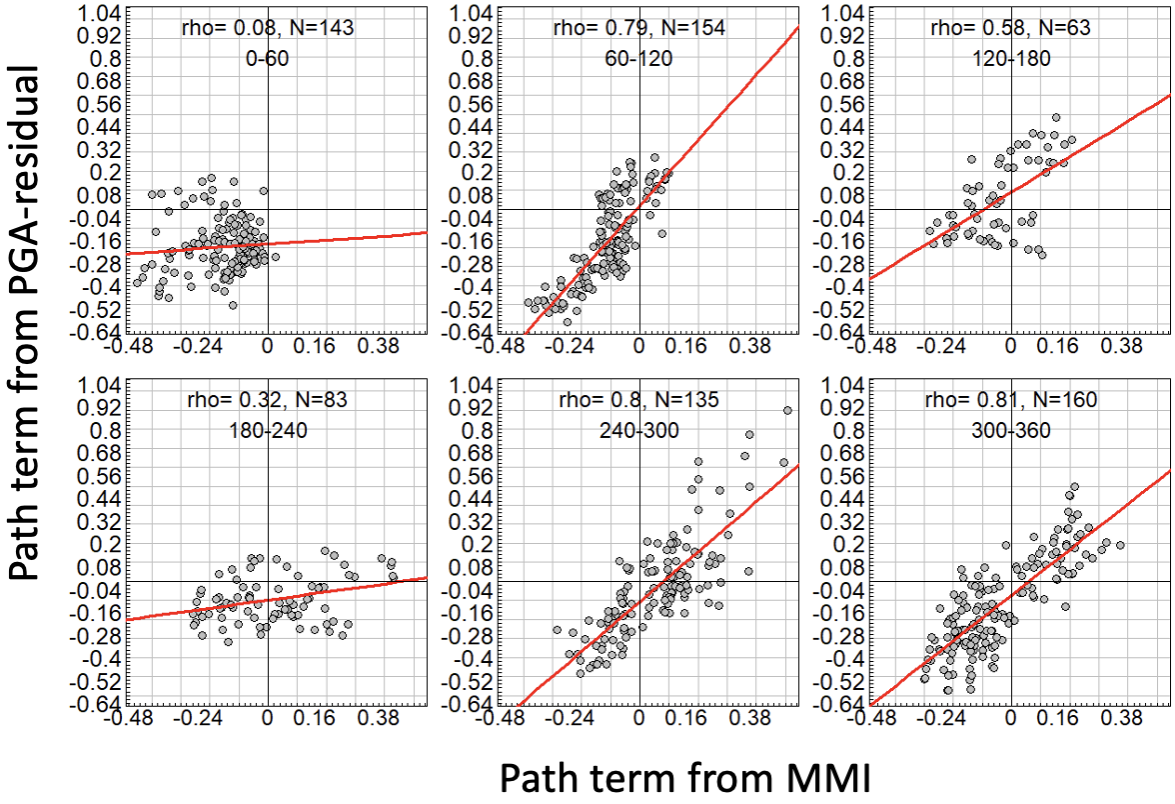

Figure 3. Example of the correlation of the path terms for ln(PGA) from the recorded ground motions and the path terms from the intensity data. The individual plots are for the azimuth bins shown in Figure 2.

Day1 (Monday, Sep. 25th, 2023) 14:05~14:40

Principal Surface Displacement of Strike-Slip Earthquakes

Brian Chiou

Senior Seismologist,
California Department of Transportation,
Sacramento, California, USA

Brian Chiou, PhD, is a Senior Seismologist in the California Department of Transportation, USA. He is a recognized expert in ground motion and seismic hazard. He was one of the ground motion prediction equation (GMPE) developers in 2008 NGA project and 2014 NGA-West2 project. Dr. Chiou has extensive experience with the SSHAC studies having been a Resource Expert for 2008-2011 BC Hydro and 2011-2013 Blue Castle SSHAC Level 3 GMC studies, and he has also served as a PPRP member for 2012-2014 Hanford and the 2011-2015 SWUS SSHAC Level 3 GMC studies, and a GMC TI for 2015-2018 Taiwan SSHAC Level 3 SSC and GMC studies.

PRINCIPAL SURFACE DISPLACEMENT OF STRIKE-SLIP EARTHQUAKES

Brian Chiou[1]
1. Senior Seismologist, California Department of Transportation, Sacramento, California, USA
Email: bc59bc@gmail.com

ABSTRACT

This paper summarizes a recently developed probabilistic distribution model for surface principal fault displacement at a location on the main rupture trace of a strike-slip earthquake in the magnitude range of $6 \leq \mathbf{M} \leq 8.3$. The model is the result of a collaborated study by a team of researchers from the California Geological Survey, Caltech, USGS, and California Department of Transportation to update the previously published model of Petersen et al. The update uses a vetted dataset of observed rupture data compiled by the Probabilistic Fault Displacement Hazard Initiative project, as well as several revisions to the formulation of Petersen et al., including the adoption of a left-skew non-normal probabilistic distribution. These revisions not only significantly improve the fit to the histogram of observed displacements but also predict more reasonable upper quantiles of displacement for large-magnitude ruptures.

Keywords: probabilistic fault displacement hazard analysis, surface rupture, principal surface displacement, strike-slip earthquake

INTRODUCTION

Coseismic surface displacement poses a geological hazard to structures and lifelines that cross active faults. Probabilistic fault displacement hazard analysis (PFDHA) (Youngs et al., 2003; Petersen et al. 2011) is a quantitative method to evaluate the displacement hazard for use in engineering design to mitigate the displacement hazard. PFDHA relies on the principal fault displacement model (FDM) to assess the probability of future principal displacement exceeding a specified test value, given there is coseismic surface rupture at the site location on or near the main fault trace. Prior to 2021, only a few published FDMs were available for use in PFDHA: Youngs et al. (2003) for normal faults, Petersen et al. (2011) for strike-slip faults, and Moss and Ross (2011) for reverse faults. The Fault Displacement Hazard Initiative (FDHI) (Borzognia et al., 2021) is a multi-year multi-agency research project to advance the state of practice by increasing the quality and quantity of the empirical rupture data and updating existing, or developing new, FDMs. The Chiou et al. (2023) FDM summarized in this paper is one of the FDMs resulting from the FDHI project. The Chiou et al. (2003) FDM is an effort to update Petersen et al. (2011) to the rupture data compiled and vetted by the FDHI project (Sarmiento et al., 2021). In addition to the data update, formulations of the Petersen et al. model are substantially revised to achieve improved fits to the histogram of observed displacements and to provide reasonable predictions of high percentiles of the predicted displacement distributions for large earthquakes. Model development and displacement predictions from the updated FDM are summarized below; details can be found in Chiou et al. (2023).

SURFACE DISPLACEMENT DATABASE

The FDHI database is the data resource used by Chiou et al. (2023), who also made two improvements to the data preparation processes. First, an objective and automated method was developed to help define the main rupture trace (Thomas et al., 2003). The resulting main trace was then used to define an earthquake-specific coordinate system in which the along-strike and the cross-strike distances of a data point or a site location are computed. The second improvement is the aggregation of net principal displacements measured along overlapped principal rupture traces. A total of 3,334 aggregated net

principal displacements from 29 strike-slip earthquakes in the $6 \leq \mathbf{M} \leq 7.9$ range were selected and used in Chiou et al. (2023, Chapter 2).

PROBABILISTIC DISTRIBUTION MODEL

Probability Distribution of *ln(D)*

It has been known that the Gaussian distribution does not appropriately match the distribution of the natural logarithm of observed principal displacement $ln(D)$. This is also the case for the selected FDHI displacement data, as shown in Figure 1.

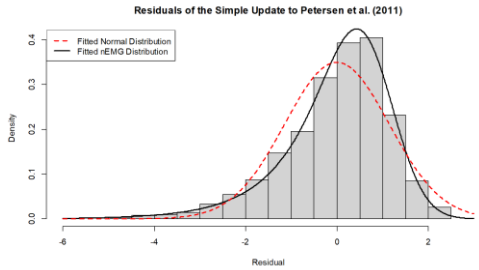

Figure 1. Histogram of the residuals of an interim simple update to Petersen et al. (2011). This update is a repeat of the regression analysis of Petersen et al. using the selected FDHI data. The model formulation, including the normality assumption for $ln(D)$, was unchanged. See Chiou et al. (2023, Section 3.2.1) for details.

To improve the distributional fit, Chiou et al. (2023) modeled $ln(D)$ as a Gaussian variate ($G \sim N(\mu, \sigma)$) minus an exponential variate ($E \sim EXP(\nu)$), G and E being independent,

$$ln(D) = Y = G - E \quad (1)$$

The Gaussian component G is analogous to the Gaussian variate used in Petersen et al. (2011). In a complex surface rupture, fault displacements near the endpoints of two or more adjacent interacting rupture segments are tapered toward the endpoints (Scholz and Lawler, 2004; Martel and Shacat, 2006). The E component in Eq. (1) models the tapering effects marginalized along the surface ruptures and over all earthquakes. Probabilistically, the subtrahend E modifies the symmetric Gaussian distribution to a left-skew distribution, matching the shape of the residual distribution shown in Fig. 1.

Chiou et al. (2023) called the distribution of $(G - E)$ the negative Exponentially Modified Gaussian distribution, or nEMG distribution for short. This distribution is characterized by the distribution parameters of the two stochastic components. The probability density function (PDF) and the cumulative distribution function (CDF) of the nEMG distribution are described in Chiou et al. (2023, Appendix C). The basic statistical measures of the nEMG distribution are as follows: mean = $\mu - \nu$; variance = $\sigma^2 + \nu^2 = \nu^2 [1 + \frac{\sigma^2}{\nu^2}]$; skewness = $-2\left[1 + \frac{\sigma^2}{\nu^2}\right]^{-1.5}$; excess kurtosis = $6\left[1 + \frac{\sigma^2}{\nu^2}\right]^{-2}$. Parameter μ affects only the mean, and ν affects all four measures. The skewness of the nEMG distribution is always negative and approaches 0 as ν decreases to 0.

Distribution Parameter Models

As in Petersen et al. (2011), the μ parameter of the $ln(D)$ distribution is modeled as a function of two predictors: the earthquake moment magnitude (**M**) and the along-strike position l normalized by the length of the main rupture trace L, $l2L = l/L$. The $l2L$ variable is folded at the midpoint of the main rupture trace to yield $l2L_f$ ($0 \leq l2L_f \leq 0.5$), which is then used in the modeling of the along-strike variation of σ. The ν parameter is modeled as a constant.

$$\mu_{ij}(\mathbf{M}_i,\ x^*_{ij}) = (c_0 + \delta_{eq,i}) + m_2(\mathbf{M}_i - m_3) + \frac{m_2 - m_1}{c_n} ln\left(\frac{1 + e^{-c_n\,(\mathbf{M}_i - m_3)}}{2}\right) + c_1\,(x^*_{ij} - 1) \quad (2)$$

$$x^*_{ij} = \sqrt{1 - \frac{(\,l2L_{ij} - 0.5)^2}{0.5^2}}$$

$$\sigma_{ij}(l2L_{f,ij}) = c_{v3}\ e^{c_{v4}\,\cdot\,max(l2L_{f,ij} - c_{cap},\ 0)} \quad (3)$$

$$v_{ij} = c_{v5} \quad (4)$$

, where index j refers to a displacement measurement in earthquake i. The above equations incorporate several upgrades to the formulation of Petersen et al. (2011): (1). Random earthquake effect δ_{eq} on the intercept c_0 of the μ parameter; $\delta_{eq} \sim N(0, \sigma^2_{eq}(\mathbf{M}))$ and $\sigma_{eq}(\mathbf{M}) = max\left(c_{v1}\ e^{c_{v2}\,\cdot\,max(\mathbf{M} - 6.1,0)}, 0.4\right)$, where σ_{eq} is capped by the value at $\mathbf{M} = 6.1$ and floored by 0.4; (2). Bi-linear scaling of the μ parameter with $\mathbf{M}$; the scaling rate transitions from m_1 to m_2 over a magnitude interval centered at $\mathbf{M} = m_3$; (3). Exponential decrease of the σ parameter with $l2L_f$; σ is capped by the value at $l2L_f = c_{cap}$ and symmetrical with respect to the midpoint of the main trace. (4). A constant v for the interior tapering effects marginalized over $l2L$ and over earthquakes.

Note that the $l2L_f$-dependence described in Eqs. 3 and 4 differ from those of Chiou et al. (2023, Eq. 3.14), where σ was modeled as a constant and v as a function of $l2L_f$. The reformulated models for σ and v, which were prompted and guided by a residuals analysis carried out after the publication of Chiou et al. (2023), supersede those of Chiou et al. (2023).

REGRESSION METHOD AND RESULTS

Estimation of the coefficients in Eqs. 2, 3, and 4 was carried out using the maximum-likelihood method provided in the R package GAMLSS (Generalized Additive Model for Location, Scale, and Shape) (Rigby et al., 2020). With coefficients c_n and m_3 being unknown, the μ model is a nonlinear mixed-effect model, which currently is not supported by GAMLSS. Therefore, for GAMLSS regression, the μ model was transformed into a linear mixed-effect model by fixing c_n and m_3 to 10 and 7.1, respectively. These two values were estimated prior to the main GAMLSS regression; the readers are referred to Chiou et al. (2023, Section 3.5) for details.

Table 1. Coefficients of nEMG Distributional Models, Conditional on Different Credible m_3

	μ					σ_{eq}		σ		v
	c_0	m_1	m_2	m_3	c_1	c_{v1}	c_{v2}	c_{v3}	c_{v4}	c_{v5}
Model8.1.nEMG	1.82276	3.23194	0.02095	7.32	2.01712	1.12867	-0.73794	0.53060	-3.88918	0.86967
Model7.nEMG	**1.33243**	**4.29242**	**0.80255**	**7.10**	**2.01751**	**1.12289**	**-0.77770**	**0.53041**	**-3.88867**	**0.86963**
Model8.2.nEMG	0.45201	4.02509	1.55817	6.75	2.01730	1.14635	-0.74292	0.52837	-3.90045	0.86969
Model8.3.nEMG	-0.56569	5.18541	1.98653	6.40	2.01927	1.11697	-0.61806	0.53081	-3.89073	0.86951

Note:
$c_n = 10$; m_3 is fixed to the value given in the table; $c_{cap} = 0.12246$

The coefficient estimates conditioned on $m_3 = 7.1$ are listed in Table 1 (*Model7.nEMG*), along with three other sets conditioned on three different m_3 values selected to represent the assessed credible range of m_3 (Chiou et al., 2023, Section 3.5). The assessed range is centered at $m_3 = 7.1$, bounded above by

m_3 = 7.32 and below by m_3 = 6.4. A m_3 value larger than 7.32 was considered untenable because the corresponding m_2 estimate would have been negative. The c_{v2} estimate (the rate of decrease of σ_{eq} with **M**) conditioned on m_3 = 6.4 differs substantially from the other three estimates, due to the large m_2 over-predicting the event terms $\delta_{eq,i}$ at the high end of **M** range. Therefore, $m_3 < 6.4$ was also considered untenable. The sets of coefficients in Table 1 are intended to be used in a PFDHA to represent the epistemic uncertainty of the probabilistic distribution for $ln(D)$ due to the estimation uncertainty of the **M**-scaling relation in the μ model.

RESIDUALS

The goodness-of-fit by the fitted FDM is examined using the normalized quantile residuals (Stasinopoulos et al., 2017), defined as $\hat{r}_{ij} = \Phi^{-1}[\mathrm{F}(ln(D_{ij}) \mid \widehat{\mu_{ij}}, \widehat{\sigma_{ij}}, \widehat{\nu_{ij}})]$, where $(\widehat{\mu_{ij}}, \widehat{\sigma_{ij}}, \widehat{\nu_{ij}})$ are the estimated distribution parameters for observation j in earthquake i; $\mathrm{F}(ln(D_{ij}) \mid \widehat{\mu_{ij}}, \widehat{\sigma_{ij}}, \widehat{\nu_{ij}})$ is the CDF of $ln(D_{ij})$ given $(\widehat{\mu_{ij}}, \widehat{\sigma_{ij}}, \widehat{\nu_{ij}})$; and $\Phi^{-1}[.]$ is the inverse CDF of the standard normal distribution. If the estimated distributional model is correct, $\hat{r}_{ij}$ will follow the standard normal distribution, aside from sampling variability. The histogram, the empirical CDF, and the Q-Q plot (Fig. 2) all indicate that $\hat{r}_{ij}$ of the fitted FDM follows closely the standard normal distribution. Based on Fig. 2, it is concluded that the assumed nEMG distribution is appropriate and the fitted FDM provides good (distributional) fits to the displacement data.

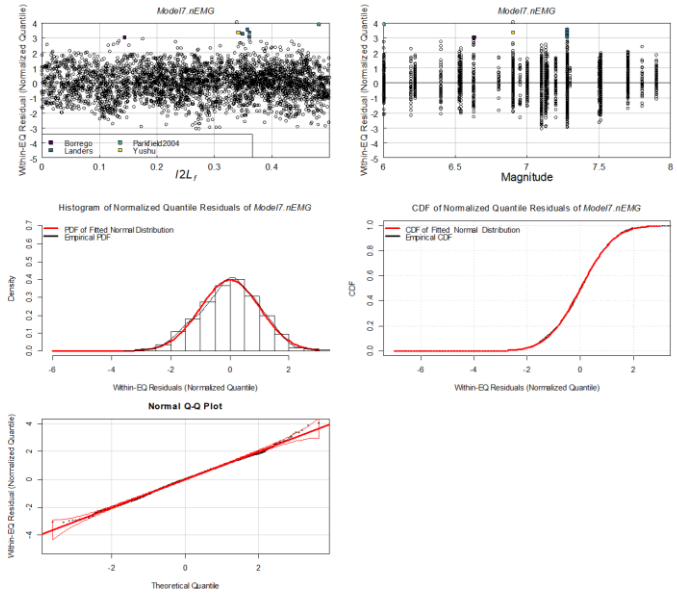

Figure 2. Diagnostic plots of normalized quantile residuals of the fitted FDM.

PREDICTIONS

The $ln(D)$ distribution predicted by any of the FDMs in Table 1 is conditioned on random earthquake effect $\delta_{eq} \sim N(0, \sigma_{eq}^2)$. The compound (unconditioned) distribution, obtained by marginalizing out δ_{eq}, is again a nEMG distribution with the same μ and ν but an increased $\sigma' = \sqrt{\sigma^2 + \sigma_{eq}^2}$. Examples of the PDF of the compound distribution are shown in Fig. 3 for several locations along a **M** 7.9 rupture trace. To further highlight the differences between the updated FDM and Petersen et al. (2011), the 5th, 50th, and 95th percentiles predicted by the two FDMs are compared in Fig. 4 as a function of **M** for $l2L$ = 0, 0.2, and 0.5. Away from the rupture edge ($l2L > 0$) and for **M** > 7.2, the 95th percentiles from the updated FDM are substantially lower than those from Petersen et al. (2011). For $l2L$ = 0.5 and **M** = 8, the predicted 95th percentile from the updated FDM is about 15 m, much smaller than the 40 m from Petersen et al. (2011). For reference, the maximum displacement of strike-slip earthquakes in the FDHI database is 13.6 m, from the **M** 7.7 Balochistan earthquake. Rodgers and Little (2006) reported a dextral slip of

18.7 m in the rupture of the 1855 New Zealand earthquake (whose magnitude is thought to be greater than 8.1) on the Wairarapa fault. Lastly, dynamic rupture modeling by Wang and Goulet (2022) yields a maximum displacement in the range of 10 to 20 m for scenarios of **M** 8 to **M** 8.2. Based on the above, it is judged that the updated FDM predicts a more reasonable 95th percentile for large magnitude than Petersen et al. (2011) does.

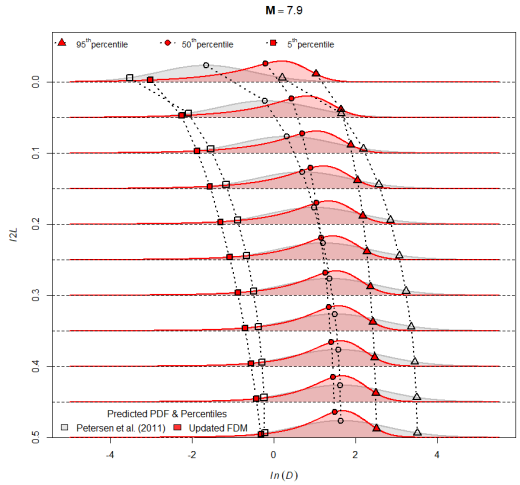

Figure 3. Probability distribution functions of $ln(D)$ predicted by the updated FDM (red curves) and Petersen et al. (2011) (gray curves) for locations along the surface rupture of an **M** 7.9 event.

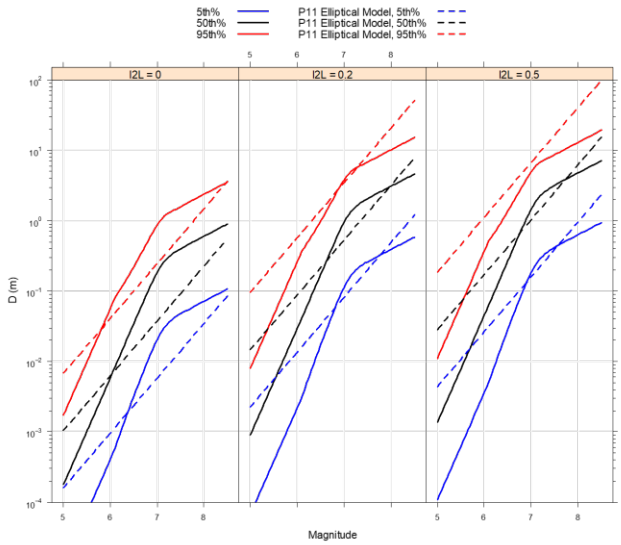

Figure 4. Predicted percentiles versus earthquake magnitude. (Left) At rupture's edge ($l2L$=0). (Middle) At $l2L$ = 0.2. (Right) At the center of the main trace ($l2L$ = 0.5).

CONCLUSIONS

The adopted nEMG distribution and the fitted FDM provide good (distributional) fits to the selected FDHI displacement data. In addition, the 95th percentile displacement predicted by the updated FDM is judged to be more reasonable than that predicted by Petersen et al. (2011) for large magnitudes. The applicable magnitude range of the updated FDM is assessed to be in the range of 6 ≤ **M** ≤ 8.3, despite the fact that the regression dataset is limited to **M** ≤ 7.9. Increasing the upper bound from **M** 7.9 to **M** 8.3 is justified by the ability of the estimated bi-linear **M** scaling relation to track the average surface displacements of **M** > 7.9 earthquakes collected in three other studies (Fig. 5).

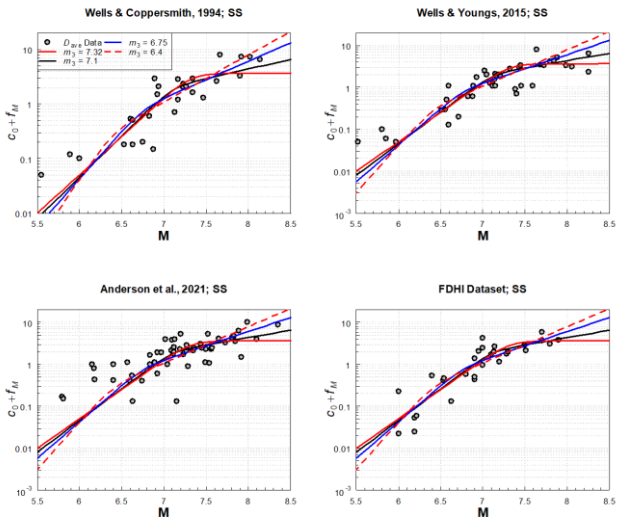

Figure 5. The **M**-scaling relations of the updated FDM and its three epistemic variants, shifted down by a factor of 2.147. For comparison, average surface displacement data collected in four studies are plotted as solid gray symbols in separate panels

REFERENCES

Anderson J. G., Biasi G. P., Angster S., Wesnousky S. G. (2021). "Improved scaling relationships for seismic moment and average slip of strike-slip earthquakes incorporating fault-slip rate, fault width, and stress drop," *Bull. Seism. Soc. Am.,* **111**(5), 2379–2392.

Bozorgnia Y., Abrahamson N., Arcos B., Baize S., Boncio P., Chao S.-H., Chen R., Chiou B., Dawson T., Donahue J., Goulet C., Hanson K., Kottke A., Kuehn N., Kuo C.-H., Lavrentiadis G., Madugo D., Mazzoni S., Milliner C., Moss R., Nurminen F., Pace B., Petersen M., Sarmiento A., Shen A., Thomas K., Thompson S., Visini F., Wang Y., Youngs R. R. (2021). "An overview of the fault displacement hazard initiative research program," *Seismological Research Letters*, **92**(2B), 1360–1361.

Chiou, B.S.J., Chen, R., Thomas, K., Milliner, C.W.D., Dawson, T.E., and Petersen, M.D. 2(023). Surface Fault Displacement Models for Strike-Slip Faults, *Report GIRS-2022-07*, University of California, Los Angeles, 186 pp, https://doi.org/10.34948/N3RG6X.

Moss R. E. S., Ross Z. E. (2011). "Probabilistic fault displacement hazard analysis for reverse faults," *Bull. Seism. Soc. Am.*, **101**(4), 1542–1553.

Petersen M. D., Dawson T. E., Chen R., Cao T., Wills C. J., Schwartz D. P., Frankel A. D. (2011). "Fault displacement hazard for strike-slip faults," *Bull. Seism. Soc. Am.*, **101**(2), 805–825.

Rigby R. A., Stasinopoulos M. D., Heller G. Z., Bastiani F. De (2020). *Distribution for Modelling Location, Scale, and Shape: Using GAMLSS in R*, Chapman & Hall/CRC: New York, 588 pp.

Stasinopoulos M. D., Rigby R. A., Heller G. Z., Voudouris V., Bastiani F. D. (2017). *Flexible Regression and Smoothing: Using GAMLSS in R*, Chapman & Hall/CRC: New York, 571 pp.

Thomas, K., Milliner, C., Chen, R., Chiou, B., Dawson, T., Petersen, M. (2023). "Least Cost Path Analysis as an Objective and Automatic Method to Define the Primary Fault Trace for Probabilistic Fault Displacement Hazard Analyses," *Earthquake Spectra*, in review.

Youngs R. R., Arabasz W. J., Anderson R. E., Ramelli A. R., Ake J. P., Slemmons D. B., McCalpin J. P., Doser D. I., Fridrich C. J., Swan F. H. III, Rogers A. M., Yount J. C., Anderson L. W., Smith K. D., Bruhn R. L., Knuepfer L. K., Smith R. B., dePolo C. M., O'Leary K. W., Coppersmith K. J., Pezzopane S. K., Schwartz D. P., Whitney J.W., Olig S. S., Toro G. R. (2003). "A methodology for probabilistic fault displacement hazard analysis (PFDHA)," *Earthquake Spectra*, **19**(1), 191–219.

Wells D. L., Coppersmith K. J. (1994). "New empirical relationships among magnitude, rupture length, rupture width, rupture area, and surface displacement," *Bull. Seism. Soc. Am.*, **84**(4), 974–1002.

Wells D., Youngs B. (2015). "Improved regression relations for earthquake source parameters," *Seismological Research Letters*, **86**(2B), 623.

Day1 (Monday, Sep. 25th, 2023) 14:40~15:15

GEER-NCREE Reconnaissance of the 2022 M_W 6.9 Chihshang, Taiwan Earthquake Sequence

Domniki Asimaki

Professor, California Institute of Technology, Pasadena, California, USA

Domniki Asimaki is a Professor of Mechanical and Civil Engineering at Caltech. She got her PhD from the Department of Civil and Environmental Engineering at MIT. Her research focuses on the understanding and simulation of 3D site effects, and their impact on the design and performance of geotechnical systems. She is an elected member of the ASCE GeoInstitute Board of Governors; she also sits on the Southern California Earthquake Center Science Planning Committee and on the editorial board of the Bulletin of Earthquake Engineering and of Earthquake Spectra. Among other awards, she has received the 2009 Arthur Casagrande Award from the ASCE Geo-Institute, the 2012 Shamsher Prakash Research Award in Geotechnical Earthquake Engineering, the 2015 Young Investigator Award in Geotechnical Earthquake Engineering from the International Society of Soil Mechanics and Geotechnical Engineering (ISSMGE), and the 2018 Bodossaki Award for Excellence in Engineering and Applied Mechanics.

GEER-NCREE Reconnaissance of the 2022 Mw 6.9 Chihshang, Taiwan Earthquake Sequence

Domniki Asimaki[1], Brian Gray[2], Grigorios (Greg) Lavrentiadis[3], Trevor Carey[4] and H. Benjamin Mason[5]

1. Professor, California Institute of Technology, Pasadena, California, USA
2. Senior Geologist, Lettis Consultants International, Inc.
3. Post-doctoral Researcher, California Institute of Technology, Pasadena, California, USA
4. Assistant Professor of Civil Engineering, University of British Columbia, Vancouver, Canada
5. Research Civil Engineer, U.S. Geological Survey, Geologic Hazards Science Center, Colorado, USA

Email: domniki@caltech.edu, bgray@lettisci.com, glavrent@caltech.edu, trevor.carey@civil.ubc.ca, hmason@usgs.gov

ABSTRACT

We performed post-earthquake reconnaissance in Taiwan following the 18 September 2022 Mw 6.9 Chihshang, Taiwan earthquake. The mainshock produced surface rupture along approximately 40 km of the plate boundary consisting of the east-dipping Longitudinal Valley fault (LVF) and the west-dipping Central Range fault. Near-field seismic stations measured PGAs exceeding 0.5 g along the fault. PGVs increased in the direction of the rupture; average amplitudes of 8 cm/sec near the epicenter increased along the fault to 89 cm/sec at the northern terminus. The ground motion recordings of the east (approximately fault parallel) component showed strong velocity pulses in the direction of the rupture. Our team investigated surface fault rupture and bridge damage using traditional reconnaissance techniques as well as unmanned aerial vehicles (UAVs) equipped with cameras and lidar. Field observations from our reconnaissance indicate that the majority of surface rupture manifested on the Yuli fault, a shallow branch of the causative Central Range fault; triggered surface rupture was also documented along the trace of the Longitudinal Valley Fault. Despite the proximity of the rupture to important locations throughout the alluvial plain from Chihshang to Ruisui, we did not observe any surface manifestations of liquefaction. We speculate that liquefaction did not occur due to a combination of short earthquake durations as well as a variation of soil types throughout the alluvial plain. The observations are important for geotechnical engineers practicing in seismically active areas with nearby, active faults capable of creating strong velocity pulses.

Keywords: 2022 Chihshang Earthquake, fault rupture, fling effects, bridge damage, pulse

INTRODUCTION

The M_W6.9 Chihshang, Taiwan earthquake occurred on 18 September 2022 at 14:44 local time. The strike-slip earthquake occurred on the north-south trending Central fault extending along the southeast coast of Taiwan. Figure 1 shows the contours of peak ground velocity (PGV) as reported in real-time by the early warning network P-Alert, composed of MEMS accelerometers across the island operated by the National Taiwan University (Wu et al., 2016). The U. S. Geological Survey (USGS) reports the earthquake's epicentral location at 23.138° N 121.344° E with an epicentral depth of 10.0 km. The fault ruptured north, leading to directivity effects. The earthquake caused bridge collapses, surface fault rupture, and landslides throughout the epicentral region. Despite the epicentral region being an alluvial plain, surficial evidence of liquefaction was sparse to non-existent. Carey et al. (2023) documents some of the prior observations. Notably, a M_W6.5 foreshock occurred on 17 September 2022 at 21:41local time (approximately 17 hours before the M_W6.9 mainshock). Figure 1 shows the location of the foreshock epicenter, which the USGS reports being at 23.119° N 121.414° E with an epicentral depth of 10.0 km. The M_W6.5 foreshock undoubtedly caused damage before the M_W6.9 mainshock, and in some cases, may have caused material yielding to bridges that subsequently collapsed during the M_W6.9 mainshock. Notwithstanding the foregoing point, our field observations focused on documenting evidence of damage associated with the M_W6.9 mainshock, because we did not have access to many field observations between the two earthquakes to isolate the M_W6.5 foreshock damage.

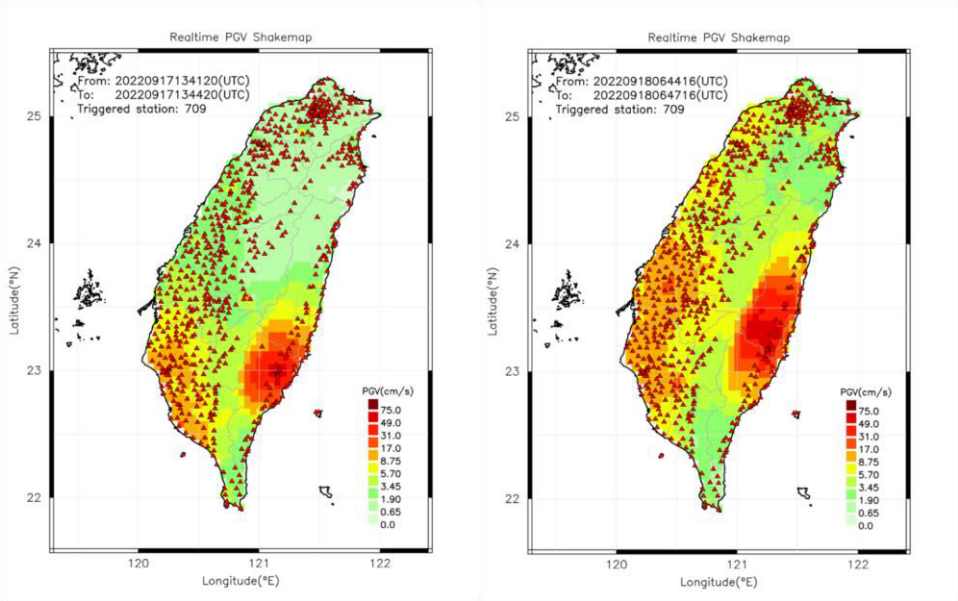

Figure 1. The real-time peak ground velocity recorded by the P-Alert network. The left panel shows the first shock on 17 Sept. The second panel shows the larger mainshock on 18 September (source: twitter.com)

The U.S. National Science Foundation (NSF)-funded Geotechnical Extreme Events Reconnaissance (GEER) team arrived in Taipei on 15 and 16 October 2022 and traveled to the affected region on 17 October. We conducted five days of fieldwork. The GEER team, which included eight U.S.-based members, was hosted by a team of geologists, geotechnical engineers, and researchers from Taiwan's National Center for Research on Earthquake Engineering (NCREE). The team was also followed in the field by Prof. Kuo-lung Wang and his graduate students from the National Chi Nan University, who documented high resolution drone imaging of structural and geotechnical damage associated with landslides and fault rupture along the affected area of our reconnaissance. We refer to the U.S.-Taiwan field reconnaissance team as the GEER-NCREE team herein. The team was separated into three focus groups to optimize our field campaign: 1) the bridge team, 2) the ground failure team, and 3) the surface fault rupture team. Figure 2 shows the location of major reconnaissance activities split by team. We have arranged the report with respect to the observations of the sub-teams. Our entire reconnaissance team bridges a wide range of expertise, so membership of the sub-teams remained fluid during our field campaign. The remainder of the paper describes our main findings in the areas of fault rupture, ground motions and bridge performance that we inspected along the Longitudinal Valley.

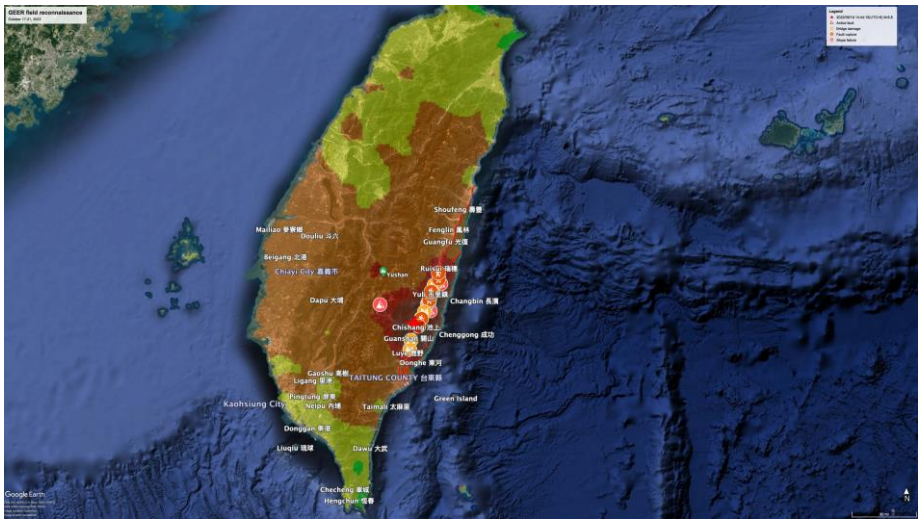

Figure 2. Location of major reconnaissance activities split by team.

SURFACE RUPTURE OBSERVATIONS

Prior to the start of field reconnaissance on October 18th, it was understood that geologists from Taiwan's Central Geological Survey and researchers from multiple Taiwanese academic institutions had been in the field documenting surface rupture in the weeks following the earthquakes. To avoid duplicating the ongoing Taiwanese efforts where possible, the surface rupture team worked to document surface rupture with a focus on engineering-related topics including: 1) surface rupture/structure interaction, 2) distribution and rupture zone width, 3) triggered/off-fault deformation, 4) oblique strain accommodation, and 5) expression of surface faulting at sites with prior historic ruptures. The takeaways of the team on the subject of surface fault ruptures were:

1. Fault deformation was complex and rarely with oblique sinistral slip. In most instances, displacement along the LVF was expressed as either nearly pure sinistral strike slip (mostly in Fuli) or nearly pure shortening (Dongli), at least where offsets could be clearly defined. Where localized changes in fault strike were observed, sense of slip was strongly influenced by these geometry changes.
2. Although the M 6.9 earthquake is well documented to have occurred on the Central Range/Yuli fault, in the region between Chihshang and Dongli School the event resulted triggered slip along the LVF only.
3. As is commonly observed, surface ruptures for the M 6.9 September 2022 earthquake were strongly influenced by the built environment. Faults consistently followed structural weaknesses where they encountered manmade structures. This manifested as fault rupture intersecting the edges of building foundations or along the edges of storm grates.
4. Multiple locations with surface rupture documented during the 1951 earthquake and subsequent events re ruptured in September 2022. In Yuli, the position, sense, and magnitude of displacement were similar, whereas along the LVF, offsets were apparently much smaller than 1951. The latter observation is consistent with triggered rather than primary displacement during the 2022 earthquake (Figure 4).
5. Existing morphology proved to be an inconsistent predictor of fault rupture position. In Fuli, rupture locations are likely to have been predicted within a few meters to a few tens of meters. In contrast, ruptures at Dongli school would have been very difficult to predict and design for without prior subsurface fault investigation and exposure.

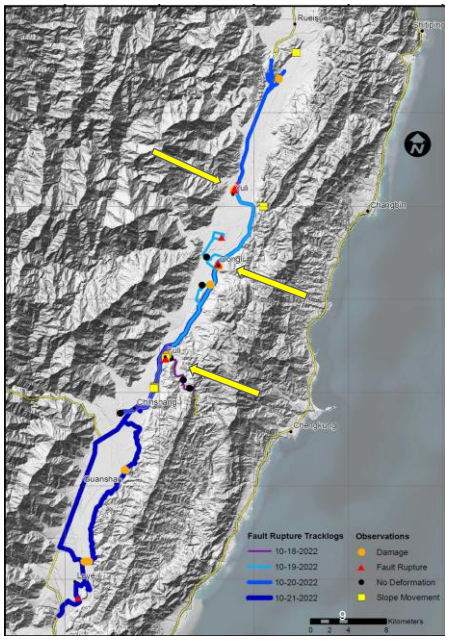

Figure 3. Tracklog and observation map from the surface fault rupture team.

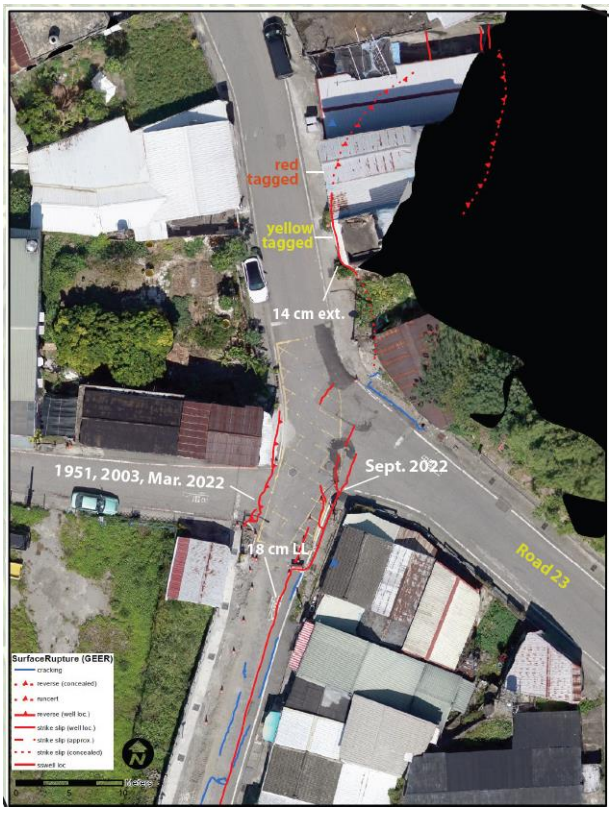

Figure 4. Detailed map of surface rupture at the Road 23 intersection in Fuli. Note position of September 2022 and prior surface ruptures at this location.

GROUND MOTIONS & TECTONIC OFFSET

Strong motion time series were collected and processed in close collaboration with NCREE engineers. We used data from four networks, specifically SANTA, CWBSN, TSMIP, EEWS. Their contribution to our work is hereby acknowledged. When the tectonic offset was computed from the strong motion records, results were verified by comparison with recordings from the GNSS dataset.
Figure 5 shows the horizontal (left) and vertical (right) displacement computed from strong motion records that were not baseline corrected to preserve the offset. Our slip estimates are consistent with the observations from the GPS stations, with the largest offset observed in the middle and northern end of the rupture. On the Central Range Fault (CRF) hanging wall we calculated 1m of right lateral slip and 1m of uplift; while on the LVF hanging wall we calculated 90cm of shortening near the fault and 30cm of shortening 14km east of the rupture. We also used the strong motion records to compute the peak-to-peak velocity pulse, also shown in Figure 5. We observed strong fault normal pulses in rupture direction and strong fault parallel pulses accommodating the permanent slip.

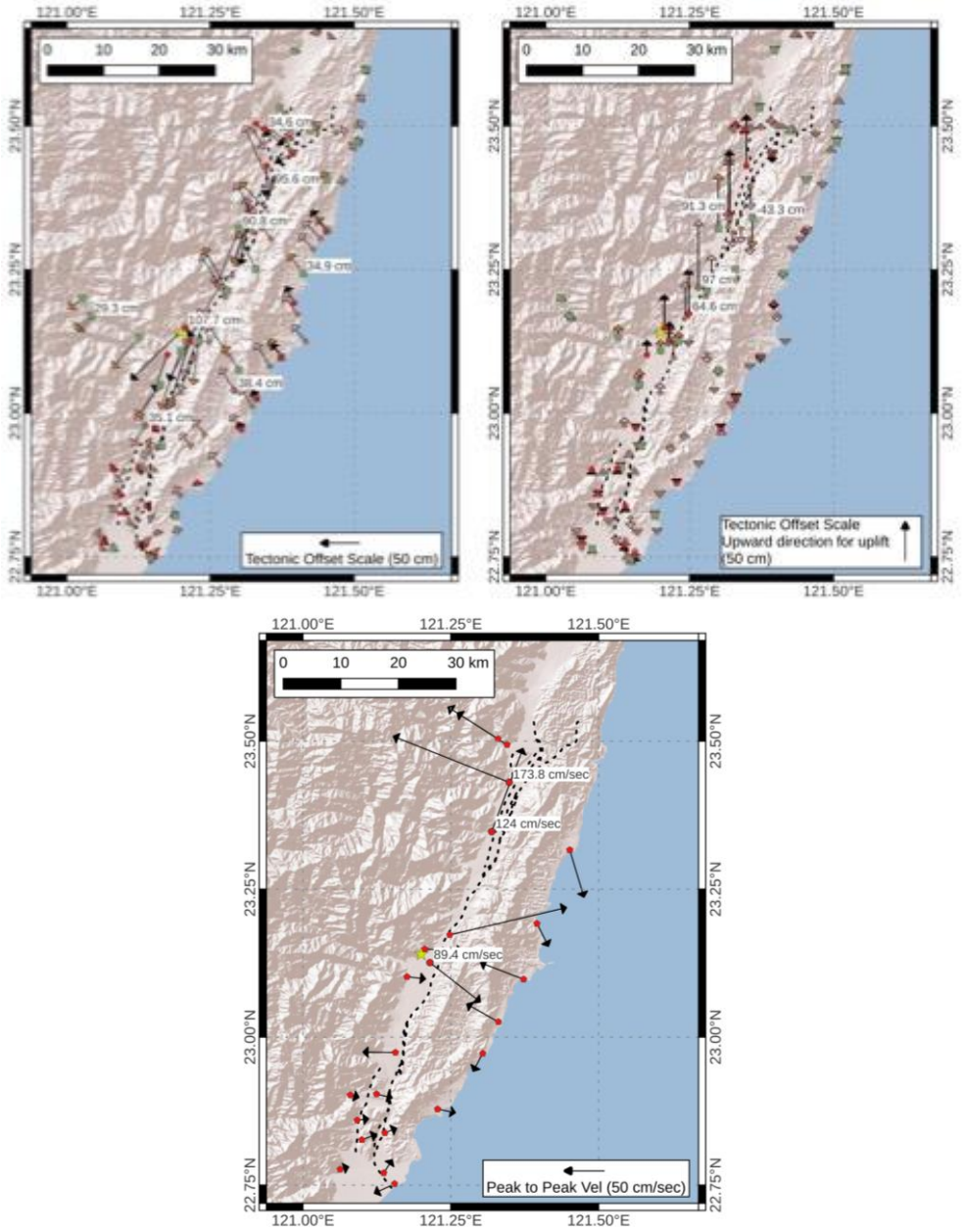

Figure 5. Mw 6.9 Chishang, Tectonic Offset (top left: horizontal; top right: vertical) and peak-to-peak velocity (bottom)

OBSERVATIONS OF BRIDGE DAMAGE

Light to heavy damage was surveyed in eight bridges as part of the reconnaissance mission. The locations of the five most heavily damaged bridges along the trace of the Longitudinal Valley fault (LVF) and M6.9 epicenter are given in Figure 6. Ground motion recordings near the bridges are also provided. All the bridges were located within 2 km of the fault due to the narrowness of the valley, but none of the bridges were identified as crossing the LVF, which would have made them susceptible to damage from fault offset. Overall, two bridges had multi-span, and foundation pier collapses, three were closed for repair, and the remaining bridges were operational but with reductions in service. The ground motion recordings in Figure 6 show a velocity pulse intensified northerly along the fault and in the direction of rupture. These directivity effects placed greater seismic demands on the bridges at the northern end of the valley than the undamaged bridges south epicenter. The displacement time histories include permanent displacements caused by fault offset.

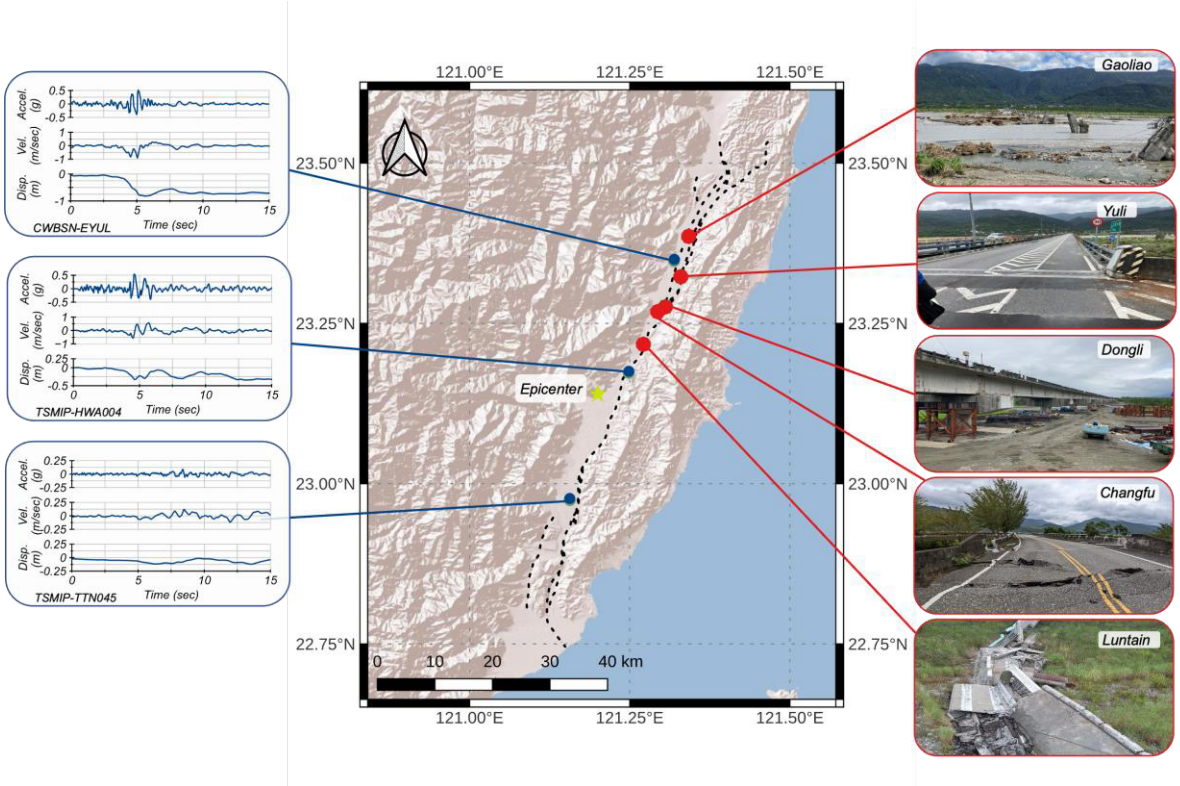

Figure 6. Locations of the five most heavily damaged bridges, the traces of the Longitudinal Valley Fault, the epicenter of the M6.9 earthquake, and select acceleration, velocity, and displacement time series from that event (from Carey et al, 2023).

Our key field observations from the bridge inspections are that most failures were caused by bridge girder unseating, which in turn was likely caused by large velocity pulses. The girder unseating triggered cascading failure in piers which resulted in some cases in catastrophic failure. Large velocity pulses also likely caused gravity wall movements and failure, while no ground failure was observed despite the soft sedimentary structure of the foundation soils in the valley.

DISCUSSION

The Chishang events nucleated on the high-angle, west-dipping Central Range Fault (CRF), which is blind in the south, and was not in the official active faults map issued by the Taiwan Geological Survey. The GEER-NCREE team performed field observations approximately a month following the events, and observed systematic bridge damage caused by large velocity pulses and differential displacements of the abutments caused by fling. The observed damage has important implications for design and retrofit of bridges in other seismically active areas. For instance, we should re-examine current seismic

design guidelines, and also start considering earthquake motions rotated in bridge normal and bridge parallel directions. The team is also assessing why liquefaction was not triggered in the alluvial sediments at the damaged bridges. Our current hypothesis is the duration of strong shaking was not long enough to cause sufficient pore water pressure buildup. We performed passive horizontal-to-vertical spectral ratio (HVSR) testing at the collapsed bridges to establish underlying ground conditions. Our analysis will use the data from HVSR testing, ground motions records, and liquefaction analysis procedures for ground motions with pulse-like directivity effects (e.g., Green et al. 2008). The findings have implications for liquefaction analysis procedures performed at sites susceptible to ground motion directivity effects. Lastly, as mentioned above, existing morphology proved to be an inconsistent predictor of fault rupture position: in some cases (Fuli), ruptures of recent events were separated by distances of a few meters, while in other cases (Dongli), ruptures would have been very difficult to predict and design for without prior subsurface fault investigation and exposure.

ACKNOWLEDGMENTS

The National Science Foundation (NSF) supported the work under the GEER Association Grant No. CMMI-1826118. We gratefully acknowledge the support of our Taiwanese colleagues, who will be co-authors on the forthcoming GEER report.

REFERENCES

Carey, Trevor & Mason, H. & Asimaki, Domniki & Athanasopoulos-Zekkos, Adda & Garcia, Fernando & Gray, Brian & Lavrentiadis, Grigorios & Nweke, Chukwuebuka. (2023). The 2022 Chihshang, Taiwan, Earthquake: Initial GEER Team Observations. Journal of Geotechnical and Geoenvironmental Engineering. 149. 10.1061/JGGEFK.GTENG-11522.

Green, R. A., J. Lee, T. M. White, and J. W. Baker. (2008). The significance of near-fault effects on liquefaction. Beijing, China.

Day1 (Monday, Sep. 25th, 2023) 15:35~16:10

Recent Advances in Evaluating the Linear and Nonlinear Dynamic Properties of Rock Subjected to Earthquake Shaking

Kenneth H. Stokoe

Professor, Jennie C. and Milton T. Graves Chair,
Department of Civil, Architectural and Environmental Engineering,
University of Texas at Austin, Austin, Texas, U.S.A.

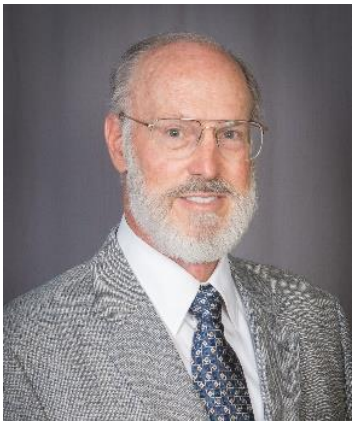

Dr. Kenneth H. Stokoe, II has been working in the areas of field seismic measurements, dynamic laboratory measurements, and dynamic soil-structure interaction for more than 45 years. He has been instrumental in developing several small-strain field seismic methods for in-situ shear wave velocity measurements and recently a large strain method for nonlinear measurements of shear wave velocity. He has also developed two types of resonant column systems that are used to evaluate dynamic soil and rock properties in the laboratory. Over the last 28 years, Dr. Stokoe has led the development of large-scale mobile field equipment for dynamic loading of geotechnical systems, foundations and structures, an activity that has been funded by the National Science Foundation, first in the NEES program for 20 years and now for 8 years in the NHERI program. The equipment has already led to the development of new testing methods to evaluate soil nonlinearity and liquefaction directly in the field. Dr. Stokoe has received several honors and awards, including election to the National Academy of Engineering, the Harold Mooney Award from the Society of Exploration Geophysicists, and the C.A. Hogentogler Award from the American Society for Testing and Materials, and the H. Bolton Seed Medal and the Karl Terzaghi Distinguished Lecturer from the American Society of Civil Engineers.

RECENT ADVANCES IN EVALUATING THE LINEAR AND NONLINEAR DYNAMIC PROPERTIES OF ROCK SUBJECTED TO EARTHQUAKE SHAKING

Kenneth H. Stokoe II[1], Shi-Yuan Li[2], and Zhong-Ze Xu[3]

1. Professor, Jennie C. and Milton T. Graves Chair, Department of Civil, Architectural and Environmental Engineering, University of Texas at Austin, Austin, Texas, U.S.A.
2. Ph.D. Student, Department of Civil, Architectural and Environmental Engineering, University of Texas at Austin, Austin, Texas, U.S.A.
3. Project Geotechnical Engineer, Haley & Aldrich, Seattle, Washington, U.S.A.

Email: k.stokoe@mail.utexas.edu, lishiyuan@utexas.edu, zhongzexu@utexas.edu

ABSTRACT

The linear and mildly nonlinear dynamic properties of basalt rock from the Idaho National Laboratory, USA, were investigated in this study. Two types of basalt rock were tested: (1) vesicular basalt which had some voids, and (2) aphanitic basalt which had almost no voids. The combined resonant column and torsional shear (RCTS) device was employed to evaluate the shear modulus (G) and the material damping ratio in shear (D) of the rock over shearing strains ranging from about 10^{-5}% to 0.02%. The elastic threshold shear strain (γ_t^e) for basalt specimens ranged from about 10^{-3}% to 10^{-2}%. The linear dynamic properties (V_s, G_{max}, and D_{min}) and nonlinear dynamic properties (G/G_{max} - log γ and D - log γ curves) exhibited little change with confining pressure. The minimum value of G/G_{max} was 0.84 at γ = 0.014%. On the other hand, the maximum value of D was 2.12% at γ = 0.013%. As a simple geotechnical engineering comparison, the nonlinear curves of basalt and sand are compared.

Keywords: rock dynamics, basalt, torsional resonant column test, shear wave velocity, shear modulus, material damping ratio, elastic threshold shear strain

INTRODUCTION

Shear modulus and material damping ratio of soil and rock are key parameters in many geotechnical engineering problems, including earthquake site response analyses, deep excavations, tunneling, and foundations of critical structures. Realistic measurements and accurate predictions of the dynamic properties are very important in many of these analyses. Over the past several decades, researchers have actively been developing approaches to measure and predict the linear and nonlinear dynamic properties of soil. However, compared to soil, very limited shear modulus reduction and material damping ratio curves for rock exist in the literature. The nonlinear behavior of rock during dynamic loading conditions in Civil Engineering has generally been treated as linear elastic and even though rock also shows nonlinear behavior. Therefore, it is of importance to investigate both the linear and nonlinear behaviors of rock and the factors influencing these behaviors. In this paper, the linear and mildly nonlinear dynamic properties of basalt rock from the Idaho National Laboratory, USA are presented. A more detailed description of this work is given in Li (2023).

EXPERIMENTAL PROGRAM

Test Device

The equipment used in this study is the combined resonant column and torsional shear (RCTS) device in the Soil and Rock Dynamics Laboratory at the University of Texas, as shown in Fig. 1. The RCTS device is of the fixed-free type, with the bottom of the specimen fixed and torsional excitation applied to the top cap at the free end. The apparatus as well as the procedures to determine the shear modulus (G), material damping ratio (D), and shear strain amplitude (γ) of the specimen in the resonant column (RC) tests are described in more detail in Keene (2017).

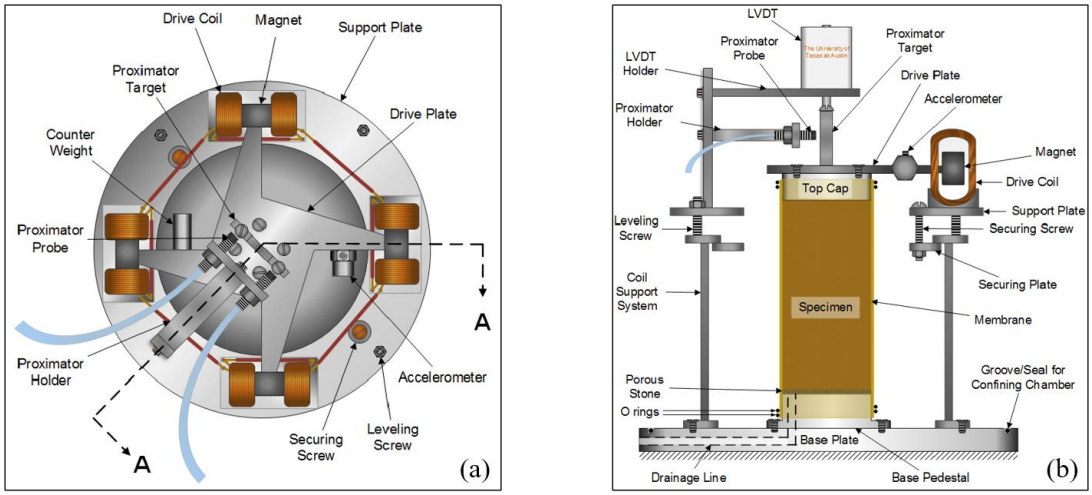

Figure 1. Combined resonant column and torsional shear (RCTS) device: (a) Top view of drive and monitoring systems and (b) Section A-A of RCTS device with a specimen in place.

Test Material and Specimen Preparation

In this study, two types of basalt from the Idaho National Laboratory (INL) are investigated: vesicular basalt and aphanitic basalt. The tested specimens included 17 basalt specimens (8 vesicular and 9 aphanitic). The two types of basalt specimens are shown in Figs. 2(a) and (b), respectively. The vesicular basalt has some voids, and the aphanitic basalt has almost no voids. The basic information on the 17 basalt specimens is presented in Table 1, including specimen ID, depth, basalt type, dimensions (diameter and length), total unit weight (γ_t), estimated void ratio (e), and estimated in-situ mean stress (σ_m). The basalt specimens are approximately 4 cm in diameter and 11 cm in length, which are the typical dimensions for test specimens in the resonant column test. It should be noted that the estimated void ratio was calculated by assuming a specific gravity (G_s) equal to 2.90 and a water content equal to 0 for all basalt specimens. Also, the estimated in-situ mean stress was computed by assuming the at-rest earth pressure coefficient (K_0) equal to 0.5. As listed in Table 1, e varies from 0.015 to 0.358 and σ_m is between 55 kPa and 3247 kPa for the basalt specimens.

The basalt specimen in place on the base pedestal and with a top cap in the RC test is shown in Fig. 2(c). Before beginning any RC testing, the basalt specimen was securely epoxied to the base pedestal, and a top cap was securely epoxied to the specimen (Choi, 2007). The curing time for the epoxy glue was at least 24 hours. Also, all basalt specimens were in an air-dried condition before any assembling.

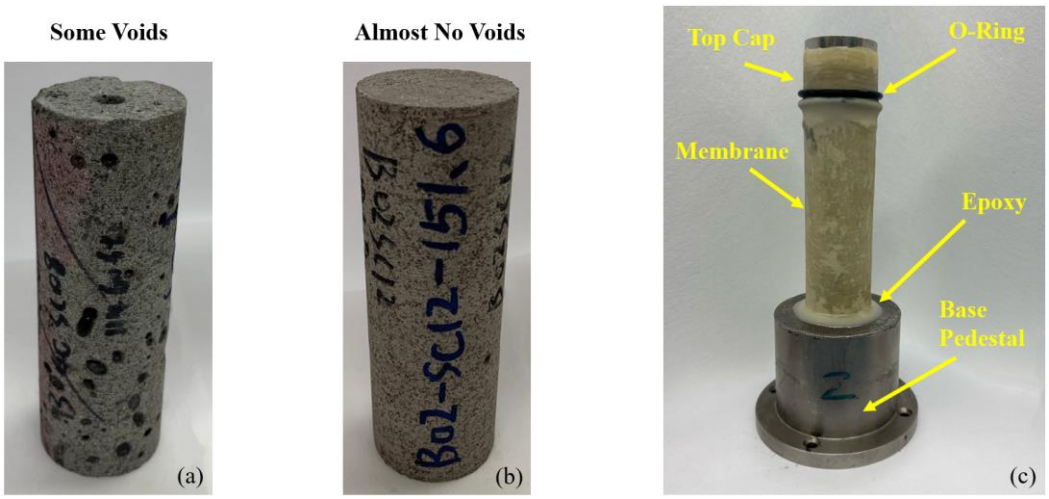

Figure 2. (a) Vesicular basalt; (b) Aphanitic basalt; and (c) Basalt specimen setup with specimen glued to the base pedestal and top cap and covered with a membrane.

Table 1. Basic information for the 17 basalt specimens

Specimen ID.	Depth (m)	Basalt Type	Diameter (cm)	Length (cm)	Total Unit Weight (kN/m^3)	Estimated Void Ratio	Estimated In-Situ Mean Stress (kPa)
1	51.6 - 52.2	Vesicular	3.8	11.1	26.0	0.093	827
2	155.9 - 156.3	Aphanitic	3.8	11.0	26.2	0.085	2586
3	115.8 - 116.2	Aphanitic	3.8	10.6	25.9	0.100	1889
4	54.1 - 54.6	Aphanitic	3.8	11.0	26.0	0.092	883
5	46.2 - 46.6	Aphanitic	3.8	11.0	26.9	0.058	745
6	34.9 - 35.4	Vesicular	3.8	11.0	24.5	0.162	552
7	63.0 - 63.4	Vesicular	3.8	11.0	21.0	0.353	1034
8	5.5 - 5.8	Aphanitic	3.8	10.6	25.6	0.112	83
9	174.5 - 174.9	Aphanitic	3.8	11.0	26.9	0.057	2903
10	57.5 - 57.9	Aphanitic	3.8	11.0	27.0	0.052	938
11	3.7 - 4.1	Vesicular	3.8	11.0	25.1	0.135	55
12	34.6 - 34.9	Aphanitic	3.8	11.0	28.0	0.015	552
13	202.1 - 202.5	Aphanitic	3.8	11.0	24.4	0.166	3247
14	90.2 - 90.5	Vesicular	3.8	10.8	23.4	0.215	1489
15	73.9 - 74.2	Vesicular	3.8	11.0	21.1	0.346	1213
16	69.2 - 69.5	Vesicular	3.8	11.0	20.9	0.358	1103
17	160.0 - 160.5	Vesicular	3.8	10.9	24.5	0.163	2661

Test Procedure and Program

Typically, the RCTS device is used to conduct resonant column tests at multiple confinement stages and over a range in shear strain levels, known as stage testing (Choi, 2007). The pressure level sequences used in the resonant column testing of the basalt specimens are listed in Table 2. In this study, each basalt specimen was tested at 6 isotropic confining pressures (σ_0), denoted as 6 stages in Table 2. The isotropic confining pressure at each stage depends on the magnitude of the estimated σ_m of the specimen. The applied confining pressures generally ranged from below, equal to, and above the estimated σ_m of the specimen. Moreover, after completing one phase of testing at a lower pressure, the confining pressure was typically increased by a factor of two. The reason why four different pressure-level sequences were used is that the maximum capacity of the pressure chamber is 2206 kPa (320 psi) and some of the specimens had either an estimated σ_m that exceeded 2206 kPa (320 psi) or, when doubled, exceeded 2206 kPa (320 psi).

Table 2. Pressure level sequences in the resonant column test for basalt specimens

Testing Pressure Levels	Stage #1	Stage #2	Stage #3	Stage #4	Stage #5	Stage #6
σ_m <= 552 kPa	0 kPa	$\sigma_m/4$*	$\sigma_m/2$	σ_m*	$2\sigma_m$	$4\sigma_m$*
552 kPa < σ_m <= 1379 kPa	0 kPa	$\sigma_m/8$	$\sigma_m/4$*	$\sigma_m/2$	σ_m*	$2\sigma_m$ or 2206 kPa*
1379 kPa < σ_m < 2206 kPa	0 kPa	$\sigma_m/16$	$\sigma_m/8$	$\sigma_m/4$*	$\sigma_m/2$*	σ_m*
σ_m >= 2206 kPa	0 kPa	138 kPa	276 kPa	552 kPa*	1103 kPa*	2206 kPa*

Note: symbol * represents the HARC test.

In this study, two types of tests were performed. These tests were low-amplitude resonant column (LARC) tests and high-amplitude resonant column (HARC) tests. In the LARC tests, only low-amplitude ($\gamma < 0.0003\%$) dynamic properties (V_s, G_{max}, and D_{min}) were measured. In the HARC tests, the traditional nonlinear measurements (from small to large strains) were performed to determine the G - log γ, G/G_{max} - log γ, and D - log γ curves of the specimens. LARC tests were performed at every confinement stage to evaluate the effects of time and magnitude of confinement on the linear dynamic properties. HARC tests were performed at 3 confinement stages to determine the nonlinear dynamic properties of basalts at different confining pressures. The details of the test program for basalt specimens in the RC tests are given in Table 2. Since negligible time-dependent changes in low-amplitude dynamic properties were found for the basalt specimens, the confinement time for each confining pressure was 30 minutes. The LARC tests were performed first at each pressure level, followed by any HARC tests (if required). Note that Specimen #17 was only tested in the unconfined state since there were too many large voids on the surface of the specimen which negated the use of a membrane.

TEST RESULTS AND DISCUSSIONS

Linear Dynamic Properties of Basalts

The variations in the estimated void ratio (e), low-amplitude shear wave velocity (V_s), low-amplitude shear modulus (G_{max}), and low-amplitude material damping ratio (D_{min}) with σ_0 for the 17 basalt specimens are shown in Figs. 3(a) - (d), respectively. It is obvious that all basalt specimens show little or no change in e, V_s, G_{max}, and D_{min} with increasing σ_0. As seen in Fig. 3(a), vesicular basalt specimens have a larger void ratio compared with aphanitic basalt specimens. However, the ranges in the linear dynamic properties (V_s, G_{max}, and D_{min}) are quite similar for the two types of basalts, as shown in Figs. 3(b) - (d). In general, for the 17 basalt specimens, V_s ranges from 1,500 m/s to 2,300 m/s, G_{max} ranges from 6,000 MPa to 13,000 MPa, and D_{min} ranges from 0.4% to 1.0%. These results show that the basalt specimens have high stiffnesses and low material damping ratios in shear. It is interesting to see, however, that D_{min} was nearly constant with increasing σ_0 below 1,000 kPa (like G_{max}) after which D_{min} increased slightly as shown in Fig. 3(d). This difference between G_{max} and D_{min} with increasing σ_0 could possibly indicate that fracturing in the specimen affects D_{min} more than G_{max} but more studies are needed.

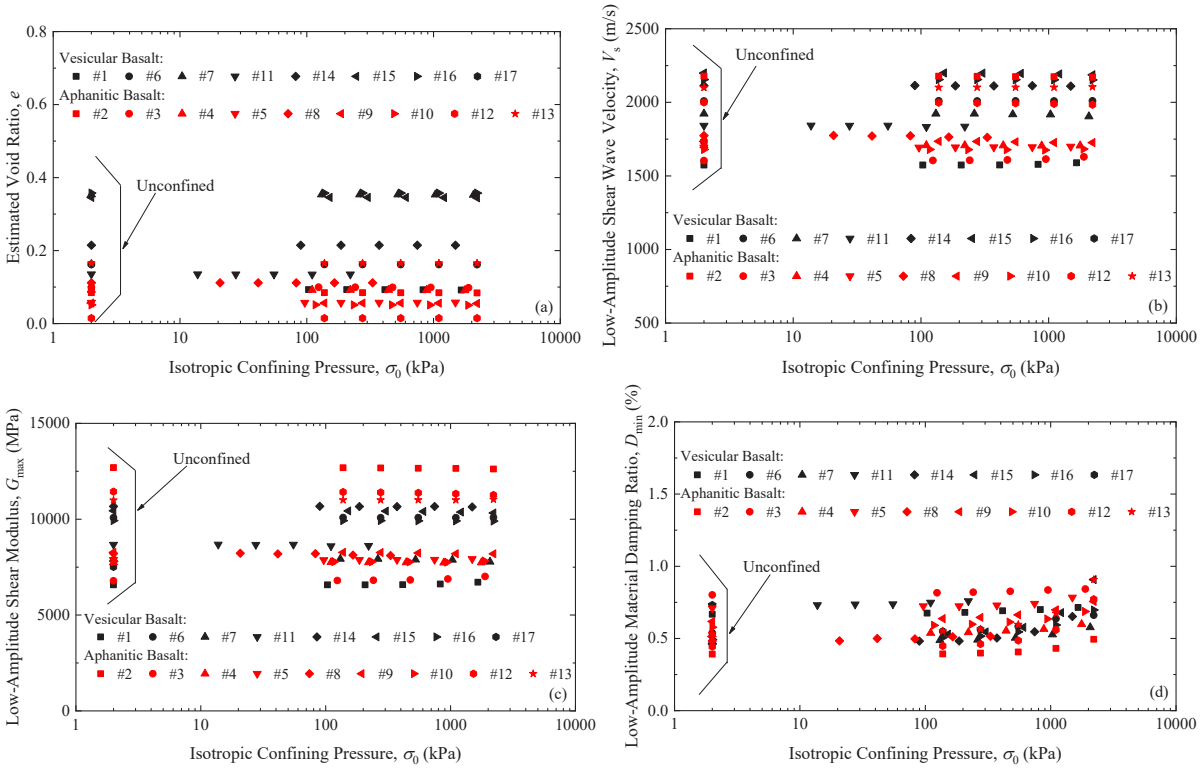

Figure 3. Effect of isotropic confining pressure on (a) e, (b) V_s, (c) G_{max}, and (d) D_{min}.

The relationship between D_{min} and V_s in the unconfined state is that D_{min} decreases slightly with increasing V_s. When V_s increases from about 1,600 m/s to 2,200 m/s, D_{min} decreases from around 0.75% to 0.50%. The database is, however, quite limited, but it is helpful to understand this relationship in terms of D_{min} versus V_s because V_s is regularly measured in the field and, the field V_s can be used as an initial indicator of D_{min}. This relationship is discussed in more detail in Li (2023).

Nonlinear Dynamic Properties of Basalts

The effect of confining pressure on the nonlinear dynamic properties of basalt Specimen #5 (aphanitic basalt) is presented in Fig. 4. The G - log γ curves, G/G_{max} - log γ curves, and D - log γ curves are almost unchanged when σ_0 increases from 186 kPa to 1,489 kPa. Thus, Specimen #5 exhibits little or no change in nonlinear dynamic properties with increasing σ_0. In fact, all vesicular and aphanitic basalt specimens in this study show essentially the same pressure-independent, nonlinear behavior.

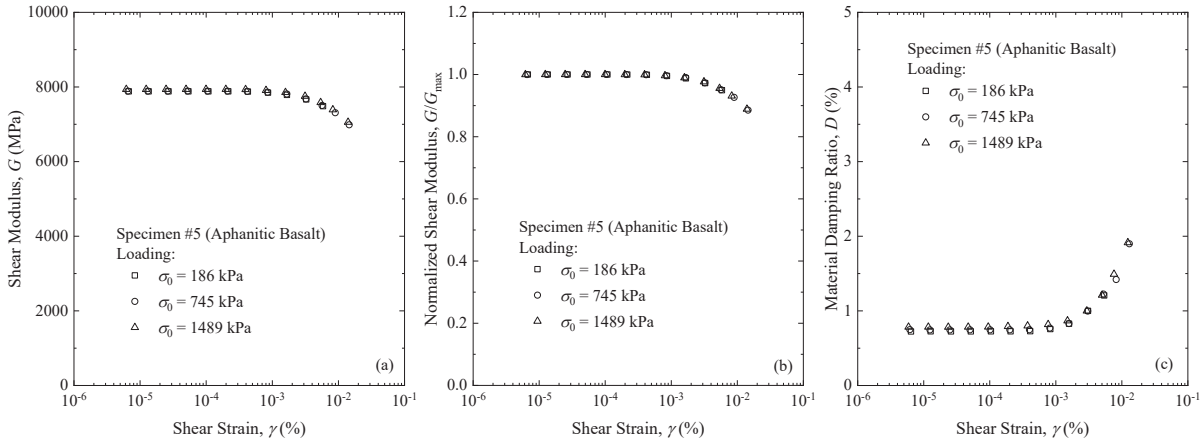

Figure 4. Nonlinear dynamic properties of Specimen #5 (aphanitic basalt) at different isotropic confining pressures: (a) G - log γ curves; (b) G/G_{max} - log γ curves; and (c) D - log γ curves.

Considering the pressure independence of the nonlinear dynamic properties of basalts, Figs. 5(a) and 5(b) show the G - log γ curves of 8 vesicular basalt specimens and 9 aphanitic basalt specimens at the highest confining pressure, respectively. It can be seen that the largest shear strains generated in the RC tests for the 17 basalt specimens are all less than 0.02% because of the power limitation of the RCTS device combined with the stiffness and dimensions of the basalt specimens. However, larger shear strains can be created in smaller rock specimens as shown by Li (2023).

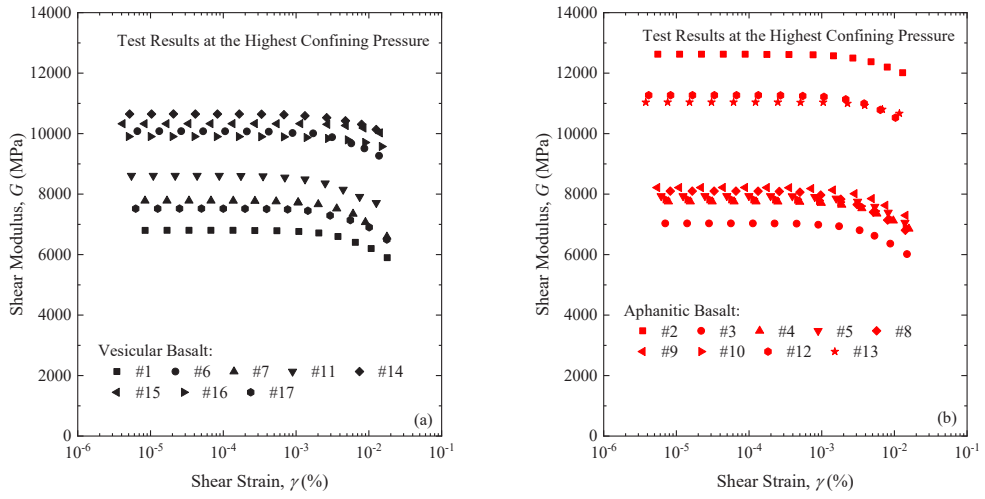

Figure 5. G - log γ curves at the highest isotropic confining pressures of (a) 8 vesicular basalt specimens and (b) 9 aphanitic basalt specimens.

The G/G_{max} - log γ and D - log γ curves of the 17 basalt specimens are compared with the same set of nonlinear curves presented by Seed and Idriss (1970) for sand in Figs. 6(a) and 6(b), respectively. It is clear that the G/G_{max} - log γ and D - log γ curves of the two types of basalt specimens are very similar and show very little nonlinearity over the shear strain range that could be generated in this study. For the 17 basalt specimens, the minimum value of G/G_{max} was 0.84 at γ = 0.014% (Specimen #8). On the other hand, the maximum value of D was 2.12% at γ = 0.013% (Specimen #3). By fitting the G/G_{max} - log γ curves of the 17 basalt specimens, the elastic threshold shear strains (γ_t^e, i.e., the shear strain when G/G_{max} equals 0.99) for the basalt specimens ranged from about 10^{-3}% to 10^{-2}%. Comparing the G/G_{max} - log γ and D - log γ curves of the basalt specimens and sand (Seed and Idriss, 1970) in Fig. 6, it is clear that the basalt specimens have a larger linear range than sands, as expected because the basalt specimens had no obvious fracturing.

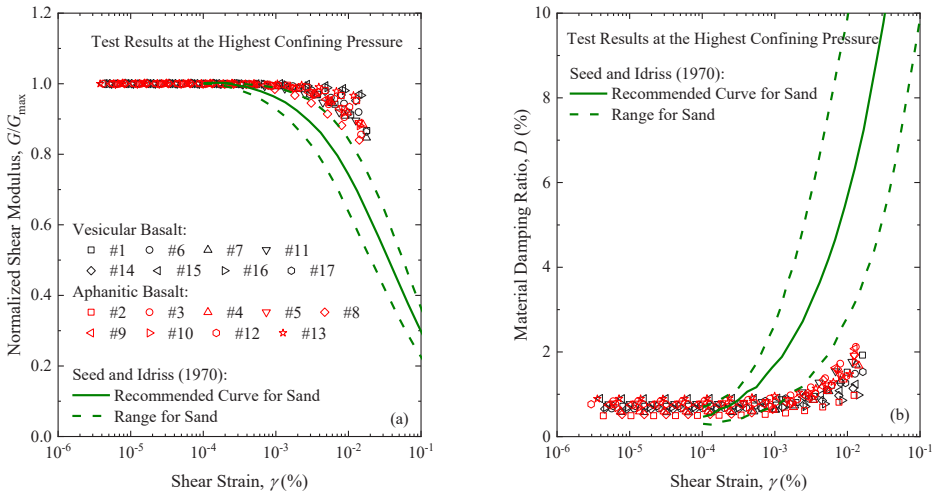

Figure 6. Comparisons between basalt specimens at the highest confining pressure and sand (Seed and Idriss, 1970): (a) G/G_{max} - log γ curves and (b) D - log γ curves.

PS4-1

CONCLUSIONS

In this study, a series of resonant column tests were performed to investigate the linear and mildly nonlinear (to shear strains of about 0.02%) dynamic properties of two types of basalts (vesicular basalt and aphanitic basalt) from Idaho National Laboratory, USA. Test results show that the linear and nonlinear dynamic properties of the basalts are both pressure independent. The ranges of linear and nonlinear dynamic properties are similar for the two types of basalts. The elastic threshold shear strain (γ_t^e) for basalts ranges from 10^{-3}% to 10^{-2}%. As expected, basalt has a larger linear range than sand.

ACKNOWLEDGMENTS

The authors would like to thank the firm of Rizzo International Inc. and Dr. Michael Rosenmeier for their support in this study.

REFERENCES

Choi, W.K. (2007). Dynamic properties of ash-flow tuffs, *Ph.D. Dissertation*, The University of Texas at Austin.

Keene, A.K. (2017). Next-generation equipment and procedures for combined resonant column and torsional shear testing, *Ph.D. Dissertation*, The University of Texas at Austin.

Li, S.Y. (2023). Investigations of: (1) the Dynamic Properties of Basalts, and (2) the Effects of High-Amplitude Shear-Strain Vibrational History on the Dynamic Properties of Sands using Combined Resonant Column and Torsional Shear (RCTS) Testing, *Ph.D. Dissertation*, The University of Texas at Austin.

Seed, H.B. and I.M. Idriss (1970). Soil moduli and damping factors for dynamic response analyses, *Report No. EERC 70-10*, University of California, Berkeley.

Day1 (Monday, Sep. 25th, 2023) 16:10~16:45

Epistemic Uncertainty in Site Response for Site-Specific PSHA

Adrian Rodriguez-Marek

Professor, Civil and Environmental Engineering Department, Virginia Tech, Blacksburg, VA, U.S.A.

Dr. Adrian Rodriguez-Marek obtained his B.S. and M.S. in Civil Engineering from Washington State University, and his Ph.D. from U.C. Berkeley in 2000 working under the guidance of Prof. Jonathan Bray. After getting his Ph.D. in August 2000 Adrian went back to WSU as an Assistant Professor. He stayed at WSU until 2010 when he moved to Virginia Tech where he is now a professor in the Civil and Environmental Engineering Department. Dr. Rodriguez-Marek's research is in the general area of geotechnical earthquake engineering. He has led NSF-funded reconnaissance teams to study the geotechnical aspects of three separate earthquakes (2001 Southern Peru; 2003 Colima, Mexico; and 2007 Pisco, Peru earthquakes). He has also made contributions to the engineering characterizations of ground motions in general and near-fault ground motions in particular. He has also been a leading developer of the concept of non-ergodic seismic hazard analysis. This concept leads to a much more rigorous treatment of uncertainty in ground motions in hazard analysis applications. Dr. Rodriguez-Marek has been a member of the ground motion characterization team in several project for the seismic hazard assessment of critical facilities in the U.S. and abroad.

EPISTEMIC UNCERTAINTY IN SITE RESPONSE FOR SITE-SPECIFIC PSHA

Adrian Rodriguez-Marek[1]
1. Professor, Civil and Environmental Engineering Department, Virginia Tech, Blacksburg, VA, U.S.A. Email: adrianrm@vt.edu

ABSTRACT

This short note presents a summary of the site response logic tree approach for capturing epistemic uncertainty in site response. Key to this approach is that the uncertainty should be sampled in ground motion space rather than in shear-wave velocity space to avoid under-representing the epistemic uncertainty. An additional component of epistemic uncertainty is model error in site response analyses. The paper includes a discussion of alternative approaches to incorporate this uncertainty.

Keywords: Site response analyses, PSHA, epistemic uncertainty

INTRODUCTION

Most project for the seismic hazard assessment of critical facilities now use the partially non-ergodic approach. This approach implies that the component of aleatory variability that corresponds to site-to-site variability is not accounted for in the hazard integral. The reduced aleatory variability (i.e., sigma) is known as the single-station sigma. The use of a reduced sigma implies that the epistemic uncertainty in site response must be fully accounted for. Recent projects have adopted the use of the site response logic tree to capture this uncertainty more systematically. This short note summarizes this approach as adopted in recent projects, with a focus of highlighting consideration in its implementation.

SITE RESPONSE LOGIC TREE

Site response analyses in seismic hazard assessment are conducted with the purpose of modifying a ground motion prediction equation (GMM) such that it is consistent with the particular characteristics of a site. This is best achieved if site response analyses are conducted both for the target profile and for a profile that is consistent with the predicted site effects in the GMM (Williams and Abrahamson, 2021; Boore *et al.*, 2022). This profile is referred to as the "host" profile (Al Atik and Abrahamson, 2021). The host-to-target conversion for site effects is quantified by *Site Adjustment Factors* (SAFs) computed as the ratio of target to host amplification factors (AF) computed using a common input motion. In PSHA applications, it is important to capture not only the best-estimated value of the SAF, but also their epistemic uncertainty. This is particularly true when the aleatory variability in hazard is the single-station sigma (Rodriguez-Marek *et al.*, 2013).

The site response logic tree is an approach to organize the epistemic uncertainty in a graphical and easy to interpret manner. Details of the site response logic tree are presented elsewhere (e.g., Rodriguez-Marek *et al.*, 2021a and b), and only a summary is presented here via a simple example extracted from Rodriguez-Marek *et al.* (2021a). Figure 1 shows a simple profile consisting of a layer of soil overlying a weathered rock which in turns rests on a stiff bedrock. There are three interpretations of the shear-wave velocity (V_S) for the soil. In addition, there is uncertainty in the transition from soil to rock, in the depth to basement, and in the presence of a low-velocity layer at an intermediate depth. These uncertainties are organized into the logic tree shown in Figure 1 (the weights are nominal interpretations and not important for this paper). Figure 2 shows the site response for the three highest weighted profiles in the logic tree. Observe how the epistemic uncertainty for some frequency ranges is small, despite the difference in the three highest-weighted profiles. Alternatively, site response analyses can be conducted for each of the end-branches of the logic tree (in this case, that is 1,350 profiles). The resulting

amplification factors can be sampled into a lower-order distribution (that preserves mean and variance) using statistical approaches (Miller and Rice, 1983). The resulting factors are shown in Figure 3.

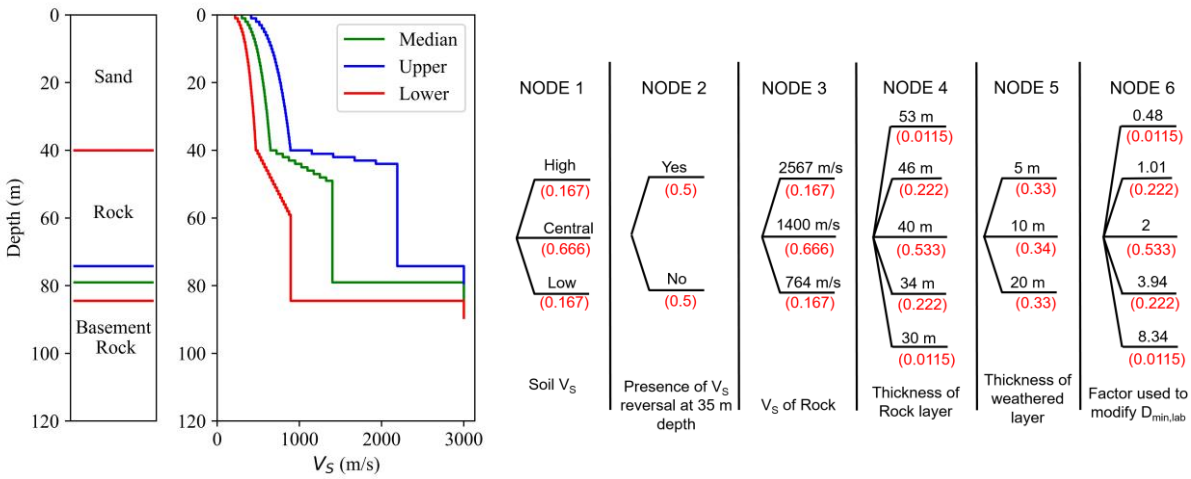

Figure 1. Left: a schematic profile showing with three interpreted velocity profiles. Right: site response logic tree representing epistemic uncertainty in the profile (from Rodriguez-Marek *et al.*, 2021).

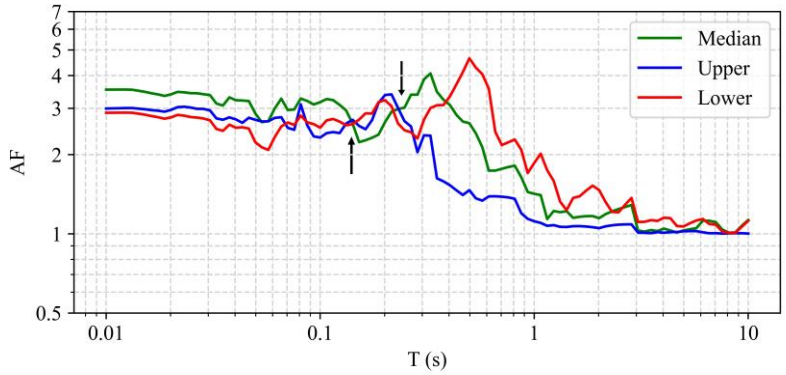

Figure 2. Amplification factors computed via equivalent linear site response analyses for the profiles shown on the left side of Figure 1. The arrows point to oscillator periods where the predicted amplification of the three profiles coincide and thus the apparent epistemic uncertainty is near zero (from Rodriguez-Marek *et al.*, 2021).

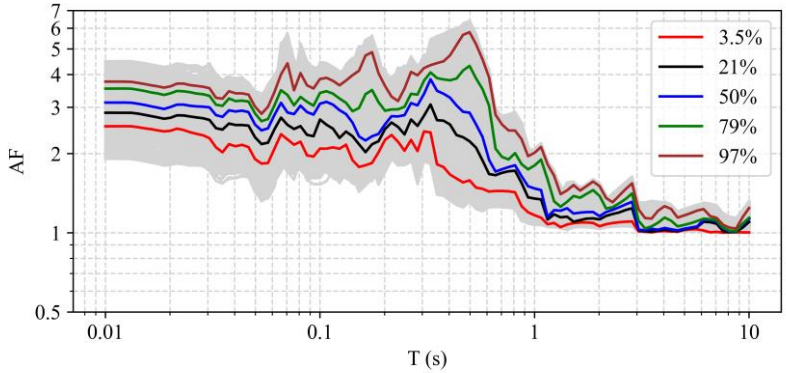

Figure 3. Gray lines represent site response analyses results for each of the end branches for the site response logic tree in Figure 1. The colored lines are the sampled Amplification Factors following the Miller and Rice (1983) sampling scheme (from Rodriguez-Marek *et al.*, 2021).

The simplicity of the site response logic tree approach often hides an important concept that underlies this approach. The onus of the analyst is not to capture uncertainties in the profile itself, but the resulting uncertainties in the resulting amplification factors. A similar concept underlies the proposed "backbone" approach for ground motion models (Atkinson *et al.*, 2014). Albeit simple, the examples shown in Figure 2 illustrates how the uncertainties in amplification function space can be underestimated even when ample uncertainties are considered in the underlying V_S profiles.

An important consideration in implementing the site response logic tree is the potential for correlations between different branches of the logic tree. These correlations can arise for several reasons and must be carefully considered by the analyst. One example is that amplification at high frequencies can occur either due to site effects (e.g., high frequency resonances), or due to low values of the site attenuation parameter (κ_0). If ground motion measurements are used to constrain the value of κ_0, then the correlation between the node in the logic tree that may control high frequency resonances (i.e., the V_S profile) and the small-strain damping noted (controlled by κ_0) must be accounted for. The recent project conducted for the Idaho National Lab (INL 2022) implemented a correlation in the site response logic tree resulting in a reduction in epistemic uncertainty.

An additional consideration that is important in site response analyses is model error. When amplification factors are computed using analytical methods, it is important to consider the potential for model error and model bias in the resulting amplification factors. Model error can be quantified using downhole arrays (Stewart and Afshari, 2021; Bahrampouri and Rodriguez-Marek, 2023). The implementation of model error into the site response logic tree can then be via two approaches:

- Alternative 1: Add model error as an additional uncertainty component (i.e., one additional branch in the site response logic tree).
- Alternative 2: Use model error as a minimum epistemic uncertainty

The two implementations are shown for a hypothetical example in Figure 4. Alternative 1 implies that model error is added (addition of variances) to the epistemic uncertainty that results from the application of the site response logic tree. This implies the assumption that estimates of model error are not contaminated by parametric uncertainty. Alternative 2 assumes that estimates of model error include potential errors in the parameters of the site response analyses, hence they constitute a lower bound to the total epistemic uncertainty. Arguments can be made for both alternatives, and the reality is likely somewhere in between both.

CONCLUSIONS

This paper presented an abbreviated discussion of use of the site response logic tree concept for capturing epistemic uncertainty in site response. The main reason for adopting a site response logic tree is that it allows for the capture of epistemic uncertainty directly in the resulting amplification factors (i.e., in ground motion space). This is analogous to the concept of a backbone model in the construction of logic trees for ground motion models. While details on the implementation of the site response logic tree are presented elsewhere (Rodriguez-Marek *et al.*, 2021a and b); this paper emphasizes two important concepts. First, the importance of considering potential correlations between different nodes of the logic tree. Second, the need to also consider model error in site response analysis in the evaluation of epistemic uncertainty.

ACKNOWLEDGMENTS

The ideas presented in this paper were developed as part of several SSHAC projects, and thus the author is indebted to colleagues that participated in these projects. These include Drs. Julian Bommer and peter Stafford from Imperial College, Dr. Ellen Rathje from the University of Texas at Austin, Dr. Robert Youngs from Wood, and Drs. Cliff Munson, Thomas Weaver, Jon Ake and Scott Stovall from the Nuclear Regulatory Commission.

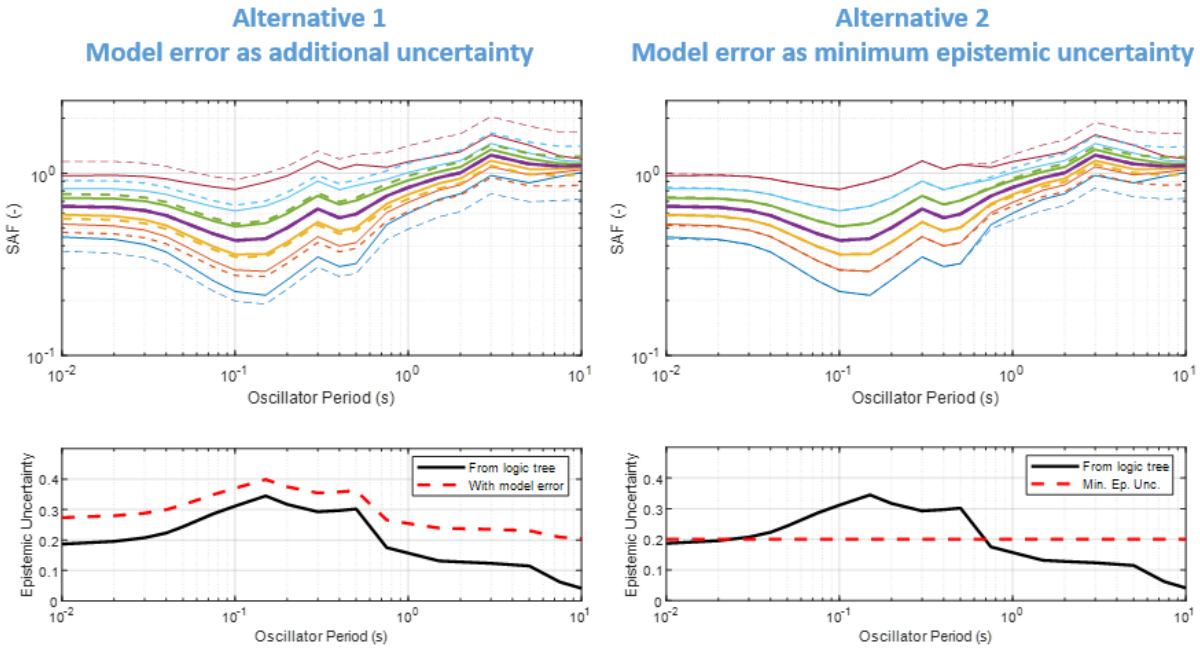

Figure 4. Alternative approaches for capturing model error Left: model error as an additional epistemic uncertainty. Right: model error as minimum epistemic uncertainty.

REFERENCES

Al Atik L. and Abrahamson N.A. (2021). A methodology for the development of 1D reference V_S profiles compatible with ground-motion prediction equations: Application to NGA-West2 GMPEs: *Bulletin of the Seismological Society of America* **111**(4), 1765-1783.

Atkinson G.M., Bommer J.J. and Abrahamson N.A. (2014). Alternative approaches to modeling epistemic uncertainty in ground motions in probabilistic seismic-hazard analysis. *Seismological Research Letters* **85**(6), 1141-1144.

Bahrampouri, M. and Rodriguez-Marek, A., 2023. One-Dimensional Site Response Analysis: Model Error Estimation. *Bulletin of the Seismological Society of America*, **113**(1), pp.401-416.

Boore D.M,. Youngs R.R., Kottke A.R., Bommer J.J., Darragh R., Silva W.J., Stafford P.J., Al Atik L., Rodriguez-Marek A. and Kaklamanos J. (2022). Construction of a ground-motion logic tree through host-to-target region adjustments applied to an adaptable ground-motion prediction model. *Bulletin of the Seismological Society of America,* **112**(6):3063-3080.

Idaho National Laboratory (2022). *Idaho National Laboratory sitewide SSHAC Level 3 probabilistic seismic hazard analysis*, Report No. INL/RPT-22-70233, 2487 p.

Miller III, A.C. and Rice, T.R. (1983). Discrete approximations of probability distributions. *Management science*, **29**, 352-362.

Rodriguez-Marek A., Bommer J.J., Youngs R.R., Crespo M.J., Stafford P.J. and Bahrampouri M. (2021a). Capturing epistemic uncertainty in site response, *Earthquake Spectra* **37**(2), 921-936.

Rodriguez-Marek, A., Cotton, F., Abrahamson, N., Akkar, S., Al Atik, L., Edwards, B., Montalva, G.A., and Dawood, H.M. (2013). "A model for single-station standard deviation using data from various tectonic regions." *Bull. Seism. Soc. Am.* **103**, 3149-3163.

Rodriguez-Marek, A., Rathje, E., Ake, J., Munson, C., Stovall, S., Weaver, T., Ulmer, K., and Juckett, M., 2021b, *Documentation Report for SSHAC Level 2: Site Response: Office of Nuclear Regulatory Research*, Research Information Letter RIL2021-15, November, 217 p.

Stewart, J. P., and Afshari, K. (2021). Epistemic uncertainty in site response as derived from one-dimensional ground response analyses. *Journal of Geotechnical and Geoenvironmental Engineering*, **147**(1), 04020146.

Williams, T. and Abrahamson, N. (2021). Site-response analysis using the shear-wave velocity profile correction approach. *Bulletin of the Seismological Society of America* **111**(4), 1989-2004.

Day1 (Monday, Sep. 25th, 2023) 16:45~17:20

Geotechnical Insights: Lessons Learned from the 2022 M_L 6.8 Chihshang Earthquake, Taiwan

Chi-Chin Tsai

Professor, National Chung Hsing University, Taichung, Taiwan

Dr. Tsai is a distinguished professor of the Department of Civil Engineering at National Chung Hsing University. He also holds the position of editorial manager for the Journal of Earthquake Engineering. Dr. Tsai obtained his Bachelor and Master degrees in 1999 and 2001, respectively, from National Taiwan University. He completed his Ph.D. at the University of Illinois at Urbana-Champaign in 2007. Prior to joining National Chung Hsing University in 2012, Dr. Tsai worked as a senior project engineer at URS, USA. Dr. Tsai's research focuses on geotechnical earthquake engineering, encompassing areas such as soil dynamics, soil liquefaction, site effect/site response analysis, and seismic slope stability assessment. In recognition of his expertise, Dr. Tsai was awarded the prestigious Humboldt Research Fellowship for Experienced Researchers in 2018. He utilized this fellowship to engage in research projects at the Bauhaus University in Weimar and Ruhr University Bochum, Germany.

GEOTECHNICAL INSIGHTS: LESSONS LEARNED FROM THE 2022 M_L 6.8 CHIHSHANG EARTHQUAKE, TAIWAN

Chi-Chin Tsai[1] and Yung-Yen Ko[2]
1. Professor, National Chung Hsing University, Taichung, Taiwan
2. Associate Professor, National Cheng Kung University, Tainan, Taiwan
Email: tsaicc@nchu.edu.tw, yyko@mail.ncku.edu.tw

ABSTRACT

On September 18, 2022, a powerful earthquake measuring a local magnitude (M_L) of 6.8 struck the southern part of Longitudinal Valley in southeastern Taiwan, causing severe damage and collapse of a number of engineering structures. This paper presents the findings of a comprehensive field reconnaissance conducted at selected sites affected by building and bridge damages. The study focuses on the geotechnical aspects, including strong ground motion, ground rupture, soil liquefaction, and their impact on the performance of engineering structures. The earthquake induced ground motions of up to 0.6 g, with similar intensities in both vertical and horizontal directions near the epicenter. Widespread ground rupture traces were observed along the officially recognized active faults, resulting in offsets of several tens of centimeters. Soil liquefaction was also prevalent in certain regions, particularly in the gravel layers of the river flood plain. The potential influence of these observed geotechnical characteristics on the damage patterns and failure modes of buildings, bridges, embankments, and levees was thoroughly discussed and interpreted. The insights presented in this paper serve as valuable references for future disaster prevention and mitigation efforts.

Keywords: 2022 Chihshang Earthquake, reconnaissance, ground rupture, soil liquefaction, embankment and levee damage

INTRODUCTION

On September 18, 2022, the southern part of Longitudinal Valley in Taiwan experienced a significant earthquake with a local magnitude (M_L) of 6.8 or a moment magnitude (M_W) of 6.9 at 14:44:15 local time. The epicenter was located in Chihshang Township, Taitung County. This earthquake was the largest inland crustal earthquake in Taiwan since the 1999 Chi-Chi earthquake with a M_W of 7.6. Despite the high seismic intensity, the damage caused by this earthquake was relatively limited due to the less populated area around the epicenter, resulting in one fatality and fewer than 200 injuries. Ground rupture traces were widespread along the Yuli and Chihshang faults, contributing to damages in buildings, pipelines, embankments, and bridges. The geotechnical and structural damages were studied by a survey team from various universities, focusing on building and bridge failures, ground rupture, foundation bearing capacity, and unexpected soil liquefaction in the gravelly alluvium of the Hualien-Taitung Longitudinal Valley (Ko, et al., 2023). The failure of geotechnical structures such as road embankments and levees were also investigated. This paper provides an overview of the earthquake event, including its strong motion characteristics and impact on engineering structures. Additionally, it presents the findings from the field reconnaissance, highlighting ground rupture, soil liquefaction, specific damage details, and insights gained from the study for future disaster prevention and mitigation efforts.

STRONG GROUND MOTION

Figure 1 shows the shake map of the Chihshang earthquake, indicating PGA and PGV, along with active faults in the region. PGA ranges from 0.3-0.5g in most areas reported with damages. Figure 2 displays velocity time histories at four selected seismic stations, showing distinct near-fault velocity pulses with periods of 1.65-4.4 seconds. Some records exhibit similar vertical and horizontal PGA values, indicating near-fault behavior. PGV along the Longitudinal Valley ranges from 50-100 cm/s, with most records showing higher values in the north-south direction, suggesting earthquake directivity.

Multiple failures occurred during the earthquake due to strong motion and a high vertical component. In Yuli Township, a three-story building collapsed, while a temple experienced floor collapse and punching shear failure. Gaoliao Bridge and Luntian Bridge both collapsed, with Gaoliao Bridge suffering shear failure of columns and Luntian Bridge experiencing pier separation from the foundation and overturning. The New Xiuguluan River Bridge underwent significant lateral displacement, damaging power lines and distorting the rail track. These failures highlight the influence of vertical motion on structures and emphasize the need for considering it in seismic design and assessment.

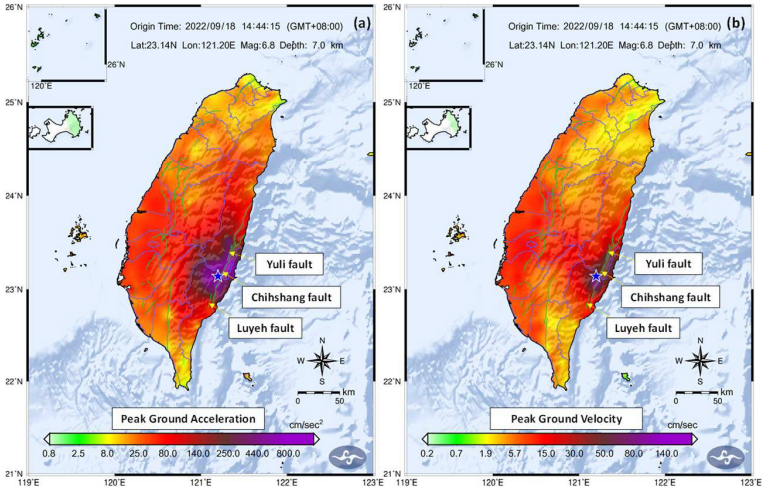

Figure 1. Shake map in terms of PGA (left, in g) and PGV (right, in cm/s) (CWB, 2022).

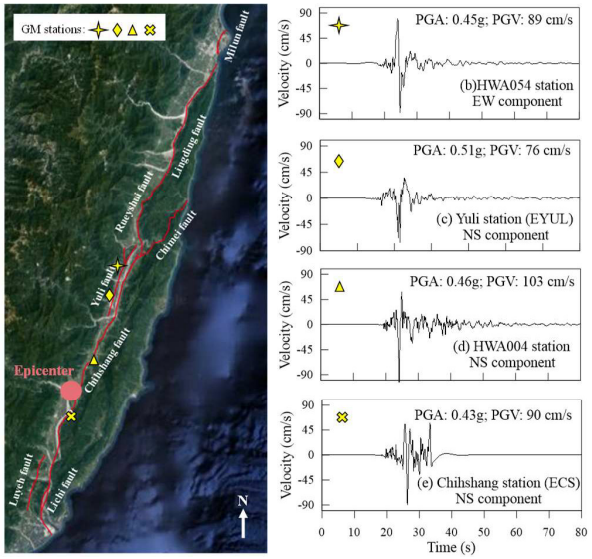

Figure 2. Pulse-like velocity time histories at selected seismic stations.

GROUND RUPTURE

Figure 3 illustrates the locations of ground rupture traces observed following the Guanshan-Chihshang earthquake sequence, as compiled by the Central Geological Survey (CGS) in Taiwan. The officially published fault lines of the Yuli and Chihshang active faults are also shown. According to CGS (2022) and their field investigation and interviews with residents, the majority of ground rupture traces were caused by the Chihshang mainshock. However, the traces observed south of Guanshan to Luyeh were induced by the Guanshan foreshock.

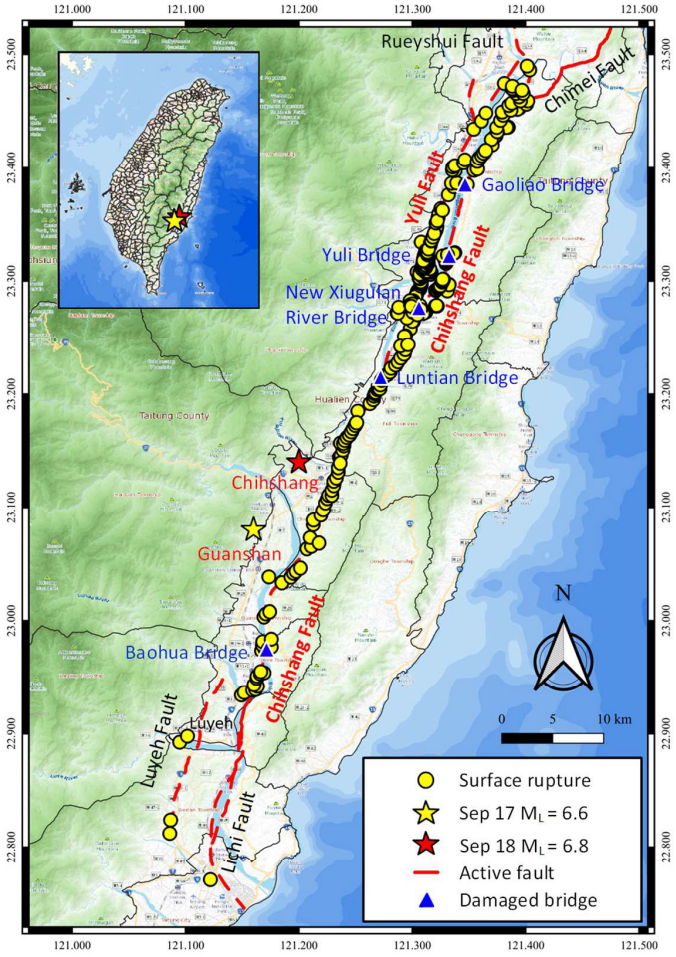

Figure 3. The locations of ground surface rupture and damaged bridges during the earthquake [after Lin (2022) and CGS (2022)].

The Yuli fault caused ground ruptures in the downtown area of Yuli Township, resulting in damage to buildings and breaks in potable water pipelines. However, the damage was not severe as the ground offsets were small, and no direct building collapses occurred. Common damages included ruptures and cracks in partition brick walls and the first-floor slab. Beams and columns had minor repairable cracks due to their reinforced structure. However, one single-family house near the collapsed Luntian Bridge experienced significant shear failure in its walls and columns, likely due to strong motions (PGA = 0.4g) and exacerbated by a ground rupture trace passing through the floor slab.

The collapse of Gaoliao and Luntian Highway Bridges, as well as the serious damage to the New Xiuguluan River Railway Bridge, was primarily caused by strong ground motions rather than ground ruptures. The Yuli Highway Bridge and the Yufu Bicycle Trail Bridge were surveyed, revealing an offset in the Yufu Bicycle Trail Bridge due to long-term fault creep. However, no new misalignment was observed on the bridge deck. Damage to the Yuli Highway Bridge was limited to certain expansion joints on the westbound bridge, caused by compression and collision induced by longitudinal excitation. A similar phenomenon was observed at the east end of the Yufu Bicycle Trail Bridge, where the old rail buried underneath the pavement buckled due to longitudinal compression.

Baohua Bridge in Luyeh Township, Taitung experienced fault-rupture induced damage during the Guanshan earthquake. Significant horizontal offsets occurred at two expansion joints near the east abutment, breaking the attached potable water pipeline. The bridge section rotated counterclockwise, causing symmetric offsets towards the center. Although a clear fault trace was not observed directly beneath the rotated section, nearby fault traces were identified (CGS, 2022). The localized damage near

the Chihshang fault suggests a connection between the damage and fault rupture. Additionally, cracking was observed in the embankment wall near the west abutment, possibly associated with a fault trace caused by the Guanshan earthquake.

SOIL LIQUEFACTION

In general, the alluvium in Hualien-Taitung Longitudinal Valley is considered less liquefiable because it is mainly composed of gravel layers. Nevertheless, soil liquefaction was observed at several locations. Although soil liquefaction is probably not the dominant cause of failure of engineering structures mentioned previously, we noticed that it was still influential to the failure mode of some of the bridge failure cases. Soil liquefaction was mostly observed in areas with sandy material near the river flood plain. Small to moderate-scale sand boils, characterized by sand eruption from ground surface cracks or vents, were found near bridges such as Yuli Bridge, Gaoliao Bridge, and Baohua Bridge. The ejecta varied in grain size and color, suggesting different local soil conditions.

At New Xiuguluan River Bridge, sand eruption occurred at pier #12 (Figure 4a), and ground surface subsidence was observed around neighboring pier #13. Soil liquefaction around bridge piers was localized, likely due to the dynamic response of the bridge structure and cyclic lateral movement of the foundation induced by intense ground motion, leading to excess pore water pressure and localized liquefaction. During the earthquake, the New Xiuguluan River Bridge experienced significant displacement of its superstructure from pier #11 to pier #1. Short columns on the cap beams of some piers were damaged. However, pier #12, despite soil liquefaction, had minimal lateral displacement and intact short columns. The superstructure on pier #13, on the other hand, had an eastward displacement of about 90 cm. Possible reasons for the limited displacement of pier #12 include significant liquefaction reducing lateral resistance and acting as an isolator, or the left-lateral slip along the Chihshang fault, with pier #12 acting as a pivot. Further study is needed to confirm these explanations.

Figure 4. Signs of soil liquefaction around pier foundations of (a) New Xiuguluan River Bridge pier #12 (view from the east side) (b) Gaoliao Bridge that is tipping-over

Most of the piers of Gaoliao Bridge were structurally demolished during the earthquake. However, one pier tipped over while its column remained undamaged. The foundation type of this pier is uncertain, but it is likely a monopile or shaft foundation commonly used in cross-river bridges in Taiwan during the 1980s and 1990s. The tipping over was likely caused by liquefaction of the surrounding soil, resulting in a loss of lateral and rotational resistance (Figure 4b). Another pier also experienced tipping over, although the liquefaction around its foundation was less significant.

EMBANKMENT AND LEVEE DAMAGE

The typical damage of the Gaoliao bridge ramp embankment includes tension cracks on the road, differential settlements, and wall movements. Two main tension cracks developed parallelly and

continuously along the longitudinal direction of the embankment as shown in Figure 5. However, the location of these cracks varies with the height of wall and vanishes or becomes very minor as wall height is less than 3 m. A comparison of the wall and culvert positions revealed a rational movement of the north wall as indicated by increasing movement with wall height. A section on the north side of the east wing of the embankment wall collapsed, spanning a length of 32 m along the main crack. The adjacent walls remained intact but experienced rotation and tilting of approximately 5 degrees. A secondary crack formed due to progressive failure after the initial collapse, and the debris of loose compacted fill (controlled low strength material, CLSM) piled up at a repose angle of approximately 23 degrees.

Minor damage was observed on the levee section along the Xiuguluan River, specifically south of the west ramp of Gaoliao Bridge. The 3 m high levee embankment with a 5 m wide crest exhibited several longitudinal cracks on the concrete facing and the access road. The damage, spanning over 400 m, was likely caused by insufficient bearing capacity of the soft foundation under strong motion, resulting in rotation/sliding of the slope face, subsidence of the crest, heave at the toe, and the development of cracks. A similar damage mechanism was observed in other earthquake events, such as the 2011 Great East Japan Earthquake and the 2016 Meinong earthquake. While there was no evidence of liquefaction, the fill material of the levee may have had inadequate strength or experienced degradation due to intense cyclic excitation.

Figure 5. Overview of ramp embankments at east and west wings of Gaoliao Bridge

CONCLUSIONS

This paper summarizes a reconnaissance conducted after the 2022 M_L 6.8 Chihshang, Taiwan earthquake. It focuses on sites in southern Hualien and northern Taitung and discusses the damage caused by ground rupture and soil liquefaction to buildings, bridges, and embankments. The findings highlight the need to consider vertical ground motion in bridge design and the importance of reinforcing non-structural elements and brick buildings for seismic resilience. Flexible pipeline parts and mechanically stabilized earth (MSE) walls are recommended for areas near fault zones prone to rupture and strong motions. Soil liquefaction was observed mainly on river flood plains, with signs of significant sand eruption near certain piers. The Hualien-Taitung Longitudinal Valley, though composed of less liquefiable gravel layers, still showed vulnerability to liquefaction in weak sandy deposits with high gravel content. Localized liquefaction near piers affected the structural failure modes, emphasizing the need to consider the complex soil-structure interaction and cyclic degradation in seismic design. The

embankment damage at Gaoliao Bridge and the levee section indicated the importance of proper compaction or reinforcement of fill materials to mitigate settlement and cyclic degradation. The failure mechanism of structures experiencing combined ground deformation and strong ground motion warrants further investigation.

ACKNOWLEDGMENTS

The authors would like to express their sincere thanks to Prof. Jin-Hung Hwang (National Central University), Prof. Yu-Wei Hwang (National Yang Ming Chiao Tung University), Prof. Louis Ge (National Taiwan University), and Dr. Min-Chien Chu (National Chung Hsing University)for their support and advice during the reconnaissance.

REFERENCES

CGS (2022) Geological investigation report on 20220917 Guanshan earthquake and 20220918 Chihshang earthquake. Central Geological Survey (CGS), Ministry of Economic Affairs, Taiwan. https://faultnew.moeacgs.gov.tw/Reports/More/63cc5a4b2020403d9f79d3c33a7aba0c. Accessed 31 March 2023 (in Chinese)

CWB (2022) Earthquake report: Earthquake No. 111 in 2022b. Central Weather Bureau (CWB), Ministry of Transportation and Communications, Taiwan, R.O.C. Accessed 7 November 2022b (in Chinese)

Lin CW (2022) Geological investigation of September 18, 2022 Chihshang earthquake, Lecture Note, Seminar on the 2022/09/18 Chihshang Earthquake Sequence on 18 October, 2022, Taipei, Taiwan

Ko, YY., Tsai, CC., Hwang, JH. et al. (2023) “Failure of engineering structures and associated geotechnical problems during the 2022 M_L 6.8 Chihshang earthquake, Taiwan,” *Nat. Hazards*, https://doi.org/10.1007/s11069-023-05993-0.

PROCEEDINGS

DAY 2

Proceedings: Day 2

Day 2 (Tuesday, Sep. 26th, 2023)				
09:00~09:35	Presentation Session 5	Prof. Jack P. Moehle	Design of Thick Foundation Mats with Special Attention on Shear Strength	page 79
09:35~10:10		Prof. Hanbin Ge	Advances in Seismic Resilience Improvement for Urban Aboveground and Underground Structures	page 86
10:30~10:55	Presentation Session 6	Prof. Tony Yang	Performance-Based Earthquake Engineering from Theory to Implementation to the Future	page 93
10:55~11:20		Prof. Carlos Ventura	Understanding Ground Motions and their Relation to Structural Damage	page 100
11:20~11:45		Prof. Murat Saatcioglu	Innovative Solutions for Seismic Retrofit of Non-Ductile Construction	page 107
11:45~12:10		Dr. Chung-Pi Luan	Introduction to the Policy of Net-Zero Building Among the Net-Zero Transition	page 114
13:20~13:45	Presentation Session 7	Dr. Trevor Nightingale	Key Issues in Decarbonizing the Built Environment	page 115
13:45~14:10		Prof. Sheryl Staub-French	A Review of Digital Transformation Efforts and Initiatives in Canada's Built Asset Industry	page 116
14:10~14:35		Prof. David Lau	New Shake Table Testing Facility for Structures and Non-structural Components	page 118
15:05~15:40	Presentation Session 8	Prof. Andres Winston Oreta	Integration of Technology in Earthquake Engineering Education: A Pathway to Enhancing Learning and Preparedness	page 124
15:40~16:15		Prof. Yi-Lung Mo	Where Do We Stand on Metamaterial-Based Seismic Design of Engineering Structures	page 133
16:15~16:50		Prof. Andrew S. Whittaker	Seismic Isolation of Advanced Reactors - A Pathway to Standardization and to Climate Targets	page 140
16:50~17:25		Dr. Daan Liang	Enabling and Accelerating Community-Based Innovation in Disaster Resilience – A US Perspective	page 147

Day2 (Tuesday, Sep. 26th, 2023) 09:00~09:35

Design of Thick Foundation Mats with Special Attention on Shear Strength

Jack P. Moehle

Professor of the Graduate School, University of California, Berkeley

Jack Moehle is a Professor of the Graduate School in Civil and Environmental Engineering at UC Berkeley. Moehle's research focuses on structural engineering, earthquake engineering, and reinforced concrete. Moehle is a member of several professional organizations, including the prestigious National Academy of Engineering, ACI 318 Building Code Committee, an Honorary Member of the American Concrete Institute & Earthquake Engineering Research Institute, and a Fellow of the Structural Engineering Institute of ASCE. He is also a recipient of several notable accolades, including the George W. Housner Medal from the Earthquake Engineering Research Institute in 2020, the Joe W. Kelly Award from the American Concrete Institute in 2019, and the ACI Wason Medal for Most Meritorious Paper for "Moment Transfer at Column-Foundation Connections: Physical Tests" in 2023.

DESIGN OF THICK FOUNDATION MATS WITH SPECIAL ATTENTION ON SHEAR STRENGTH

Jerry Zhai[1] and Jack P Moehle[2]
1. Ph.D. Candidate, University of California, Berkeley
2. Professor of the Graduate School, University of California, Berkeley
Email: jerryzhai@berkeley.edu, moehle@berkeley.edu

ABSTRACT

The shear stress at failure of concrete elements without shear reinforcement decreases with increased member depth in accordance with the size effect, which is particularly sensitive in foundation mats. This paper summarizes seven beam tests conducted at UC Berkeley that show the extent of the size effect in beams with high-strength longitudinal reinforcement. It also addresses key design considerations for foundation mats with and without shear reinforcement. Tests show that minimum shear reinforcement greatly increases the shear strength, while tests without shear reinforcement show a clear size effect that should be considered when designing thick mats.

Keywords: Mat Foundations, Shear, Size Effect, High Strength Reinforcement, UC Berkeley

INTRODUCTION

Mat foundations are commonly used for high-rise buildings on the West Coast of the United States. During large seismic or wind events, these mass concrete elements must resist immense forces from the overturning moments due to lateral load. Traditionally, mat foundations have been designed to avoid the need for shear reinforcement by sizing them deep enough to accommodate the shear demands, and then placing sufficient longitudinal steel to meet the moment demands. The potential for substantially reduced shear strength due to the size effect may make this traditional design approach uneconomical.

Under ACI 318-14 and prior versions of the code, mat foundations without shear reinforcement were permitted to use $2.0\sqrt{f_c'}$ psi ($0.17\sqrt{f_c'}$ MPa) as its unit one-way shear strength. Buildings adopting performance-based approaches on the other hand typically used $1.0\sqrt{f_c'}$ psi ($0.083\sqrt{f_c'}$ MPa) to account for the size effect, which refers to the decrease in unit shear strength with increasing member depth. In the 2019 update to ACI 318, the effects of size and low longitudinal reinforcement ratio (ρ) were recognized in the revised one-way shear equations. The combination of large depth and low ρ commonly pushes unit shear strengths in mat foundations down to $0.5\sqrt{f_c'}$ psi ($0.041\sqrt{f_c'}$ MPa) or even lower depending on ρ and mat thickness. Prior to the tests conducted at UC Berkeley in 2021, only two beams without shear reinforcement of depths representing foundation mats were tested. These tests reported unit shear strengths of $0.7\sqrt{f_c'}$ psi ($0.06\sqrt{f_c'}$ MPa) by Shioya et al. (1984) and $0.8\sqrt{f_c'}$ psi ($0.07\sqrt{f_c'}$ MPa) by Collins et al. (2015), much lower than the permissible $2.0\sqrt{f_c'}$ psi ($0.17\sqrt{f_c'}$ MPa) and lower than the $1.0\sqrt{f_c'}$ psi ($0.083\sqrt{f_c'}$ MPa) adopted in performance-based approaches.

Most research on shear is conducted via beam tests, the results of which require interpretation for a foundation. In a foundation, the shear forces may partially be mitigated by arch action between points of applied load above the mat and points of support in the soil (Uzel, 2011). However, this mechanism does not apply at points about 1.5 mat thicknesses away from the applied loads and decreases in effectiveness for sufficiently soft soils. The scatter in strength predictions by different approaches, and concerns of further reductions on shear strength due to emerging use of high-strength reinforcement in foundations, prompted the research at UC Berkeley into full depth mat foundations.

UC BERKELEY TEST SPECIMENS 1 AND 2

Test beam 1 is configured like that of a mat foundation and loaded in symmetrical 3-point bending plus

self-weight, with details in Figure 1. The overall dimensions of this beam are 76 ft (23.2 m) long, 140 in (3.6 m) deep, and 10 in (0.25 m) wide, with supports centered at 3 ft (0.91 m) from each end. The beam is divided into two tests designated Phase 1 and Phase 2 on opposite sides of the loading point at midspan. Each side of the beam has the same shear span to depth ratio (a/d = 3.23) but different reinforcement configurations, requiring different applied loads to fail each side. All longitudinal steel is ASTM A1035 Gr. 100 steel, which exhibits 120 ksi (830 MPa) yield strengths. Concrete compressive strengths from cylinder testing yielded 4600 psi (32 MPa) for both Phase 1 and Phase 2 testing.

The beam is monotonically loaded until failure is reached on the weaker right side by design, which is referred to as Phase 1. Phase 1 has no shear reinforcement and a reinforcing ratio of 0.45%, which is representative of a typical mat foundation reinforcement ratio. The low reinforcement ratio results in relatively high longitudinal steel stresses during shear failure. Following a shear repair and moment strengthening procedure where the shear and moment strengths on Phase 1 are increased, the beam is reloaded until failure is reached on the opposite span (Phase 2). Phase 2 has ACI 318-19 minimum shear reinforcement to determine if the size effect is overcome. The shear reinforcement is headed to reduce congestion and verify the effectiveness of headed bars as shear reinforcement.

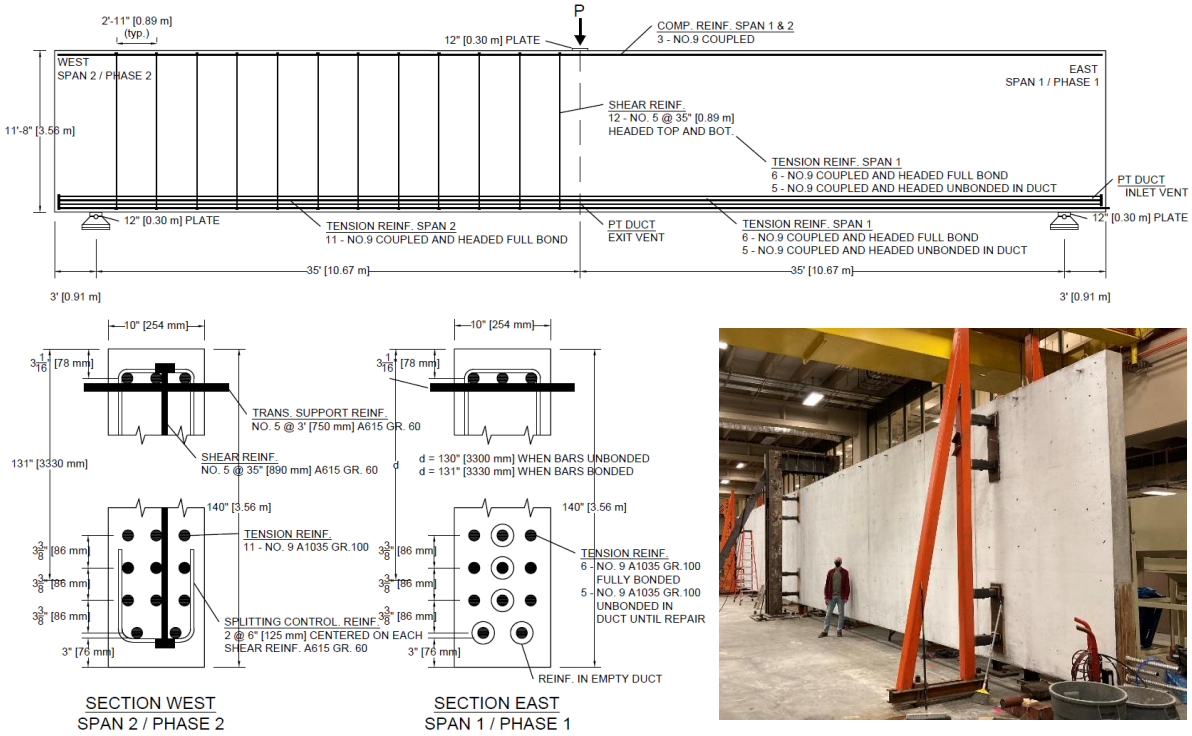

Figure 1: UCB Beam 1 specimen details for Phase 1 and Phase 2.

The second specimen was designed based on the findings of Test Beam 1 and pressing questions from the profession regarding differences between shear in beams and shear in foundations. As shown in Figure 2, the beam is 73.5 ft (22.4 m) long, 96 in (2.44 m) deep, and 10 in (0.25 m) wide. The beam is reinforced uniformly on both spans using the same Gr. 100 steel as Test Beam 1. This reinforcement was installed at a very low ratio of 0.22%, which is just above the minimum ratio of 0.18% for footings to represent very lightly reinforced footings that are still code permissible. Concrete compressive strengths were 4600 psi (32 MPa) and 5000 psi (34 MPa) for Phase 3 and Phase 4 respectively.

The testing conditions for Phase 3 are similar to the conditions of a mat foundation. During an earthquake, the soil pressure distribution under the compression side of the mat will vary depending on relative stiffness of the soil and foundation. A uniform soil pressure is representative for common conditions encountered on the West Coast of the United States. To replicate this condition, the west span representing Phase 3 was loaded with a line of jacks that applied equal upward force, applied through a force-distributing medium, with the midspan and the opposite end pinned as shown for Phase 3 in Figure

2. Following failure of the Phase 3 span, a shear repair was conducted so that further loading in 3-pt bending results in failure on the Phase 4 span.

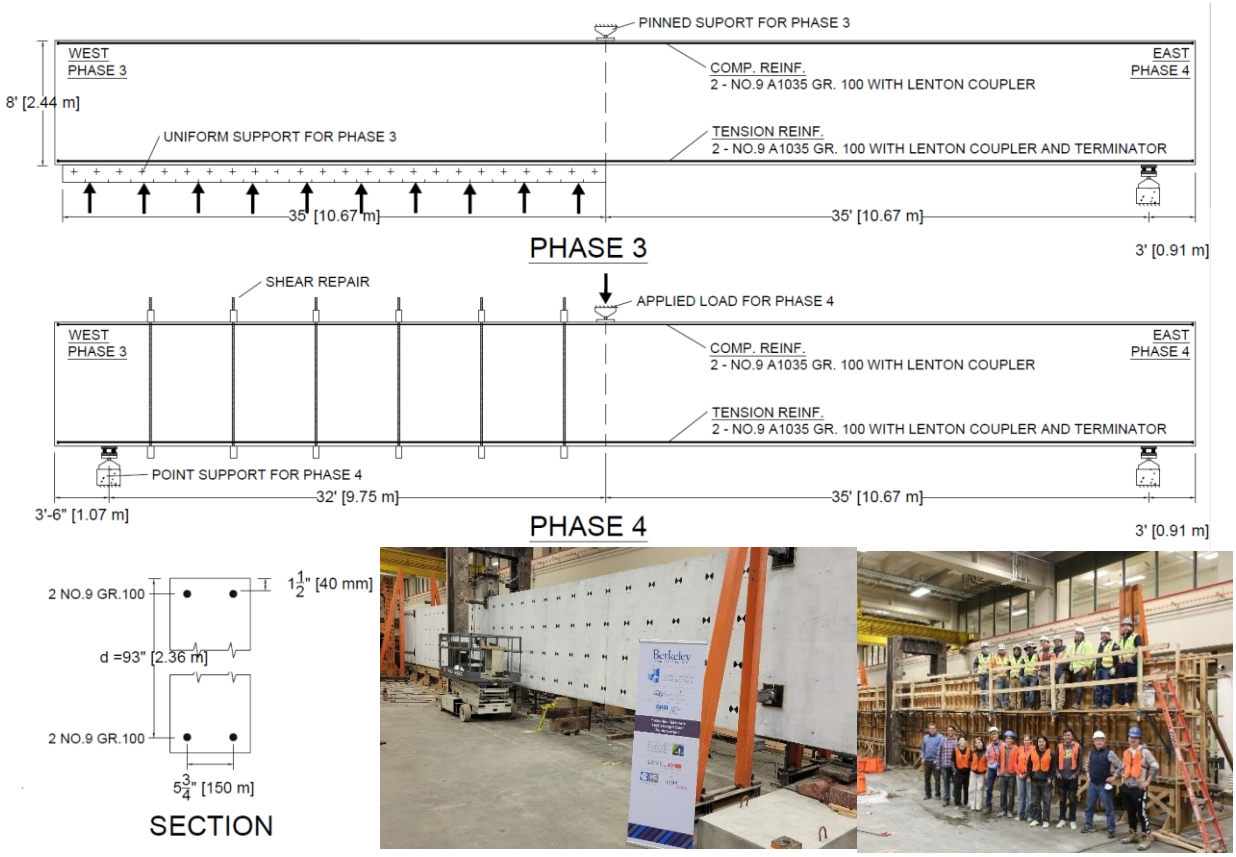

Figure 2: UCB Beam 2 specimen details and loading configurations for Phase 3 and Phase 4.

Results of phase 1 and phase 2

Phase 1 is the test of a beam without shear reinforcement. Figure 3 shows the measured relationship between midspan applied force P and midspan deflection. Following the formation of the first flexural cracks at LS1, the slope of the load-displacement curve decreases but maintains a somewhat linear relationship all the way up to failure at LS7a. Between these points, cracks progressively form on the bottom of the tension face as flexural cracks grow vertically at first, then incline towards the loading point when shear stresses increase, eventually reaching the beam failure state in Figure 4.

At LS7a, East Crack 1 had reached a width of approximately 0.1 in (3 mm), indicating significant reduction in the shear-carrying capacity along that inclined crack. The steel strains along the span at failure also show significant tension shift, with the tensile strains remaining nearly constant for much of the Phase 1 span. This effect may be important to consider if bar cutoffs are included in the construction of mat foundations. Over the relatively small increase in vertical displacement from LS7a to LS7b, an irrecoverable reduction in the load-carrying capacity was observed along with the rapid formation of East Crack 2. With a sharp cracking sound, this crack formed rapidly and grew to about 0.2 in (5 mm) in width while slipping by 0.08 in (2 mm) along the crack plane. In contrast, East Crack 1 did not slip appreciably. As shear slip is necessary for shear forces to be carried at large crack widths, it was determined that East Crack 2 was unlikely to have additional capacity and the test was stopped to preserve the integrity of the compression zone so that the beam could be repaired more readily.

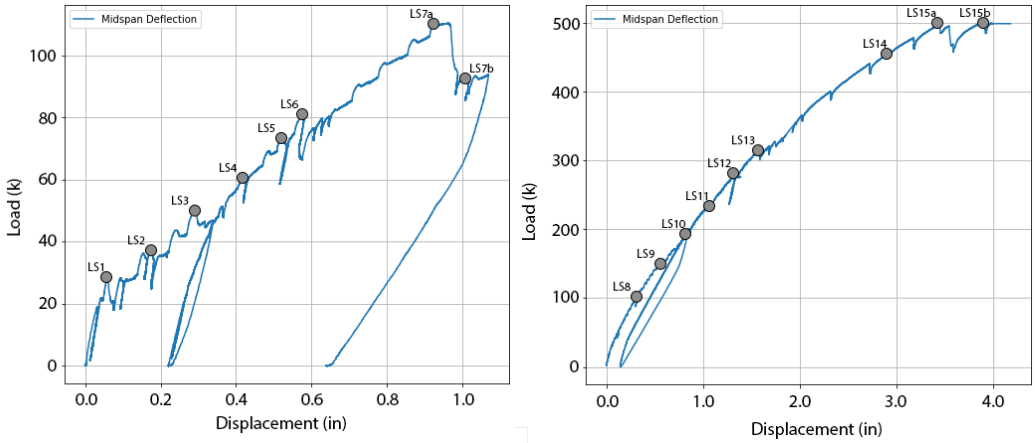

Figure 3: Load displacement response at midspan of Phase 1 (left) and Phase 2 (right).

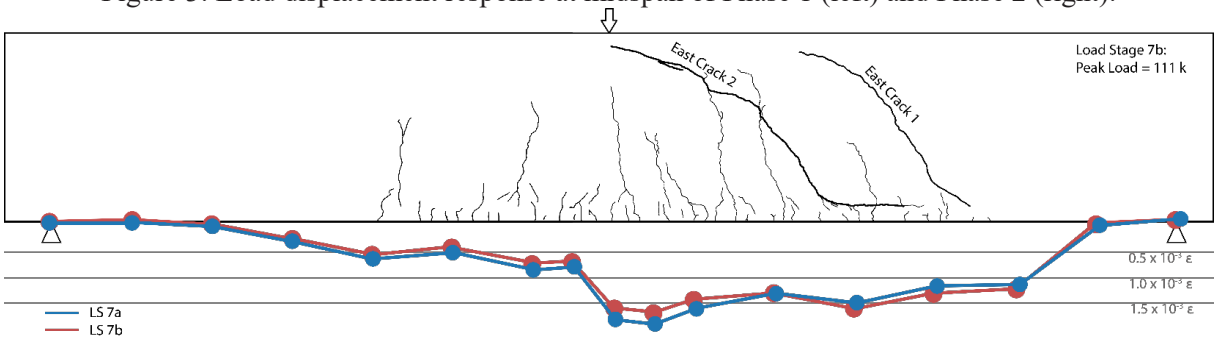

Figure 4: Phase 1 state at failure with reinforcement strains at LS7a and LS7b

Following a repair procedure whereby the moment and shear strength of Phase 1 is increased, the beam is reloaded in the same configuration to induce a shear failure in the opposite span for Phase 2. The presence of just twelve No. 5 bars evenly spaced over 35 ft (s = 35 in (890 mm)) increased the failure load to 4.6 times the failure load of Phase 1 (Figure 3). The shear reinforcement also allows for multiple load paths, resulting in a more complex and well distributed crack pattern (Figure 5) when compared with Phase 1. This also mutes the large tension shift effect observed in Phase 1. Evidence from the test showed that the size effect is suppressed when minimum shear reinforcement is used, allowing the concrete contribution to shear strength V_c to reach close to $2.0\sqrt{f_c'}$ ($0.17\sqrt{f_c'}$ MPa).

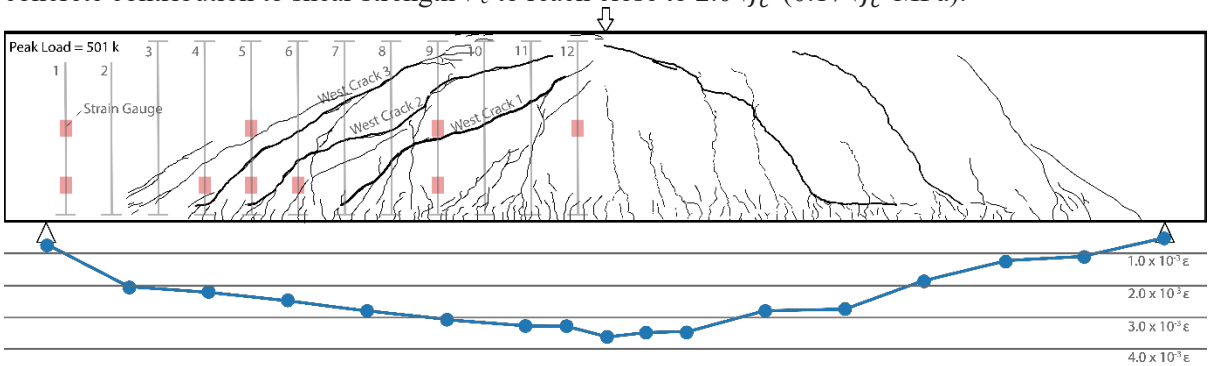

Figure 5: Phase 2 state at failure with reinforcement strains at LS15a.

RESULTS OF PHASE 3 AND PHASE 4

The load displacement plot for Phase 3 and Phase 4 are presented in Figure 6. The y-axis for Phase 3 should be interpreted as the vertical applied load that is resolved by a uniform support reaction on the left and a point support on the right. For Phase 3, displacements are measured at the tip of the beam as Phase 3 is loaded as an upside-down cantilever. Phase 4 is tested using a point load in 3-pt bending with displacements recorded at midspan. To connect the results of Phase 3 to Phase 4 for the east span, displacement and load data from the uniform load in Phase 3 are transformed into an equivalent point

load response. This results in the equivalent midspan load on the y-axis starting at -22 k (-98 kN) as less self-weight is carried on the right support in Phase 3 than in Phase 4.

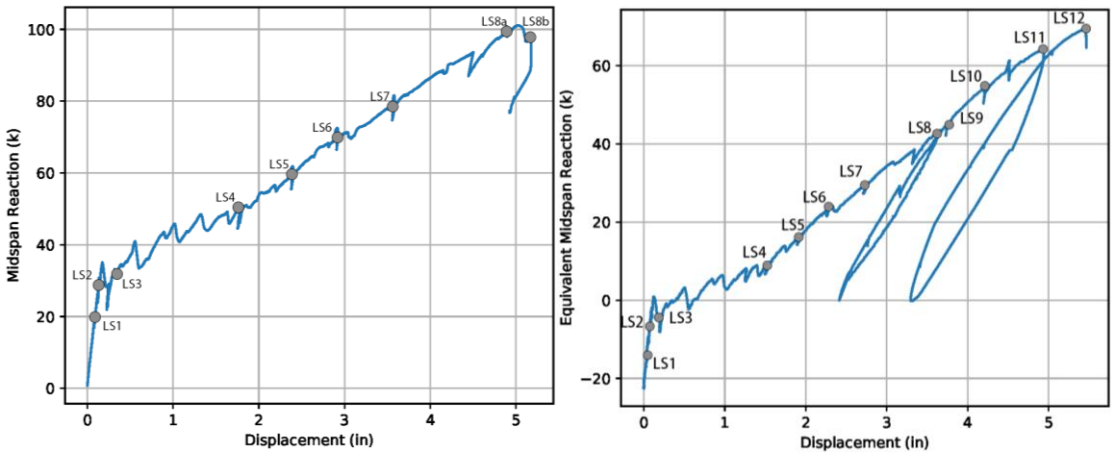

Figure 6: Load displacement response of Phase 3 (left) and Phase 4 (right).

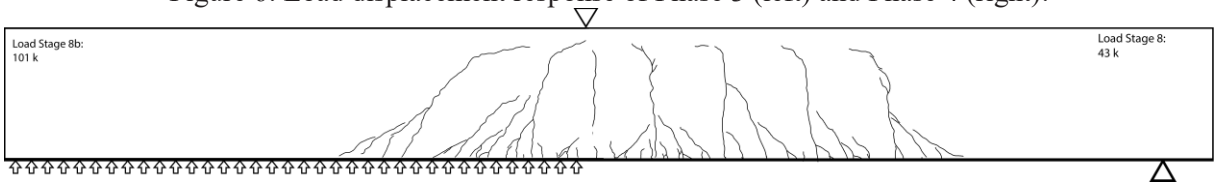

Figure 7: Phase 3 cracked state at failure.

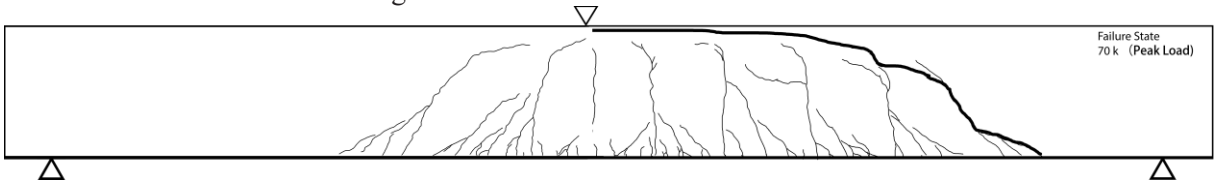

Figure 8: Phase 4 cracked state at failure.

The shear span for both Phase 3 and Phase 4 was 35 ft (10.7 m) to provide a direct comparison between the shear response of a beam versus a footing. During Phase 3 loading on the west (left) span in Figure 7, the uniform load results in cracking only in the vicinity of the top restraint. In direct comparison with this, the opposite side, representative of a beam, has multiple flexural cracks distributed evenly along the shear span. Despite the observed differences in the crack pattern, failure of Phase 3 and Phase 4 occurs at very similar sectional shear forces. Failure of Phase 3 occurred with the formation of the left-most crack, corresponding to a shear of 63.5 k (282 kN) at a section located *d* (93 in = 2.36 m) away from the top restraint in accordance with ACI 318-19 practices. Phase 4 failed along the thick crack in Figure 8, at a similar load of 61 k (271 kN) located a section located *d* away from the right support.

Peak longitudinal steel stresses were 86 ksi (593 MPa) and 113 ksi (779 MPa) in Phase 3 and Phase 4 respectively. Despite the relatively high steel stresses and associated flexural crack widths, the beam did not fail prematurely and carried more load than predicted using calibrated FEM models. It appears that use of high-strength reinforcement does not result in additional penalties on the shear strength when compared with using Gr. 60 steel, even in cases where the observed steel stresses exceed the conventional yield stress of 60 ksi (414 MPa) for Gr. 60 steel.

UC Berkeley Size Effect Series

In addition to the above tests, 3 smaller specimens of 3 ft, 2 ft, and 1 ft (914 mm, 610 mm, and 305 mm) depth were tested as companion specimens to the larger beams. The series of 6 tests form a size effect series that illustrates how unit shear strengths decrease with increased depth when high-strength reinforcement is used. This is plotted alongside various other size effect series (Bentz, 2018) in Figure 9. The lines for each size effect series show a clear reduction in unit shear strength with increased size

and show that the "Low Rho Size Effect" series of beams reinforced with Gr. 60 steel at 0.35% is very similar to the "UC Berkeley Size Effect" series using high-strength reinforcement at 0.22%, suggesting that the responses are very similar.

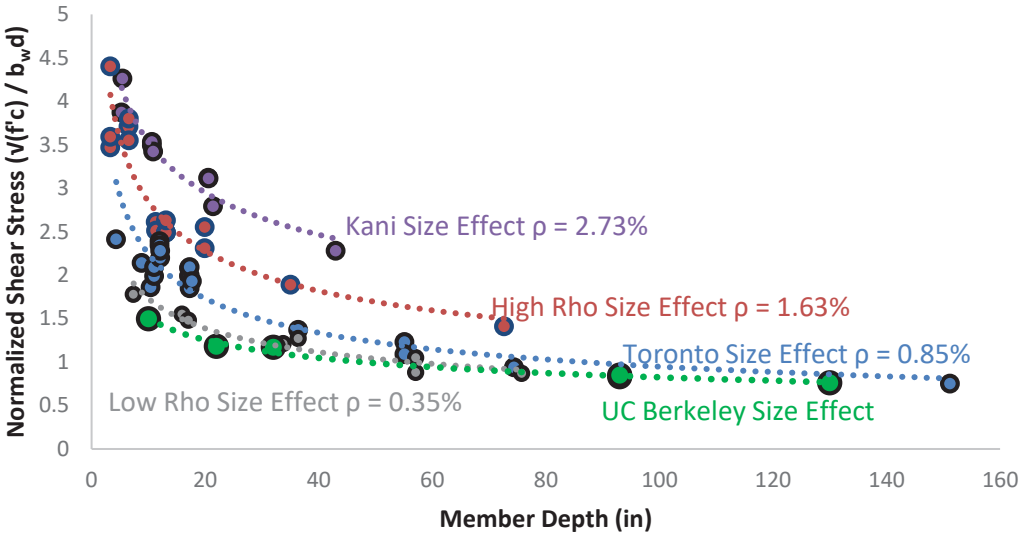

Figure 9: Size effect series for various longitudinal reinforcement ratios (UC Berkeley series in green).

DESIGN RECOMMENDATIONS AND CONCLUSIONS

Seven shear tests were conducted at UC Berkeley on beams with and without shear reinforcement. The findings show a clear size effect when shear reinforcement is not used. The experiments also suggest that shear strength is not sensitive to the use of high-strength longitudinal reinforcement. Minimum shear reinforcement is effective in overcoming the size effect.

The following recommendations are made based on results of the test program:

- ACI 318 minimum shear reinforcement is effective in overcoming the size effects when designing deep mats. Headed shear reinforcement was demonstrated to be effective. There may also be economic or environmental incentives to use shear reinforcement to decrease the mat depth, reducing construction time and concrete quantities.
- If shear reinforcement is absent, the penalties of the size effect and low reinforcement ratio effect on shear strength can be severe, though the combined penalty is not as severe as indicated by ACI 318-19 one-way shear strength equations. A lower bound near $1.0\sqrt{f_c'}$ psi ($0.083\sqrt{f_c'}$ MPa) seems reasonable.
- Where shear reinforcement is not used, conservative bar cutoff locations need to account for the significant tension shift that occurs.

ACKNOWLEDGMENTS

The authors thank the sponsoring agencies and donors Pankow Foundation, ACI Foundation, MKA Foundation, Level 10 Construction, nVent Lenton, Concrete Reinforcing Steel Institute, Cascade Steel Rolling Mills, and Sika Corp for their generous financial, material, and labor donations.

REFERENCES

Bentz, E.C., and Collins, M.P., "The Toronto Size Effect Series," *Symposium Paper*, **328**, 2.1-2.12.

Collins, M.P., Quach, P.T., Bentz, E.C., "Shear Behavior of Thick Slabs," *ACI Structural Journal*, **117**, 115-126.

Shioya, T.; Iguro, M.; Nojiri, Y.; Akiyama, H.; and Okada, T., "Shear Strength of Large Reinforced Concrete Beams," *Symposium Paper*, **118**, 259-280.

Uzel, A., B. Podgorniak, E.C. Bentz, and M.P. Collins (2011). "Design of Large Footings for One-Way Shear," *ACI Structural Journal*, **108**, 131-138.

Day2 (Tuesday, Sep. 26th, 2023) 09:35~10:10

Advances in Seismic Resilience Improvement for Urban Aboveground and Underground Structures

Hanbin Ge

Professor, Department of Civil Engineering, Meijo University, Nagoya, Japan

Dr. Hanbin Ge is a full Professor of Structural Engineering at Meijo University, Japan since 2008, fellow of Japan Society of Civil Engineers (JSCE) since 2013, and member of Engineering Academy of Japan (EAJ) since 2018. He graduated from Huazhong University of Science and Technology, China in 1986, studied for both master and doctor degrees and then worked at Nagoya University, Japan for about 20 years. Professor Ge is co-author of 19 books including seismic design codes and more than 400 journal papers. His research interests include behavior of structural members and systems, with particular emphasis on developing high-performance seismic dampers, seismic and damage control design, seismic performance evaluation, fractural behavior and retrofit of steel and steel-concrete composite structures. Professor Ge received The JSCE (The Japan Society of Civil Engineers) Thesis Award in 1995, The JSCE Structural Engineering Thesis Award in 1999, The JSCE Bridge Engineering Thesis Award (Tanaka Award) in 2016 and 2020.

ADVANCES IN SEISMIC RESILIENCE IMPROVEMENT FOR URBAN ABOVEGROUND AND UNDERGROUND STRUCTURES

Zhiyi Chen[1], Pengfei Huang[2,3], Hanbin Ge[4]

1. Professor, Department of Geotechnical Engineering, Tongji University, Shanghai, China
2. PhD candidate, Department of Geotechnical Engineering, Tongji University, Shanghai, China
3. Visiting scholar, Department of Civil Engineering, Meijo University, Nagoya, Japan
4. Professor, Department of Civil Engineering, Meijo University, Nagoya, Japan

Email: zhiyichen@tongji.edu.cn, pfhuang@tongji.edu,cn, gehanbin@meijo-u.ac.jp

ABSTRACT

The importance of seismic resilient engineering structures is highlighted as it not only reduces the seismic-induced damage during earthquakes but also reduces the time and financial costs associated with post-earthquake recovery, known as robustness and recoverability. Therefore, improving structural seismic resilience has become one of the research hotspots in the structural earthquake engineering. The present paper systematically summarizes the current status of research on seismic resilience for both aboveground and underground structures considering the variations in their damage mechanism and seismic control theory, and highlights the differences in seismic resilience between aboveground and underground structures. It emphasizes that while there has been considerable research on seismic resilience for aboveground structures, the same cannot be said for underground structures, particularly regarding the research on functional recovery. Most resilience designs for underground structures primarily follow those developed for aboveground structures. Given the distinct seismic response characteristics of underground structures, it is imperative to further develop a regional seismic control strategy and functional recovery theory specifically tailored to underground structures.

Keywords: Seismic resilience, underground structures, aboveground structures, seismic resilience design

INTRODUCTION

Strong earthquakes, including the 1995 Kobe earthquake (An et al., 1997; Iida et al., 1996), the 1999 Chi-Chi earthquake (Chang et al., 2004), and the 2008 Wenchuan earthquake (Kawashima et al., 2009), have inflicted severe damage on both aboveground and underground structures. These earthquakes have not only led to numerous casualties and substantial economic losses but have also resulted in a profound impact on economic development. Consequently, ensuring seismic safety for engineering structures has remained a prominent area of global research interest (Huang and Chen, 2021a).

Seismic research on engineering structures should consider not only the casualties and property losses caused by structural damage but also the time and financial costs required for post-earthquake recovery or reconstruction. Take the 1995 Kobe earthquake as an example where the restoration of Daikai Station took a year and cost nearly 10 billion yen (Ma et al., 2022). Recently, seismic research for urban structures has gradually evolved from “performance-based seismic design” to "resilience-based seismic design". Resilience refers to the system's capacity to absorb or endure disturbances while maintaining and restoring its normal functions. A resilience-based seismic design not only focuses on effective resistance to seismic disasters during earthquakes but also emphasizes rapid functional recovery afterward, encompassing the notions of robustness and recoverability. Seismic resiliency can be conceptualized at both city and structure levels, and the present study primarily focuses on the latter. At the structural level, reducing the structural damage and eliminating the post-earthquake residual deformation emerge as two crucial factors for seismic resilience (Miller, 1998). Additionally, there are differences in the seismic control theory between aboveground and underground structures owing to their distinct seismic damage mechanisms. The seismic response of aboveground structures is closely associated with structural vibration characteristics, whereas the seismic response of underground structures is controlled by the surrounding soil and exhibits less sensitivity to structural vibration characteristics (Huang and Chen, 2021b). The current paper presents a systematic and comprehensive

review of the seismic resilience for both aboveground and underground structures, as well as a comparative analysis of resilience theories and measures between the aboveground and underground structures.

SEISMIC RESILIENCE FOR ABOVEGROUND STRUCTURES

There are mainly two approaches to enhance the robustness of aboveground structures. The first approach is to obstruct the propagation path of seismic motion from the ground to structures, and the second approach is to install dampers within structures to reduce seismic responses.

The first approach is achieved by installing isolation bearings between the main structure and its foundation. Various types of isolation bearings, such as lead rubber bearing (LRB) and friction pendulum bearing (FPB) are commonly used. These bearings effectively reduce the horizontal stiffness of the structure and extend its natural period. By adjusting the structural natural period away from the predominant period, the seismic responses of the structure can be reduced.

The second approach is generally achieved by installing hysteretic dampers within structures to dissipate seismic energy concentratedly and thereby reduce structural seismic responses (Figure 1). Commonly used hysteretic dampers include Buckling-Restrained Brace (BRB) (Feng et al., 2021a; Gu et al., 2022; Yang et al., 2019; Feng et al., 2021b; Yamazaki et al., 2016a), Shear Panel Damper (SPD) (Ge et al., 2011; Ge et al., 2012; Li et al., 2017), Buckling Restrained Rippled Plate (BRRP) (Yamazaki et al., 2016b), etc. as shown in Figure 2. These hysteretic dampers employ friction, plastic deformation, or other mechanical behaviors during earthquakes to dissipate seismic energy concentratedly so that the main structural components can be undamaged or slightly damaged. The seismic performance of dampers can be further improved by optimizing their structural design and configuration within damper systems. One example of an improved damper design is the Rippled Plate Buckling-Restrained Brace (PR-BRB) proposed by Yamazaki et al. (2016a) (Figure 2a). The PR-BRB replaces the flat plate in the traditional BRB with a rippled plate, resulting in longer and multiple-wave core members. This innovation enhances the energy dissipation capabilities of the BRB compared to conventional designs. In addition, Feng et al. (2021a) introduced a novel energy dissipation system called the multi-toggle brace damper (MTBD) system. Compared to the traditional toggle brace damper systems, the proposed MTBD system exhibits a larger amplification factor, a fuller hysteresis loop, and a more obvious energy dissipation effect. Consequently, it enhances the vibration control effect.

(a) (b)

Figure 1. The installation of hysteretic dampers: (a) in buildings, (b) under bridges

To improve the recoverability of aboveground structures, researchers improved traditional BRB by incorporating self-centering or replaceability design. Wang et al. (2022) proposed a novel resilient system known as the dual self-centering variable friction brace (DSC-VFB) as shown in Fig. 3. The DSC-VFB system exhibits self-centering behavior and possesses energy-dissipating capabilities that effectively reduce residual deformation of structures. The grooved friction plates and self-centering system can be conveniently disassembled and replaced, improving its recoverability.

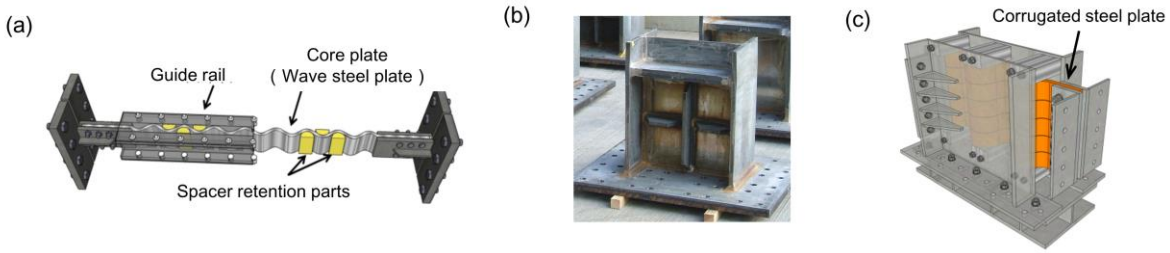

Figure 2. Hysteretic dampers: (a) RP-BRB (Yamazaki et al., 2016a), (b) SPD, and (c) BRRP (Yamazaki et al., 2016b)

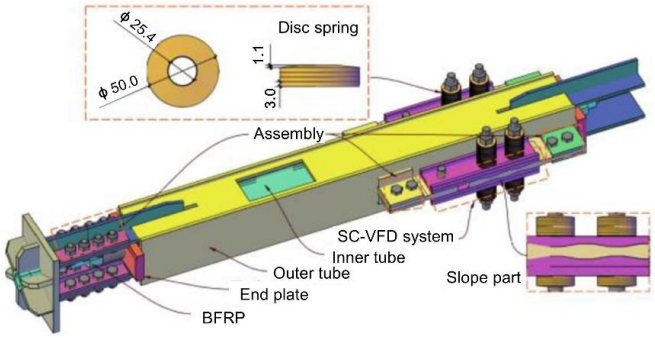

Figure 3. Dual self-centering variable friction brace (DSC-VFB) (Wang et al., 2022)

SEISMIC RESILIENCE FOR UNDERGROUND STRUCTURES

Compared to aboveground structures, the development of seismic control techniques for underground structures has lagged behind and those techniques for underground structures differ significantly from those used for aboveground structures. This disparity arises from the distinct response characteristics exhibited by underground structures. Due to the constraints of the surrounding soil, the seismic responses of underground structures are mainly controlled by the deformation of the surrounding soil and not strongly influenced by its vibration characteristics (Huang et al., 2023; Chen et al., 2021). Given this, the main seismic control strategies for underground structures can be divided into two categories according to structural forms. Linear structures such as tunnels and tubes employ the strategy of setting isolation layers around the surface of underground structures. This approach transforms the original dynamic system from a ground-underground structures system into a ground-isolation layer-underground structures system. It weakens the constraints exerted by the surrounding soil and absorbs seismic energy, thus reducing structural seismic responses (Chen et al., 2018; Chen and Shen, 2014). To validate the effectiveness of this approach, Chen and Shen (2014) carried out dynamic centrifuge tests on a tunnel model with an isolation layer around its surface. The results demonstrated that the isolation layer can significantly reduce the seismic responses of tunnels by absorbing earthquake-induced ground deformation as shown in Figure 4.

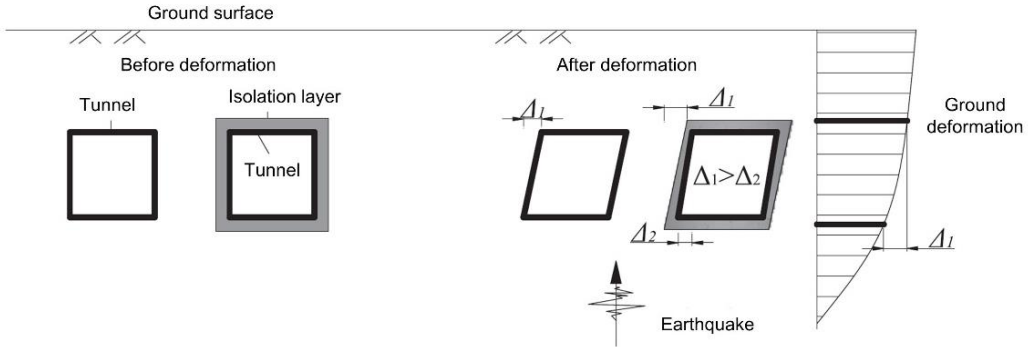

Figure 4 Mechanism of isolation layer on shock absorption

For underground spatial structures such as subway stations, studies have revealed that the central columns are the most vulnerable components. Earthquake records show that the limited horizontal

deformation capacity of central columns under high axial pressure is the primary factor contributing to the damage of subway stations during earthquakes (Chen et al., 2016). Given this, current research efforts have predominantly focused on installing seismic control devices at the ends of central columns, such as flexible rubber bears (Liu et al., 2020), sliding isolation bears (Zhuang et al., 2020), SPD (Chen et al., 2014), and FPB (Jia and Chen, 2021; Chen and Jia, 2021) as shown in Figure 5. Liu et al. (2020) carried out a series shaking table tests on a subway station with rubber bearings equipped at the column ends. The results showed a significant decrease in bending moment (60%-80%) and shear force (90%) at the column ends. However, the installation of flexible bearings led to a reduction in the lateral stiffness of the structure, resulting in increased lateral deformation. The study by Liu et al. (2020) revealed that the layer drift of the subway station increased by 30%-50%, and the bending moment of the sidewall increased by 5%-25%. In contrast, flexible energy-dissipation bearings can mitigate the increase in lateral deformation through energy dissipation. The study by Chen and Jia (2021) reveals that the FRB can reduce the internal forces on the central column and at the same time without causing a significant increase in lateral deformation of subway stations.

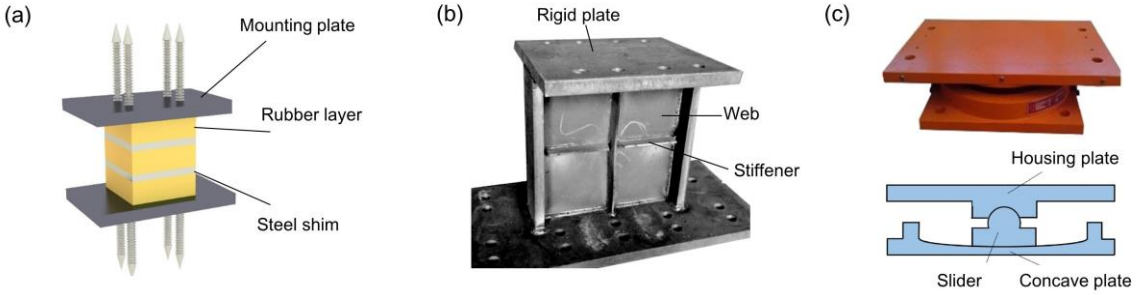

Figure 5. The bearings for underground structures: (a) rubber bearing (Liu et al., 2020), (b) SPD (Chen et al., 2014), (c) FPB (Jia and Chen, 2021)

The research aimed at improving the recoverability of underground structures mainly focuses on addressing the vulnerability of the central column. These studies can be categorized into two approaches: self-centering central column and replaceable central column, by which the recoverability of underground structures can be improved (Du et al., 2018; Chen and Zhou, 2019). Some researchers combined the concept of replaceability and self-centering to propose replaceable self-centering structural forms for central columns. Chen and Zhou (2019) proposed a self-centering energy-dissipation column base for underground structures. The self-centering mechanism primarily relies on the unbonded prestressed tendons, self-weight, and the overlying soil pressure. Replaceable energy-dissipating devices at the column foot are employed to dissipate seismic energy concentratedly through rocking behavior during earthquakes. By employing self-centering or replaceable design strategies, the recoverability of underground structures, particularly in relation to the central column, can be improved.

DISCUSSION AND CONCLUSION

Compared to aboveground structures, the resilience strategy for underground structures is still in its early stage, with most of these resilience designs being adapted from those used for aboveground structures, such as the isolation bearings and rocking structural components. However, it is noteworthy that there are notable differences in the seismic control mechanism between aboveground and underground structures.

Firstly, both isolation bearings for aboveground structures and the isolation layer for underground structures are employed to obstruct the propagation path of seismic energy. However, their specific functions differ. The isolation bearings for aboveground structures are used to prolong the structural natural period and keep it away from the predominant period. In contrast, for underground structures, structural vibration characteristics are not the main factors influencing structural seismic responses. The main purpose of the isolation layer around underground structures is to weaken the constraints imposed by surrounding soils and to absorb seismic shocks.

Secondly, similar types of isolation bearings can be used for both aboveground and underground structures. However, in the case of underground structures, the isolation bearings are typically installed

at the ends of central columns and serve to weaken the horizontal connection between central columns and beams. As mentioned earlier, central columns are the most vulnerable components of underground structures. By installing flexible isolation bearing, the internal forces of the central column can be significantly reduced, but at the same time, the structural layer drift and internal forces of sidewalls may increase. In contrast, the installation of hysteretic dampers in aboveground structures can reduce the seismic responses of the whole structure.

Thirdly, both the aboveground and underground structures can utilize the rocking structure or rocking structural components to reduce the seismic deformation of the structure or structural components. In the aboveground structures, the rocking behavior typically occurs at the structure level, and the seismic energy is dissipated through collisions at the rocking interface rather than structural deformation. However, achieving large rigid body rotational deformations is challenging for underground structures. Rocking behavior in underground structures commonly occurs at the component level, particularly in the central column. The rocking interface weakens the connection between columns and beams, thereby cutting off the stress transfer path and protecting the central column.

Compared to aboveground structures, seismic control strategies for underground structures are still insufficient. While some resilience design concepts from aboveground structures can be applied to underground structures, it is crucial to consider the unique characteristics and response mechanisms specific to underground environments. While the use of isolation layers can effectively reduce the overall seismic responses of underground structures, current research primarily focuses on tunnel structures characterized by small cross-sectional areas and spans. For underground spatial structures with large structural span, complex structural form, and high structural density, such as subway stations, the application of the isolation layer is limited to some extent. Although the isolation bearings can be used in underground spatial structures to improve their seismic performance, they can also lead to a reduction in structural stiffness and result in an increase in structural layer drift and internal force of sidewalls. Considering the seismic response characteristics of underground structures, it is crucial to develop a regional seismic control strategy that addresses these challenges.

REFERENCES

An X., Shawky A.A. and Maekawa K. (1997). "The collapse mechanism of a subway station during the Great Hanshin earthquake," *Cement Concrete Comp.*, **19**(3), 241-257.

Chang K.C., Mo Y.L., Chen C.C., Lai L.C. and Chou C.C. (2009). "Lessons learned from the damaged Chi-Lu cable-stayed bridge," *J. Bridge Eng.*, **9**(4), 343-352.

Chen Z.Y, Chen W. and Bian G.Q. (2014). "Seismic performance upgrading for underground structures by introducing Shear Panel Dampers," *Adv. Struct. Eng.*, **17**(9), 1343-1357.

Chen Z.Y., Chen W., Zhang W. and Lou M.L. (2016). "Effects of axial compression ratio of central columns on seismic performance of a multi-story underground structure," *Int. J. Comp. Meth.*, **13**(04), 1641014.

Chen Z.Y., Huang P.F. and Chen W. (2021). "Seismic response characteristics of multi-story subway station through shaking table test," *Adv. Struct. Eng.*, **24**(10), 2185-2200.

Chen Z.Y. and Jia P. (2021). "Seismic response of underground stations with friction pendulum bearings under horizontal and vertical ground motions," *Soil Dyn. Earthq. Eng.*, **151**, 106984.

Chen Z.Y., Liang S.B., Shen H. and He C. (2018). "Dynamic centrifuge tests on effects of isolation layer and cross-section dimensions on shield tunnels," *Soil Dyn. Earthq. Eng.*, **109**, 173-187.

Chen Z.Y. and Zhou Y. (2019). "Seismic performance of framed underground structures with self-centering energy-dissipation column base," *Adv. Struct. Eng.*, **22**(13), 2809-2822.

Chen Z.Y. and Shen H. (2014). "Dynamic centrifuge tests on isolation mechanism of tunnels subjected to seismic shaking," *Tunn. Undergr. Sp. Tech.*, **42**, 67-77.

Du X.L., Wang Z.L. and Liu H.T. (2018). "Study of a seismic new system of underground frame structure based on toughness design," *Technol. Earthq. Disaster Prevention*, **13**(03), 493-501. (In Chinese)

Feng H., Zhou F.Y, Ge H.B., Zhu H.P. and Zhou L.M. (2021a). "Energy dissipation enhancement through multi-toggle brace damper systems for mitigating dynamic responses of structures," *Structures*, **33**, 2487-2499.

Feng H., Zhou F.Y., Ge H.B., Zhu H.P. and Zhou L.M. (2021b). "Seismic performance enhancement of buildings using multi-limb brace damper systems," *Struct. Des. Tall Spec.*, **30**(3), e1825.

Ge H.B., Chen X. and Kang L. (2012). "Demand on stiffened steel Shear Panel Dampers in a rigid-framed bridge pier under repeated seismic ground motions," *Adv. Struct. Eng.*, **15**(3), 525-546.

Ge H.B., Chen X. and Matsui N., (2011). "Seismic demand on Shear Panel Dampers installed in steel-framed bridge pier structures," *J. Earthq. Eng.*, **15**(3), 339-361.

Gu T.Y., Li J.H., Sun J.B., Jia L.J., Liu T. and Ge H.B. (2022). "Experimental study on miniature buckling-restrained brace with corrugated core bar," *J. Earthq. Eng.*, **26**(13), 6633-6655.

Huang P.F. and Chen Z.Y. (2021a). "Fragility analysis for subway station using artificial neural network," *J. Earthq. Eng.*, **26**(13), 6724-6744.

Huang P.F. and Chen Z.Y. (2021b). "Deep learning for nonlinear seismic responses prediction of subway station," *Eng. Struct.*, **244**, 112735.

Huang P.F., Chen Z.Y. and Liu Z.Q. (2023). "Nonparametric probabilistic seismic demand model and fragility analysis of subway stations using deep learning techniques," *Undergr. Space*, **11**, 63-80.

Iida H., Hiroto T., Yoshida N. and Iwafuji M. (1996). "Damage to Daikai subway station," *Soils Found.*, **36**, 283-300.

Jia P. and Chen Z.Y. (2021). "Seismic reduction effectiveness of friction pendulum bearings in underground station structures," *Int. J. Comp. Meth.*, **18**(3), 2041008.

Kawashima K., Takahashi Y., Ge H.B., Wu Z.S. and Zhang J.D. (2009). "Reconnaissance report on damage of bridges in 2008 Wenchuan, China, earthquake," *J. Earthq. Eng.*, **13**(7), 965-996.

Li R., Ge H.B. and Maruyama R. (2017). "Assessment of post-earthquake serviceability for steel arch bridges with seismic dampers considering mainshock-aftershock sequences," *Earthq. Struct.*, **13**(2), 137.

Liu Z.Q., Chen Z.Y., Liang S.B. and Li C.X. (2020). "Isolation mechanism of a subway station structure with flexible devices at column ends obtained in shaking-table tests," *Tunn. Undergr. Sp. Tech.*, **98**, 103328.

Ma C., Lu D.C., Zhao Y.Q., Wang Z.H. and Du X.L. (2022). "Performance of an underground structure seismic mitigation system improved by frictional deformation absorbing braces." *Structures*, **37**, 1-16.

Miller D.K. (1998). "Lessons learned from the Northridge earthquake," *Eng. Struct.*, **20**(4-6), 249-260.

Wang Y.W., Zhou Z., Ge H.B., Yao J.H. and Xie Q. (2022). "Experimental validation and numerical simulation of a dual-self-centering variable friction braced frame under strong ground motions," *J. Build. Eng.*, **56**, 104761.

Yamazaki S., Kato H., Usami T. and Ge H.B. (2016a). "An experimental and analytical study on buckling-restrained braces with rippled core plate (RP-BRB)," *J. JSCE. Ser. A1*, **72**(4), 264-278. (In Japanese)

Yamazaki S., Usami T. and Nonaka T. (2016b). "Developing a new hysteretic type seismic damper (BRRP) for steel bridges," *Eng. Struct.*, **124**, 286-301.

Yang S., Guan D.Z., Jia L.J., Guo Z.X. and Ge H.B. (2019). "Local bulging analysis of a restraint tube in a new buckling-restrained brace," *J. Constr. Steel Res.*, **161**, 98-113.

Zhuang H.Y., Zhao C., Chen S., Fu J.S., Zhao K. and Chen G.X. (2020). "Seismic performance of underground subway station with sliding between column and longitudinal beam." *Tunn. Undergr. Sp. Tech.*, **102**, 103439.

Day2 (Tuesday, Sep. 26th, 2023) 10:30~10:55

Performance-Based Earthquake Engineering from Theory to Implementation to the Future

Tony Yang

Professor, Department of Civil Engineering,
The University of British Columbia, Vancouver, Canada

Professor Tony T.Y. Yang is a fellow of Canadian Academy of Engineering, Director of Smart Structures Laboratory and Head of Structural Engineering division at the Department of Civil Engineering at The University of British Columbia. He is a world-renowned for his ground-breaking innovation in performance-based design, structural simulation and testing, robotic inspection and construction and high-performance, carbon-neutral and resilient infrastructure. Prof. Yang is one of the 19 voting members of the Standing Committee for Earthquake Design, which is responsible for writing the seismic design provision of the 2020/2025 National Building Code of Canada (NBCC). Prof. Yang is also a committee member of S16, which is responsible for writing the design provision of steel structures in the Canada. Prof. Yang's work has been well recognized by his colleagues, he is the recipient of the 2020 Meritorious achievement award from Engineers & Geoscientists British Columbia Canada, which is the highest achievement award given to a professional engineer (P. Eng.) in British Columbia, Canada, 2019 Technology award from the New Zealand Concrete Society and the 2014 CISC H.A. Krentz award for the highest impacted steel research from the Canadian Institute of Steel Construction.

PERFORMANCE-BASED EARTHQUAKE ENGINEERING FROM THEORY TO IMPLEMENTATION TO THE FUTURE

T.Y. Yang[1], Xiao Pan[2], Yifei Xiao[3], Zhongwei Chen[4]

1. Professor, Department of Civil Engineering, The University of British Columbia, Vancouver, Canada
2. Postdoctoral research fellow, Department of Civil Engineering, The University of British Columbia, Vancouver, Canada
3. PhD student, Department of Civil Engineering, The University of British Columbia, Vancouver, Canada
4. MASc student, Department of Civil Engineering, The University of British Columbia, Vancouver, Canada

Email: yang@civil.ubc.ca

ABSTRACT

Performance-based earthquake engineering (PBEE) aims to assess the performance of structures using metrics that are immediately valuable to both engineers and stakeholders. The PBEE framework encompasses the assessment of seismic hazards, structural responses, resulting damage, loss and downtime involved in recover the building to its original state, through a coherent probabilistic analysis. In this paper, the performance-based earthquake engineering framework is first described. Then, two previous case studies of PBEE were reviewed. Finally, the paper describes the future vision on the potential integration of PBEE with novel AI and smart technologies.

Keywords: Performance-based earthquake engineering, seismic analysis, artificial intelligence, computer vision.

INTRODUCTION

Recent seismic events in various regions, including Japan, Chile, New Zealand, and others, have effectively demonstrated that even countries with well-established building codes are still susceptible to substantial financial devastation when faced with significant seismic activities. Historically, code-based design aimed to provide minimum safety to prevent complete or partial structural failure during intense seismic occurrences. Nevertheless, this conventional approach to design has led to considerable financial losses in previous earthquake incidents (Lee and Mosalam 2006). In order to efficiently address seismic vulnerabilities, it is imperative to identify the structural elements that suffer notable damage due to seismic activity and accurately assess the associated monetary losses. For this reason, in the past decades, the performance-based earthquake engineering (PBEE) methodology has been developed and applied to numerous case studies to quantify the performance of structural and nonstructural components in the event of earthquake, which enable decision makers to have a well-defined tool to rapidly quantify the seismic resilience of structures.

GENERIC PBEE FRAMEWORK

Within the PBEE framework, four essential steps are defined in the performance assessment including the probabilistic seismic hazard analysis (PSHA), response analysis, damage analysis, and loss analysis. Figure 1 shows the framework of performance assessment. Seismic hazard analysis is to quantify the mean annual rate of exceeding a given value of the seismic intensity measure (im) and determine what types of earthquakes are most important to the seismic hazard. Response analysis is to analyze the responses of structural and nonstructural components under the selected ground motions and determine response statistics related to engineering demand parameters. Damage analysis is to quantify the structural and nonstructural component damage and obtain fragility curves. Finally, loss analysis is to provide decision variables for stakeholders based on the damage quantities. The mean annual rate of the decision variable exceeding a threshold value is expressed in Equation 1.

$$\lambda(dv < DV) = \int_{im}\int_{dm}\int_{edp} G(dv|dm)dG(dm|edp)dG(edp|im)|d\lambda(im)| \quad (1)$$

where im is the seismic intensity measure. dm is the damage measure. edp is the engineering demand parameter. dv is the statistically independent of edp and im. $\lambda(dv < DV)$ represents the mean rate of events $\{dv < DV\}$. Function $dG(a|b)$ represents the conditional complementary cumulative distribution function.

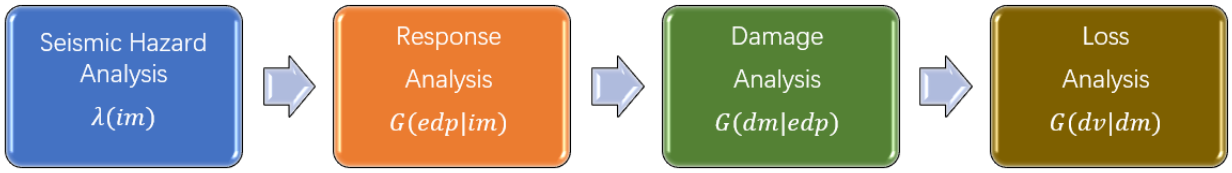

Figure 1. Framework of PBEE framework.

CASE STUDIES

To illustrate the implementation procedures, a case study (Yang et al., 2015) is reviewed which includes the theory and implementation of the PBEE framework on a multi-storey building. In that study, a five-story steel frame building located in Vancouver, British Columbia (Figure 2), Canada, was selected and designed using 9 pre-qualified SFRS methods which included the ductile moment resisting frame (MRF), moderately and limited ductility concentrically braced frame (CBF and CBFLD), ductile eccentrically braced frame (EBF), ductile buckling restrained braced frame (BRBF), ductile and limited ductility steel plate shear wall (SPSW and SPSWLD), X-braced frame (XBF), and suspended zipper-braced frame (SZBF) to verify the proposed art performance-based assessment procedure. The building has a bay width of 9 m, a first-story height of 4.25 m, and a floor height of 3.65 m for 2 to 5 floors. The building is symmetric in both the north-south and east-west directions.

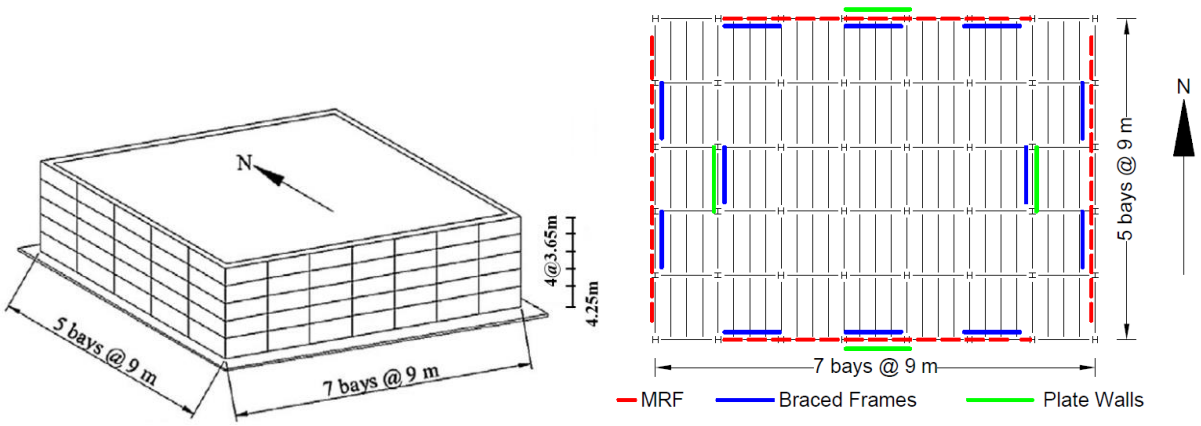

(a) 3D view (b) Plan view

Figure 2. (a) 3D view of the prototype building. (b) Location of the SFRS on the plan view

In this study, the prototype building was divided into 26 performance groups (PGs). Table 1 shows the summary of the PGs included in this study.

Table 1. Summary of Performance Group

PG	Name	Location	EDP
1	SH12	Between levels 1 and 2	ISD_1
2	SH23	Between levels 2 and 3	ISD_2
3	SH34	Between levels 3 and 4	ISD_3
4	SH45	Between levels 4 and 5	ISD_4
5	SH5R	Between levels 5 and R	ISD_5
6	CW12	Between levels 1 and 2	ISD_1
7	CW23	Between levels 2 and 3	ISD_2
8	CW34	Between levels 3 and 4	ISD_3
9	CW45	Between levels 4 and 5	ISD_4
10	CW5R	Between levels 5 and R	ISD_5
11	INTD12	Between levels 1 and 2	ISD_1
12	INTD23	Between levels 2 and 3	ISD_2
13	INTD34	Between levels 3 and 4	ISD_3
14	INTD45	Between levels 4 and 5	ISD_4
15	INTD5R	Between levels 5 and R	ISD_5
16	Contents2	Below level 2	a_2
17	Contents3	Below level 3	a_3
18	Contents4	Below level 4	a_4
19	Contents5	Below level 5	a_5
20	ContentsR	Below level R	a_R
21	Ceiling2	Below level 2	a_2
22	Ceiling3	Below level 3	a_3
23	Ceiling4	Below level 4	a_4
24	Ceiling5	Below level 5	a_5
25	CeilingR	Below level R	a_R
26	Elevator	at level R	a_R

where the ISD and a are the inter-story drift and floor acceleration, respectively.

The seismic hazard analysis was conducted with three hazard levels, including 2%probability of being exceeded in 50 years (2⁄50), 10%probability of being exceeded in 50 years (10⁄50) and 50% probability of being exceeded in 50 years (50⁄50). The ground motions were selected from PEER (2012) according to the requirements in the National Building Code of Canada. Figure 3 presents an illustrative example of the scaled spectra for the 2⁄50 hazard level.

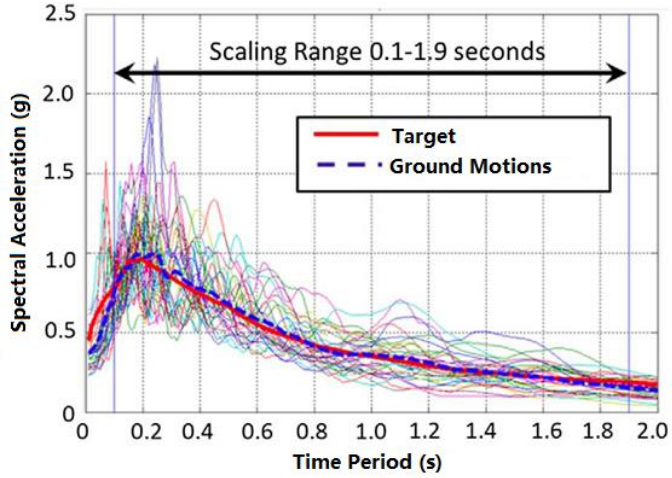

Figure 3. Ground motion scaling for the 2⁄50 hazard

The finite element model for the 9 different design methods was built using OpenSees (UCB 2012) to simulate the structural response by conducting a dynamic response analysis for each of the selected and scaled ground motion records. The engineering demand parameter (*edp*) associated with each PG was monitored. The peak *edp* values would be summarized in a matrix for each ground motion record. Three *edp* matrices should be defined for each seismic hazard level considered in this case. Table 2 summarize the sample peak structural response at 2⁄50 hazard level.

Table 2. Peak structural response at 2/50 hazard level

EDP [units]	EBF	CBF	CBFLD	SZBF	BRBF	XBF	SPSW	SPSWLD	MRF
ISD_2^* [%]	0.88	0.48	0.44	0.55	0.63	0.33	0.28	0.27	1.43
ISD_3 [%]	0.35	0.46	0.53	0.49	0.49	0.39	0.30	0.20	1.11
ISD_4 [%]	0.21	0.51	0.28	0.44	0.59	0.33	0.40	0.20	0.93
ISD_5 [%]	0.18	0.23	0.26	0.23	0.6	0.39	0.63	0.30	0.84
ISD_R [%]	0.10	0.12	0.13	0.04	0.34	0.32	0.52	0.20	0.72
a_g [g]	0.36	0.36	0.36	0.36	0.36	0.36	0.36	0.36	0.36
a_2 [g]	0.49	0.61	0.69	0.67	0.56	0.61	0.51	0.63	0.53
a_3 [g]	0.42	0.65	0.77	0.67	0.56	0.81	0.53	0.69	0.51
a_4 [g]	0.36	0.70	0.78	0.62	0.57	0.96	0.54	0.86	0.51
a_5 [g]	0.41	0.65	0.90	0.65	0.55	1.1	0.58	1.01	0.50
a_R [g]	0.60	0.92	1.14	0.76	0.82	1.56	0.82	1.33	0.80

Table 3 summarizes the initial costs, median repair costs at three hazard levels, mean annualized loss (MAL) and the total life cycle costs using the proposed PBEE methodology.

Table 3. Summary of Performance Assessment

Design type	Median repair cost (million)				Mean annualized loss (MAL) (10^4)	50-year life-cycle costs @ 3.5% annual interest(10^6)
	Initial costs	2/50	10/50	50/50		
EBF	$46.59	$1.83	$1.22	$0.31	$3.36	$49.11
EBF	$47.32	$1.72	$1.08	$0.10	$1.98	$49.15
SPSW	$46.76	$1.74	$1.38	$0.37	$3.13	$49.16
BRBF	$46.86	$1.72	$1.32	$0.31	$3.54	$49.48
SZBF	$46.95	$1.69	$1.36	$0.31	$3.76	$49.48
SPSWLD	$46.91	$1.73	$1.59	$0.61	$3.99	$49.76
XBF	$46.84	$1.85	$1.59	$0.61	$4.76	$50.07
CBFLD	$47.10	$1.76	$1.56	$0.34	$4.30	$50.10
CBF	$47.32	$1.69	$1.56	$0.34	$3.93	$50.13

where the life cycle costs were obtained by starting with the initial construction costs and adding the mean cumulative annual repair cost every year with 3.5 % annual interest.

The results show that the proposed PBEE procedure can provide a more intuitive perspective to the engineers to select the most economical system for a specific project in the financial aspect.

FUTURE VISION

Past development in the field has been focused on enhancing various methodological components within the PBEE framework, such as development of different probabilistic seismic hazard analysis models, more advanced finite element models, new fragility functions with new experimental data. Recently, with the advancement of AI technologies (Pan & Yang, 2022, Pan & Yang, 2022; Pan & Yang, 2023a; Pan & Yang, 2023b; Pan et al., 2023) have used the presented a generic framework to evaluates the system-level and component-level damage. The result shows that the PBEE can incorporate advanced robotic technologies for efficient data collection (e.g., Pan, Tavasoli, & Yang, 2023; Tavasoli, Pan, & Yang, 2023; Xiao et al., 2023). These novel robotic technologies, image processing and AI algorithms will be continuously developed in the near future. Integrating these technologies into the PBEE framework will provide a more rapid and comprehensive performance assessment.

Figure 4 shows the prediction by the AI model on the system state and component state of the reinforced concrete structures. It is shown that the proposed AI models can assess the damage status from these on-site images at high accuracy.

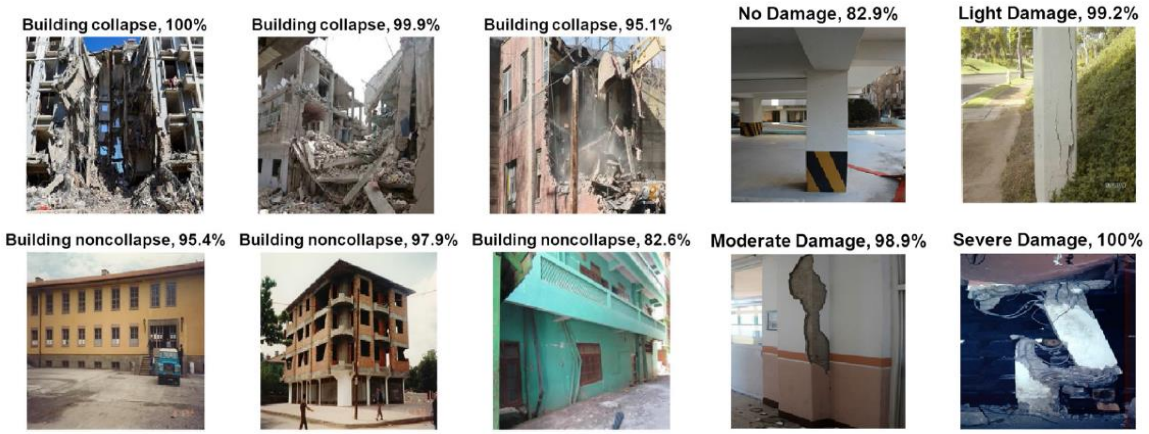

Figure 4. AI-based evaluation of structural damage state (a) system level; (b) component level

Once the damage states of components are identified, the consequence functions can be used to identify the associated losses. Figure 5 shows the cumulative loss function in a case study presented in Pan & Yang (2020). The cost simulation results can provide critical risk data for decision making and resource allocation during post disaster reconstruction. For example, the decision maker can use the 50% probability of non-exceedance to identify the median repair cost for the building.

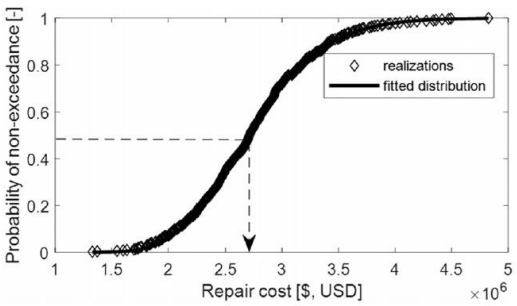

Figure 5. Cumulative loss function

CONCLUSIONS

In this paper, the theory and applications of the PBEE framework have been reviewed. In the past decades, numerous studies have been conducted to enhance different methodological components of the PBEE framework including PSHA, finite element modelling, fragility function development, and loss quantification. In addition, the paper also discussed future research directions on the integration of PBEE with AI technologies, which offers new solutions to provide a more comprehensive assessment using the PBEE framework.

REFERENCES

1. Lee, T. H., and Mosalam, K. M., 2006. Probabilistic Seismic Evaluation of Reinforced Concrete Structural Components and Systems, PEER Report No. 2006/04, University of California, Berkeley.
2. National building code of Canada. (2015). National Research Council Canada, Institute for Research in Construction.
3. Pacific Earthquake Engineering Research Center (PEER), 2012. Open System for Earthquake Engineering Simulation (Opensees) Framework, University of California, Berkeley, available at http://opensees.berkeley.edu/.

4. Pan, X., & Yang, T. Y. (2020). Postdisaster image-based damage detection and repair cost estimation of reinforced concrete buildings using dual convolutional neural networks. Computer-Aided Civil and Infrastructure Engineering, 35(5), 495-510.

5. Pan, X., & Yang, T. Y. (2022). Image-based monitoring of bolt loosening through deep-learning-based integrated detection and tracking. Computer-Aided Civil and Infrastructure Engineering, 37(10), 1207-1222.

6. Pan, X., & Yang, T. Y. (2023a). 3D vision-based out-of-plane displacement quantification for steel plate structures using structure-from-motion, deep learning, and point-cloud processing. Computer-Aided Civil and Infrastructure Engineering, 38(5), 547-561.

7. Pan, X., & Yang, T. Y. (2023b). 3D vision-based bolt loosening assessment using photogrammetry, deep neural networks, and 3D point-cloud processing. Journal of Building Engineering, 70, 106326.

8. Pan, X., Tavasoli, S., & Yang, T. Y. (2023). Autonomous 3D vision-based bolt loosening assessment using micro aerial vehicles. Computer-Aided Civil and Infrastructure Engineering.

9. Pan, X., Yang, T. Y., Xiao, Y., Yao, H., & Adeli, H. (2023). Vision-based real-time structural vibration measurement through deep-learning-based detection and tracking methods. Engineering Structures, 281, 115676.

10. Pan, Y., Wang, H., Li, X., & Yu, H. (2017). Adaptive command-filtered backstepping control of robot arms with compliant actuators. IEEE transactions on control systems technology, 26(3), 1149-1156.

11. Tavasoli, S., Pan, X., & Yang, T. Y. (2023). Real-time autonomous indoor navigation and vision-based damage assessment of reinforced concrete structures using low-cost nano aerial vehicles. Journal of Building Engineering, 68, 106193.

12. Xiao, Y., Pan, X., & Yang, T. T. (2022). “Nonlinear backstepping hierarchical control of shake table using high-gain observer”. Earthquake Engineering & Structural Dynamics, 51(14), 3347-3366

13. Xiao, Y., Pan, X., Tavasoli, S., M. Azimi, Bao Y., Noroozinejad Farsangi E., & Yang T.Y. (2023) “Autonomous Inspection and Construction of Civil Infrastructure Using Robots” Automation in Construction toward Resilience: Robotics, Smart Materials, and Intelligent Systems, edited by Ehsan Noroozinejad Farsangi, Mohammad Noori, Tony T.Y. Yang, Paulo B. Lourenço, Paolo Gardoni Izuru Takewaki, Eleni Chatzi, Shaofan Li. Publisher: CRC Press - Taylor & Francis. DOI: 10.1201/9781003325246-1

14. Yang, T. Y., Moehle, J., Stojadinovic, B., and Der Kiureghian, A. (2009). Performance evaluation of structural systems: theory and implementation, Journal of Structural Engineering, ASCE, 135, 1146–1154.

15. Yang, T. Y., & Murphy, M. (2015). Performance evaluation of seismic force–resisting systems for low-rise steel buildings in Canada. Earthquake Spectra, 31(4), 1969–1990. doi:10.1193/022314eqs032m

16. Zheng, K., Zhang, Q., Hu, Y., & Wu, B. (2021). Design of fuzzy system-fuzzy neural network-backstepping control for complex robot system. Information Sciences, 546, 1230-1255.

Day2 (Tuesday, Sep. 26th, 2023) 10:55~11:20

Understanding Ground Motions and their Relation to Structural Damage

Carlos Ventura

Professor, Department of Civil Engineering,
The University of British Columbia, Vancouver, Canada

Dr. Carlos Ventura is a Civil Engineer with specializations in structural dynamics and earthquake engineering. He has been a faculty member of the Department of Civil Engineering at the University of British Columbia (UBC) in Canada since 1992. He is currently the Director of the Earthquake Engineering Research Facility (EERF) at UBC, and is the author of more than 600 papers and reports on earthquake engineering, structural dynamics and modal testing. Dr. Ventura has conducted research about earthquakes and structural dynamics for more than thirty-five years. Three of his most significant contributions in recent years are the development and implementation of performance-based design methods for seismic retrofit of school buildings, known as the Seismic Retrofit Guidelines (SRG) Project; a unique seismic structural health monitoring program for bridges in BC, known as the BCSIMS project; and the first network-based earthquake early warning system for schools and public institutions in BC. These projects have contributed in a very significant manner to the seismic risk reduction efforts in BC. He has been involved in the field testing and instrumentation or seismic monitoring of more than one hundred buildings, bridges and dams in several countries. In addition to his academic activities, Dr. Ventura is a recognized international consultant on structural vibrations and safety of large Civil Engineering structures. The quality of his research work has been recognized by several national and international awards, as well as being appointed as member of the Canadian Academy of Engineering, the Engineering Institute of Canada, and Fellow of Engineers Canada. He is also a member of several national and international professional societies, advisory committees and several building and bridge code committees.

UNDERSTANDING GROUND MOTIONS AND THEIR RELATION TO STRUCTURAL DAMAGE

Carlos E. Ventura
Department of Civil Engineering, the University of British Columbia, Canada
E-mail: ventura@civil.ubc.ca

ABSTRACT

In recent years, the strong ground motion records database has significantly expanded, mostly as a consequence of the seismic events in Chile, Japan, New Zealand, Turkey, and other countries. Engineers are facing many challenges in dealing with these particular records, mainly associated with methods for selection and scaling of the motions to use as input for dynamic structural analysis. One of the aspects which has not been thoroughly investigated is the link between the characteristics of strong motions and observed damage. A striking example is given by the field observations at Tsukidate and Sendai after the Tohoku 2011 earthquake in Japan. The PGA at Tsukidate was approximately 3.0 g and it was 1.5 g at Sendai. Despite this extremely large difference in PGA, the damage was much greater in Sendai than in Tsukidate, confirming that the PGA is not necessarily a good index of damage potential. In this paper, we explore what other characteristics of ground motion record may significantly contribute to structural damage. Specifically, we explored the effects of intensity of shaking, duration, frequency content and elastic and constant ductility response spectra. The impact of these variables will be assessed using reported structural damage data.

Keywords: Strong motion, damage, intensity, duration, response spectrum.

INTRODUCTION

When the Tohoku earthquake hit the Japanese coastline on March 11th 2011, the rupture involved three different locations in sequence, resulting in a maximum slip of about 40 m and a significant amount of energy released in a three- minute span (Shojiro *et al.,* 2011*)*. The moment magnitude associated with this event is Mw 9.0. According to the JMA (Japan Meteorological Agency) intensity scale, the maximum seismic intensity was 7 in the city of Kurihara (K-NET Tsukidate) (Ochi and Suzuoki, 2011) and the rating in Sendai was 6+.

A PGA of 3.0 g was recorded in Tsukidate (MYG004), while at Sendai (MYG013) the PGA was 1.5 g. As shown in Figure 1, both sites are at comparable epicentral distances (Nishiyama *et al.,* 2011). The observed damage at the two locations is not related to the PGA: much more severe damage was observed in Sendai than in Tsukidate (Ventura 2011). In particular, wood houses in Tsukidate experienced some level of damage, but it was not as severe as expected given the high seismic intensity. Figure 5 shows typical examples of damage in Tsukidate. Despite the very high acceleration in Tsukidate, many containers and stacked items did not overturn (Figure 2 to 4).

In the city of Sendai, significant damage was observed in wooden houses. Reinforced concrete buildings were also damaged (Figure 6 through 9). Post-earthquake evaluations reported several types of damage in reinforced concrete buildings, such as: collapse of first and mid-stories, shear failures in columns and failure of walls in multi- storey buildings. The structural damage was widespread overall and not just isolated to some specific types of structures.

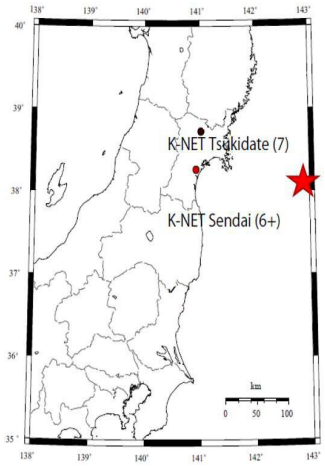

Figure 1: Location of the epicenter and the stations of Tsukidate and Sendai, adjusted from [3].

Figure 2: Not overturned objects in Tsukidate - Example 1 (Source: Midorikawa Lab).

Figure 3: Not overturned objects in Tsukidate - Example 2 (Source: Midorikawa Lab)

Figure 4: Not overturned objects in Tsukidate - Example 3 (Source: Midorikawa Lab).

Figure 5: Overturned objects in Tsukidate - Example 1 (Source: Midorikawa Lab).

Figure 6: Damage to the pavements in Sendai - Example 3 (Source: Midorikawa Lab).

Figure 7: Structural Damage in Sendai - Example 1 (Source: Midorikawa Lab).

Figure 8: Structural Damage in Sendai - Example 2 (Source: Midorikawa Lab).

Figure 9: Structural Damage in Sendai - Example 3 (Source: Midorikawa Lab).

CASE STUDY OF DAMAGE IN TSUKIDATE AND SENDAI

The ground motion records for Tsukidate and Sendai were downloaded from the Japanese Kyoshin network K-NET and KiK-net database (NIED). In addition to the traditional ground motion parameters, such as PGA, PGV and maximum displacement, attention was focused as well on the waveform type, the frequency content and the significant duration $D_{5\text{-}95}$. Table 1 provides a summary of the main characteristics of the motions recorded at Tsukidate and Sendai stations.

The seismic intensity expressed in JMA *shindo* levels (Japan Meteorological Agency, 2017), which represents the degree of shaking at different locations, was estimated to be 6+ in Sendai while at the Tsukidate station reached the highest scale degree of 7. The station of Tsukidate recorded an extremely high acceleration, about 3 g, while the maximum acceleration in Sendai was 1.5 g. Less significant differences were observed in terms of velocity, while the maximum displacements were similar and about 22 cm for both stations.

Table 1: Characteristics of the Japanese Ground Motion Records.

	Tsukidate	Sendai
Record Name	MYG0041103111446-NS	MYG0131103111446-NS
Seismic Intensity	7	6+
Max. Acceleration	2.91 g	1.46 g
Max. Velocity	110 cm/sec	86 cm/sec
Max. Displacement	22.5 cm	22.4 cm
Waveform	2-wave groups	2-wave groups
Frequency Content	Short Period (0.2 sec)	Intermediate period (0.5-1.0 sec)
5-95 Significant Duration	80.85 sec	89.72 sec

From a qualitative point of view, both records have similar time history shapes, which can be described by two waves groups as shown in Figure 10.

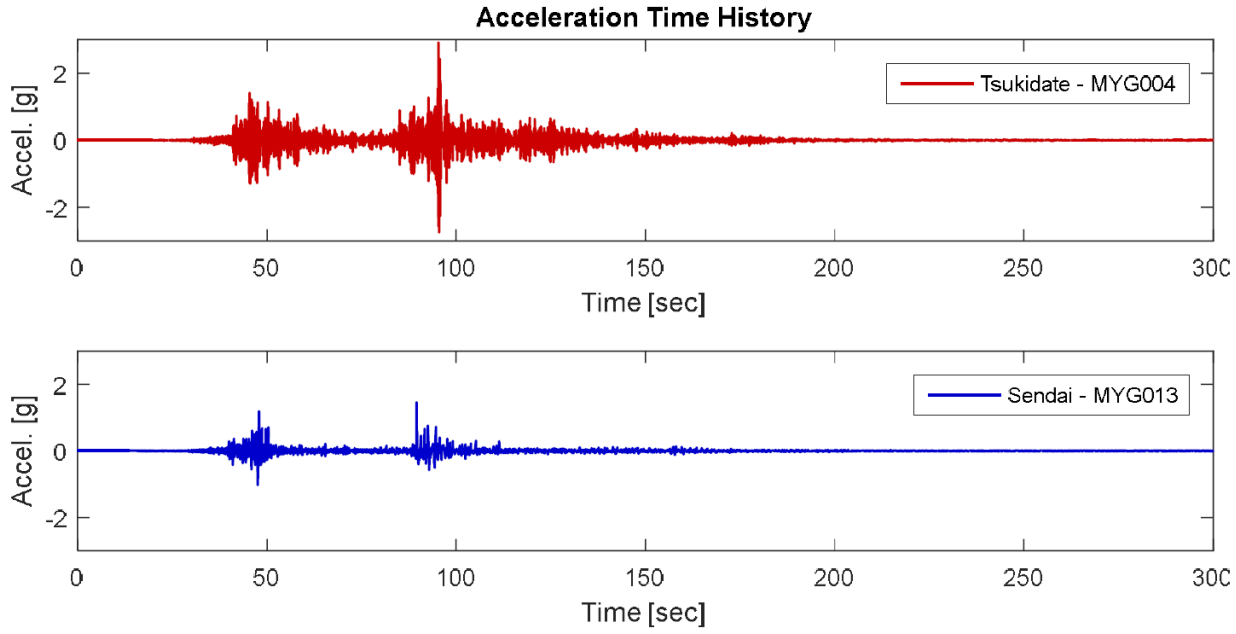

Figure 10: Acceleration Time Histories for the NS components in Tsukidate and Sendai

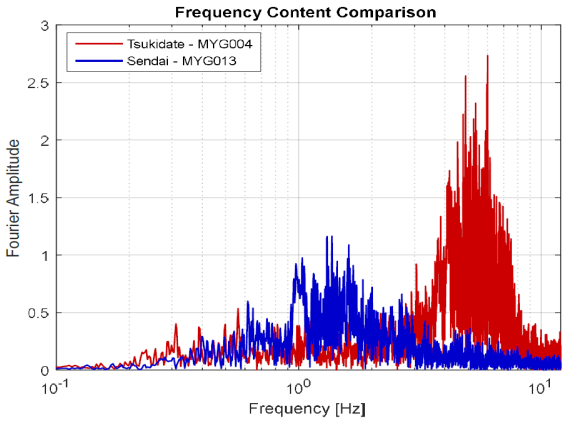

Figure 11: Frequency content of the NS component records for Tsukidate and Sendai.

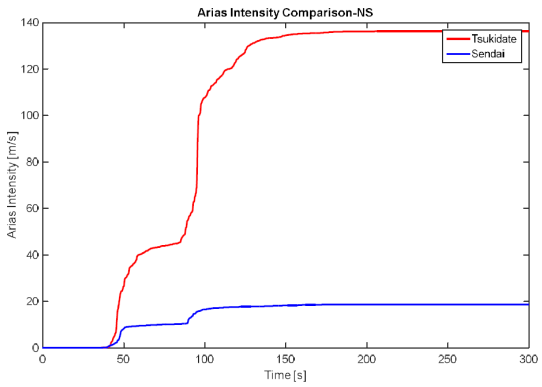

Figure 12: Arias Intensity for Tsukidate and Sendai.

One of the characteristics of the records which underlines the different nature of the ground motions is the frequency content (Figure 11). Tsukidate motions have a much higher frequency content.

The Arias Intensity is a common measure of the energy content of the ground motion (Bommer and Boore, 2004). It is defined as the time integral of the ground acceleration squared (Arias, 1970). The Arias Intensity of Tsukidate and Sendai are shown in Figure 12. It is clear that the Arias intensity for Sendai is only a small fraction of the Arias Intensity of the Tsukidate record. However, the damage in Sendai was much greater than the damage in Tsukidate, despite the fact that the Arias Intensity is supposed to be a measure of the energy in the ground shaking. Clearly, the Arias Intensity is not a good measure of potential damage to structures.

ELASTIC RESPONSE SPECTRA ANALYSIS

We next probe the relevance of the elastic response spectrum as an index of damage potential. This is a logical step because the elastic spectrum is used as the basis for design.

Elastic response spectra for pseudo acceleration (PSA), pseudo velocity (PSV) and spectral displacements have been calculated and plotted for both sites as showed respectively in Figure 13 and Figure 14 and Figure 15.

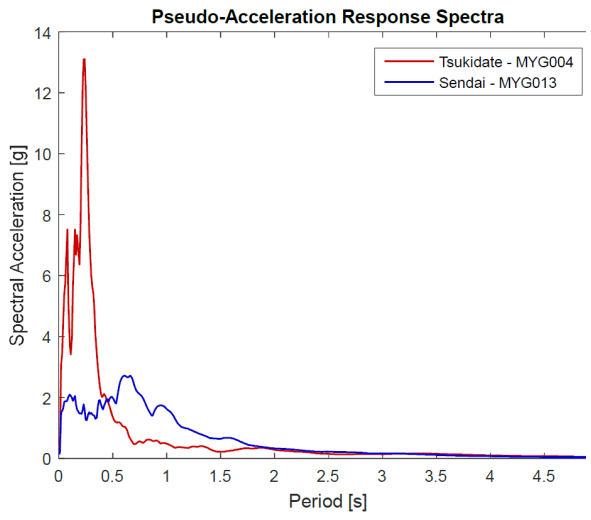

Figure 13: PSA Response Spectra of the NS components in Tsukidate and Sendai.

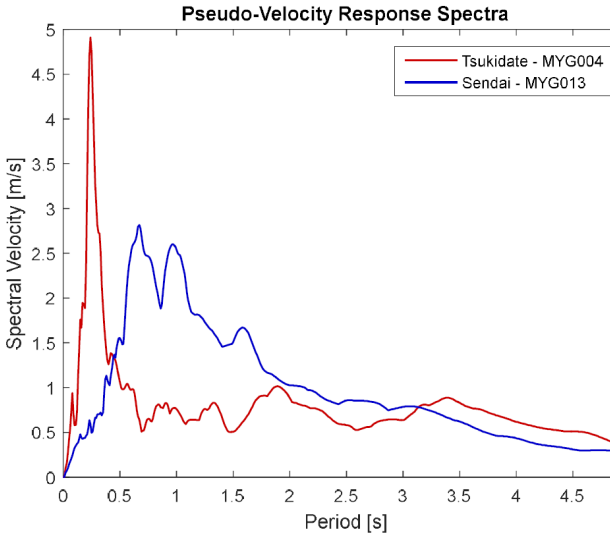

Figure 14: PSV Response Spectra of the NS components in Tsukidate and Sendai.

Results show how the most distinctive characteristic is related to the spectral shape of the two records. The motion recorded in Tsukidate is associated with a spectral shape featuring a very sharp spike at 0.24 seconds in the acceleration response spectrum with the maximum response reaching 13 g and much lower amplitudes at other spectral periods. On the other hand, the motion recorded in Sendai generates responses with significantly lower amplitudes but a broader spectral shape ranging from 0.1 to 1.5 seconds.The same features characterize the velocity response spectra as well, with the difference in spectral shape more evident and a relative difference in the maximum velocity responses less pronounced.

The analyses of the elastic response spectra give information about the maximum responses of a variety of structures with different fundamental periods but it does not provide a meaningful insight into the relationship with potential for structural damage.

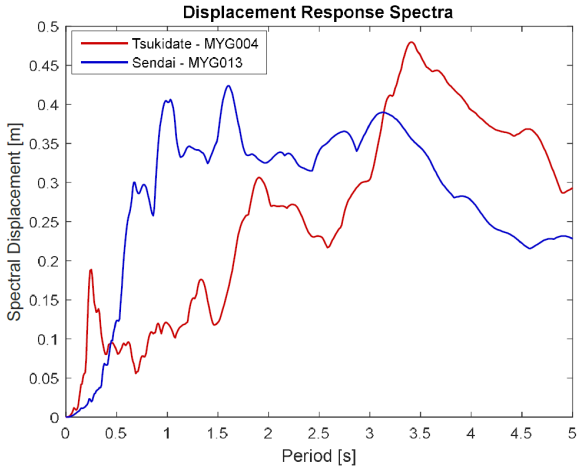

Figure 15: Displacement Response Spectra of the NS components in Tsukidate and Sendai.

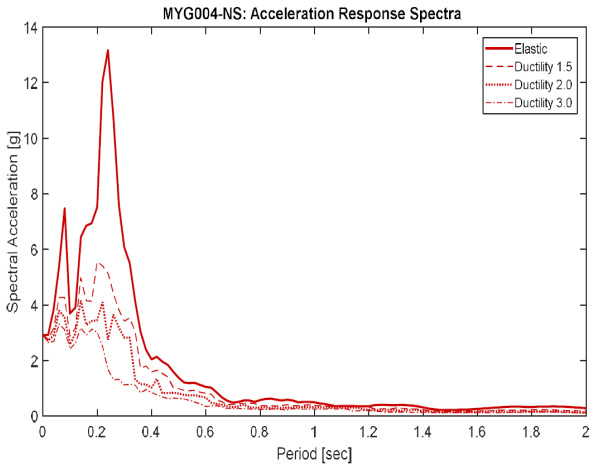

Figure 16: Constant Ductility Spectrum for Tsukidate.

CONSTANT DUCTILITY SPECTRA ANALYSIS

The Constant Ductility Spectrum is a tool used to calculate the lateral resistance of a system to ensure that a target ductility is achieved in design (Scott and Mason, 2017). Constant ductility spectra have been calculated for Tsukidate and Sendai using Bispec V2 computer program (Earthquake Solutions, 2017). Different levels of ductility (1.5, 2 and 3) have been considered to explore a broad range of nonlinear capacities. Figure 16 and Figure 17 show the constant ductility spectra for the Tsukidate and Sendai.

The nonlinear spectra for the motion recorded in Tsukidate show how the spectral shape significantly changes for each level of ductility when considering a nonlinear system. This rapid decrease in spectral amplitudes is particularly significant in comparison with the very sharp peak at the period of 0.24 sec. A slight increase of ductility to 1.5, results in a decrease of about 60% in spectral amplitude, reaching a spectral acceleration of about 5 g, much less than the elastic spectral value of 13 g. This shows that even a small amount of inelastic behaviour would reduce high intensity low period peaks to significantly lower values.

As for the inelastic spectra generated with the Sendai record, the spectral shape is quite similar to the broad banded shape of the elastic spectra and the decreases in amplitudes, even for very low value of ductility are about than 40%.

In general, it can be seen that the displacement demands for Sendai are higher than the ones generated with the ground motion at Tsukidate for a period range from 0.4 to 3.3 sec, for a variety of ductility capacities. Based on the results shown in Figure 18 it would seem that the constant ductility displacement spectra might be a useful tool for discriminating between the damage potential of the different earthquake records.

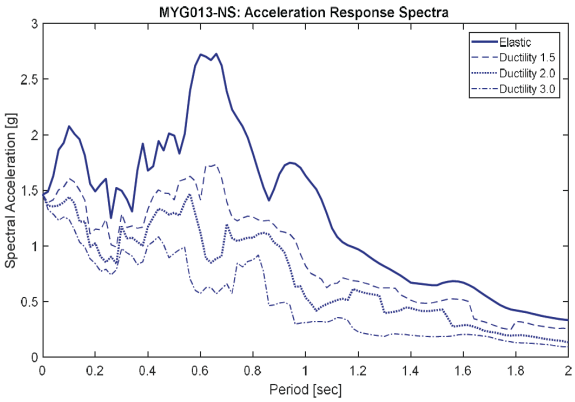

Figure 17: Constant Ductility Spectrum for Sendai.

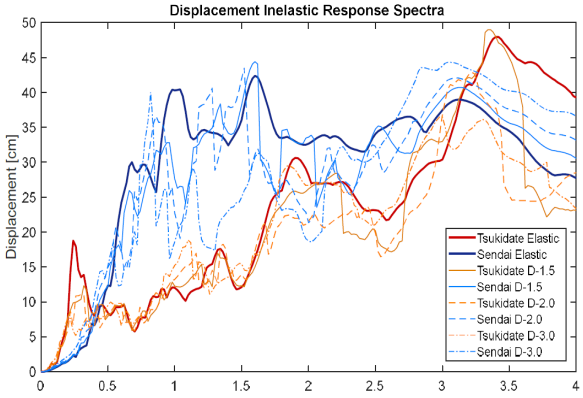

Figure 18: Comparison of Constant Ductility Spectrum for Displacement Response.

CONCLUSIONS

This paper is a preliminary exploration at understanding how the characteristics of the subduction ground motions affect their damage potential. To this purpose, several characteristics have been considered for comparison. Peak Ground Acceleration (PGA) has been shown not to be a good index for structural damage potential. The Arias intensity was found to be poorly correlated to the structural damage observed in the field. Elastic response spectra and constant ductility spectra were generated for the two ground motions under consideration. Except for the constant-ductility displacement spectra, these spectra did not show a meaningful correlation to the damage potential of the motions.

ACKNOWLEDGMENTS

The author would like to acknowledge the financial support of the Natural Sciences and Engineering Research Council (NSERC) of Canada. This paper used data recorded by the Japanese strong motion network (K-NET and KiK-net) administrated by the National Research Institute for Earth Science and Disaster Prevention (NIED). Dr. Ilaria Capraro helped with the data processing part of this study.

REFERENCES

Arias, A. (1970) "A measure of earthquake intensity," *Seismic Design for Nuclear Power Plants*, pp. 438-483.

Bommer, J. and D. Boore (2004). "Engineering Seismology," in *Encyclopaedia of Geology*, R. Selley, R. Cocks and I. Plimer, Eds., Oxford, Elsevier, pp. 499-514.

Earthquake Solutions (2017). "*Providing State-of-the- Art Software for Structural and Earthquake Engineering*,"[Online].Available: http://www.eqsols.com/Pages/Bispec.aspx. [Accessed 4 July 2017].

Japan Meteorological Agency. (2017). "Tables explaining the JMA Seismic Intensity Scale," [Online]. Available: http://www.jma.go.jp/jma/en/Activities/inttable. html#ryuui. [Accessed 4 July 2017].

National Research Institute for Earth Science and Disaster Prevention (NIED), "Strong-motion eismograph networks (K-NET, Kik-net)," National Research Institute for Earth and Disaster Resilience.

Nishiyama, I., I. Okawa, H. Fukuyama and Y. Okuda (2011). "Building Damage by the 2011 off the Pacific coast of Tohoku earthquake and coping activities by NILIM and BRI collaborated with the administration," in *43rd Joint Meeting of U.S.-Japan Panel on Wing and Seismic Effects,* Tsukuba, Japan.

Ochi, S. and M. Suzuoki, (2011) "The lessons of the Great East Japan Earthquake 2011 and the countermeasures against earthquakes and tsunamis in future - Fundamental Concepts behind Future Tsunami Disaster Prevention," in *43rd Joint Meeting of U.S.-Japan Panel on Wing and Seismic Effects*, Tsukuba, Japan.

Scott, M.H. and H.B. Mason, (2017), "Constant-ductility response spectra for sequential earthquake and tsunami loading," *Earthquake Engineering and Structural Dynamics*.

Shojiro, K., N. Kazuhiro, M. Kazunari and K. Masahiro, (2011), "Strong Mootion and Earthquake Response Records of the 2011 off the Pacific Coast of Tohoku Earthquake," in *43rd Joint Meeting of U.S.-Japan Panel on Wing and Seismic Effects*, Tsukuba, Japan.

Ventura, C.E. (2011), "Ground Shaking during the 2011 Japan Earthquake: what have we learned?". Presentation to Structural Engineers Association of BC, Vancouver, BC. Canada.

Day2 (Tuesday, Sep. 26th, 2023) 11:20~11:45

Innovative Solutions for Seismic Retrofit of Non-Ductile Construction

Murat Saatcioglu

Distinguished University Professor,

Department of Civil Engineering, University of Ottawa, Ottawa, Canada

Dr. Murat Saatcioglu is a Distinguished University Professor in the Department of Civil Engineering of the University of Ottawa, Ottawa, Canada. He received his B.S. in Civil Engineering from the Middle East Technical University, Ankara Turkey, his MASc. in Structural Engineering from the University of Toronto, Toronto, Canada, and his Ph.D. in Structural Engineering from Northwestern University, Evanston, Ill., USA. He is a Fellow of the Canadian Academy of Engineers, Engineering Institute of Canada, American Concrete Institute (ACI), and the Canadian Society for Civil Engineering (CSCE). Dr. Saatcioglu's research interests include analysis, design, and retrofit of structures subjected to extreme loads, including those caused by earthquakes and bomb blasts. He has conducted extensive experimental and analytical research on earthquake and blast resistant structures, and contributed towards the development of codes and standards, nationally and internationally.

Professor Saatcioglu is the recipient of numerous national and international research and teaching awards and medals, including the 2015 A.B. Sanderson Award of CSCE for outstanding contributions to the development and practice of structural engineering in Canada; the 2014 Whitman Wright Award of CSCE for significant contributions to the advancement of innovation and information technology in civil engineering; the 2001, 2004 and 2015 Casimir Gzowski Medals for best papers in the Canadian Journal of Civil Engineering; the 2004 Wason Medal of ACI, the 2000 Raymond C. Reese Research Prize of the American Society of Civil Engineers for outstanding contributions to the application of structural engineering research, the 2005 CCEDS-1 Award for Best Paper from McMaster University; and the 1989 Charles Whitney Medal of ACI. In 2021 he was listed among the World's Top 2% Scientists in all categories by Stanford University.

INNOVATIVE SOLUTIONS FOR SEISMIC RETROFIT OF NON-DUCTILE CONSTRUCTION

Murat Saatcioglu
Distinguished University Professor, Department of Civil Engineering, University of Ottawa, Ottawa CANADA
Email: Murat.Saatcioglu@uOttawa.ca

ABSTRACT

Non-ductile reinforced concrete frame buildings and unreinforced masonry (URM) infill or load bearing walls suffer significant damage when subjected to strong earthquakes. Existing inventory of buildings worldwide includes such non-ductile structures either because they were designed prior to the enactment modern seismic design codes or built in regions of the world where code enforcement creates challenges. Seismic retrofit of these buildings offers a viable strategy for seismic risk mitigation. This has created the impetus for developing innovative retrofit methodologies at the University of Ottawa through experimental and analytical research. The retrofit techniques include column jacketing either through transverse prestressing or by providing carbon fibre reinforced polymer (CFRP) jackets; reinforced concrete frame bracing either by diagonal prestressing strands or buckling restrained braces (BRB); and unreinforced masonry (URM) infill or load bearing walls with internal reinforcement and/or CFRP sheets. The results, summarized in this paper, show successful enhancement of inelastic deformability, and/or seismic force resistance of otherwise seismically deficient buildings, while also resulting in improved drift control.

Keywords: CFRP, concrete column jacketing, drift control, earthquake engineering, FRP, infill walls, load bearing walls, prestressing, seismic retrofitting, seismic bracing, unreinforced masonry, URF.

INTRODUCTION

Performance of buildings during previous earthquakes has consistently demonstrated that non-ductile reinforced concrete frame buildings, with or without masonry infill walls are vulnerable to seismic excitations. Load bearing masonry buildings also exhibit brittle behavior under strong earthquake forces. Both types of buildings represent a significant proportion of building inventory in the world, especially if they were designed and built prior to the enactment of modern building codes which call for ductile response with energy dissipation capabilities and capacity protection of non-ductile elements. The same type of seismic deficiency can also be found in newer buildings if the implementation of seismic design requirements cannot be ensured, and code enforcement creates challenges. It is economically not feasible to replace a large number of seismically deficient buildings with newer structures that are code compliant. Hence, seismic retrofitting of these seismically deficient buildings remains to be a viable seismic risk mitigation strategy. A comprehensive seismic retrofit research program has been underway at the Structures Laboratory of the University of Ottawa to develop retrofit methodologies for brittle concrete columns and URM walls for buildings that benefit from local seismic improvements, as well as seismic bracing of non-ductile frames at the system level for overall building protection. The details of individual projects that make up the research program are summarized in the following sections.

CONCRETE COLUMN RETROFITS

Columns are critical elements, responsible for strength and stability of the structure above, especially if located at the critical lower levels. In frame structures they play a key role in providing resistance to seismic forces. Seismically deficient columns may suffer damage due to lack of inelastic moment capacity and/or inelastic deformability (ductility) in flexure, or brittle shear damage associated with insufficient diagonal tension capacity. These deficiencies result from lack of properly designed transverse column reinforcement. Sometimes lack of proper splicing of longitudinal reinforcement in the plastic hinging region results in bar slippage, reducing seismic resistance and energy dissipation. All of these seismic deficiencies in existing buildings benefit from externally provided additional transverse

reinforcement. Two techniques were researched, as described below, one providing transverse prestressing to columns and the other involves the use of CFRP jackets.

Transverse Prestressing for Column Retrofits (RetroBelt)

Transverse reinforcement in reinforced concrete columns (known as a RetroBelt system of seismic retrofitting) fulfils three main functions: restraining longitudinal reinforcement against buckling; increasing shear resistance; and confining concrete for improved deformability. Lateral confinement also improves bond between steel and concrete, playing a crucial role in the performance of spliced longitudinal reinforcement. The Retro-Belt system externally applies a lateral prestressing force, which improves all three mechanisms, enhancing strength and deformability of concrete columns. The system consists of specially designed anchors, which hold the stress in the prestressing strands, placed as individual hoops at a designed spacing and prestress level. The resulting high active lateral pressure provides improved concrete confinement as well as diagonal tension (shear) crack control, increasing strength and ductility of columns. It also enhances bond between steel and concrete, improving behavior in splice deficient regions.

An experimental investigation of the Retro-Belt system was conducted, involving 19 large-scale R/C columns tested under simulated seismic loading. The test columns were designed to investigate shear-dominant and flexure-dominant columns, as well as the problems associated with lap-splices. Figure 1 shows application on a circular column and comparison of hysteretic behavior of columns with and without the application of RetroBelt system.

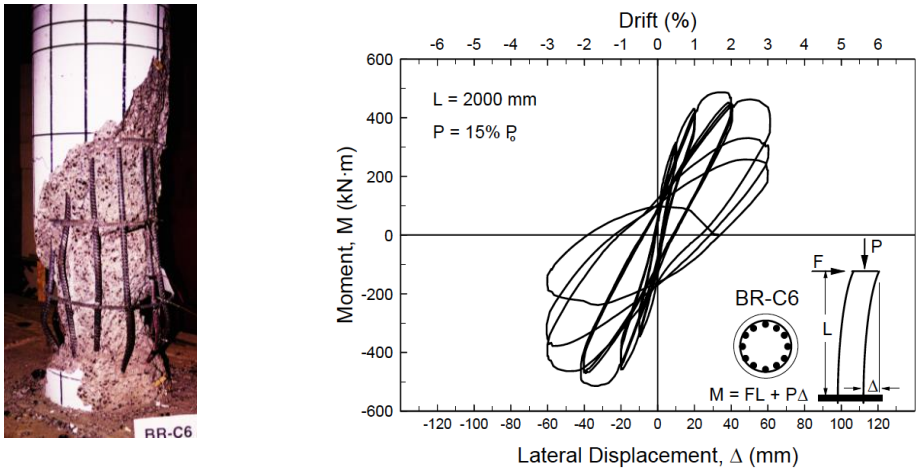

a) Seismically deficient Column BR6

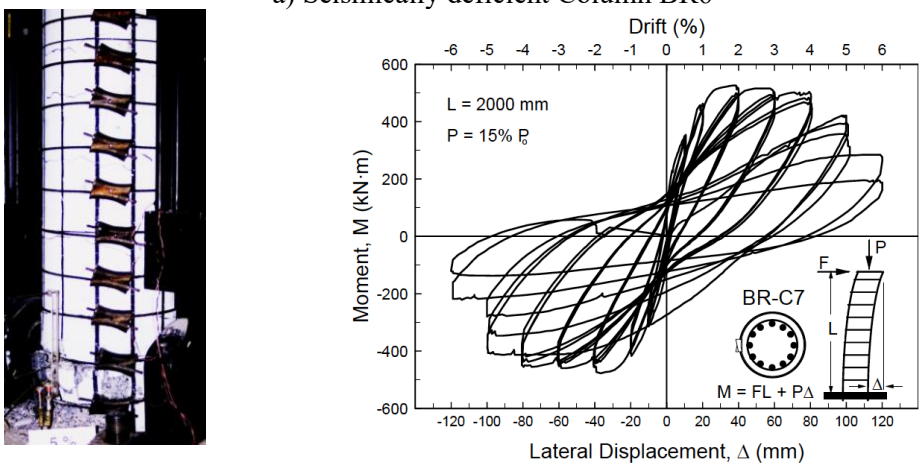

b) Column BR7 retrofitted with RetroBelt

Figure 1. Flexure-dominant column with and without the application of the RetroBelt system.

Columns with CFRP Jackets

Large-scale square and circular reinforced concrete columns were tested under simulated seismic loading with and without carbon FRP (CFRP) sheets. The tests included flexure-dominant and shear-dominant columns under different levels of constant axial load, accompanied by incrementally increasing drift reversals. They were representative of bridge columns having 500 mm to 610 mm cross-sectional dimensions subjected to 15% of column concentric capacity and building columns having a 270 mm cross section subjected to 30% to 43% of their concentric capacities. The columns were jacketed with different plies of CFRP sheets to assess their effectiveness under different geometric and stress conditions. Figure 2 (a) illustrates typical test columns during testing. The concrete strength in the columns ranged between 38 MPa for bridge columns and 50 MPa to 90 MPa for building columns. The results indicate that CFRP jackets can increase column deformability up to 4% to 6% drift ratios in shear dominant columns and 6% to 8% in flexure dominant columns depending on the number of plies, the level of axial compression, and the degree of rounding of the corners in square columns prior to the application of the CFRP sheets. Figure 2 (b) and (c) show sample hysteretic relationships obtained from the test program. Both normal-strength and high-strength concrete columns benefited from CFRP jackets with higher number of plies required for high-strength concrete columns. An important parameter for jacket design was the effectiveness of the CFRP jacket, which improved with the level of axial compression as more concrete in the critical section expanded in transverse direction, bringing CFRP strains close to 1.5%. Columns with low levels of axial compression, on the other hand, experienced limited transvers strains with CFRP strains approaching between 0.6% and 1% for square and circular columns. Some of the columns were designed to have insufficient splice lengths for longitudinal reinforcement (20 times the bar diameter) in potential plastic hinge regions as representatives of older practice. These columns showed limited benefits from CFRP jacketing. The drift capacity was limited to 2% and 3% for square and circular columns, respectively, also exhibiting severe pinching of hysteresis loops.

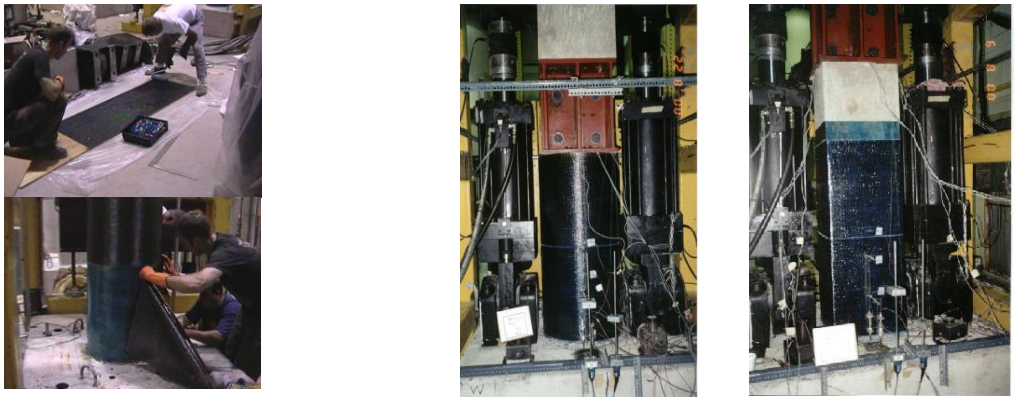

a) Application of CFRP jackets and column tests

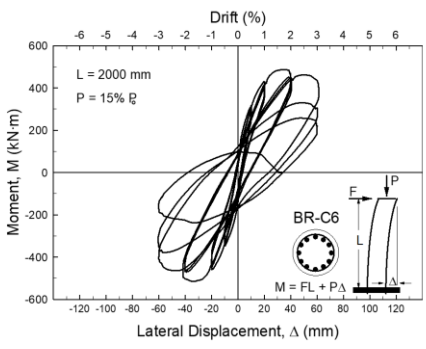

b) Unretrofitted column

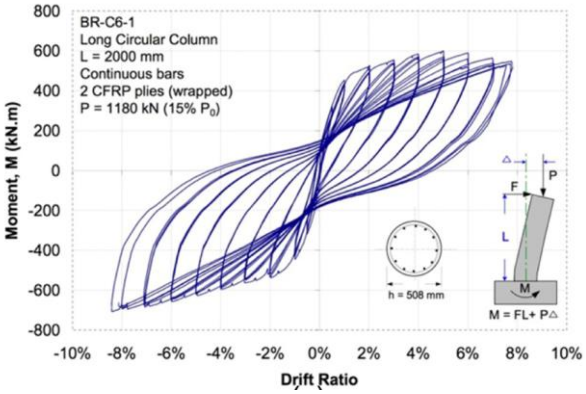

c) CFRP retrofitted column

Figure 2. Comparisons of two flexure-dominant columns one with and the other without a CFRP jacket.

BRACING OF NON-DUCTILE REINFORCED CONCRETE FRAMES

When the number of seismically deficient elements in a multistory building is high, it is more feasible to provide a system level retrofit. These frame buildings benefit from increased seismic force resistance and drift control while the frames continue fulfilling their gravity load carrying functions. Two frame bracing systems were developed experimentally, one involving a buckling restrained brace (BRB) and the other involving progressively engaging diagonal prestressing cables. The details are summarized below.

Non-ductile Concrete Frames Braced with a Newly Developed BRB System of Retrofitting

An experimental investigation was conducted to assess the performance of a new Buckling Restrained Brace (BRB) system for retrofitting seismically deficient reinforced concrete frames. The BRB consists of a ductile inner steel core bar designed to yield in tension and compression without buckling, while controlling response to seismic forces. The core bar is contained within a tubular steel section, which in turn is housed in a larger tubular steel section infilled with mortar providing lateral restraint against buckling. Self-consolidating mortar is used as filler material between the two tubular sections to increase the buckling resistance. The inner core bar is connected to innovative end units that allow extension and contraction during tension-compression cycles while providing lateral restraint against buckling. The new BRB system has been verified experimentally by using two large-scale reinforced concrete frames and conducting a reference un-retrofitted frame test, as well as 4 retrofitted frame tests. Tests demonstrated substantial increases in the lateral load and energy dissipation capacities of retrofitted frames with satisfactory drift control. Three different types of steel bars with different strength and elongation characteristics were considered. Among the three, stainless steel provided the best strength, stiffness and ductility enhancements. Figure 3 shows two companion frames, one with and the other without the BRB system of retrofitting.

a) Unretrofitted control frame

b) BRB braced frame

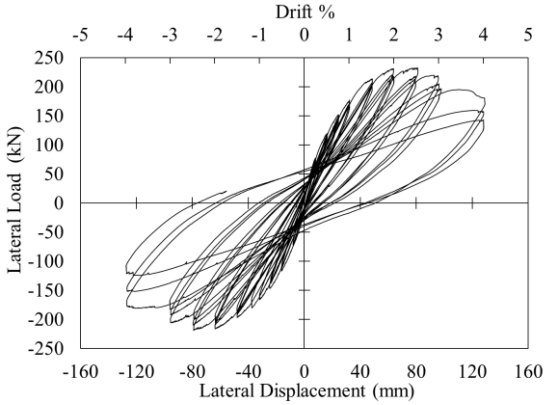

c) Hysteretic behavior of control frame

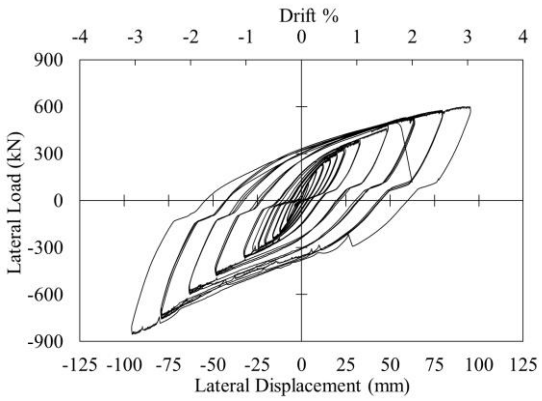

d) Hysteretic behavior of braced frame

Figure 3. Application of BRB to brace a non-ductile reinforced concrete frame.

Progressively Engaging Diagonal Cables for Seismic Bracing

Existing bracing systems for seismic retrofitting used in practice can be intrusive and result in lengthy down times and expensive structural interventions. An alternative to conventional techniques is the use of high-strength prestressing strands or cables, diagonally placed as tension elements. This technique was researched at the University of Ottawa through experimental and analytical research in two-phase research program. The use of steel strands as tension brace elements proved to be an effective technique during the first phase of research. However, the resulting stiffening effects on the frames led to increased seismic force demands as well as increased axial forces on the attached columns, potentially generating net tension in columns, foundation uplift, and excessive compression in columns on the other side. Relatively low elongation characteristics of high-strength cables and slack caused by yielding strands and associated pinching of hysteresis curves reduced potential energy dissipation capacity. In the second phase of research the technique was improved by developing progressively engaging, initially loose multiple strands as tension cables. These cables were placed loosely to engage during seismic response at pre-determined drift levels, thereby eliminating premature increase in seismic force demands until their participation was required. Tests of a large-scale reinforced concrete frames were conducted as proof of concept with subsequent numerical research to expand the results. Figure 4 shows the hysteretic response of two frames with cables engaging at different levels of lateral drift.

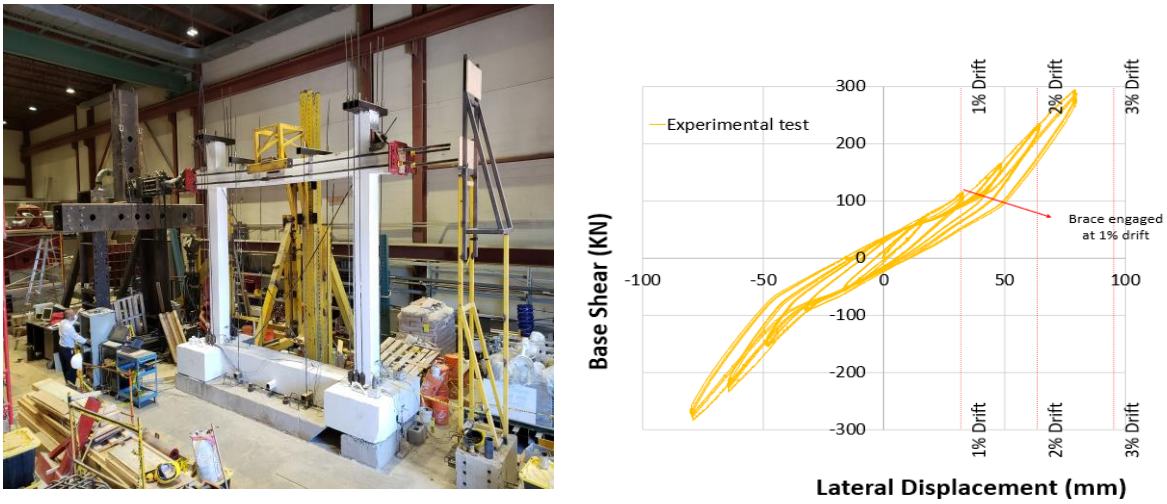

a) Frame with single loose strand along each diagonal engaging at 1% drift.

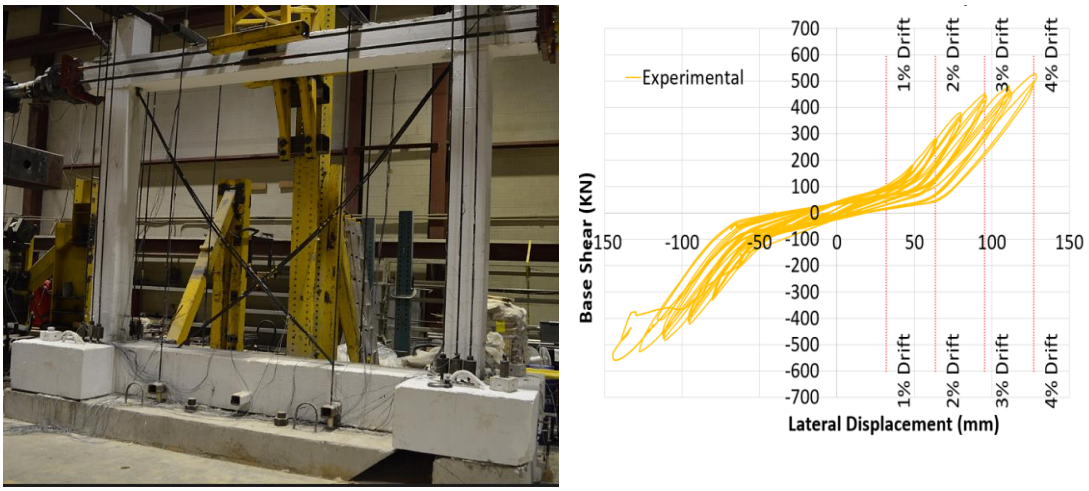

b) Frame with three loose cables along each diagonal designed to have the first cable engage at 1.5% drift and the other two at 2% drift.

Figure 4. Application of progressively engaging tension only cable braces.

MASONRY WALL RETROFITS

Masonry walls (unreinforced or partially reinforced), perform in a brittle manner, often resulting in catastrophic failures during strong earthquakes. Innovative retrofit techniques were developed for these walls through experimental research involving surface bonded CFRP sheets for shear strengthening and different types of flexural reinforcement for improved flexural resistance. The reinforcement for flexural strengthening involved the following materials, well anchored to the foundation concrete:

i. CFRP anchors, shown in Figure 5(a), resulting in limited improvement.
ii. Ductile steel sheets, shown in Figure 5(b), resulting in energy dissipation.
iii. Internal reinforcement, shown in Figure 5(c), developing significant flexural strength enhancement, but premature shear failure due to diagonal compression crushing.
iv. Prestressing strands in boundary regions, shown in Figure 5(d), resulting in significant strength enhancement with self-centering characteristics.

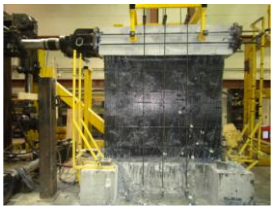

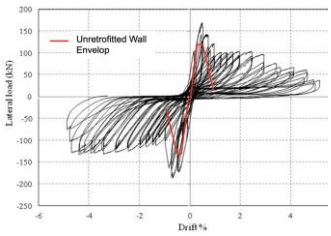

a) Wall with CFRP anchors

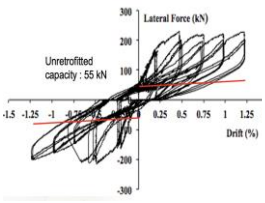

b) Wall with steel sheets as anchors

c) Wall with internal reinforcement for flexure

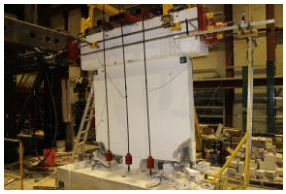

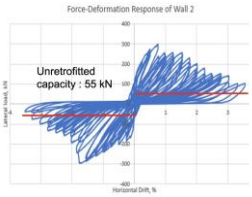

d) Prestressing at the ends for flexure

Figure 5. Masonry wall retrofit techniques involving CFRP sheets for diagonal tension control and different vertical reinforcement for flexural strengthening.

CONCLUSIONS

The following conclusions can be drawn from the experimental research program reported in this paper for the development of seismic retrofit methodologies:

- Transverse prestressing of concrete columns induces active and passive lateral pressure on concrete, which improves concrete confinement resulting in enhanced ductility. It also controls diagonal tension caused by shear, improving column shear capacity.
- CFRP jackets result in significant improvements in column flexural and shear capacities while also enhancing inelastic deformability.
- Non-ductile reinforced concrete frames can be braced by BRBs for enhanced lateral force resistance and drift control, improving overall seismic response of the entire building.
- Progressively engaging tension only cable braces can control lateral drift of frame buildings and increase seismic force resistance when needed (when engaged at different design drift levels) without prematurely stiffening the frames and increasing seismic force demands.
- Surface mounted CFRP sheets applied on masonry walls increase diagonal tension capacity associated with seismic shear force reversals. However, the CFRP sheets cannot prevent diagonal compression crushing of masonry units unless the masonry units are filled with concrete. The same walls can be strengthened for flexure either by providing CFRP anchors or steel sheet anchors externally or reinforcing steel internally. Prestressing the walls by inserting strands in boundary regions increases flexural strength while promoting self-centering.

Day2 (Tuesday, Sep. 26th, 2023) 11:45~12:10

Introduction to the Policy of Net-Zero Building Among the Net-Zero Transition

Chung-Pi Luan

Chief Secretary, Architecture and Building Research Institute

Chung-Pi Luan obtained his Master of Architecture from University of Pennsylvania and a Ph.D. of Architecture from National Taiwan University of Science and Technology. Presently, he holds the position of Chief Secretary at the Architecture and Building Research Institute under the Ministry of Interior. He has served in the government for decades, and is mainly responsible for the formulation, management, and research of regulations related to architectural technology. He represented as Chinese Taipei to participate in the Meeting of APEC Architect Plan, and promoted mutual recognition agreement of architects with other countries. These years, in response to the pressing issues of global warming and environmental crises, his research interest is focused on sustainable development, such as strategies for promoting net-zero buildings.

Day2 (Tuesday, Sep. 26th, 2023) 13:20~13:45

Key Issues in Decarbonizing the Built Environment

Trevor Nightingale

Director General, National Research Council of Canada

Trevor is Director General of the Construction Research Centre at the National Research Council Canada where he oversees 265 research and technical professionals who push the frontiers of building science and engineering and publish the National Model Codes.

Prior to becoming Director General in 2019, Trevor led NRC's High-performance Buildings program, which helped industry develop and commercialize energy-saving retrofit technologies for commercial and institutional buildings. A major thrust was the effective integration of buildings with smart grid to realise benefits to both the system operator and the building/home owner. With industry and the provincial utility, he championed several large scale technology development and pilot projects in New Brunswick that help the utility company to develop products and programs to address winter peak reduction.

Trevor was the Director of Research and Development for the Intelligent Building Operations research unit from 2010 to 2015, where he guided research in the areas of lighting, heating, ventilation, human factors, building controls, and energy measurement and verification.

Trevor began his career at NRC in 1992 as a researcher and holds a Bachelor of Science in Physics from the University of British Columbia, and a Ph.D. in Building Engineering, from Heriot Watt University in the United Kingdom.

Day2 (Tuesday, Sep. 26th, 2023) 13:45~14:10

A Review of Digital Transformation Efforts and Initiatives in Canada's Built Asset Industry

Sheryl Staub-French

Professor, Department of Civil Engineering
in the Faculty of Applied Science,
The University of British Columbia, Vancouver, Canada

Dr. Staub-French is a Professor in the Department of Civil Engineering in the Faculty of Applied Science. She is Director of the BIM TOPiCS Lab where she leads inter-disciplinary research focused on developing methods and tools to support the digital delivery of sustainable building construction projects through effective and collaborative use of building information modeling (BIM). She has published over 100 papers in leading journals and conferences on BIM and related topics. Her lab has made significant contributions in developing BIM guidelines and best practices; collaborating with industry and government to advance technology transfer; and developing tools to support virtual design and digital delivery.

As the first Associate Dean of Equity, Diversity and Inclusion (EDI) in the Faculty of Applied Science, Dr. Staub-French is a strong leader and advocate in advancing EDI in engineering and leading the Faculty's EDI initiatives. She received her BS in Civil Engineering from Santa Clara University and her MS and PhD from Stanford University.

A REVIEW OF DIGITAL TRANSFORMATION EFFORTS AND INITIATIVES IN CANADA'S BUILT ASSET INDUSTRY

Sheryl Staub-French[1] and Erik A. Poirier[2]

1. Professor, Department of Civil Engineering, University of British Columbia, Vancouver, BC, Canada
2. Professor, Department of Construction Engineering, École de Technologie Supérieure, Montreal, QC, Canada

Email: ssf@civil.ubc.ca, erik.poirier@etsmtl.ca

ABSTRACT

As with other countries around the world, Canada has put forward several efforts and initiatives to support the digital transformation within its built asset industry. Being essentially characterized by the adoption and implementation of building information modeling (BIM) and its complimentary technologies, these efforts and initiatives have emerged and been driven at various levels within industry, academia and government and with different objectives guiding them. Moreover, the scale and scope of their deployment have differed as has their impact within industry. After more than two decades of such efforts, several lessons can be extracted and reflected upon to inform the next generation of initiatives aimed at supporting and accelerating the digital transformation of Canada's built asset industry. This keynote aims to provide an overview of the past and current initiatives across Canada, their remit and aim, their high-level impact, and the lessons to be taken to inform future initiatives. The results will be presented across three critical domains: Creating and systematizing demand for digital project delivery and built asset management, upskilling industry stakeholders across industry segments, as well as structuring practice and harmonizing capabilities across supply and value chains through standardization. The results show that despite the lack of a structured or harmonized approach at the national level, significant gains have been obtained in certain areas and certain jurisdictions. Emerging efforts have enabled a more consistent approach across the country. In this light, several governmental bodies are now mobilizing resources and laying the groundwork for a more common and harmonized approach to digitalization of Canada's built asset industry.

Keywords: BIM, Digital transformation, Digitalization initiatives, Canadian built asset industry

Day2 (Tuesday, Sep. 26th, 2023) 14:10~14:35

New Shake Table Testing Facility for Structures and Non-structural Components

David Lau

Professor, Department of Civil and Environmental Engineering, The University of Carleton University, Ottawa, Canada

Dr. David T. Lau is a Professor in the Department of Civil and Environmental Engineering of the University of Carleton University, Ottawa, Canada. His research interests on structural dynamics and earthquake engineering; monitoring and assessment of large structures including the Confederation Bridge; development of measurement and high speed computer data processing techniques for real-time monitoring; repair, retrofit and strengthening techniques and strategies for existing bridges, buildings, liquid storage tanks and other infrastructures, including the seismic application of advanced composite materials and other innovative devices; dynamic response and earthquake resistant design of bridges, buildings, liquid storage tanks and concrete arch dams; ritz vector approach or finite element method for nonlinear structural analysis.

NEW SHAKE TABLE TESTING FACILITY FOR STRUCTURES AND NON-STRUCTURAL COMPONENTS

David Lau[1], Jeffery Erochko[2], Cameron Flude[3], and Geoffrey Davidson
1. Professor, Carleton University, Ottawa, Ontario, Canada
2. Associate Professor, Carleton University, Ottawa, Ontario, Canada
3. Ph.D. Candidate, Carleton University, Ottawa, Ontario, Canada
4. Former Graduate Student, Carleton University, Ottawa, Ontario, Canada
Email: davidlau@cunet.carleton.ca, jeffreyerochko@cunet.carleton.ca, cameronflude@cmail.carleton.ca, geoffreydavidson@cmail.carleton.ca

ABSTRACT

As part of a new facility for multi-hazard testing of built infrastructure protection and resilience, a new mobile multi-unit shake table system has been developed and recently commissioned at Carleton University. The new shake table system consists of four fully reconfigurable 6-degree-of-freedom hexapod motion tables that are electro-mechanical powered. The motion tables can be operated individually or utilized in any combinations to impose multiple support excitation motions for testing of large size or long-span structures. The four motion tables can also be operated in synchronization as a single large shake table with four times the payload capacity of the individual table. The paper briefly describes the unique and flexible capabilities of the new mobile reconfigurable shake table system. A research program using the new shake table system for suspended ceilings in tall buildings is also presented.

Keywords: Shake Table, Super-tall Building, Suspended Ceiling, Non-structural Component.

INTRODUCTION

New state-of-the-art seismic testing facilities at Carleton University utilize four independent mobile shake tables by MTS Systems Corporation and their subsidiary E2M Technologies B.V. Each table can duplicate motions in six degrees-of-freedom and the four tables can be controlled such that they move individually, each table independent of the movement of the other tables, or such that they move together as a single large platform in translation and rotation about one reference location. Since there are four separate mobile tables, they can be re-positioned relatively easily into any configuration. This gives the researcher a great amount of flexibility in how their tests can be set up. The tables can be used as one large table with a test frame connected between the tables or as individual tables that can move independently to simulate multiple support excitations such as bridge piers or as a building with structural separations. The mobility of the tables is also advantageous in that the tables can be placed in storage when not in use and there does not need to be a designated shake table laboratory.

SHAKE TABLE CAPABILITIES

Each table has a relatively large stroke length and can reproduce translational displacements of over +/- 500mm in both horizontal directions and over +/- 400mm in the vertical direction as well as rotational displacements of over 23° about all three axes. Figure 1, Figure 2 and Figure 3 show one of the shake tables with displacements in vertical, horizontal and rotational directions. The result is a unique system with flexible capabilities for seismic testing for a wide range of applications of different structural systems. Because of its unique combination of 6-degree-of-freedom and large range of stroke lengths and rotation angles, it is especially suitable for testing of non-structural or operational and functional components (OFC).

Figure 1. Shake table with vertical displacement

Figure 2. Shake table with horizontal displacement

Figure 3. Shake table with rotational displacement

TEST SETUP FOR NON-STRUCTURAL COMPONENT TESTING

Over the past decades there have been significant advancements in earthquake engineering in building design, resulting in stronger, more resilient, and safer structures. However, over the same period there has been more limited development of improvement in other areas concerning building safety, especially in the performance of non-structural building components during earthquakes. A modern structure designed in accordance with current building codes can be expected to survive a significant earthquake, remaining intact even though it may suffer a controlled amount of damage. In contrast, experiences from recent major earthquakes, such as the 1994 Northridge (Norton et al., 1994), 2011 Christchurch (Dhakal et al., 2011), and the 2011 Tohoku earthquakes (Motosaka and Mitsuji, 2012) have clearly demonstrated that non-structural components are susceptible to suffer significant damage which affect the operation and functional performance of their hosting structures.

A steel test frame which can be supported by the four tables in a 5.4m x 5.4m square, shown in Figure 1, was specially designed for testing non-structural components (Davidson, 2021). The test frame is a steel braced structure with perimeter beams and open web steel joists forming the roof/floor structure. Steel angles can be installed on the perimeter of the test frame at varying heights below the underside of the joists to simulate the perimeter support conditions for suspended non-structural components, such as suspended ceilings, and allow for different suspension heights. The test frame was designed with the intention to reduce the amplification of the input excitations in both the vertical and horizontal directions and as such the bare frame's fundamental frequency in the horizontal and vertical directions was designed to be greater than 20 Hz. The relatively high stiffness of the frame will reduce amplification and therefore allow desired floor motion responses to be inputted directly and give greater control of the response motion to the researchers. In addition, if a lower vertical frequency is desired for specific testing, weight can be added to the roof of the frame to lower the frequency. Accelerometers mounted on the test frame measure the response of the test frame when it is subjected to different input excitations. The measured values are inputted into the shake table control software which uses an iterative approach to alter the table input motions and reduce the error between the desired response of the test frame and the measured response.

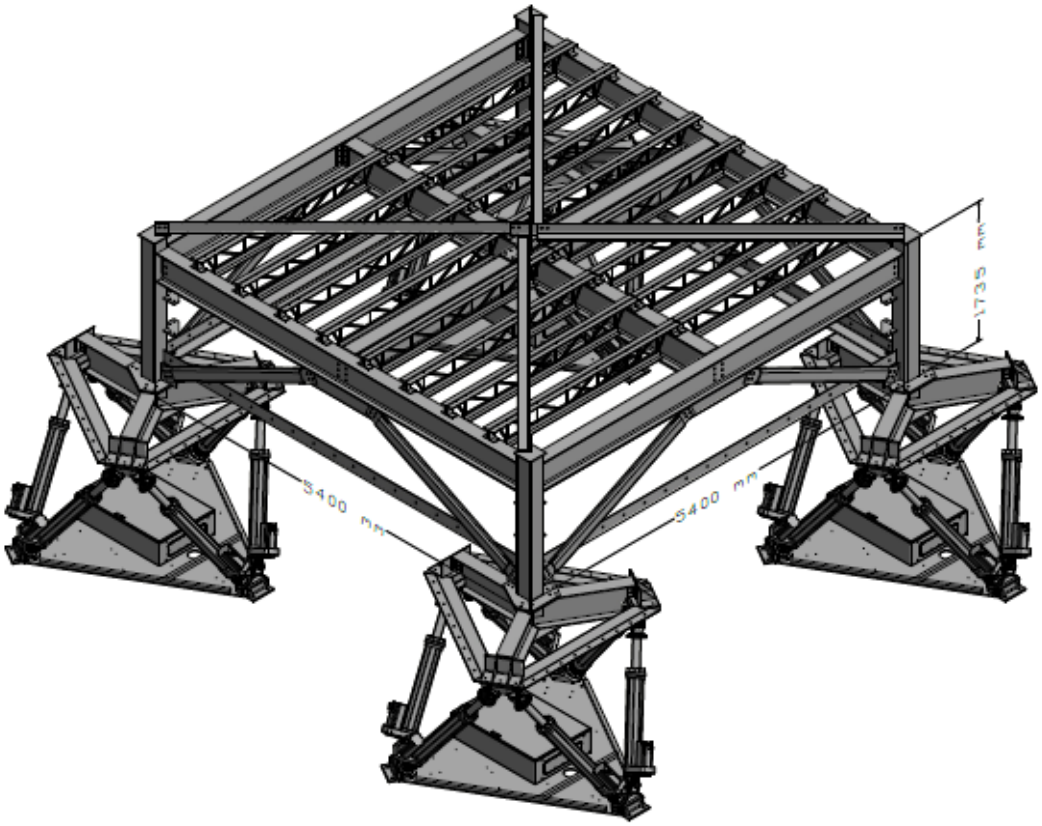

Figure 4. Test frame setup (Davidson, 2021)

The first testing program using this facility will investigate the seismic performance of suspended ceilings. The test program will use floor motions from a range of building types including supertall buildings which include a rotational component. Suspended ceilings are among the many types of non-structural components commonly used in commercial, office and institutional buildings such as schools and some medical facilities. Ceiling failure poses a major life safety hazard as falling ceilings are a serious threat to building occupants and can cause significant damage to other collocated components like electrical wiring or gas lines, resulting in loss of building function or possibly starting fires within the building. Furthermore, fallen ceilings create additional hazards as they can severely impede evacuation of the building and subsequent emergency search and rescue response. Damage to suspended ceilings has been reported as one of the most commonly observed types of damage to non-structural components even in moderate earthquakes that have higher probability of occurrence (Phan & Taylor, 1996). The capabilities of the tables make these facilities especially suitable for of non-structural or operational and functional components (OFC) including suspended ceilings because they can accurately replicate the floor motion responses from different types of buildings including the rotational components of floor motions.

ACKNOWLEDGMENTS

The authors would like to acknowledge the funding support from Canadian Foundation for Innovation for the new shake table test facilities, which are essential for this research.

REFERENCES

Davidson, G.A. (2021). “Development of testing facilities and procedures for seismic performance of suspended ceilings,” Master’s thesis, Department of Civil Engineering, Carleton University, Ottawa, Ontario, Canada.

Dhakal, R.P., MacRae, G.A., and Hogg, K. (2011). “Performance of ceilings in the February 2011 Christchurch earthquake,” *Bulletin of the New Zealand Society for Earthquake Engineering*, **44**(4), 379-389.

Motosaka, M., and Mitsuji, K. (2012). "Building damage during the 2011 off the Pacific coast of Tohoku Earthquake," *Soils and Foundations*, **52**(5), 929–944.

Norton, J.A., King, A.B., Bull, D.K., Chapman, H.E., McVerry, G.H., Larkin, T.J., and Spring, K.C. (1994). "Northridge earthquake reconnaissance report," *Bulletin of the New Zealand Society for Earthquake Engineering*, **27**(4), 235-344.

Phan, L.T. and Taylor, A.W. (1996). "State of the art report on seismic design requirements for nonstructural building components," U.S. Department of Commerce. National Institute of Standards and Technology.

Day2 (Tuesday, Sep. 26th, 2023) 15:05~15:40

Integration of Technology in Earthquake Engineering Education: A Pathway to Enhancing Learning and Preparedness

Andres Winston C. Oreta

Professor, Department of Civil Engineering, De La Salle University, Manila, Philippines

Andres Winston C. Oreta is a professor at the Department of Civil Engineering (Structural Engineering Division) of De La Salle University (DLSU), Manila, Philippines.

He is a member of the Disaster Resilience Unit of DLSU Center for Engineering and Sustainable Development Research (CESDR). He served as consultant for UNISDR for the development of the concept and website for the "One Million Safe Schools and Hospitals Campaign." He organized a Newton Fund Workshop on "Localising Strategies for Making Cities Resilient to Disasters" with University of Huddersfield in Manila, Philippines. He has also collaborative research projects with University College of London on the project, Philippines Resilience of Schools to Mulit-Hazards (PRISMH) and Cultural Heritage Resilience and Sustainability to Multi-Hazards (CHeRiSH). He is a fellow of the Association of Structural Engineers of the Philippines (ASEP) and chair of the Philippine Group of the International Association for Bridge and Structural Engineering (IABSE). He is a key organizer of the Asia Conference on Earthquake Engineering (ACEE).

INTEGRATION OF TECHNOLOGY IN EARTHQUAKE ENGINEERING EDUCATION: A PATHWAY TO ENHANCING LEARNING AND PREPAREDNESS

Andres Winston C. Oreta[1]
[1]Professor, Department of Civil Engineering, De La Salle University, Manila, Philippines
Fellow, Association of Structural Engineers of the Philippines (ASEP)
Chair, Philippine Group of International Association for Bridge & Structural Engineering (IABSE)
Email: andres.oreta@dlsu.edu.ph

ABSTRACT

Earthquake engineering plays a crucial role in mitigating the devastating effects of seismic events on infrastructure and communities. As the field evolves, the integration of technology into earthquake engineering education has emerged as a new direction in the design of courses related to earthquakes in universities to enhance learning outcomes, promote experiential learning, and bolster preparedness. This presentation presents the author's exploration on the significance of technology in earthquake engineering education and highlights its impact on both students and future professionals. Collaborative platforms and online resources like PEER (earthquake time history database), SeismoSignal (data visualization tools), PHIVOLCS (seismic hazard assessment in the Philippines), STERA-3D (free software for seismic performance assessment of buildings) among others provide students and researchers important tools and data for understanding earthquakes and their impact to the built environment. Video presentations from various sites including YouTube enhances the classroom and online lectures. The affordability of bench-scale shake table testing equipment has now provided opportunities for the students to immerse themselves in realistic scenarios, allowing for hands-on experiences in a controlled and safe environment. As seismic events continue to pose significant challenges, the incorporation of technology in earthquake engineering education becomes increasingly vital in preparing the next generation of engineers to safeguard communities and infrastructure against the destructive forces of earthquakes.

Keywords: earthquake engineering education, shake table, earthquake, seismic hazard, STERA-3D, SeismoSignal, PHIVOLCS

INTRODUCTION

Recognizing the need for future civil and structural engineers to understand the importance of earthquake engineering in professional practice especially in earthquake-prone countries, the current directions is to introduce earthquake engineering as a major or elective course in the curriculum in civil engineering. Many universities all over the world including the United States do not have a course in earthquake engineering at the undergraduate level (Jayamon 2018). As a result, there have been proposals on sample syllabi for a course on earthquake engineering and structural dynamics in civil engineering undergraduate curriculum. Jayamon (2018) proposed a syllabus that highlights lectures on basic concepts in structural dynamics (modeling and dynamic analysis of damped and undamped single and multi-degree of freedom systems) and earthquake engineering (different lateral load resisting systems, equivalent lateral load analysis of the building structure based on the provisions in ASCE 7 and requirements of seismic design guidelines for strength and serviceability limits). The proposed syllabus by Jayamon (2018) has almost the same content as existing syllabi in earthquake engineering from other universities like CE447 Seismic Design of Structures Syllabus by J. Kent Hsiao of Southern Illinois University Carbondale and CE 184 Introduction to Earthquake Engineering by Richard Armstrong of California State University - Sacramento.

Project-based learning is also emphasized in many proposed syllabi. In the syllabus proposed by Jayamon (2018), the major requirement is a case study based project where the students complete the design of an office building in a specific geographical location. The project requires students to do

assignments like use appropriate tools to find the seismicity of the given location and select suitable ground motions that can be used in the analysis of the building, modeling of single and multi-degree of freedom systems and solving the system for computing strength and deflections, design simple frame structures based on equivalent lateral force methods to apply code provisions. The last stage of the project includes the design and detailing of different elements in the lateral load resisting system. Current directions now in earthquake engineering education is to integrate "hands-on experiments" using a bench-scale shake table with classroom lectures. S.J. Dyke et al (2000) integrated a series of "hands-on" experiments into the civil engineering curriculum at Washington University. Students are expected to tie the theoretical concepts discussed in class to their experimental observations. The laboratory activities are based on the use of a bench-scale seismic simulator, or shake table. Creative utilization of the equipment has offered numerous opportunities to supplement the rather conventional content of several courses by integrating "hands-on" experiments in earthquake engineering. S.J. Dyke et al (2002) did not just focus on Washington University but advanced earthquake engineering education through the University Consortium of Instructional Shake Tables (UCIST). The universities that compose the consortium have each purchased an instructional shake table lab station. Several tutorials, experiments and videos have been developed, and several more are in progress. Each university is also integrating at least three experiments into their undergraduate curriculum.

Basic earthquake engineering is also being introduced in the Senior High School level in some schools. Doyle et al (2013) presented experiential hands-on tools (instructional table-top earthquake simulators, or "shaking tables") that can be used to teach learners about fundamental physics principles and can stimulate their interest in physical science, engineering, mathematics and technology (STEM) careers. The activities involving shaking tables are used to introduce complicated topics such as seismology, vibration response, and structural performance and design to students. The beauty of the activities is that they can utilize shaking tables that range from expensive, higher technology simulators to low cost, low technology solutions. One innovative program which was implemented for K-12 students during the pandemic was a summer hands-on earthquake engineering curriculum for the virtual classroom at California Polytechnic State University (S. Navias 2022). In this program, each student received a $60 mail-home engineering kit consisting of materials like basswood, cardboard, craft foam and low-cost accelerometers. The instructional objectives of the week-long summer program were to spend one hour of lecture each day introducing earthquake engineering concepts interspersed with questions and discussion, followed by an hour for students to work on a hands-on activity in break-out rooms with instructors virtually. These activities formed a project highlighting the engineering design process: (i) assemble a shake-table, (ii) design, construct, instrument, test, and analyze a basswood structural model, (iii) retrofit and retest the model, and (iv) present to the class on their decision process and original/retrofitted structure's performance. Through the mail-home engineering kit, students were able to participate in the hands-on activities. The development of an inexpensive mail-home engineering kit (with construction materials and an accelerometer) proved to be critical to these sessions' success since students most appreciated and learned from the hands-on activities. The hands-on component was coupled with lectures of varied and engaging content to provide background knowledge on what generates earthquake hazard and how structural engineers design buildings and infrastructure to insure the seismic resiliency of communities (S. Navias 2022).

With the advancement of online resources, applications and technology and the affordability of bench-scale shake table testing equipment, engaging student-centered learning activities that complement the lectures and quizzes and enhance the learning about earthquakes and their impacts to the built environment can now be introduced in the courses related to earthquake engineering. The author and his collaborators, explored the integration of technology to enhance the teaching and learning in the course syllabi of courses related to earthquake engineering at De La Salle University. These activities including traditional exams and problem sets are integrated into an outcomes-based course syllabus.

COURSES RELATED TO EARTHQUAKE ENGINEERING

At De La Salle University, Manila Philippines, a three-unit course on Earthquake Engineering (Course Code: STERQUA) is required in the undergraduate civil engineering curriculum for structural engineering majors. The course content of STERQUA consists of topics which are common to many syllabi on introduction to earthquake engineering. The general topics that are discussed in lectures and videos with corresponding assignments and projects are described as follows:

- *Earthquakes and Disasters* – Basic concepts on seismology (faults, magnitude, intensity, focus, epicenter), lessons learned from earthquake hazards and disasters (liquefaction, landslide, surface rupture, ground shaking)
- *Earthquake Hazards* – Seismic Zones in the Philippines, Hazard Maps and Online Tools by the Philippine Institute of Volcanology and Seismology (PHIVOLCS)
- *Basic Structural Dynamics & Earthquake Engineering* – Dynamic modeling and analysis of undamped and damped single-degree-of-freedom (SDOF) systems, forced vibration of SDOF systems, SDOF systems subjected to ground motion, Response spectra
- *Earthquake Engineering and Seismic Design* – Seismic provisions of the National Structural Code of the Philippines (NSCP), Static lateral force procedure, Irregular structures, Special Provisions on Seismic Detailing of RC Structures, Seismic retrofitting concepts

In the graduate program for Master's and PhD in Civil Engineering, there are also courses related to earthquake engineering (DLSU CE Graduate Program website). These courses with their course codes and description are:

- *CIV573M (Structural Dynamics)* - This course deals with the theory and principles of structural dynamics. Highlights of the course are modeling and analysis of structures modeled as single and multi-degree of freedom systems considering viscous and proportional damping. Dynamic analysis methods like the modal method, response spectra and time-history analysis are included.
- *CIV574M (Seismic Analysis and Design of Buildings)* - This course deals with Behavior of Buildings (RC, Steel, Masonry) under Seismic Loading; Responses of Structural Elements to Earthquake-Type Loading; Ductility; Inelastic Behavior; Damping; Earthquake Damage; Earthquake Resistant Design; Seismic Detailing; Recent Studies on Seismic Analysis and Design of Structures (Push-over analysis)
- *CIV575M (Earthquake Disaster Mitigation)* - This course covers topics such as Introduction to Disaster Management with special focus to earthquake hazards; Earthquake Damage, Lessons learned from earthquakes, Seismic Vulnerability, Seismic Hazards Rating, Seismic Retrofitting, and Recent Studies in Earthquake Disaster Mitigation.
- *CIV602M (Advanced Earthquake Engineering)* - This is the equivalent of STERQUA in the graduate curriculum but more topics are included like analysis of multi-degree-of-freedom systems due to ground motion, lessons learned from earthquakes; and seismic codes.

Integrated in these courses are various activities and assignments where online resources and laboratory equipment are used by the teacher and the students in understanding concepts and accomplishing assignments on earthquake engineering. The following section describes these online platforms and resources and hands-on laboratory exercises and their relevance to understanding earthquake engineering.

ONLINE RESOURCES AND TECHNOLOGY

In the present times, the internet has become the source not only of rich and comprehensive information but also online tools and applications which makes it an alternative to the traditional library when it comes to research. Many websites and publications related to earthquake engineering are accessible for public use in the internet. Videos from YouTube are accessible for download or viewing. Hence, several exercises and projects can be designed using online platforms in the learning and application of earthquake engineering principles. Among these online-based activities are:

1. The **Philippine Institute on Volcanology and Seismology (PHIVOLCS)** has developed online and mobile applications specifically applied to the Philippine context. Among the online resources used in both the undergraduate and graduate courses are:
    a) *Fault Finder* is an application capable to do proximity searches to active faults (Figure 1). These tool is used by the students to determine the shortest distance between an active fault and a specific site which is an important parameter in the base shear computation in the National Structural Code of the Philippines (NSCP). The latest version of The PHIVOLCS Fault Finder is now on Google Play.

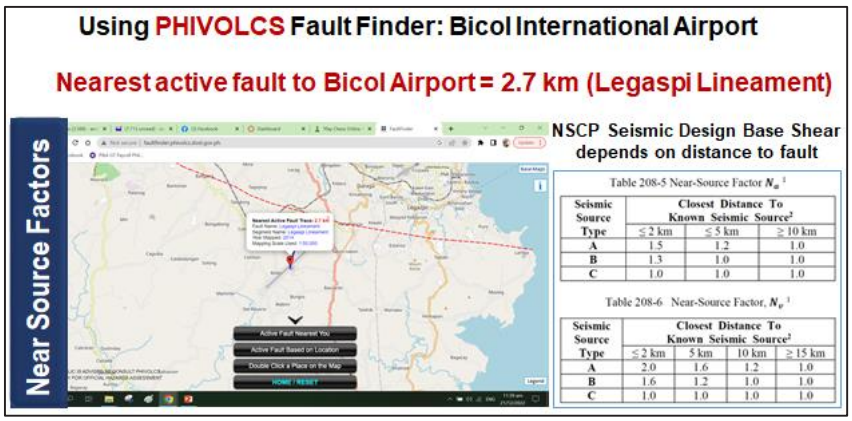

Figure 1. PHIVOLCS Fault Finder

    b) *Hazard Hunter* is the country's one-stop shop for hazard assessment (Figure 2. You will be informed if a location is prone to seismic, volcanic, or hydrometeorologic hazards. Reports on hazard assessment and critical facilities and areas in the vicinity of the site that are prone to different hazards can be generated. This tool is useful when the students conduct hazard assessment at a site which is an important step in is disaster risk assessment and mitigation of a project. Hazard Hunter is also at Google Play.

    c) *"How safe is my house?"* is a rapid assessment and self-check for earthquake safety of Concrete Hollow Block (CHB) Houses in the Philippines developed by PHIVOLCS, JICA and ASEP. The checklist is used by students in their assignment on sell-check of their respective houses (Figure 3). A mobile app is now available at Google Play.

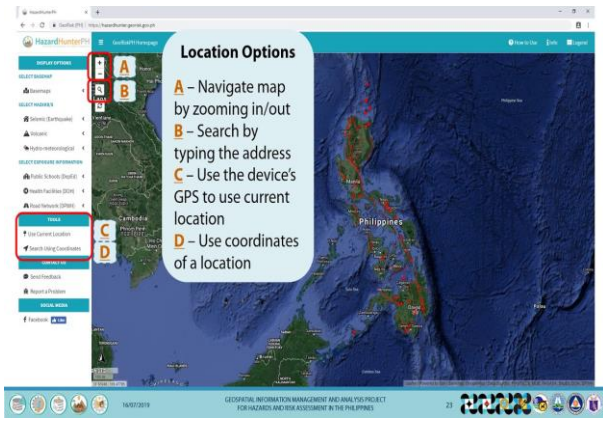

Figure 2. Hazard Hunter

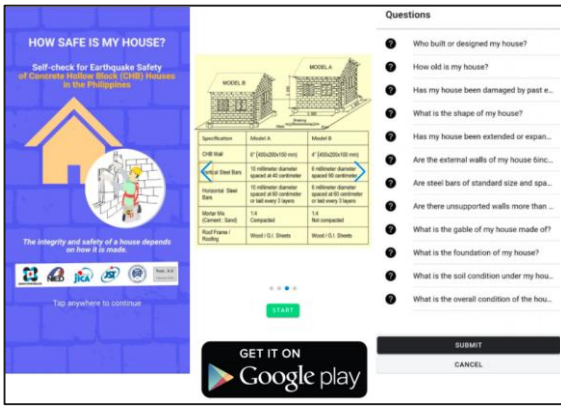

Figure 3 How safe is my house assessment

2. **"Understanding Earthquakes and Disasters: Photo-Video Presentations"** consists of eight short photo-video presentations (Figure 4) developed by the author (Oreta 2008). Before online lectures were conducted and YouTube was not yet popular then, the author played these videos in the classroom and conferences using a DVD player or a computer with Windows Media Player. The photo-video presentations present images with text and music on a specific topic on the

PS8-1

impact of earthquake hazards – ground shaking, surface rupture, liquefaction, tsunami, landslides – to the community and infrastructures. The photo-video presentations were used in the classroom lectures in the courses on Earthquake Engineering and Disaster Management. In an online class, students watch the videos asynchronously and then write a reaction paper. The materials were also used in public awareness campaigns and conferences for professional organizations. The video files are accessible at Digital Structures Blogspot and at YouTube.

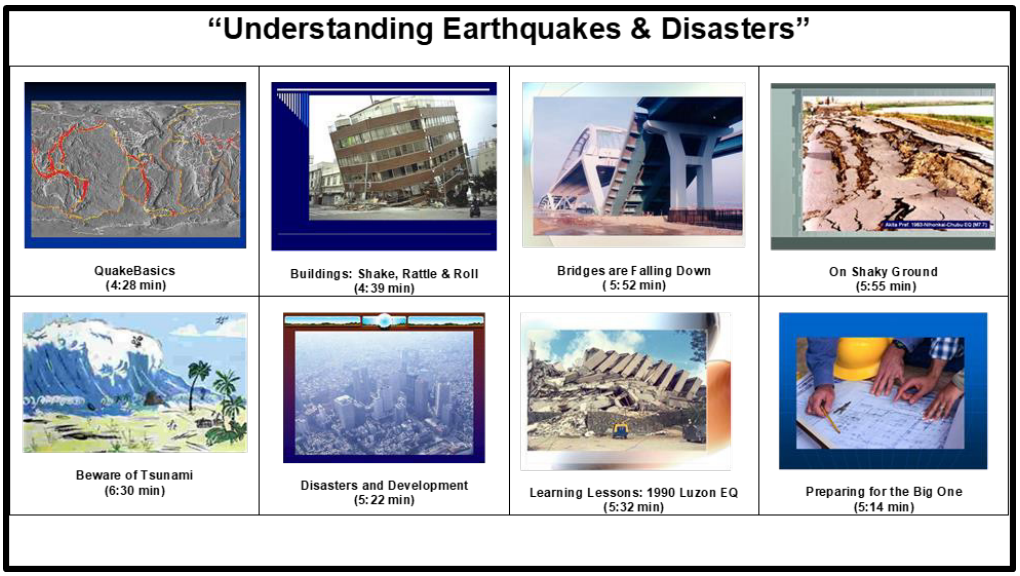

Figure 4. Titles of the Photo-Videos on Understanding Earthquakes and Disasters (Oreta 2008)

3. **FEMA 154 RVS Level 1 Screening Method** was applied on selected essential buildings. The FEMA 154 is a side walk survey of a building where a Rapid Visual Screening (RVS) method is used to assist decision makers in classifying the buildings into those that require detailed investigation and those that do not. Sample outputs are shown in Figure 5. Through this tool and exercise, students understand concepts on seismic vulnerability of buildings. The document is available at FEMA website.

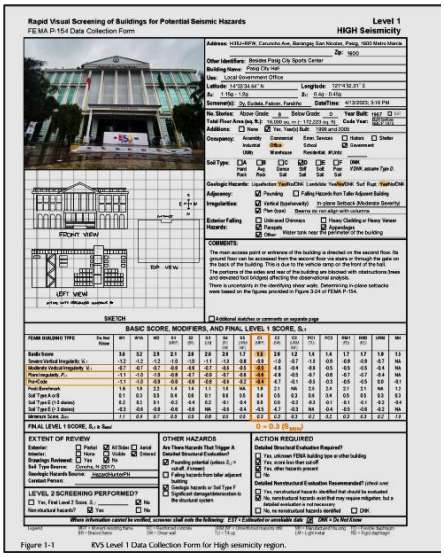

Figure 5. Sample FEMA 154 RVS

4. The web-based **Pacific Earthquake Engineering Research Center (PEER)** ground motion database provides tools for searching, selecting and downloading ground motion data. The NGA-West2 ground motion database includes a very large set of ground motions recorded in worldwide shallow crustal earthquakes in active tectonic regimes. The database has one of the most comprehensive sets of meta-data, including different distance measure, various site characterizations, earthquake source data, etc. A student exercise on Earthquake Ground Motion Analysis is one activity where the PEER website was utilized. The students were first required to select and describe a recent significant earthquake – its location, impact with respect to damages and loss of lives accompanied by photos. Then they download a ground motion data related to the earthquake and analyze for for acceleration, velocity and displacement for maximum responses and Fourier/Power spectra.

5. The free academic license software, **SeismoSignal** was used to process the earthquake time history data downloaded from PEER for acceleration, velocity and displacement for maximum responses and Fourier/Power spectra (Figure 7). The extracted time history acceleration data was then

transferred to MS Excel for the application of dynamic analysis of a damped SDOF or MDOF system subjected to ground acceleration using Newmark's Beta numerical integration method. Various problems on seismic performance using earthquake data can be designed like the investigation on how the system be modified or retrofitted by changing the dynamic properties of the SDOF or MDOF system so that the maximum displacement can be reduced. SeismoSignal is very useful in a course on Structural Dynamics.

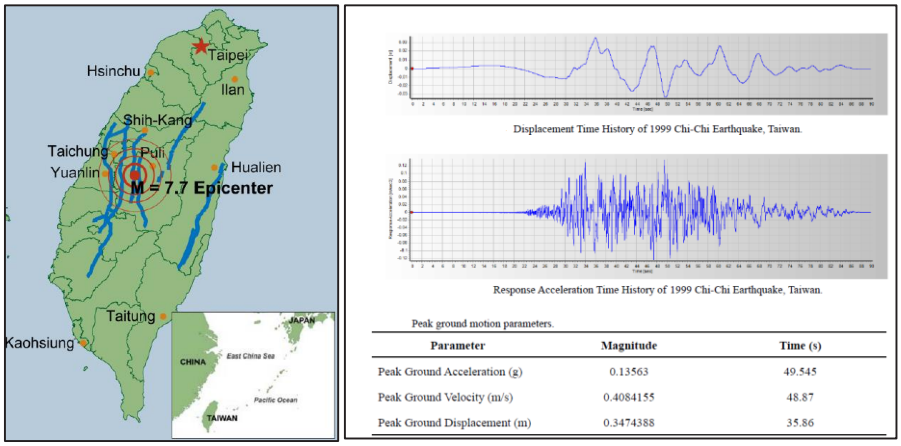

Figure 7. 1999 Chi-Chi Earthquake Time History Data downloaded from PEER and processed by SeismoSignal

6. **Structural Earthquake Response Analysis 3D or STERA3D** is an integrated software for seismic analysis of buildings with various structures (reinforced concrete, steel, masonry, base isolation, response control, etc.) in three dimensional space developed for research and educational purposes. STERA_3D has a visual interface to create building models and show the results easily and rapidly. In the graduate seminar on Earthquake Disaster Mitigation, a case study about "Seismic Performance of an Irregular Building," Each group modeled and analyzed a specific type of irregular building using STERA3D. They perform both push-over analysis and time-history analysis to determine the performance of the irregular building and identify potential weaknesses. They reanalyzed using STERA3D at least one retrofit method and compared to the original model. A sample output is shown in Figure 8.

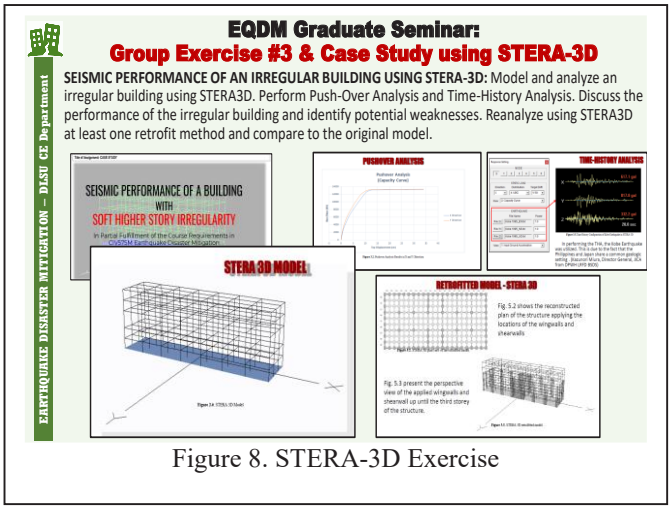

Figure 8. STERA-3D Exercise

SHAKE THE TOWER CHALLENGE – A SHAKE TABLE TESTING EXERCISE

Current directions now in earthquake engineering education is to integrate "hands-on experiments" using a bench-scale shake table with classroom lectures. Recently, DLSU purchased a Quanser Shake Table II, an instructional shake table device that can be used for earthquake simulation, structural dynamics, vibration control, and data acquisition through use of sensors and digital control systems on scale models. To maximize and test the capability and performance of the shake table, a hands-on group exercise, "Shake the Tower Challenge" is introduced as a fourth hour activity in the undergraduate course on earthquake engineering with course code, STERQUA. A fourth hour activity is a student-centered learning activity which is accomplished outside of the regular class meetings at their own time and place. The main objective of the exercise is for the students to develop an understanding and an

PS8-1

intuition regarding the dynamic nature of structures when subjected to ground shaking. The "Shake the Tower Challenge" is a group exercise where the students construct a 24-inch tall tower made of sticks glued together by glue stick (Figure 9). The stick towers were subjected to shaking with varying amplitude and frequency until collapse (Figure 10). Through this exercise the students observed the swaying of the tower at different frequencies and the change of the swaying with respect to frequency and amplitude as the tower is damaged. The student feedback on the exercise is positive, to quote one student: "*The Shake the Tower Challenge was a very interesting activity because I was able to view various towers and how they performed under various shake table settings. It helped me understand and appreciate the concepts related to structure stiffness, period, frequency, and displacement. It was fun building towers and experimenting with the shake table to create the competition parameters because I was able to apply the lessons learned (in structural dynamics). I noticed that the best towers were the ones that had designs that minimized the number of joints while still being able to provide bracings. This helped reinforce my understanding of building retrofitting and the design of earthquake resistant structures. I would definitely recommend this type of activity for future reference*."

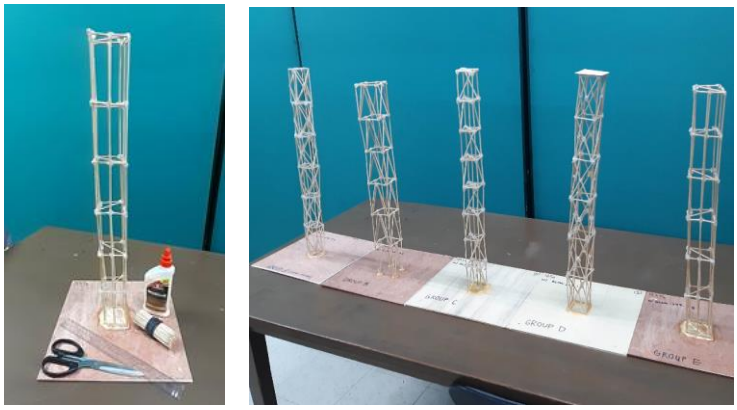

Figure 9. The Stick Towers constructed using sticks and glue.

Figure 10. Testing the Stick Towers on the Shake Table

CONCLUSIONS

In conclusion, the integration of technology in earthquake engineering education offers immense benefits for students and professionals alike. The use of the internet for learning and research developed in the student's life-long learning skills and addressed specifically the student outcome on the "ability to use techniques, skills, and modern engineering tools necessary for engineering practice." The shake table exercise, on the other hand, provided an opportunity for the students to observe the performance of model towers under ground shaking which addressed the student outcome on "an understanding of the impact of solutions in global, economic, environmental, and societal contexts." More problem-based and experiential activities can be developed using the internet and the shake table in courses on earthquake engineering as demonstrated in some universities in the United States (S.J. Dyke et al 2002). This will be the direction that the DLSU Department of Civil Engineering will pursue.

ACKNOWLEDGMENT

Dr. Lessandro Garciano and his research team for allowing the students to use the Shake Table. BSMS students (Jade Ching, Rafael Chan and Aldrei Ong) and CES representatives (Miles Louis Lim and Stiffany Caira Lopez) for managing the Shake the Tower Challenge. Prof. Taiki Saito for his advice on the use of STERA-3D.

REFERENCES

Armstrong, Richard. "CE 184: Introduction to Earthquake Engineering," California State University, Sacramento, https://www.csus.edu/faculty/a/richard.armstrong/docs/ce_184_course_syllabus_armstrong.pdf

Dyke, Shirley J. (2000). "Current Directions in Earthquake Engineering Education," Proc. of the 2000 Engrg. Mech. Spec. Conf., ASCE, Austin, TX, May 21–24, 2000.

Dyke, Shirley J. et al (2000). "Earthquake Engineering Education: A Modern Approach," American Society for Engineering Education (ASEE)

Dyke, Kelly et al (2002), "Advancing Earthquake Engineering Education Through a Cooperative Effort Based On Instructional Shake Tables," 7th US National Conference on Earthquake Engineering, EERI, Boston, MA, July 21–25, 2002. https://engineering.purdue.edu/TeachEE/publications/Advancing%20Earthquake%20Engineering%20Education.pdf

Doyle, Kelly et al. (2013.) "Using Educational Hands-On Experiential Tools to Introduce Math, Science and Engineering Concepts to K-16 Students (Research to Practice)," Paper ID #7191, 120th ASEE Annual Conference and Exposition, June 23-26, 2013.

Hsiao, J. Kent. "CE447 Seismic Design of Structures Syllabus," Southern Illinois University Carbondale, Department of Civil and Environmental Engineering, https://engineering.siu.edu/civil/_common/documents/syllabus-ce%20447.pdf

Jayamon, Jeena Rachel (2018). "Syllabus for a Proposed Course on Earthquake Engineering in Undergraduate Civil Engineering Curriculum," Eleventh U.S. National Conference on Earthquake Engineering, Integrating Science, Engineering & Policy, June 25-29, 2018, Los Angeles, California

Navias, S. et al (2022). "Hands-on Earthquake Engineering Curriculum for the Virtual Classroom," 12th National Conference on Earthquake Engineering, Salt Lake City, Utah, 27 June – 1 July 2022, Hosted by Earthquake Engineering Research Institute, https://digitalcommons.calpoly.edu/cgi/viewcontent.cgi?article=1147&context=aen_fac

Oreta, A.W.C. (2008). "Understanding Earthquakes & Disasters: Photo-Video Presentations for Public Awareness and Education," PICE Midyear Convention, June 26-28, 2008, Clark, Pampanga

Online Resources Links:

- DLSU CE Graduate Program Website. https://www.dlsu.edu.ph/colleges/gcoe/academic-departments/civil-engineering/graduate-studies/
- Fault Finder. http://faultfinder.phivolcs.dost.gov.ph/
- Hazard Hunter. https://hazardhunter.georisk.gov.ph/
- How safe is my house?: https://howsafeismyhouse.phivolcs.dost.gov.ph/
- Digital Structures. http://digitalstructures.blogspot.com/search/label/Understanding%20Earthquakes%20and%20Disasters
- Understanding Earthquakes & Disaster at YouTube. https://www.youtube.com/playlist?list=PLyZ8LqQdRYisw5RjghvQ4Yc2Gvbj5S0hh
- FEMA 154. https://www.fema.gov/sites/default/files/2020-07/fema_earthquakes_rapid-visual-screening-of-buildings-for-potential-seismic-hazards-a-handbook-third-edition-fema-p-154.pdf
- PEER NGA West. https://ngawest2.berkeley.edu/
- SeismoSignal. https://seismosoft.com/products/seismosignal/
- STERA_3D. https://rc.ace.tut.ac.jp/saito/software-e.html

Day2 (Tuesday, Sep. 26th, 2023) 15:40~16:15

Where Do We Stand on Metamaterial-Based Seismic Design of Engineering Structures

Yi-Lung Mo

Moores Prof., Dept. of Civil and Env. Eng., University of Houston, Houston, Texas, U.S.A.

Dr. Y.L. Mo, P.E., F.ASCE, F.ACI, F.Humboldt, F.IAAM, is Moores Professor at the Civil and Environmental Engineering Department, University of Houston (UH), Houston, Texas. Dr. Mo's expertise is structural/earthquake engineering, including constitutive models, finite element simulations, nano-scale material and large-scale infrastructure testing, and field investigations of complex structures, on which he has more than 500 research publications, including 282 referred journal papers, many conference, keynote and prestige lectures, research reports, books and book chapters, magazine articles and earthquake field mission reports. His Google scholar citations, h-index and i10-index are 9448, 51 and 164, respectively.

WHERE DO WE STAND ON METAMATERIAL-BASED SEISMIC DESIGN OF ENGINEERING STRUCTURES

Y.L. Mo[1], Nagesh H Ramaswamy[2], Priyanka Shrestha[3], Xiaoliang Li[4], Kalyana Babu Nakshatrala[5], Xiaonan Shan[6]
[1] Moores Prof., Dept. of Civil and Env. Eng., University of Houston, Houston, Texas, U.S.A.
[2] Ph.D. Student, Dept. of Civil and Env. Eng., University of Houston, Houston, Texas, USA
[3] MS Student, Dept. of Civil and Env. Eng., University of Houston, Houston, Texas, USA
[4] Ph.D. Student, Dept. of Elec. and Computer Eng., University of Houston, Houston, Texas, USA
[5] Assoc. Prof., Dept. of Civil and Env. Eng., University of Houston, Houston, Texas, USA
[6] Assist. Prof., Dept. of Elec. and Computer Eng., University of Houston, Houston, Texas, USA
Email: yilungmo@central.uh.edu, nhoraked@cougarnet.uh.edu, pshrest5@cougarnet.uh.edu, xli67@cougarnet.uh.edu, knakshatrala@uh.edu, xshan@central.uh.edu

ABSTRACT

Conventional seismic isolation systems for engineering structures are effective in reducing the damaging effects of the horizontal components of a vibration, but they are not well suited for protection against the vertical components of dynamic loads. They are also prone to rocking, further complicating the design. Metamaterial-based seismic isolators are very attractive because they can overcome the disadvantages existing in conventional seismic isolation systems. These metamaterial-based seismic isolators use the foundation of engineering structures to block or reflect the damaging seismic motion being transmitted to the engineering structures. This paper presents both the analytical and experimental studies to demonstrate the feasibility and effectiveness of the metamaterial-based seismic isolators. To date, where we stand on metamaterial-based seismic design of engineering structures is critically examined. Guided by solid-state physics, the seismic isolators can be made by the metamaterial to exhibit frequency band gaps that are useful in resisting the seismic waves imposed on engineering structures from earthquake disturbances. Possessing distinct frequency band gaps, this metamaterial will block, or reflect, the incoming seismic motion with the frequencies falling between these gaps. We properly designed the frequency band gaps to match the fundamental frequency of an earthquake, so that its dynamic response is greatly reduced.

Keywords: metamaterial, seismic design, engineering structure, frequency band gap, periodic foundation

IDEA

A novel idea on passive seismic isolation created by adopting the concept of phononic crystals in solid-state physics (Liu et al., 2000; Sigalas et al., 2005; Kittel, 2005; Thomas et al., 2006; Xiao et al., 2008; Maldovan, 2013; Khelif et al., 2003; Pennec et al., 2010, Cheng et al., 2013), also called a metamaterial-based seismic isolation system or periodic foundation, was proposed for seismic-based isolation eleven years ago (Xiang et al., 2012), and a feasibility study and experimental investigations were performed (Yan et al., 2014; Yan et al., 2015; Witarto et al., 2018; Ramaswamy et al., 2023). Different from the conventional seismic isolation, the metamaterial doesn't lengthen the natural period to reduce the seismic load but simply doesn't let the seismic wave propagate through the metamaterial when the frequency of the incoming seismic waves is within a certain range of frequency (frequency band gaps) of well-designed metamaterials.

THEORY

The theoretical frequency band gaps of periodic foundations can be solved using Finite Element Analysis (FEA). For continuous, isotropic, perfectly elastic and small deformation material, the governing equation of motion is shown in Eq. (1) (Cheng and Shi, 2013) without consideration of damping,

$$\rho(\mathbf{r})\frac{\partial^2 \mathbf{u}}{\partial t^2} = \nabla\{[\lambda(\mathbf{r})+2\mu(\mathbf{r})](\nabla\cdot\mathbf{u})\} - \nabla\times[\mu(\mathbf{r})\nabla\times\mathbf{u}] \quad (1)$$

where $\mathbf{r}$ is the coordinate vector; $\mathbf{u}(\mathbf{r})$ is displacement; $\rho(\mathbf{r})$ is the density; $\lambda(\mathbf{r})$ and $\mu(\mathbf{r})$ are Lame constants; ∇ is Laplace operator. Applying the periodic boundary conditions to the governing equation, Eq. (1), Eq. (2) can be obtained:

$$(\mathbf{\Omega}(\mathbf{K}) - \omega^2\mathbf{M})\cdot\mathbf{u} = \mathbf{0} \quad (2)$$

where $\mathbf{\Omega}$ is the stiffness matrix and $\mathbf{M}$ is mass matrix of the unit cell. In this way, the wave equations can be transferred into an Eigen-value equation, as shown in Eq. (2), which is the so-called dispersion equation. Finite Element Analysis (FEA) can be adopted to solve the Eigen-value problem using the commercial software.

FEASIBILITY STUDY

As presented above, the theoretical derivation for the concept of periodic foundations is promising. Several challenges must be addressed in order to experimentally demonstrate the practical application of the concept. One such challenge is to achieve a good understanding of the effect of the high heterogeneity in materials at the scale of a full-size foundation (base isolator). This is important because any heterogeneity is likely to hinder the desired performance of the isolation system. Another issue concerns the effect of de-bonding on the performance of the isolator. In order to begin to address these and other practical design issues and to validate the theoretical results, a scaled model and a periodic foundation were fabricated and tested using the shake table facility at the National Center for Research on Earthquake Engineering (NCREE) in Taiwan (Xiang et al., 2012).

As shown in Figure 1, the three-story steel frame on a 1-D layered periodic foundation (i.e., Specimen A) and its fixed-base counterpart (i.e., Specimen B) were installed together on the shake table, in order to have a good comparison under the same excitation inputs.

The main frequency of the recorded ambient vibration, i.e., about 50Hz, falls into the fourth band gap of the periodic foundation. The horizontal acceleration time histories at the top story of the frames with and without the periodic foundation are shown in Figure 2. It can be seen from Figure 2 that for the frame on the periodic foundation (i.e., Specimen A), the acceleration response history is reduced significantly compared to that of the frame without the periodic foundation (i.e., Specimen B). The peak acceleration responses of Specimens A and B are 0.003g and 0.046g, respectively (the reduction attributed to the implementation of the periodic foundation is about 93.5%). The test result indicates that the periodic foundation is capable of being an effective filter to isolate the vibration in which the frequency contents fall into the desired band gap.

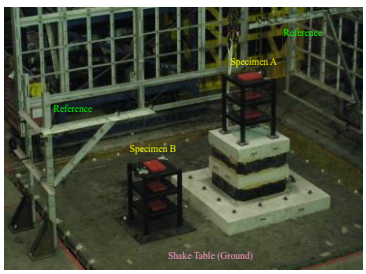

Figure 1. Shake Table Test

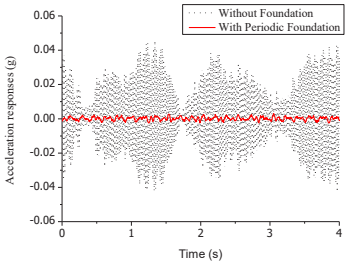

Figure 2. Acceleration Response-Time History

SENSITIVITY ANALYSES

Sobol' sensitivity analysis is a global sensitivity analysis method using variance decomposition that can handle linear and nonlinear mathematical models. The advantage of Sobol' decomposition that allows the reduction of the dimension of the objective function is very beneficial for predicting the first frequency band gaps without the need to solve the wave equation. Sobol' sensitivity analysis is applied

to 1D periodic materials to characterize the influential parameters in obtaining the frequency band gaps (Witarto et al., 2019). It is found that the density ratio and height ratio are the most significant in determining the frequency band gaps.

EXPERIMENTAL PROGRAM

Field tests were conducted to verify the effectiveness of a 3D periodic foundation. Figure 3 shows the RC footing with an upper steel column as Specimen E, and the 3D periodic foundation with an upper steel column as Specimen F.

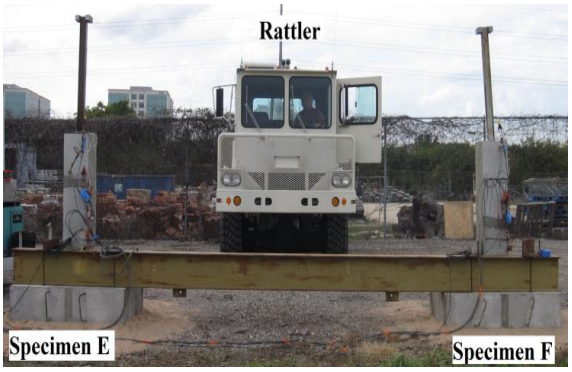

Figure 3. Test Setup of 3D periodic foundation.

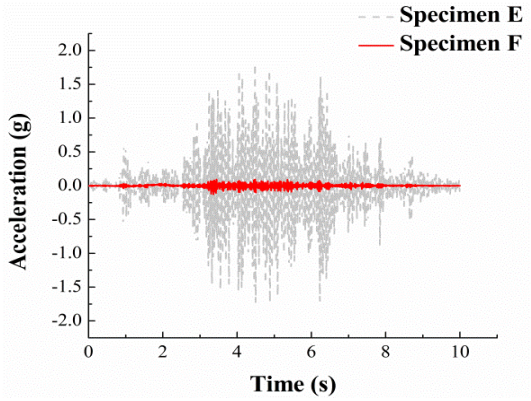

Figure 4. Acceleration in X direction at the top of the column under modified BORAH.AS/HAU090 with a main frequency of 35.1Hz

Figure 4 shows that, for the steel column on the 3D periodic foundation, i.e., with a peak acceleration of 0.14g, the peak acceleration in the X direction was reduced to 8.08% as compared to that of the steel column with the conventional foundation, i.e., with a peak acceleration of 1.73g (Yan et al., 2015).

IMPLEMENTATION

The concept of the periodic foundation is implemented in a real small modular reactor building (Witarto et al., 2018). A periodic foundation was designed (Figure 5) and tested at NCREE (Figure 6). The isolation mechanism of the 1D periodic foundation can be observed from the Fourier spectra of the recorded time series. Figure 7 shows the Fourier spectra of the test results of Case 4. The spectra show that the majority of the main frequency contents of all four earthquakes are located within 3.7-50 Hz, which is overlapping with the tested attenuation zone and the theoretical frequency band gaps. As one can clearly see, the frequency content of the input waves in this region is effectively filtered out.

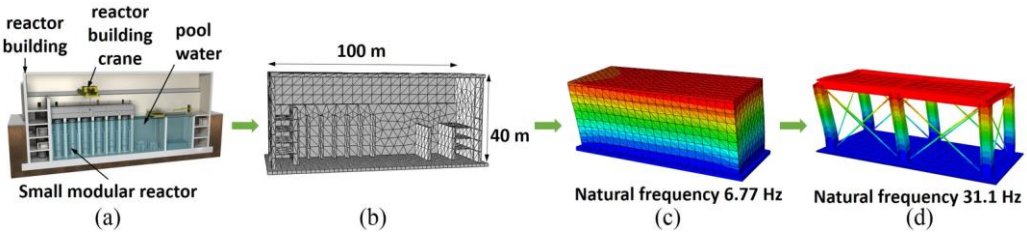

Figure 5. Design process of superstructure model: (a) NuScale SMR Building; (b) Finite element model of prototype building; (c) Modal analysis result of prototype building; (d) Modal analysis result of scaled model.

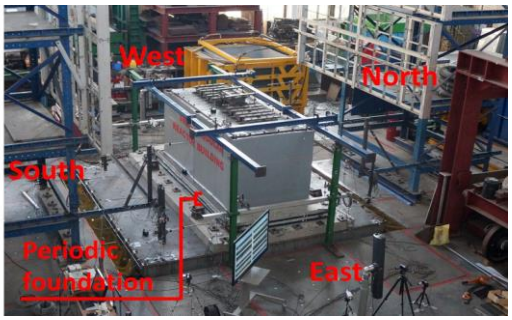

Figure 6. Test setup of 1D periodic foundation with SMR building structure

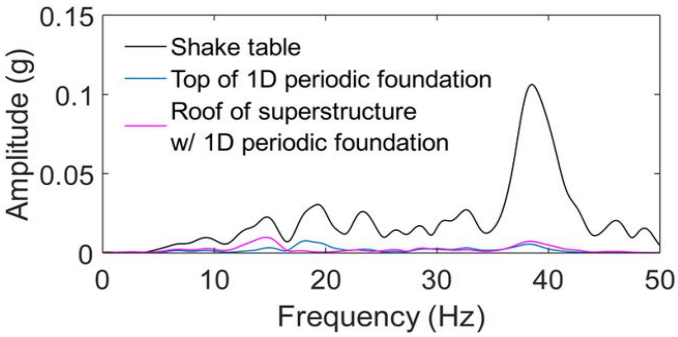

Figure 7. Fourier spectra of seismic test results of Case 4 in the horizontal direction: Bishop Earthquake

In addition, a non-invasive periodic barrier is a combination of a trench and a 1D periodic barrier (Huang et al., 2021; Zhang et al., 2022; Ramaswamy et al., 2023). The advanced seismic isolation performance of the periodic barrier is developed based on the selective vibration isolation property of the existing periodic foundation. The periodic barrier is expected to provide both advantages of wave barrier and periodic material when infilled in a trench type barrier. The periodic barrier is installed away from the structure, acting as a non-invasive vibration isolation system. The disadvantages of the periodic foundation are overcome with this trench-type periodic barrier since it is easy to be installed and maintained. It does not need to carry the superstructure load since it is independent of the structure. The proposed trench-type periodic barrier will add immense value to seismic isolation systems and the field of earthquake engineering.

The specimen used in this field test program is a 1D unit cell periodic barrier consisting of two reinforced concrete layers and one polyurethane layer (Figure 8).

Figure 8. Far Field Excitation Setup

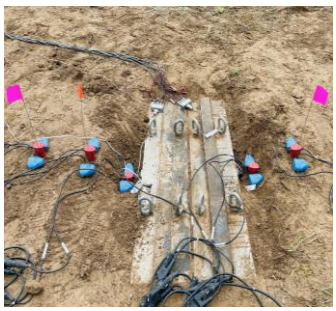

Figure 9. Test case P0B2T

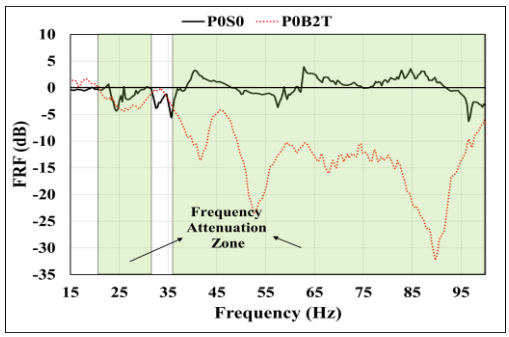

Figure 10. FRFs of P0S0 and P0B2T cases under vertical direction of excitation

In the test case P0B2T (Figure 9), one thick periodic barrier with a length of 4 feet, depth of 5 feet, and width of 1.84 feet is installed in a trench. The series of polyurethane pads will screen a wide range of frequencies, which provides a very wide frequency attenuation zone. The response is calculated in the same direction as the excitation direction. Figure 10 shows the FRF and frequency curves of Cases P0S0 and P0B2T under vertical direction of excitation. The colored areas denote the frequency attenuation zone for the P0B2T case to be 21 Hz-31.5 Hz, and 36.5 Hz-100 Hz.

CURRENT STATE

Although the metamaterial-based foundation can mitigate seismic excitation with a certain frequency range, it may amplify the response if the excitation is in the pass band of the metamaterial. Hence, the tunable metamaterial-based foundation will be the next milestone that is highly desirable for base isolation under seismic ground motions with a wide frequency range and significant variation and uncertainty in both the frequency domain and time domain. Magnetorheological Elastomers (MREs, also referred to as magneto-sensitive elastomers) are a class of solids composed of a polymeric matrix

with embedded micro- or nano-sized ferromagnetic particles such as carbonyl iron. As a result of this composite microstructure, the mechanical properties (elastic modulus and shear modulus) of these materials can be controlled by the application of a magnetic field. Based on MRE and traditional construction materials, the MRE-based metamaterial foundation will be put forward in the next step with tunable frequency band gaps, which can be automatically adjusted based on the state-of-the-art control algorithms. With increased input current, the magnetic field intensity increases, the elastic modulus and shear modulus of MRE increase (Figure 11), and the frequency band gap of the MRE-based metamaterial foundation can be adapted to varying engineering needs in seismic engineering. The test setup is shown in Figure 11.

Young's modulus is determined using a test-obtained stress-strain curve. The comparison of Young's modulus for various magnetic field intensities from 0 to 250 mT for three types of MRE is shown in Figure 11.

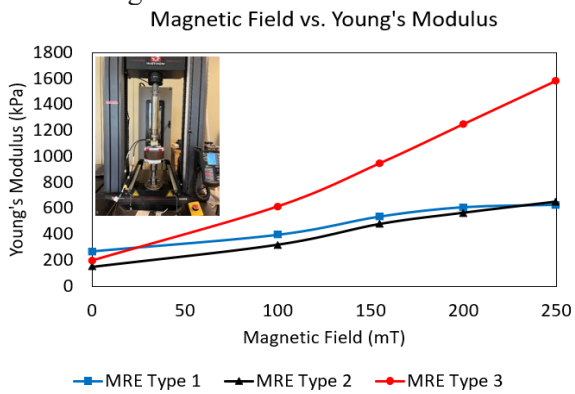

Figure 11. Magnetic Field Vs Young's Modulus for different types of MRE in Uniaxial Compression

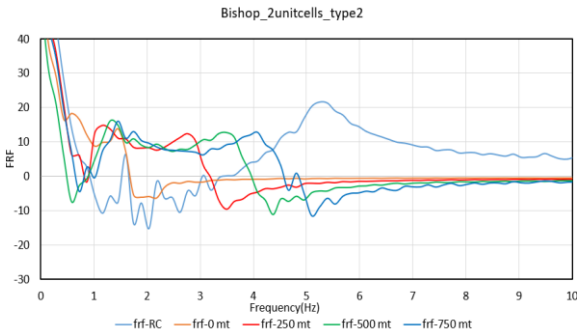

Figure 12. FRF of the FEM with RC foundation and MRE based foundation

The results depicted in the figure above show that the applied magnetic field significantly influences Young's modulus of MREs regardless of their types. Young's modulus values are used in the finite element simulation of the MRE-based metamaterial foundation based on the experimental results. Two-story RC frames with a RC foundation and MRE-RC layer are modeled in ABAQUS with the Bishop earthquake as the input ground motion. The ground motion data is extracted from the PEER Ground Database. The FEM model is simulated from a 0 to 750 mT magnetic field with a variety of Young's modulus of MRE.

It is shown in Figure 12 that the FRF of MRE-based metamaterial from 0 to 750 mT shows a reduction of seismic response at various frequency ranges. The frequency range shifts as the magnetic field increases from 0 to 750 mT. The lowest FRF is -10, so the vibration reduction is 68.5% for the MRE-based metamaterial foundation.

CONCLUSIONS

Guided by the solid-state physics, the seismic isolators can be made by the metamaterial to exhibit frequency band gaps that are useful in resisting the seismic waves imposed on engineering structures from earthquake disturbances. From both the analytical and experimental studies, it is found that metamaterial-based seismic design is an innovative method. In practice, the frequency band gap needs to cover all the possible frequencies of seismic disturbance. It is suggested that Magnetorheological Elastomers be used as adjustable metamaterial to broaden the frequency band gap in real time.

ACKNOWLEDGMENTS

The research reported in this paper is financially supported by the National Science Foundation. the U.S. Department of Energy and National Center for Research on Earthquake Engineering, Taiwan. During the course of this study, the strong support of Professor Kenneth H. Stokoe from the University of Texas at Austin and Professor K. C. Chang from National Taiwan University are also acknowledged.

REFERENCES

Cheng, Z. and Z. Shi, (2013). “Novel Composite Periodic Structures with Attenuation Zones,” Engineering Structures, 56, 1271.

Cheng, Z., Z. Shi, Y. L. Mo and H. Xiang, (2013). "Locally resonant periodic structures with low-frequency band gaps.," Journal of Applied Physics, vol. 114, p. 033532.

Huang, H. W., B. C. Zhang, J. J. Wang, F. -Y. Menq, K. B. Nakshatrala, Y.L. Mo, K. H. Stokoe. (2021) “Experimental Study on Wave Isolation Performance of Periodic Barriers,” Soil Dynamics and Earthquake Engineering., 147(2): 04020150. https://doi.org/10.1016/j.soildyn.2021.106602

Khelif, A., P. A. Deymier, B. Djafari-Rouhani, J. O. Vasseur and L. Dobrzynski, (2003). "Two-Dimensional Phononic Crystal with Tunable Narrow Pass Band Application to a Waveguide with Selective Frequency.," Journal of Applied Physics, vol. 94, no. 3, pp. 1308-1311.

Kittel, C., (2005). “Introduction to Solid State Physics.,” New York: John Wiley & Sons.

Liu, Z., X. Zhang, Y. Mao, Y. Zhu, Z. Yang, C. T. Chan and P. Sheng, (2000). "Locally resonant sonic materials.," Science, vol. 289, pp. 1734-1736.

Maldovan, M., (2013). "Sound And Heat Revolutions in Phononics.," Nature, vol. 503, pp. 209-217.

Pennec, Y., J. O. Vasseur, B. Djafari-Rouhani, L. Dobrzyński and P. A. Deymier, (2010). "Two-dimensional phononic crystals: examples and applications.," Surface Science Reports, vol. 65, no. 8, pp. 229-291.

Ramaswamy, N., Joshi, B., Wang, J., Li, X., Menq, F. Y., Shan, X., Babu Nakshatrala, K., Stokoe, K. H., & Mo, Y. L. (2023). Experimental study of passive seismic vibration isolation by trench-type periodic barrier. Engineering Structures, 276. https://doi.org/10.1016/j.engstruct.2022.115308

Sigalas, M., M. S. Kushwaha, E. N. Economou, M. Kafesaki, I. E. Psarobas and W. Steurer, (2005). "Classical Vibrational Modes in Phononic Lattices: Theory and Experiment.," Zeitschrift für Kristallographie-Crystalline Materials, vol. 220, no. 9-10, pp. 765-809.

Thomas, E.L., T. Gorishnyy and M. Maldovan, (2006). "Phononics: Colloidal Crystals Go Hypersonic.," Nature Materials, vol. 5, pp. 773-774.

Witarto, W., K. B. Nakshatrala and Y. L. Mo, (2019). “Global Sensitivity Analysis of Frequency Band Gaps in One-Dimensional Phononic Crystals,” Mechanics of Materials, 134, 38-53. https://doi.org/10.1016/j.mechmat.2019.04.005

Witarto, W., S. J. Wang, C. Y. Yang, X. Nie, Y. L. Mo, K. C. Chang, Y. Tang and R. Kassawara, (2018). “Seismic Isolation of Small Modular Reactors Using Metamaterials,” AIP Advances, 8, 045307. https://doi.org/10.1063/1.5020161

Xiang, H.J., Z. F. Shi, S.J. Wang and Y.L. Mo, (2012). “Periodic Materials-based Vibration Attenuation in Layered Foundations: Experimental Validation,” Smart Materials and Structures, 21(11): 112003, Highlight of 2012 Collection. https://doi.org/10.1088/0964-1726/21/11/112003

Xiao, W., G. W. Zeng and Y. S. Cheng, (2008). "Flexural Vibration Band Gaps in a Thin Plate Containing a Periodic Array of Hemmed Discs.," Applied Acoustics, vol. 69, no. 3, pp. 255-261.

Yan, Y., A. Laskar, Z. Cheng, F. Menq, Y. Tang, Y. L. Mo and Z. Shi, (2014). "Seismic Isolation of Two Dimensional Periodic Foundations.," Journal of Applied Physics, vol. 116, no. 4, p. 044908.

Yan, Y., Z. Cheng, F. Menq, Y. L. Mo, Z. Shi and Y. Tang, (2015). "Three Dimensional Periodic Foundations for Base Seismic Isolation.," Smart Materials and Structures, vol. 24, no. 7, p. 075006.

Zhang, B., H. W. Huang, F. Menq, J. Wang, K. Nakshatrala, K. H. Stokoe, and Y. L. Mo. (2022). “Field experimental investigation on broadband vibration mitigation using metamaterial-based barrier-foundation system,” Soil Dynamics and Earthquake Engineering, 155, 107167. https://doi.org/10.1016/j.soildyn.2022.107167

Day2 (Tuesday, Sep. 26th, 2023) 16:15~16:50

Seismic Isolation of Advanced Reactors - A Pathway to Standardization and to Climate Targets

Andrew S. Whittaker

SUNY Distinguished Professor,
University of Buffalo, Buffalo, NY USA.

Andrew Whittaker is a SUNY Distinguished Professor in the Department of Civil, Structural and Environmental Engineering at the University at Buffalo. He is a registered civil and structural engineer in the State of California. Whittaker served as the Vice-President and President of the Consortium of Universities for Research in Earthquake Engineering from 2003 to 2011, and on the Board of Directors of the Earthquake Engineering Research Institute and the World Seismic Safety Initiative from 2008 to 2010, on the Advisory Board for the Southern California Earthquake Center from 2010 to 2017, and on the Board of Directors for TerraPraxis since 2023. He serves on a number of national committees including ASCE 4, ASCE 7, ASCE 43, ASCE 59, and ASCE Codes and Standards, and ACI 349. Whittaker is Chair of the ASCE Nuclear Standards Committee. Whittaker is a member of ANS, contributing to its Non LWR working group on PRA and serving on the ANS Rapid Response Taskforce, responding to man-made and natural hazard threats to operating nuclear power plants. His research interests are broad and include earthquake, blast and impact engineering of nuclear structures, buildings, long-span bridges, and transportation infrastructure.

SEISMIC ISOLATION OF ADVANCED REACTORS: A PATHWAY TO STANDARDIZATION AND TO CLIMATE TARGETS

Andrew Whittaker
SUNY Distinguished Professor, University of Buffalo, Buffalo, NY USA.
Email: awhittak@buffalo.edu

EXTENDED ABSTRACT

A range of innovative low-carbon technologies will be needed very soon to achieve the Paris Agreement and limit global temperature rise this century to below 2 degrees Celsius below pre-industrial levels, with the aspirational goal to limit the increase to 1.5 degrees Celsius. Nuclear power could play a very significant role in achieving the goals of the Paris Agreement, decarbonizing the global economy, and meeting future demands for energy (e.g., Buongiorno *et al.* (2018), Partanen *et al.* (2019), IEA (2019), ETI (2020), Ingersoll and Gogan (2020), IAEA (2020a; 2020b; 2020c)), and it is a subject of this paper. At the time of this writing, nuclear power represents about one quarter of the global low-carbon electricity production (EMBER, 2023).

ETI (2020) deconstructed the capital cost of nuclear projects in the United States and Western Europe, and elsewhere in the world. The data suggests that aside from the higher direct costs of materials, equipment, and labor in the United States and Western Europe, the long build times of First-of-a-Kind (FoaK) projects lead to substantially greater time-based indirect costs (e.g., engineering, supervision, project management, rental site infrastructure), greater interest payments, and much higher interest rates due to project risk. The high cost, budget overruns, and time delays for FoaK plants have stymied the deployment of nuclear energy at scale (i.e., Nth-of-a-Kind (NoaK) construction) in the United States. The cost and time savings associated with *learning from doing* and *standardization* have not been realized in the nuclear industry in the United States and Western Europe.

Malhotra and Schmidt (2020) described the fundamental differences in carbon-technology uptake using the typology of Fig 1. Type 1 technologies access large and growing international markets, spurring continued innovation, because they are simple, standardized, and mass produced. Type 2 technologies "…provide opportunities for national green industrial policies fostering technological adaptation, and participation in global value chains." Type 3 technologies require "…a combination of national green industrial policies and measures to promote international coordination for inter-project and inter-context learning at a regional or global scale." The authors note that the "…need for international coordination increases as one moves to the top-right of the figure." Complex, customized systems are expensive and challenging to deliver: the nuclear power experience in the United States and Western Europe. So how do we move from complex, customized (FoaK) nuclear construction (Type 3, top right in Fig 1) to simple, standardized (NoaK) standardized construction (Type 1, bottom left in Fig 1) and tackle climate change?

The advanced nuclear reactors being developed in the United States are fundamentally different from the large light water reactors in the US operating fleet, offering a range of power outputs from 1 MWe to 300 MWe, using accident tolerant fuels, coolants other than water enabling operation near atmospheric pressure, and passive safety systems. The wide range of power outputs of these advanced reactors makes possible the repowering of coal and gas plants in the US and abroad. To repower the 250 GWe (2 TWe) of coal in the US (global) will require the design, licensing, and construction, of 1000+ (10,000+) advanced reactors. Simple, standardized advanced reactors is the only nuclear-energy pathway to decarbonizing this energy sector.

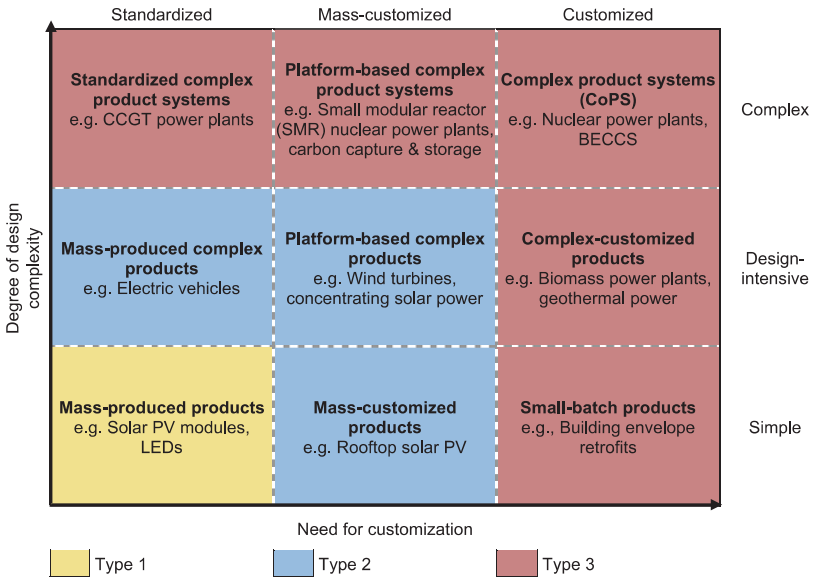

Figure 1. Binning of clean energy technologies based on design complexity and need for customization (adapted from Malhotra and Schmidt (2020)).

The seismic load case is a key contributor to the complexity and customized construction of US nuclear power plants (Parsi *et al.*, 2022). The near-surface geology and seismic hazard are different at each power plant site, requiring site-specific geotechnical investigations, probabilistic seismic hazard analyses, seismic soil-structure-interaction analysis, design, engineering, equipment qualification, and licensing: all thwarting standardization. The impact of the seismic load case on direct and indirect cost, and the standardization it thwarts, must either be substantially reduced or eliminated to deploy advanced reactors at the scale needed to support decarbonization. Seismic isolation can mitigate the impact of the seismic load case on safety-class structures, systems, and components and is, in my opinion, the pathway to standardized advanced reactors: an idea first proposed by Gluekler *et al.* (1991) but never acted upon.

The benefits of seismically isolating nuclear reactors, in terms of reduced seismic demands and risk, are well and long established (e.g., Tajirian *et al.* (1989), Tajirian (1992), Tajirian and Patel (1993), Clark *et al.* (1995), Aiken *et al.* (2002), Huang *et al*. (2008; 2009; 2011a; 2011b), Kumar *et al*. (2015; 2017a; 2017b), Yu *et al.* (2018)). (Earthquake-simulator experiments on isolated advanced reactors were undertaken by Professor Kelly at the University of California, Berkeley in the late 1980s when the author and a few others in the audience with grey hair were PhD students.) Despite the benefits of seismic isolation being well known, it has yet to be applied to a nuclear power plant in the US, in part due to a lack of new builds. (Two nuclear power plants, in Cruas, France and Koeberg, South Africa were seismically isolated in the early 1980s to enable the re-use of a French design developed for a site of lower seismic hazard: an approach indirectly pursued here.)

In the late 2000s, the two key impediments to industry's implementation of seismic isolation in NPPs were: 1) a lack of technical guidance and standards for analysis and design of seismically isolated NPPs, and its associated regulatory and financial risks, and 2) a lack of data on the financial costs and benefits of seismic isolation. Both impediments have been addressed. Tools and guidelines for base isolation of nuclear facilities have been developed through research projects funded by the U.S. Department of Energy (DOE) and the U.S. Nuclear Regulatory Commission (NRC). Consensus standards, ASCE/SEI 4-16 (ASCE, 2017) and ASCE/SEI 43-19 (ASCE, 2021), now include chapters specific to seismic isolation. Three technical reports on the analysis and design of seismically isolated nuclear power plants have been published by the NRC: 1) NUREG/CR-7253, Technical considerations for seismic isolation of nuclear facilities (Kammerer *et al.*, 2019), 2) NUREG/CR-7254, Seismic isolation of nuclear power plants using sliding bearings (Kumar *et al.*, 2019a), and 3) NUREG/CR-7255, Seismic isolation of nuclear power plants using elastomeric bearings (Kumar *et al.*, 2019b). A topical report on the seismic

isolation of advanced reactors, written to enable analysis, risk-based design, and licensing, is being submitted to the NRC. Journal articles, conference papers, and technical reports support and complement the standards, with many identified in Whittaker *et al.* (2018). Studies on the seismic isolation of safety-class equipment in NPPs have been completed and published (e.g., Lal *et al*. (2023a; 2023b), Mir *et al*. (2022; 2023a; 2023b)) and outcomes will be included in future editions of ASCE/SEI 4 and ASCE/SEI 43.

The impact of seismic isolation on the cost of advanced reactors is being quantified. Studies funded by the Electric Power Research Institute and the U.S. Department of Energy (e.g., Lal *et al*. (2020; 2022)) quantified the reductions in the capital cost of key safety-class equipment, in two very different types of reactors, made possible by seismic isolation and standardization: factors of 3 to 5, depending on the site seismicity. Fig 2 presents sample results for a reactor vessel (RV) and a steam generator (SG) in a molten chloride fast reactor for sites characterized by peak horizontal ground acceleration (0.3g and 0.5g): compare the normalized FoaK conventional and NoaK isolated costs to judge the reductions in capital cost of equipment.

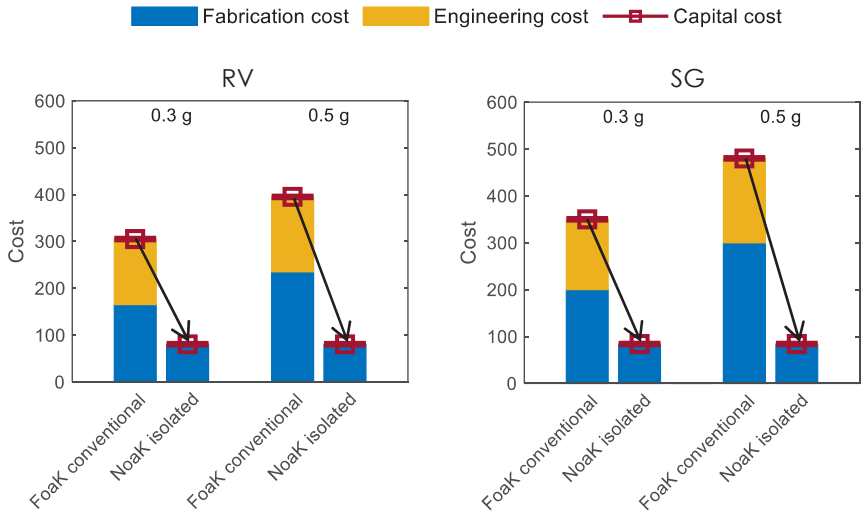

Figure 2. Capital cost of safety-class equipment in a molten chloride fast reactor, RV = reactor vessel, SG = steam generator (adapted from Lal *et al.* (2022)).

Quantifying the percentage reduction in capital cost of advanced reactors enabled by standardization and seismic isolation is a work in progress. The goal is cartooned in Fig 3: standardized reactor buildings and isolation systems, all pre-licensed by the NRC, with an adequate treatment of other external hazards, including flooding and wind-borne missile impact. The customer selects her/his site and a reactor type. Soil-structure-interaction analysis will not be needed for isolated advanced reactors, enabling the use of surface free-field United States Geological Survey (USGS) seismic hazard data requiring only location coordinates and site-specific geotechnical studies. The site and reactor type will dictate the choice of a pre-licensed isolation system.

The increment in cost attached to additional excavation (if needed), casting of a foundation and pedestals, and supply of the isolation system, is expected to be a small percentage of the building construction cost, with preliminary estimates available in Yu *et al.* (2018). The percentage reduction in the cost of the building framing will be reactor specific and may be relatively small because component thicknesses might be driven by non-seismic considerations such as shielding around the reactor vessel and protection from wind-borne missiles, affecting the building envelope. However, the standardization of the building framing will enable the use of modular construction, including precast reinforced concrete, driven by innovative design approaches used in non-nuclear construction sectors such as Design for Manufacturing and Assembly.

The greatest reductions in capital cost will accrue from the de-engineering of the project and the standardization of all components above the foundation supporting the pedestals and isolators and dampers. Eliminating the need for site-specific probabilistic seismic hazard assessment, soil-structure-interaction analysis, design of structures, systems, and components (aside from the foundation), probabilistic risk assessment and release calculations, and licensing, will cut 5+ years from the schedule for design and construction, drastically reducing interest rates, financial risk, and indirect costs. This is the plan to move from complex, customized (FoaK) nuclear construction (Type 3, top right in Fig 1) to simple, standardized (NoaK) standardized construction (Type 1, bottom left in Fig 1), tackle climate change, and do our part to achieve the Paris Agreement.

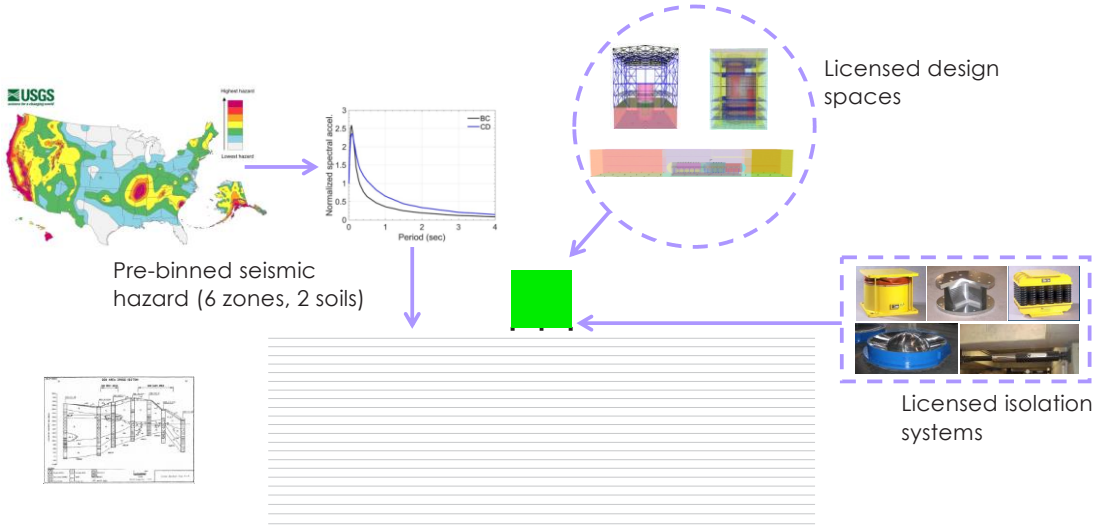

1) Site selected. 2) Pick a licensed heat source (MWe). 3) Pick a licensed isolation solution. 4) Price time and construction. 5) Evaluate alternatives and iterate on 2, 3, and 4.

Figure 3. Simple, standardized, safe, inexpensive advanced reactors.

ACKNOWLEDGMENTS

Many faculty and design professionals contributed, directly or indirectly, to the work described in this extended abstract and in the list of references. Early work on the seismic isolation of nuclear reactors was completed by Professor James Kelly and his co-workers at the University of California, Berkeley, as part of the DOE-funded ALMR program in the late 1980s and early 1990s. More recent contributors include Dr. Charles Kircher (CKA), Professor Yin-Nan Huang (NTU, Taiwan), Dr. Robert Budnitz (retired, LBNL), Dr. Robert Kennedy (dec.), Dr. Annie Kammerer (USDOD), Drs. Chandrakanth Bolisetti and Justin Coleman (INL), Professor Manish Kumar (IITB), Professor Manish Kumar (IITGN), Dr. Ching-Ching Yu (TerraPower), Professor Michael Constantinou (UB), Dr. Faizan Ul Haq Mir (UB), Mr. Sai Sharath Parsi (UB), Mr. Kaivalya Lal (UB), Dr. Ben Kosbab (SGH), Messrs. Ben Carmichael and Brandon Chisholm (Southern Company), Professors Koroush Shirvan and Jacopo Buongiorno (MIT), and Mr. Eric Ingersoll and Ms. Kirsty Gogan (TerraPraxis). These contributions are gratefully acknowledged.

REFERENCES

Aiken, I. D., Clark, P. W., and Kelly, J. M. (2002). Experimental testing of reduced-scale seismic isolation bearings for the advanced liquid metal reactor, *IAEA TECDOC-1288*, International Atomic Energy Agency (IAEA), Vienna, Austria.

American Society of Civil Engineers (ASCE). (2017). Seismic analysis of safety-related nuclear structures and commentary, *ASCE/SEI 4–16*, Reston, VA.

American Society of Civil Engineers (ASCE). (2021). Seismic design criteria for structures, systems, and components in nuclear facilities, *ASCE/SEI 43–19*, Reston, VA.

Buongiorno, J., Corradini, M., Parsons, J., and Petti, D. (2018). The future of nuclear energy in a carbon constrained world - an interdisciplinary MIT study, MIT Energy Initiative, Massachusetts Institute of Technology, Cambridge, MA, USA.

Clark, P. W., Aiken, I. D., Kelly, J. M., Gluekler, E. L., and Tajirian, F. F. (1995). "Tests of reduced-scale seismic isolation bearings for the US advanced liquid metal reactor (ALMR) program." *Proceedings: Joint ASME/JSME Pressure Vessels and Piping Conference*, August 2019, Honolulu, HI.

Sandbag Climate Campaign CIC (EMBER). (2023). Global electricity review 2023 (https://ember-climate.org/data/data-tools/data-explorer/), England.

Energy Technologies Institute (ETI). (2020). The ETI nuclear cost drivers project: Full technical report, Loughborough, UK.

Gluekler, E. L., Bigelow, C. C., DeVita, V., Kelly, J. M., Seidensticker, R. W., and Tajirian, F. F. (1991). "Seismic isolation development for the US advanced liquid-metal reactor program." *Nuclear Engineering and Design*, **127**(3), 295-301.

Huang, Y.-N., Whittaker, A. S., and Luco, N. (2008). Performance assessment of conventional and base-isolated nuclear power plants for earthquake and blast loadings, *Technical Report MCEER-08-0019*, University at Buffalo, The State University of New York, Buffalo, NY.

Huang, Y.-N., Whittaker, A. S., Kennedy, R. P., and Mayes, R. L. (2009). Assessment of base-isolated nuclear structures for design and beyond-design basis earthquake shaking, *Technical Report MCEER-09-0008*, University at Buffalo, The State University of New York, Buffalo, NY.

Huang, Y.-N., Whittaker, A. S., and Luco, N. (2011a). "A seismic risk assessment procedure for nuclear power plants: (I) Methodology." *Nuclear Engineering and Design*, **241**(9), 3996-4003.

Huang, Y.-N., Whittaker, A. S., and Luco, N. (2011b). "A seismic risk assessment procedure for nuclear power plants: (II) Application." *Nuclear Engineering and Design*, **241**(9), 4004-4011.

International Atomic Energy Agency (IAEA). (2020a). Climate change and nuclear power, *STI/PUB/1911*, Vienna, Austria.

International Atomic Energy Agency (IAEA). (2020b). Driving deeper decarbonization with nuclear energy, *IAEA Bulletin*, **61**(3), Vienna, Austria.

International Atomic Energy Agency (IAEA). (2020c). Seismic isolation systems for nuclear installations, *IAEA-TECDOC-1905*, Vienna, Austria.

International Energy Agency (IEA). (2019). Nuclear power in a clean energy system, Paris, France.

Ingersoll, E., and Gogan, K. (2020). Missing link to a livable climate: How hydrogen-enabled synthetic fuels can help deliver the Parsi goals, Lucid Catalyst, MA.

Kammerer, A. M., S., W. A., and Constantinou, M. C. (2019). Technical considerations for seismic isolation of nuclear facilities, *NUREG/CR-7253*, United States Nuclear Regulatory Commission, Washington, D.C.

Kumar, M., Whittaker, A. S., and Constantinou, M. C. (2015). "Response of base-isolated nuclear structures to extreme earthquake shaking." *Nuclear Engineering and Design*, **295**, 860-874.

Kumar, M., Whittaker, A. S., and Constantinou, M. C. (2017a). "Extreme earthquake response of nuclear power plants isolated using sliding bearings." *Nuclear Engineering and Design*, **316**, 9-25.

Kumar, M., Whittaker, A. S., Kennedy, R. P., Johnson, J. J., and Kammerer, A. (2017b). "Seismic probabilistic risk assessment for seismically isolated safety-related nuclear facilities." *Nuclear Engineering and Design*, **313**, 386-400.

Kumar, M., S., W. A., and Constantinou, M. C. (2019a). Seismic isolation of nuclear power plants using sliding bearings, *NUREG/CR-7254*, United States Nuclear Regulatory Commission, Washington, D.C.

Kumar, M., S., W. A., and Constantinou, M. C. (2019b). Seismic isolation of nuclear power plants using elastomeric bearings, *NUREG/CR-7255*, United States Nuclear Regulatory Commission, Washington, D.C.

Lal, K. M., Parsi, S. S., and Whittaker, A. S. (2020). Cost basis for utilizing seismic isolation for nuclear power plant design, *03002018345*, Electric Power Research Institute, Idaho Falls, ID.

Lal, K. M., Parsi, S. S., Kosbab, B., Ingersoll, E., Charkas, H., and Whittaker, A. S. (2022). "Towards standardized advanced nuclear reactors: Seismic isolation and the impact of the earthquake load case." *Nuclear Engineering and Design*, **386**(11487).

Lal, K. M., Whittaker A. S., and Sivaselvan, M. V. (2023a). "Mid-height seismic isolation of equipment in nuclear power plants: Numerical simulations and design recommendations." *Nuclear Engineering and Design*, **408**(112286).

Lal, K. M., Whittaker, A. S., and Constantinou, M. C. (2023b). "Mid-height seismic isolation of equipment in nuclear power plants." *Earthquake Engineering & Structural Dynamics*, **52**(4), 998-1015.

Malhotra, A., and Schmidt, T. S. (2020). "Accelerating low-carbon innovation." *Joule*, **4**(11), 2259-2267.

Mir, F. U. H., and Whittaker, A. S. (2022). "Dynamic responses of submerged components in advanced reactors: experimental and numerical studies." *Earthquake Spectra*, **38**(4), 3063–3088.

Mir, F. U. H., S., W. A., Kosbab, B., and Nguyen, N. (2023a). "Recommendations for seismic analysis of a molten salt reactor." *Nuclear Engineering and Design*, **413**(112504).

Mir, F. U. H., Whittaker, A. S., Kosbab, B. D., and Nguyen, N. (2023b). "Characterizing the seismic response of a molten salt nuclear reactor." *Earthquake Engineering & Structural Dynamics*, **52**(7), 2025-2046.

Parsi, S. S., Lal, K. M., Kosbab, B., Ingersoll, E., Shirvan, K., and Whittaker, A. S. (2022). "Seismic isolation: A pathway to standardized advanced nuclear reactors." *Nuclear Engineering and Design*, **387**(111445).

Partanen, R., Qvist, S., Gogan, K., and Ingersoll, E. (2019). Sustainable nuclear: An assessment of sustainability of nuclear power for the EU taxonomy consultation 2019, Prepared by Lucid Catalyst and Think Atom for EDF, United Kingdom.

Tajirian, F. F., Kelly, J. M., and Gluekler, E. L. (1989). "Testing of seismic isolation bearings for the PRISM advanced liquid metal reactors under extreme loads." *Transactions: 10th International Conference on Structural Mechanics in Reactor Technology (SMiRT-10)*, Anaheim, CA.

Tajirian, F. F. (1992). "Seismic analysis for the ALMR." *Proceedings: International Atomic Energy Agency (IAEA) Specialists' Meeting on Seismic Isolation Technology*, San Jose, CA.

Tajirian, F. F., and Patel, M. R. (1993). "Response of seismic isolated facilities: A parametric study of the ALMR." *Transactions: 12th International Conference on Structural Mechanics in Reactor Technology (SMiRT-12)*, Stuttgart, Germany.

Whittaker, A. S., Sollogoub, P., and Kim, M. K. (2018). "Seismic isolation of nuclear power plants: Past, present and future." *Nuclear Engineering and Design*, **338**, 290-299.

Yu, C.-C., Bolisetti, C., Coleman, J. L., Kosbab, B., and Whittaker, A. S. (2018). "Using seismic isolation to reduce risk and capital costs of safety-related nuclear facilities." *Nuclear Engineering and Design*, **326**, 268-284.

Day2 (Tuesday, Sep. 26th, 2023) 16:50~17:25

Enabling and Accelerating Community-Based Innovation in Disaster Resilience – A US Perspective

Daan Liang

Program Director, Division of Civil, Mechanical and Manufacturing Innovation, National Science Foundation, Alexandria, VA, USA

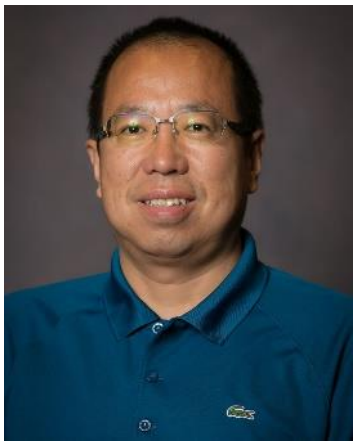

Dr. Daan Liang is the Program Director for the Humans, Disasters, and Built Environment (HDBE) program at the US National Science Foundation. The program supports fundamental, multidisciplinary research on the interactions between humans and the built environment within and among communities exposed to natural, technological, and other types of hazards and disasters. His portfolio also includes cross-cutting disaster-related solicitations and DCLs. In addition, Dr. Liang represents the NSF on interagency working groups for the National Windstorm Impact Reduction Program (NWIRP), Subcommittee on Resilience Science and Technology, and Science for Disaster Reduction. Prior to his NSF IPA assignment, Dr. Liang was a Professor in the Department of Civil, Construction, and Environmental Engineering and the Director of the Center for Sustainable Infrastructure (CSI) at the University of Alabama. Dr. Liang co-founded and co-directed an NSF Industry-University Cooperative Research Center (IUCRC) on Wind Hazard and Infrastructure Performance (WHIP). He received his bachelor's degree in engineering management from Tianjin University, China in 1997 and both his MS (1999) and PhD (2001) in civil engineering from University of Buffalo, New York. He is a licensed Professional Engineer in Texas.

ENABLING AND ACCELERATING COMMUNITY-BASED INNOVATION IN DISASTER RESILIENCE – A US PERSPECTIVE

Daan Liang
Program Director, Division of Civil, Mechanical and Manufacturing Innovation, National Science Foundation, Alexandria, VA, USA
Email: dliang@nsf.gov

ABSTRACT

The frequency and force of extreme events have been increasing while more people live in places susceptible to natural hazards. This complex and compounding interactions of engineering, social, environmental, and climatic processes play out over large spatial and temporal scales but remain poorly understood. This paper outlines the US Government strategies for tackling climate change and building resilience to disasters. It then points to the engagement between scientists and non-scientists as effective means to co-create research agenda, form trust relationships, and produce implementable community-based outcomes. A primary goal of both Smart and Connected Communities and CIVIC Innovation Challenge programs is to deepen the partnership between researchers and stakeholders and co-produce innovative pathways to a more prosperous, equitable, and resilient future. Transferability, scalability, and sustainment are key features of funded projects. It concludes with reaffirming the importance of convergent approach and scholarship in community engagement.

Keywords: disaster resilience, community engagement, climate change adaptation, the United States

INTRODUCTION

Driven by a changing climate, the frequency and force of extreme events such as storms, wildfires, floods, droughts, and heat waves have been increasing and new diseases are emerging (NOAA 2023). At the same time, many of nation's critical infrastructures are well beyond their service life while more people choose to live in places susceptible to natural hazards. This complex and compounding interactions of engineering, social, environmental, and climatic processes play out over large spatial and temporal scales but remain poorly understood.

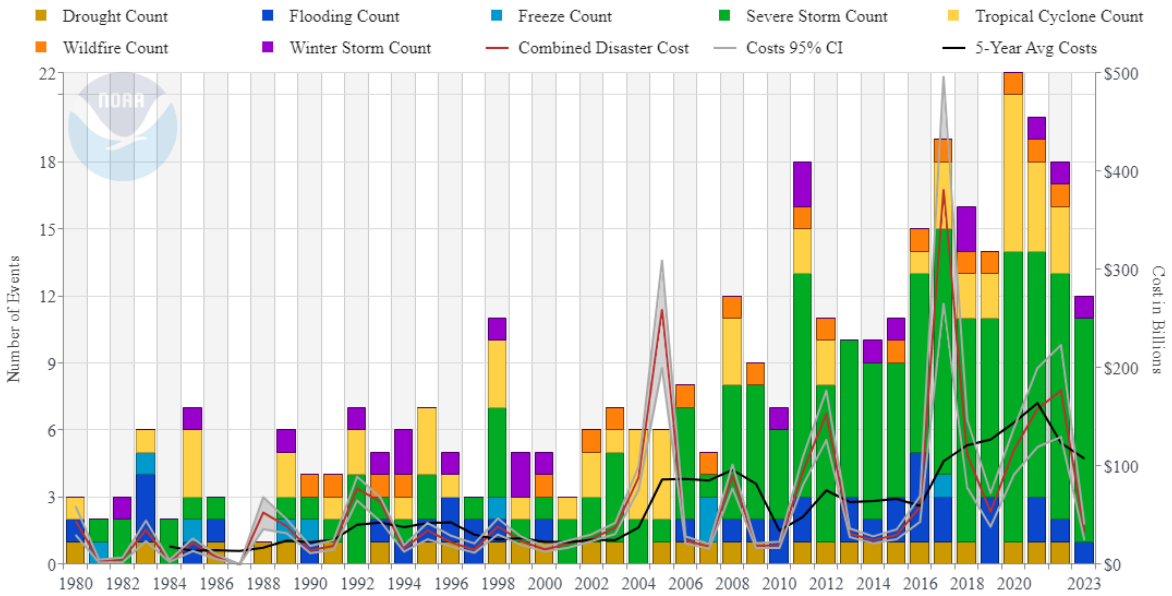

Figure 1. United States Billion-Dollar Disaster Events 1980 – 2023, CPI-Adjusted (NOAA 2023).

RESILIENCE PATHWAYS AND ENGAGED RESEARCH

Disaster resilience is an ever-evolving challenge, influenced by new threats and structural factors. President Biden's Executive Order 14008, titled *Tackling the Climate Crisis at Home and Abroad*, organizes and deploys the full capacity of US Government Agencies to combat the climate crisis and increase resilience to the impacts of climate change (WH, 2021). In Moser et. al (2019), resilience was characterized as a trait of a system, as a process or set of processes, or as an outcome. To support decisionmakers in achieving the goal of resilience, science-based solutions the United States National Science and Technology Council's (NSTC) Subcommittee on Resilience Science and Technology (SRST) established a Resilience Science and Technology Grand Pathways Framework focusing on strengthening specific societal dimensions of resilience to better identify, align, and prioritize investments in science and technology (NSTC 2023). The Grand Pathways Framework considered a community to be people connected through common physical, social, virtual, or hybrid characteristics. It includes individuals and families, businesses, nonprofit groups, faith-based and community organizations, media outlets, and government at all levels.

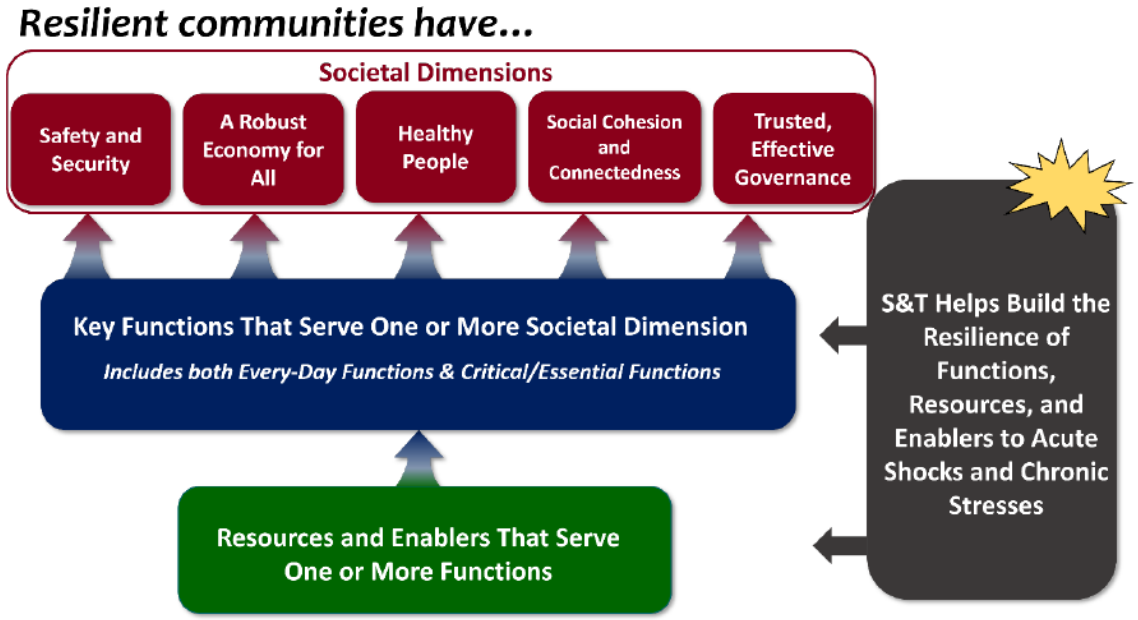

Figure 2. Construct of Resilience Communities as Defined by Social Dimensions, Enablers, and Functions (NSTC 2023).

Five societal dimensions of resilience were identified: safety and security, financial/economic resilience, healthy people, social cohesion, and trusted effective governance. The integration of societal dimensions, cross-cutting enablers, and key functions would allow for identification of the critical gaps that impede resilience and that can be addressed by the advancement in science and technology.

Participation by and collaboration with local communities are essential to resilience building. Motivated by the fact that scientific expertise alone is not always sufficient to address our society's grand challenges, engaged research is a mode of research conducted via collaboration among scientist and non-scientist actors (ACERE 2023). Principles for engaged research include matching partners and modes of engagement with the scale and scope of the project goals; anticipating problematic power dynamics; allowing sufficient time for sustained engagement; and maintaining flexible processes that facilitate ongoing learning.

Engagement with people and communities could lead to co-created research agenda, trust relationships between scientists and non-scientists, implementable outcomes, and other benefits. It's necessary especially for equitable resilience building as not all people experience disasters in the same way. A person's demographic background and economic status are shown as strong determinants of his/her outcomes following disaster events. The post-disaster recovery of minority and low-income neighborhoods is often slower than do their well-resourced counterparts. This is in part because many communities lack the resources and know-how for risk reduction, mitigation, and planning (NASEM 2022). Investment in disaster resilience competes for funding with other local needs such as public safety, education, and economic development.

It should note that engaged research may lead to unintended harms if not designed or executed properly: amplification of inequitable power dynamics, fatigue and resentment among collaborators, and un-sustained demands on time and resource.

SMART AND CONNECTED COMMUNITIES AND CIVIC INNOVATION CHALLEGENS

The NSF has made significant investment in disaster resilience research through core programs and special solicitations. The Smart and Connected Communities (S&CC) program solicitation is to accelerate the scientific and engineering advances and enable communities to attain new levels of economic opportunity and growth, safety and security, health and wellness, accessibility and inclusivity, and overall quality of life (NSF 2021). This solicitation defines communities as having geographically-delineated boundaries—such as towns, cities, counties, neighborhoods, community districts, rural areas, and tribal regions—consisting of various populations, with the structure and ability to engage in meaningful ways with proposed research activities. Intelligent technologies are then synergistically integrated with the natural and built environments in those communities to improve the social, economic, and environmental outcomes.

Figure 3. The Scope of S&CC Solicitation Outlining Core Science Domains and Applications

Researchers are expected to work closely with community stakeholders to translate local challenges into use-inspired research questions in control, privacy, safety, security, and other the scientific domains (as depicted as the core in Figure 3). Community stakeholders include residents, community groups, NGOs, businesses, municipal organizations, and agencies. Two distinct features of S&CC funded projects are 1) integrative research that addresses fundamental technological and social science dimensions of smart

and connected communities and 2) solutions that are piloted together with communities. The sustainability of the research outcomes beyond the life of the project is also important, as well as the scalability and transferability of the proposed solutions.

The Civic Innovation Challenge (CIVIC) takes the community engagement to a higher level (NSF 2022). By addressing priorities at the local scale that are relevant across the US, CIVIC is aimed at enabling a broader and more fluid exchange of research and technology capabilities and civic priorities through joint partnerships involving civic stakeholders and the research community. CIVIC funds projects that pilot state-of-the-art solutions over 12 months, following a six-month planning phase, and have the potential for lasting impact in the partnering community as well as the potential to be scaled and implemented in other places.

The CIVIC is uniquely designed, flipping the community-university dynamic by asking communities to identify civic priorities ripe for innovation and then to partner with researchers to address those priorities. Research-based solutions shall be ready for piloting in and with communities on a short timescale, where their effectiveness can be evaluated. A coalition of civic partners, stakeholders and researchers are determined to co-create and execute pilot projects. Civic partners and stakeholders may include local, state, or tribal government officials; non-profit representatives; community organizers or advocates; community service providers; and/or others working to improve their communities. The outcomes will be curated and shared as nationwide best practice for tackling common problems.

CONCLUSIONS

As an independent and the only federal agency in the U.S. whose mission supports all fields of science and engineering disciplines, from mathematics, engineering and geosciences to biological, behavioral and computer sciences, the National Science Foundation has funded research and researchers, innovations and innovators, and infrastructure, resulting in transformational technologies empowering the economic competitiveness and sustainability (NSF 2023). Advanced manufacturing, advanced wireless, artificial intelligence, biotechnology, microelectronics and semiconductors, quantum information science and engineering are all benefitted from sustained NSF investment. In NSF's FY 2024 Budget Request, four major themes are presented: *Advance Emerging Industries for National and Economic Security, Build a Resilient Planet, Create Opportunities Everywhere, Strengthen Research Infrastructure*. The *Build a Resilient Planet* initiative engages scientists and engineers across disciplines through convergent research that addresses societal needs and integrates research and education. Understanding and supporting responses to global change, improving computing capacity, and maintaining needed observational capabilities over time are examples of priority actions.

Scholarships in community engagement and citizen science are still emerging. Developing new and enhancing methodologies to scale up the practice of engaged research and its impact, by harvesting generalizable insights and ubiquitous technologies, are important frontier topics for future NSF investment. Equally important are methods for design and evaluation of engaged research, particularly in relation to stimulating foundational discovery, the translation of discovery into impact, broadening participation, and assessing short- and long-term impacts, positive and negative.

ACKNOWLEDGMENTS

Any opinions, findings, and conclusions or recommendations expressed in this material are those of the author(s) and do not necessarily reflect the views of the National Science Foundation or the US Government.

REFERENCES

Advisory Committee for Environmental Research and Education. (ACERE) 2022. Engaged Research for Environmental Grand Challenges: Accelerating Discovery and Innovation for Societal Impacts. A report of the NSF Advisory Committee for Environmental Research and Education. Prepared by the Advisory Committee on Environmental Research and Education.

Moser, S., Meerow, S., Arnott, J. and Jack-Scott, E. (2019) The turbulent world of resilience: interpretations and themes for transdisciplinary dialogue. Climatic Change 153, 21–40 (2019). https://doi.org/10.1007/s10584-018-2358-0

National Academies of Sciences, Engineering, and Medicine (NASEM) 2022. Equitable and Resilient Infrastructure Investments. Washington, DC: The National Academies Press. https://doi.org/10.17226/26633.

National Science and Technology Council (NSTC) Subcommittee on Resilience Science and Technology, 2023, The Resilience Science and Technology Grand Pathways Framework, available at https://www.whitehouse.gov/ostp/news-updates/2023/03/22/nstc-resilience-science-and-technology-grand-pathways-framework/

National Science Foundation (NSF), 2021, Smart and Connected Communities (S&CC), NSF 22-529, available at https://www.nsf.gov/pubs/2022/nsf22529/nsf22529.htm

National Science Foundation (NSF), 2022, Civic Innovation Challenge: A research and action competition driven by community priorities, NSF 22-565, available at https://www.nsf.gov/pubs/2022/nsf22565/nsf22565.htm

National Science Foundation (NSF), 2023, Fiscal Year 2024 Budget Request to Congress, https://new.nsf.gov/budget

NOAA National Centers for Environmental Information (NCEI) U.S. Billion-Dollar Weather and Climate Disasters (2023). https://www.ncei.noaa.gov/access/billions/, DOI: 10.25921/stkw-7w73

White House (WH), 2021, Executive Order on Tackling the Climate Crisis at Home and Abroad, https://www.whitehouse.gov/briefing-room/presidential-actions/2021/01/27/executive-order-on-tackling-the-climate-crisis-at-home-and-abroad/

PROCEEDINGS

DAY 3

Proceedings: Day 3

Day 3 (Wednesday, Sep. 27th, 2023)				
09:00~09:35	Presentation Session 9	Prof. Shyh-Jiann Hwang	Seismic Retrofitting Programs of RC Buildings after the 1999 Chi-Chi Earthquake in Taiwan	page 155
09:35~10:10		Prof. Takuya Nagae	System-Level and Component-Level Verification by Seismic-Response Building Tests Towards PBEE	page 161
10:30~11:05	Presentation Session 10	Prof. Gilberto Mosqueda	Hybrid Simulation of Steel Moment Frame Structures with Column Shortening	page 168
11:05~11:40		Prof. Tracy Becker	Multi-Degree of Freedom Hybrid Testing with Model Updating of an Isolated Bridge	page 175
no presentation		Prof. Peter Fajfar	Floor Acceleration Spectra Based on Structural Dynamics	page 181

Day3 (Wednesday, Sep. 27th, 2023) 09:00~09:35

Seismic Retrofitting Programs of RC Buildings after the 1999 Chi-Chi Earthquake in Taiwan

Shyh-Jiann Hwang

Professor, Department of Civil Engineering, National Taiwan University, Taipei, Taiwan, R.O.C.

Dr. Hwang is a Professor of Civil Engineering at the National Taiwan University, Taipei, Taiwan. He had served as the Director General of National Center for Research on Earthquake Engineering (NCREE) in Taiwan. He received his Master and PhD form the University of California, Berkeley. Dr. Hwang has been awarded the Distinguished Chair Professor of National Taiwan University. He serves as a member of seismic code committee in Taiwan and is very active in Taiwan concrete society. His research interests include shear behavior of reinforced concrete members, and seismic design and retrofitting of reinforced concrete structures. He had been responsible for providing technical supports to a national project that evaluates and retrofits all the non-code compliant school buildings in Taiwan. He is now participating the seismic retrofitting project by phases issued by the Ministry of Interior Affairs. This project is aimed to remove the seismic deficiency of the soft first story as a first priority for the residential buildings.

SEISMIC RETROFITTING PROGRAMS OF RC BUILDINGS AFTER THE 1999 CHI-CHI EARTHQUAKE IN TAIWAN

Shyh-Jiann Hwang[1]
1. Professor, Department of Civil Engineering, National Taiwan University, Taipei, Taiwan, R.O.C.
Email: sjhwang@ntu.edu.tw

ABSTRACT

Prior to the introduction of modern seismic codes in the late 1990s for Taiwan, many reinforced concrete buildings were designed without adequate detailing and reinforcement for seismic protection. For these vulnerable buildings, enhancements to the seismic capacities through retrofitting are urgently needed. The objective of this paper is to report the current seismic retrofitting projects of Taiwan. One was the school retrofitting project issued by the Ministry of Education 15 years ago. This school retrofitting project had upgraded the seismic capacities of approximately 10,000 school buildings in Taiwan. The other is the seismic retrofitting project by phases issued by the Ministry of Interior Affairs. This project is aimed to remove the seismic deficiency of the soft first story as a first priority for the residential buildings. The progress and technological development of these seismic projects are introduced in this paper.

Keywords: 1999 Chi-Chi Earthquake, residential building, school building, seismic assessment, seismic retrofitting

INTRODUCTION

Reinforced concrete buildings account for 75% of the total floor area in Taiwan. More than three quarters of these existing concrete buildings were constructed before 1999. Because of the less seismic demand and the inadequate seismic detailing, these older reinforced concrete buildings are prone to severe earthquake damage and even collapse. Recent reconnaissance reports revealed that the school buildings with cantilever corridors and the residential buildings with the soft first stories are the particularly vulnerable structures in Taiwan. Therefore, enhancements to the seismic capacities of these buildings through retrofitting are urgently required.

The school retrofitting program issued by the Ministry of Education started from 2009 and continued to 2020. This program was completed and yielded substantial results. Firstly, the progress and technology of this seismic project for school buildings in Taiwan are reported. The seismic retrofitting program for residential buildings by phases issued by the Ministry of Interior Affairs started from 2018. This program is still in process. Then the objective and technology development of this seismic project for residential buildings in Taiwan are discussed in this paper.

PROGRAM FOR UPGRADING SEISMIC CAPACITY OF SCHOOL BUILDINGS

The 921 Chi-Chi Earthquake demonstrated that the safety level of school buildings in Taiwan was of great concern. During this earthquake, more than half of the school buildings in Nantou County were either partially or fully destroyed (Fig. 1). Therefore, it is without a doubt that the seismic capacity of the school buildings in Taiwan should be a cause for concern, and that the seismic capacity of the school buildings needs to be urgently improved through retrofitting.

There are 3,783 public elementary and high schools in Taiwan, and the total number of buildings may be as high as approximately twenty seven thousands. The government of Taiwan had launched a project to upgrade the seismic performance of school buildings, and a total of $130 billion Taiwan dollars was budgeted from 2009 to 2022. This school retrofitting program have upgraded the seismic capacities of 10,163 school buildings in Taiwan (Fig. 2).

Fig. 1- School damages by Chi-Chi Earthquake

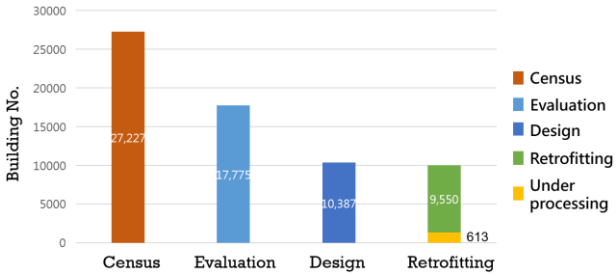

Fig. 2- Results of school retrofitting program

PROGRAM FOR UPGRADING SEISMIC CAPACITY OF RESIDENTIAL BUILDINGS

Reinforced concrete buildings account for 75% of the total floor area in Taiwan. More than three quarters of these existing concrete buildings were constructed before 1999. Because of the less seismic demand and the inadequate seismic detailing, these older reinforced concrete buildings are prone to severe earthquake damage and even collapse. Worst of all is the deficiency of the soft first story due to the residential and commercial mixed usage (Fig. 3). This retrofitting program by phases, started from 2018, is aimed to remove the seismic deficiency of the soft first story as a first priority for the residential buildings. A newly completed example is shown in Fig. 4. It's a 6-story condominium with a parking lot in the first story. Ten shear walls were added in the first story. The floor area of the first story is 690 m^2 and the retrofitting cost is TD$3,700/$m^2$.

Fig. 3- Collapsed buildings with soft first story

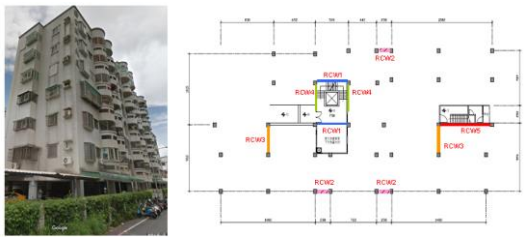

Fig. 4- Retrofitting example for soft first story

TECHNOLOGY DEVELOPMENT

National Center for Research on Earthquake Engineering (NCREE) suggested that the detailed evaluation of the seismic capacity of school buildings should be carried out using the method of performance-based design [1, 2], i.e., first conduct the nonlinear lateral pushover analysis to find the capacity curve of the school building, and then carry out the spectrum analysis to obtain the performance curve of the school building. By selecting the performance point, the associated peak ground acceleration can be determined, as shown in Fig. 5.

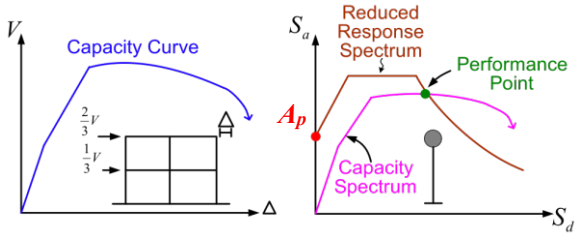

Fig. 5- Detailed evaluation for seismic capacity

The older reinforced concrete buildings in Taiwan were constructed with non-ductile detailing and low concrete compressive strength. Therefore their vertical members are prone to the shear or the flexural shear failures by earthquake loading and can be termed as shear-critical members. The shear strength of the deep reinforced concrete members can be reasonably predicted by the Softened Strut-and-Tie Models [3,4]. Based on the experimental and analytical studies, the lateral load-displacement curves of the shear critical members [5-9] were derived (Figs. 5 and 6).

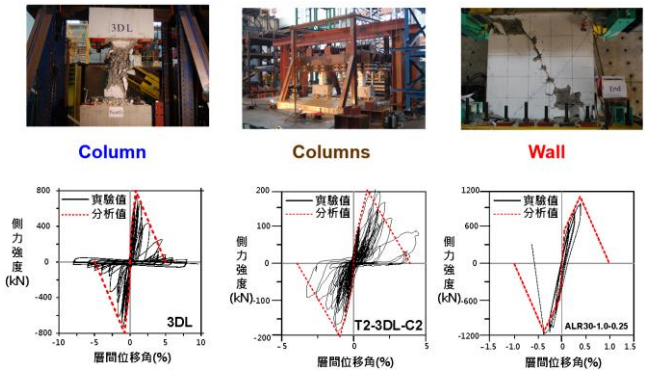

Fig. 6- Experimental and analytical studies in NCREE

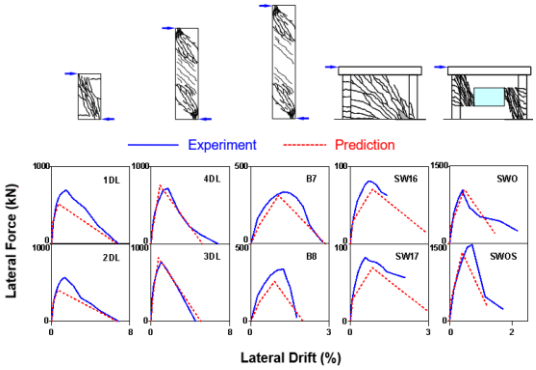

Fig. 7- Lateral load-displacement Curves [5-9]

A nonlinear time-domain analysis is considered more appropriate for the seismic evaluation of mid-rise to high-rise reinforced concrete buildings where the contributions from higher modes of dynamic analysis cannot be negligible. The hysteresis rules of vertical members can be easily modeled by the Pivot Hysteresis Model [10] with two pivot points that control unloading stiffness and pinching behavior (Fig. 8).

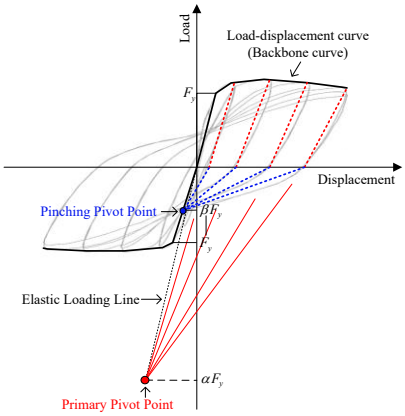

Fig. 8- Pivot Hysteresis Model

Using the simulated annealing technique, the parametric equations for the Pivot hysteretic model to predict the hysteretic behavior of rectangular reinforced concrete columns was derived [11] and test verification is shown in Fig. 9.

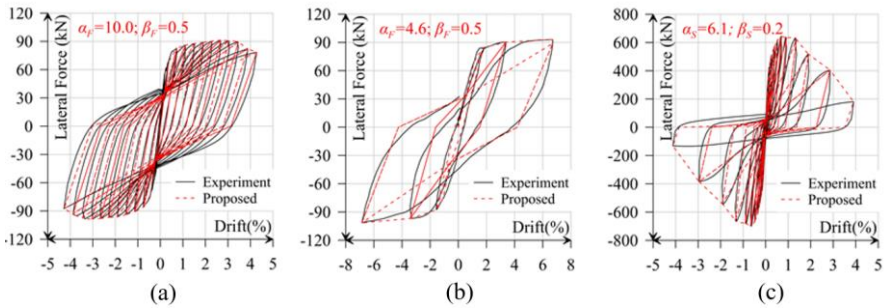

Fig. 9- Test verification: (a) Flexural failure, (b) Flexural shear failure, (c) Shear failure

Similarly, the parametric equations for the Pivot hysteretic model to predict the hysteretic behavior of rectangular reinforced shear walls was derived [12] and test verification is shown in Fig. 10.

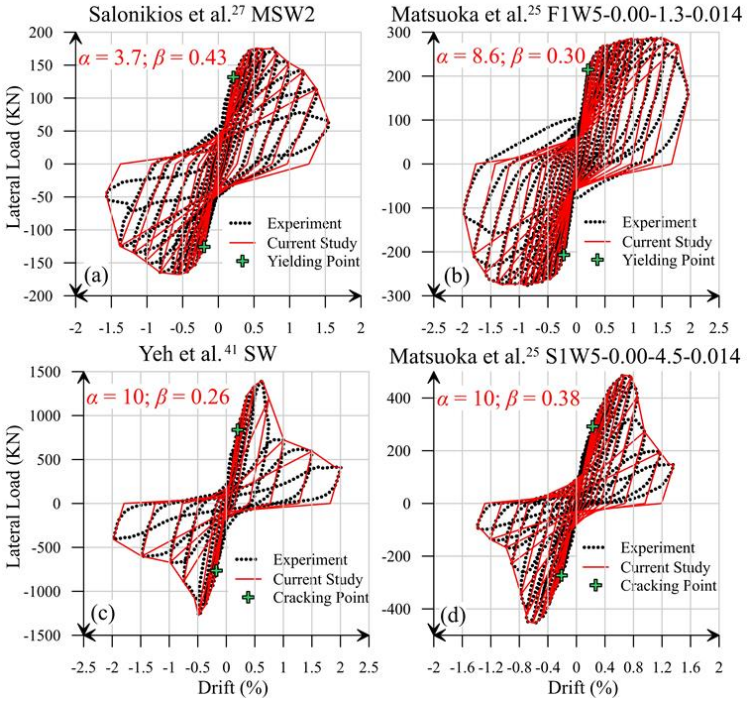

Fig. 10- Test verification: (a) Flexural shear failure of rectangular wall, (b) Flexural failure of barbell wall, (c)Shear failure of rectangular wall, (d) Shear failure of barbell wall

CONCLUSIONS

The school retrofitting program issued by the Ministry of Education started from 2009 and continued to 2022. This program was fully developed and yielded substantial results. The seismic retrofitting program for residential buildings by phases issued by the Ministry of Interior Affairs started from 2018. This program is in the demonstration stage. It is hoped that, by seismic evaluation and retrofitting of school buildings and residential buildings, the general public of Taiwan would understand the importance of seismic retrofitting. This work may be continued and extended to more existing buildings in order to create a much secure homeland.

ACKNOWLEDGMENTS

The author would like to thank the officials of the Ministry of Education and the Ministry of Interior Affairs for providing information and guidance. These works done by the members of the National Center for Research on Earthquake Engineering are much appreciated.

REFERENCES

[1] Chung, L. L., Yeh, Y. K., Chien, W. Y., Chai, J. F., Hsiao, F. P., Shen, W. C., Chiou, T. C., Chow, T. K., Chao, Y. F., Yang, Y. S. and Hwang, S. J. (2008). Technology Handbook for Seismic Evaluation and Retrofit of School Buildings. Technical Report NCREE-08-023, *National Center for Research on Earthquake Engineering*, Taipei, Taiwan. (In Chinese)

[2] Hsiao, F. P., Chung, L. L., Yeh, Y. K., Chien, W. Y., Shen, W. C., Chiou, T. C., Chow, T. K., Chao, Y. F., Weng, P. W., Yang, Y. S., Chu, Y. L., Tu, Y. S., Chai, J. F. and Hwang, S. J. (2013). Technology Handbook for Seismic Evaluation and Retrofit of School Buildings - Third edition. Technical Report NCREE-13-023, *National Center for Research on Earthquake Engineering*, Taipei, Taiwan. (In Chinese)

[3] Hwang, S. J. and Lee, H. J. (2002). "Strength Prediction for Discontinuity Regions by Softened Strut-and-Tie Model," *Journal of Structural Engineering*, ASCE, **128**(12), 1519-1526.

[4] Hwang, S. J., Tsai, R. J., Lam, W. K. and Moehle, J. P. (2017). "Simplification of Softened Strut-and-Tie Model for Strength Prediction of Discontinuity Regions," *ACI Structural Journal*, **114**(5), 1239-1248.

[5] Li, Y. A. and Hwang, S. J. (2017). "Prediction of Lateral Load Displacement Curves for Reinforced Concrete Short Columns Failed in Shear," *Journal of Structural Engineering*, ASCE, **143**(2), 04016164. doi: 10.1061/(ASCE)ST.1943-541X.0001656

[6] Li, Y. A., Weng, P.W. and Hwang, S. J. (2019). "Seismic Performance of RC Intermediate Short Columns Failed in Shear," *ACI Structural Journal*, **116**(3), 195-206.

[7] Shen, W. C., Hwang, S. J., Li, Y. A., Weng, P. W. and Moehle, J. P. (2021). "Force-Displacement Model for Shear-Critical Reinforced Concrete Columns," *ACI Structural Journal*, **118**(1), 241-249.

[8] Weng, P. W., Li, Y. A., Tu, Y. S. and Hwang, S. J. (2017). "Prediction of Lateral Load Displacement Curves for Reinforced Concrete Squat Walls Failed in Shear," *Journal of Structural Engineering*, ASCE, **143**(10), 04017141. doi:10.1061/(ASCE)ST.1943-541X.0001872

[9] Tsai, R. J., Hsu, Y. C., and Hwang, S. J. (2021). "Prediction of Lateral Load-Displacement Curve of Reinforced Concrete Walls with Openings under Shear Failure," *ACI Structural Journal*, **118**(5), 275-284.

[10] Dowell, R. K., Seible, F. and Wilson, E. L. (1998). "Pivot Hysteresis Model for Reinforced Concrete Members," *ACI Structural Journal*, **95**(5), 607-617.

[11] Ling, Y. C., Mogili, S., and Hwang, S. J. (2022). "Parameter Optimization for Pivot Hysteresis Model for Reinforced Concrete Columns with Different Failure Modes," *Earthquake Engineering and Structural Dynamics*, **51**(10), 2167-2187.

[12] Ling, Y. C., Mogili, S., and Hwang, S. J., (2022) "Parameter Optimization for Pivot Hysteresis Model for Reinforced Concrete Shear Walls with Different Failure Modes," The 8th Asia Conference on Earthquake Engineering, Taipei, Taiwan.

Day3 (Wednesday, Sep. 27th, 2023) 09:35~10:10

System-Level and Component-Level Verification by Seismic-Response Building Tests Towards PBEE

Takuya Nagae

Associate Professor, Disaster Mitigation Research Center, Nagoya University, Japan

Takuya Nagae worked in Nagoya University from 2014 to 2022 and in E-Defense (NIED) from 2006 to 2014. He has completed a series of large-scale tests on RC, Steel and Wood structures in Nagoya University as well as in E-Defense. Sub-structure representations regarding high-rise building responses were also developed in his career. He has enthusiastically promoted a various of international joint projects. He will complementally introduce the process that he proceeded such projects.

SYSTEM-LEVEL AND COMPONENT-LEVEL VERIFICATION BY SEISMIC-RESPONSE BUILDING TESTS TOWARDS PBEE

Takuya Nagae[1], Kazuki Takaya[2], Ryota Nishi[3]
1. Associate Professor, Disaster Mitigation Research Center, Nagoya University, Japan
2. Ph.D. Student, Graduate School of Environmental Studies, Nagoya University, Japan
3. Contract Researcher, EERC/E-Defense, NIED (Ph.D. Student, Nagoya University), Japan
Email: nagae.takuya.h9@f.mail.nagoya-u.ac.jp, takaya.kazuki.f6@s.mail.nagoya-u.ac.jp, nishi.r@bosai.go.jp

ABSTRACT

In the wood dwelling full-structure test, the foundation sliding occurred at the interface of foundation and soil. Even in sequential inputs of MCE motions, a slight damage state was kept. Once the structural system changes from the upper structure failure mode to the foundation sliding soil failure mode, the collapse probability becomes very low in the MCE events. Thus, if the upper structure failure as well as the foundation-sliding soil failure are precisely evaluated, such different ultimate stage scenario can be adopted in practice. The PBEE method has a potential to assess this seismic response mechanism. Outcomes from systematic testing will be contributing not only to the individual building system verification but also to the comprehensive PBEE strategy.

Keywords: Shaking table test, System level assessment, Wood dwelling structure

INTRODUCTION

The Tokyo Metropolitan Resilience Project was done in the period from 2017 to 2022, sponsored by MEXT, Japan. A comprehensive test plan for the current/future wood dwellings in densely populated urban areas was proposed in this Project. Figure 1 shows the background of the test using the two generic Grade-3 index buildings. One adopted the Post-and-beam structure (P&B structure), and the other the Shear-wall structure (SW structure). A series of tests were planned with different physical boundary conditions surrounding the reinforced concrete (RC) foundations. In the Phase 1, A-building equipped a base-isolation system, while B-building represented a generic foundation constructed on real soil by preparing a soil box. In the Phase 2, the foundation of A-building was firmly fixed, while cast-iron plates were installed beneath the foundation of B-building. In the third Phase 3, the damaged first-story of A-building was retrofitted, and the foundation of B-building was firmly fixed.

Figure 1. Wood dwellings represented in the E-Defense shaking table facility

TEST BUILDING AND TEST SCHEDULE

The design criteria of the Grade-3 building were adopted for both of the two test buildings. The allowable stress design was applied; The base shear force coefficient of 0.2 to the standard, 0.25 to the Grade-2 index building and 0.3 to the Grade-3 building. The margin in the design requirement was minimized to evaluate the capacities of both test buildings. Thus, the earthquake resisting capacities of the upper structures of A-building and B-building were assumed to be equivalent in this design process.

Figure 2 shows the setups of A-building and B-building on the shake table. The X-direction of the test buildings was set to the shorter direction of the shake table. In the first Phase 1, A-building was equipped with a Base-isolation system, while B-building represents a foundation supported on soil (Soil-foundation system). Figure 3 shows the condition of A-building. The base-isolation layer was composed of fifteen sliding bearings having the friction coefficient of 0.065, six laminated rubbers and six oil dampers (three for each of the X and Y-directions). Figure 4 shows the condition of B-building. The test system of B-building accommodated real 1.5 m-high soil beneath the foundation by preparing a reinforced concrete soil box. Well compacted Silica sand was utilized for the soil.

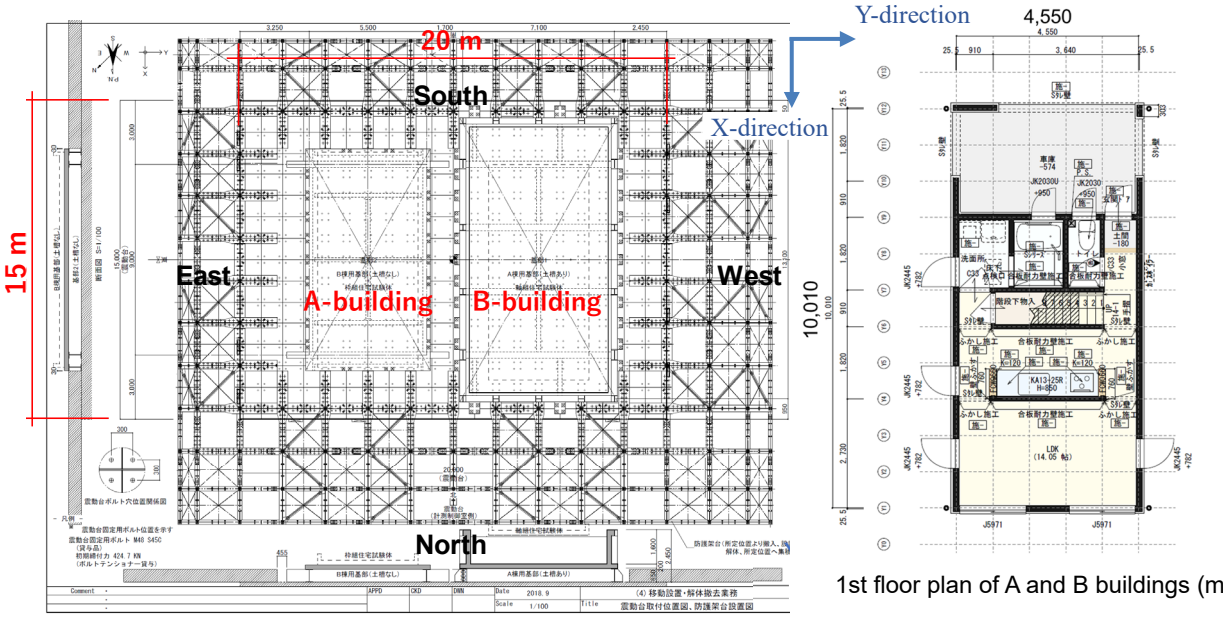

Figure 2. Setup locations of two test buildings on the E-Defense shaking table

(1) Base-isolation layer (sliding bearings, rubbers and oil dampers) (2) P&B structure

Figure 3. A-building with Base-isolation system (Upper structure: P&B structure)

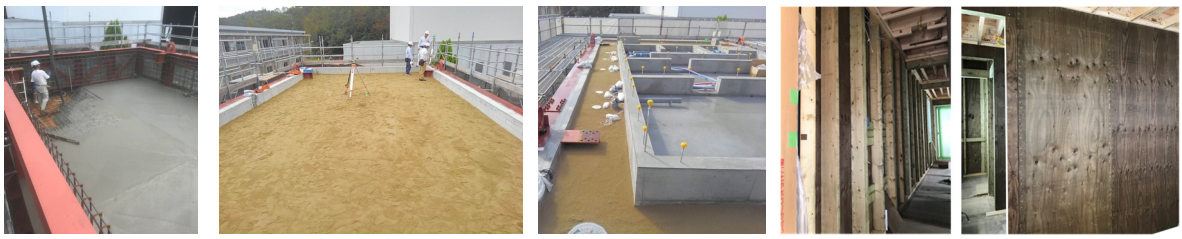

(1) Soil box (2) Soil (3) RC foundation (4) SW structure

Figure 4. B-building with Foundation-soil system (Upper structure: SW structure)

Figure 5 shows the depiction on the sequential tests in Phase 1, Phase 2 and Phase 3. The same upper structures were used from beginning to end. Table 1 shows the input motion schedules in each

Phase. The JMA-Kobe motion and JR-Takatori motion of the 1995 Kobe earthquake were adopted. JMA-Kobe 50% is equivalent to the Design-Based Earthquake.

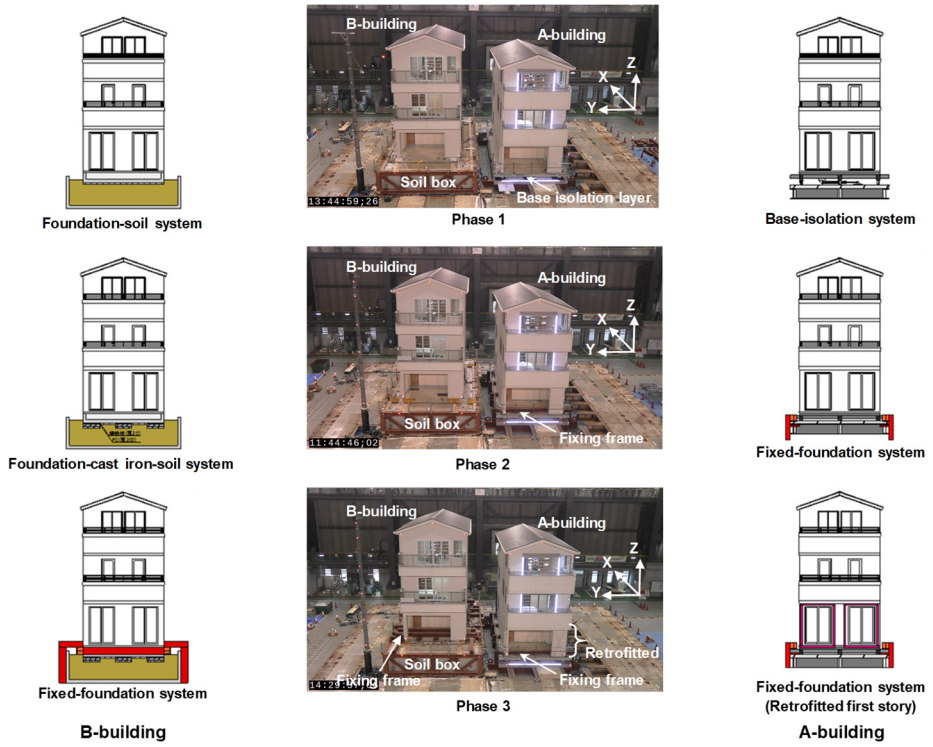

Figure 5. Depiction on the sequential Phase 1, Phase 2 and Phase 3 (tested in 2019)

Table 1 Test schedule and input motions

	Input motion	A-building	B-building
Phase 1	(1) JMA-Kobe 25%, 50% (2) JR-Takatori 25%, 50% (3) JMA-Kobe 100% (4) JR-Takatori 100%	Base-isolation system	Foundation-soil system
Phase 2	(1) JMA-Kobe 25%, 50%, 100% (2) JR-Takatori 100%	Fixed-foundation system	Foundation-cast iron system
Phase 3	(1) JMA-Kobe 100%	Fixed-foundation system	Fixed-foundation system

ACCELERATION DISPLACEMENT RESPONSE SPECTRA AND TEST ASSESSMENT

Nonlinear response systems can be discussed using the Acceleration-Displacement (*Sa-Sd*) Response Spectra format. The maximum deformation distributions can be assessed given the first mode shape. Figure 6 shows the mode vectors adopted for (1) A-building with Base-isolation (4-DOF) system, (2) B-building with Foundation-soil (4-DOF) system and (3) A-building with Fixed-foundation (3-DOF) system.

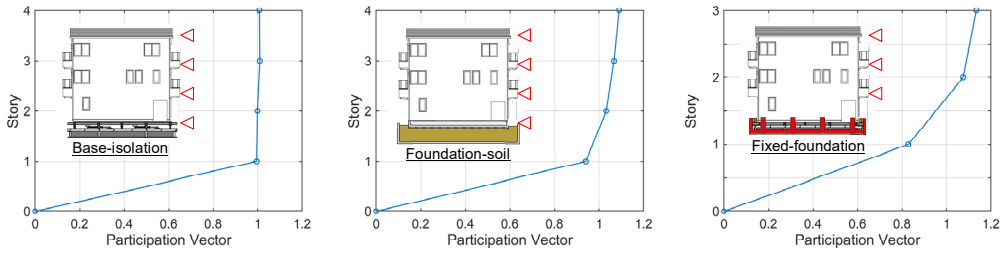

(1) A-building / Phase 1 (2) B-building / Phase 1 (3) A-building / Phase 2

Figure 6. Adopted mode vectors / JMA-Kobe 100% / X-direction

By using these mode vectors, the equivalent SDOF systems were implemented in the *Sa-Sd* Response Spectra format, as shown in Figure 7. The results of A-building with the Base-isolation system and B-building with the Foundation-soil system showed consistent peak displacements to the Spectra, as well as A-building with the Fixed-foundation system showing inelastic responses in the upper.

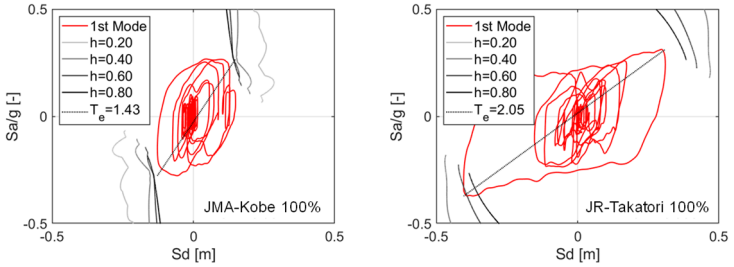

(1) A-building / Phase 1 (Base-isolation system) / X-direction

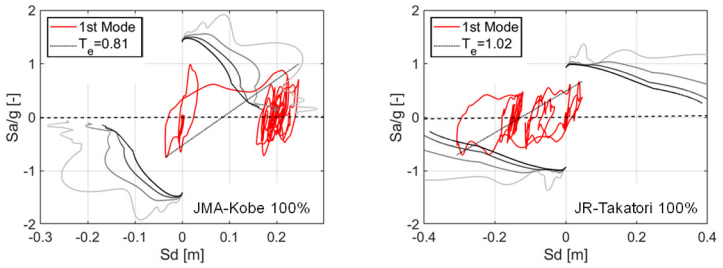

(2) B-building / Phase 1 (Foundation-soil system) / X-direction

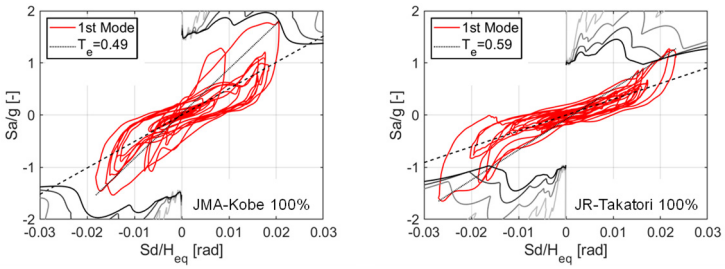

(3) A-building / Phase 2 (Fixed-foundation system) / X-direction

Figure 7. Comparison of test results and Acceleration Displacement Response Spectra

DIFFERENT ULTIMATE FAILURE MODES IN THE UPPER STRUCTURES

Figure 8 shows the base shear force coefficient v.s. the story drift angle, when subjected to JMA-Kobe 100%. Regarding A-building with the fixed-foundation, the maximum drift angle reached 0.03 rad, due to shear failures in the first story components. The Base-isolation system significantly reduced the responses in the upper structure. Regarding B-building with the fixed foundation, the maximum drift angle exceeded 0.10 rad due to very brittle tension fracture at the bases in the first story. On the other hand, the Foundation-soil system also had a story drift limit. Here, different ultimate failure modes were confirmed in the P&B and SW structures. And similar input reduction effects due to the Base-isolation and Foundation-soil systems were confirmed.

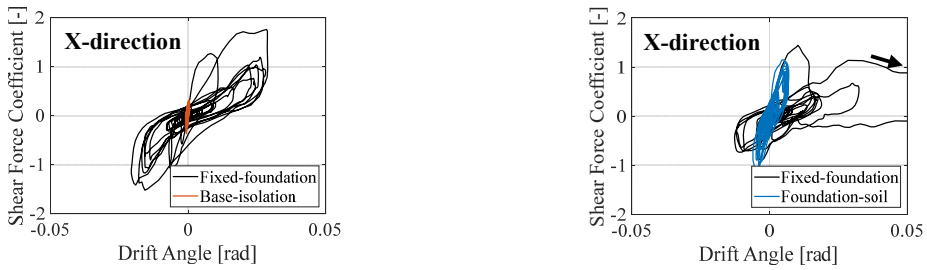

(1) A-building (Shear failure when foundation fixed) (2) B-building (Tension fracture when foundation fixed)

Figure 8. Different ultimate failure modes in the P&B and SW structures and impacts by foundation boundaries

PBEE APPLICATION INCLUDING COMPARATIVE TESTING

Figure 9 and 10 are showing preliminary discussions by the 2009 test results, in advance of the 2019 test. IMK model was calibrated given the full-scale collapse tests conducted in 2009. The first-mode response in the tests were represented by the SDOF system. The stiffness and strength deteriorating parameters were adjusted in addition to the maximum strength capacity as well as negative slope angle. The test responses were well traced by dynamic response analysis using such IMK models and input ground motions. Such numerical analyses would be used in the probabilistic performance assessment, reasonably, through an IDA statistical approach with GM intensity factor of 1.0 when PGA is 0.5 g. From base sliding tests conducted separately, sliding foundation models assuming different friction coefficients were combined with the IMK upper model, and the impacts of sliding foundations were clearly indicated, through the same IDA statistical approach in Figure 9. The variation due to ground motion uncertainties becomes small in the upper when the foundation sliding dominates. Needed in the PBEE here is the precise assessment of both the upper ultimate strength and the sliding strength before seeing the test results.

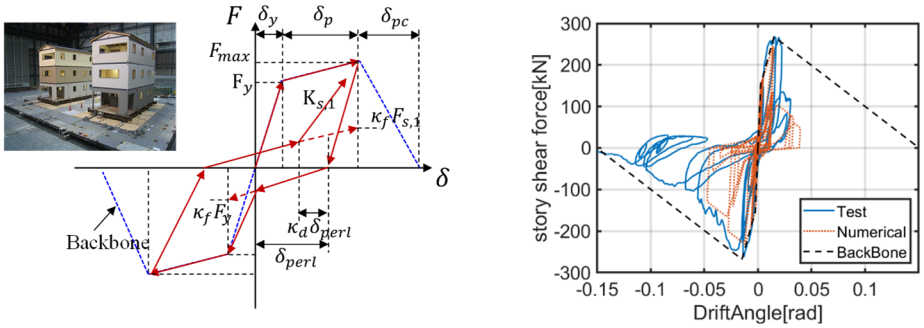

(1) Application of IMK model given a collapse test result (Grade 2)

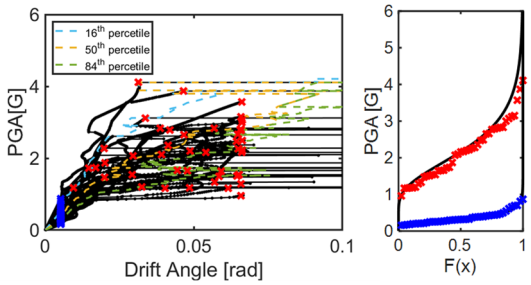

(2) IDA using the calibrated IMK model (FEMA P695, Far-Field GMs; 2-direction 22 sets)

Figure 9. Preliminary discussions based on the 2009 test results

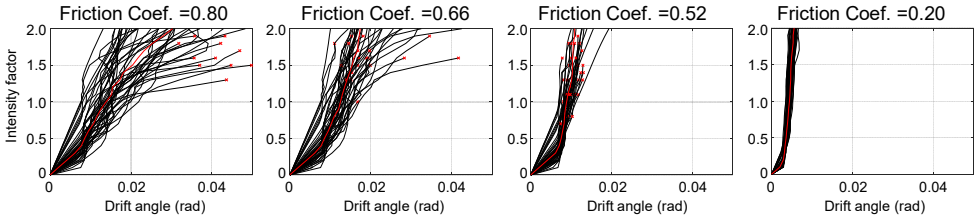

(1) Ground motion intensity vs Upper-structure drift angle

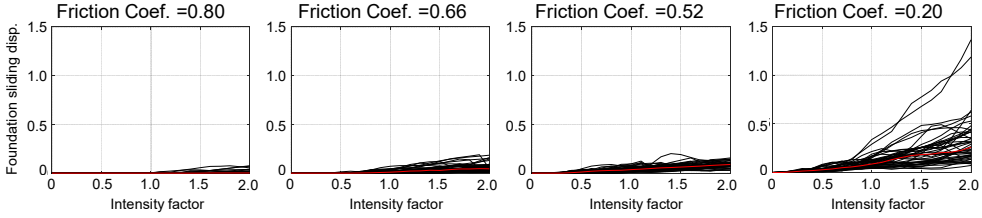

(2) Ground motion intensity vs Foundation sliding displacement

Figure 10 Response impacts by sliding foundation based on the 2009 test assumption

In Figure 11 regarding the upper structure capacity in the 2019 test results, the allowable strength capacities corresponding to the design limit were assessed and arranged in reference to the separatedly conducted component level tests. Shown in A-building is about 4 times the allowable stress limit in the Grade-3 criteria while in B-building about 3 times. In design practice, the system capacity is the sum of component evaluations, which show the ratios less than 1.5. Now, a numerical analysis using 3-D frame system is assigned and verified to realize a procedure making a reference instead of the system tests.

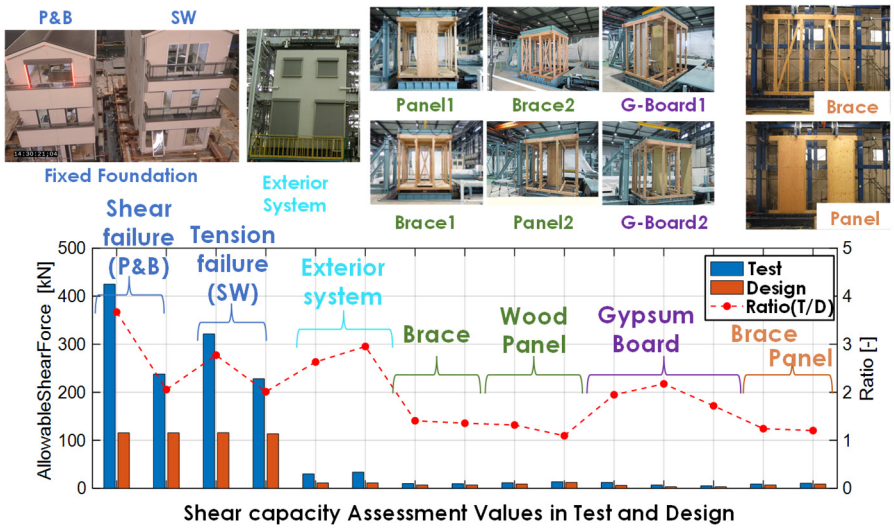

Figure 11. Strength capacities in system level against component level

CONCLUSIONS

Given the test results including soil and foundation, numerical analysis can be calibrated to trace the overall test response. In PBEE, this should be done in advance. Wood dwelling upper structures shows much larger strength capacities than the design evaluations. The uppers should be assessed as precisely as possible, representing the relevant ultimate failure modes. A promising numerical analysis software is assigned already for the upper. The foundation sliding behaviors should be assessed too, and the test data acquirement and compatible numerical analysis development are the intense future work.

REFERENCES

T. Nagae, S. Uwadan, K. Takaya, C. Yenidogan, S. Yamada, H. Kashiwa, K. Hayashi, T. Takahashi, T. Inoue (2020) Sliding-rocking combined actions at base foundation influencing global and local deformations of upper wood structure, 17th WCEE, 2020, Japan

T. Takahashi, S. Uwadan, T. Nagae, C. Yenidogan, S. Yamada, H. Kashiwa, K. Hayashi, T. Inoue (2020) Stiffness, ultimate strength capacity and cyclic loading deterioration characteristics of two different wood-structure dwellings following the current Japanese practice, 17th WCEE, 2020, Japan

Aghababaei Mohammad, Okamoto Christian, Koliou Maria, Nagae Takuya, Pantelides Chris P., Ryan Keri L., Barbosa Andre R., Pei Shiling, van de Lindt John W., Dashti Shideh (2021) Full-Scale Shake Table Test Damage Data Collection Using Terrestrial Laser-Scanning Techniques, Journal of Structural Engineering, 147-3, March 2021

Yenidogan Cem, Nishi Ryota, Uwadan Seiya, Nagae Takuya, Isoda Hiroshi, Tsuchimoto Takahiro, Inoue Takahiro, Kajiwara Koichi (2021) Full-scale shake table tests of P&B type of Japanese three-story wood dwellings for the collapse characterization, Soil Dynamics and Earthquake Engineering, Volume 150, November 2021, DOI : 10.1016/j.soildyn.2021.106898 ISSN

Yenidogan Cem, Nishi Ryota, Nagae Takuya, Inoue Takahiro, Kajiwara Koichi (2020) Full-scale cyclic test of a Japanese post and beam wood shearwall assembly, Bulletin of Earthquake Engineering, 18-10, 4985-5008

Chung Yu-Lin, Kuo Kuan-Ting, Nagae Takuya, Kajiwara Koichi (2019) Seismic responses of a free-standing two-story steel moment frame equipped with a cast iron-mortar sliding base, Earthquake and Structures, 17-3, 245-256

PS10-1

Day3 (Wednesday, Sep. 27th, 2023) 10:30~11:05

Hybrid Simulation of Steel Moment Frame Structures with Column Shortening

Gilberto Mosqueda

Professor, University of California San Diego, California, USA

Gilberto Mosqueda is a professor in the Department Structural Engineering, Director of the Seismic Response Modification Device Test Facility, and Associate Dean for Equity Diversity and Inclusion for the Jacobs School of Engineering at UC San Diego. His research focus is on developing experimental and numerical capabilities to simulate the response of structures including building and their contents from the onset of damage through failure. He has contributed towards the development of hybrid testing methods for large-scale structural models and the application of earthquake protections systems including seismic isolation and damping devices in buildings and bridges. He has led teams of investigators in reconnaissance missions following earthquakes to investigate damage, most recently following the 2017 Puebla-Morelos Earthquake that affected Mexico City. Professor Mosqueda is the recipient of the NSF CAREER Award, the American Society of Civil Engineering Moisseiff Award, and the Mexico College of Civil Engineering Jose A. Cuevas Award.

HYBRID SIMULATION OF STEEL MOMENT FRAME STRUCTURES WITH COLUMN SHORTENING

Gilberto Mosqueda[1], Claudio Sepulveda[2], Chia-Ming Uang[1], Gulen Ozkula[3], Kung-Juin Wang[4], Chung-Che Chou[5], Po-Chia Huang[6], Cheng-Wei Huang[6], Mao Cheng[7] and Tracy Becker[8]

1. Professor, University of California San Diego, California, USA
2. Graduate Student Researcher, University of California San Diego, California, USA
3. Assistant Professor, University of Wisconsin, Platteville, USA
4. Principal Engineer, National Center for Research on Earthquake Engineering, Taipei, Taiwan, R.O.C
5. Director General, National Center for Research on Earthquake Engineering, Taipei, Taiwan, R.O.C
6. Research Assistant, National Center for Research on Earthquake Engineering, Taipei, Taiwan, R.O.C
7. Graduate Student Researcher, University of California Berkeley, California, USA
8. Professor, University of California Berkeley, California, USA

Email: gmosqueda@ucsd.edu

ABSTRACT

Deep columns in steel moment frames are susceptible to local buckling and subsequent axial shortening when subjected to combined high axial forces and cyclic lateral loads. Deep column members have been studied extensively, however, experimental simulations at the subassembly or the full system level are more limited including the interaction between the shortening columns and the surrounding structural framing system. Four full-scale steel moment frame cruciform subassemblies are tested as part of this program using quasi-static and hybrid simulations. The hybrid simulations are conducted using advanced algorithms with new capabilities developed for this project. A mixed displacement and force control strategy enables compatible displacements between the numerical and experimental models for force-controlled degrees of freedom, in this applying a controlled axial load on the column that is susceptible to shortening. The experimental cruciform subassembly includes beam-to-column connections with reduced beam sections for which the response is measured and utilized with online model updating of parameters in the nonlinear numerical beam models. These experiments provide new capabilities for hybrid testing and data that provides insight into the seismic response of steel moment frame structures with deep columns under more realistic boundary conditions.

Keywords: Hybrid simulation, steel moment frames, axial shortening, online model updating

INTRODUCTION

A series of experiments have been carried out on individual deep column members that demonstrate their susceptibility to bucking and subsequent column shortening (Ozkula et al., 2021; Elkady and Lignos, 2017). Past quasi-static testing of isolated columns and subassemblies have shown the importance of the axial load, inelastic deformation, and boundary conditions on the severity of axial shortening (Chansuk et al., 2021; Chou et al., 2022). The effects of column shortening on the frame system-level behavior has only been addressed through pure numerical simulations (Wu et al., 2018), without experimental system-level testing and only limited subassembly testing. This project aims to experimentally assess the system behavior of moment frame structures with deep columns by conducting quasi-static tests and hybrid simulations with full-scale cruciform subassemblies. To capture axial shortening in the hybrid simulation, a new mixed displacement and force control method is proposed and implemented to achieve equilibrium of forces and displacement compatibility. Past hybrid simulations that have utilized force control for stiff degrees of freedom have neglected deformations (Del Carpio et al. 2015). Moreover, to overcome limitations in the experimental setup, an overlapping substructuring method is applied to simplify the boundary conditions of the physical substructure. An online model updating scheme is integrated with the substructuring method that utilizes data measured during the test to update parameters of hysteretic models for the reduced beam section.

PROTOTYPE MODEL AND SUBSTRUCTURING

The prototype structure considered is a steel moment frame with 18ft height at the first story plus five floors at 14ft each over four bays each spanning 26ft. Column sections are W24x176 and considered deep sections while beams are W27x129 for the first three stories. The upper stories columns are W24x131 and beams are W27x94. Reduced beam section (RBS) are considered for beam-column connection. The numerical nonlinear model for the hybrid simulation is developed in OpenSees. Columns are modeled using distributed plasticity elements with a displacement-based formulation. The panel zone deformation is simulated using the parallelogram approach (Gupta and Krawinkler 1999) with a rotational spring in one corner. Beams are modeled considering an elastic beam-column element for the middle section with each end having rigid offsets plus a lumped plasticity spring. Above the second story, the beam hinges are simulated using Ibarra-Medina-Krawinkler (IMK) model (Ibarra et al. 2005). However, for beam hinges at the first story, a modified version of Bouc-Wen model (Chen and Becker 2021) is used with the ability of having updatable parameters to be used in the online model updating scheme. The numerical model and experimental substructure including the actuator configuration are illustrated in Figure 1.

The physical substructure is a cruciform beam-column subassembly depicted in Figure 2. The column is one and one-half story heigh with a pair of parallel pinned-connected actuators located on top of the specimen to control the horizontal displacement of the system. The control point of the actuators is located at the top end of the first story column to ensure displacement compatibility at first floor level with the numerical substructure. Since axial shortening is expected at the base of the column and the specimen is an interior column, one vertical pinned-connected actuator controls each beam end following the vertical displacement measured at the control point. To impose the axial forces, four hydraulic jacks are located on top of the specimen in force control mode. Preliminary numerical studies indicate that the three interior columns are expected to have similar behavior, thus, the one experimental specimen is selected to represent the three interior columns. To overcome the large number of DOFs at the boundaries of the experimental substructure (rotation at the member ends and horizontal displacement at the first story) an overlapping substructure approach is implemented for this test (Hashemi and Mosqueda 2014). A zone is overlapped in both domains in order to minimize the effects of limiting the controlled DOFs such as neglecting rotation at the boundaries. For this test, the commanded signals from the numerical substructure are the horizontal displacement at the floor level, and the axial load obtained from the second story column. The feedback signals are the moment M and shear force V calculated at the top end of the first story column in the physical substructure, plus the vertical displacement measured at the same point. This last signal is converted into an equivalent vertical force *Feq*, which imposes the measured displacement coming from the test on the numerical model.

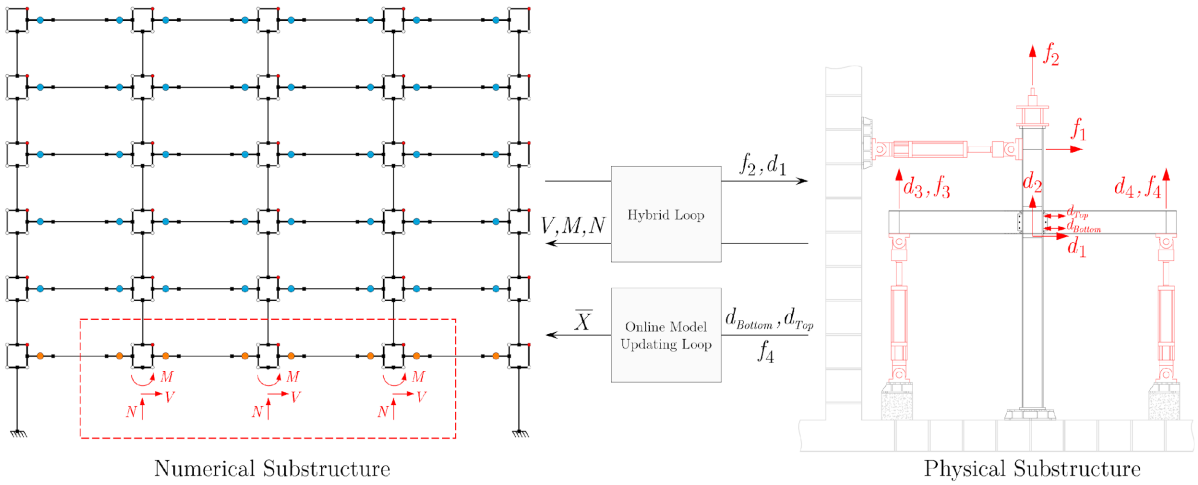

Figure 1. Detailed nonlinear numerical model of frame and experimental substructure representing three interior first story columns in numerical model.

Figure 2. Photo of full-scale cruciform subassembly with lateral support system at NCREE.

Closed-loop Mixed Displacement and Force Control

A closed-loop mixed displacement and force control approach is used to apply the axial load using force control on the stiff column and enforce the compatible displacement due to shortening in the numerical model. The control loop is implemented within the conventional displacement based finite element framework and applied here in OpenSees. The force command for the column axil load is obtained from the numerical substructure as the internal axial force of the second story columns. The axial force is applied using four hydraulic jacks on top of the specimen. The vertical displacement or shortening of the first story column is measured in the physical substructure and sent as a feedback displacement to the numerical model. The measured shortening is converted into the equivalent force applied in the numerical model to achieve displacement compatibility between both substructures. To account for nonlinearities in the numerical model, the equivalent force is calculated using a closed-loop proportional-integral (PI) controller. The target variable is the axial shortening displacement measured in the column, while the observed displacement refers to the the vertical displacement at the node above the column in the numerical substructure. For every time integration step, the equivalent force is adjusted based on the error and imposed in the numerical substructure as an external force.

Online Model Updating

An online model updating (OMU) algorithm is included in the hybrid simulation to improve the numerical model of the reduced beam section plastic hinge in the first story since these elements are likely to experience a similar loading history as the experimental substructure. The experimental response of the beam RBS is measured and model parameters for the Bouc-Wen material model are identified through an unscented Kalman filter algorithm. Thus, in each updating step, the numerical RBS hinges parameters are updated based on the observed experimental behavior.

RESULTS

An overview of the results for one of the hybrid simulations labeled HS-B is presented. The ground motion sequence consisted of an elastic (Kobe 1995), Design-basis Earthquake (DBE) (Kobe 1995) and Maximum Considered Earthquake (MCE) (Northridge 1994) motions scaled based to the seismic hazard used for the design of the prototype structure. The maximum drift observed was 5% in the first story, which is near the capacity of the experimental setup. The first story drift ratio is shown in Figure 3 and the local response of the column base is shown in Figure 4.

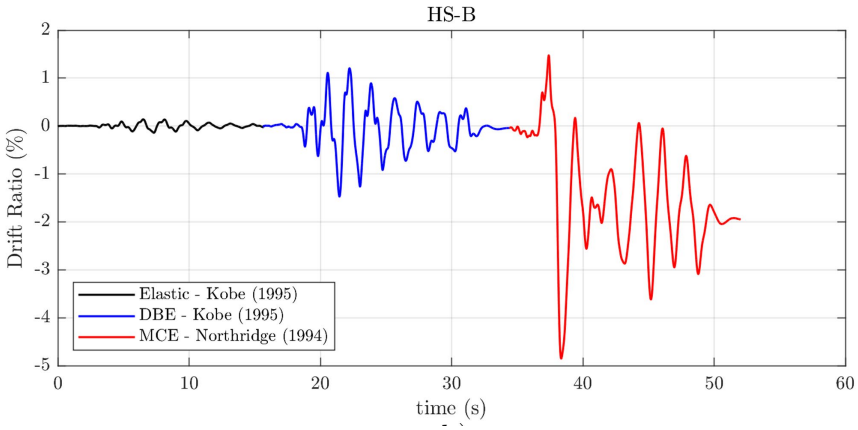

Figure 3. First story drift ratio during hybrid simulation.

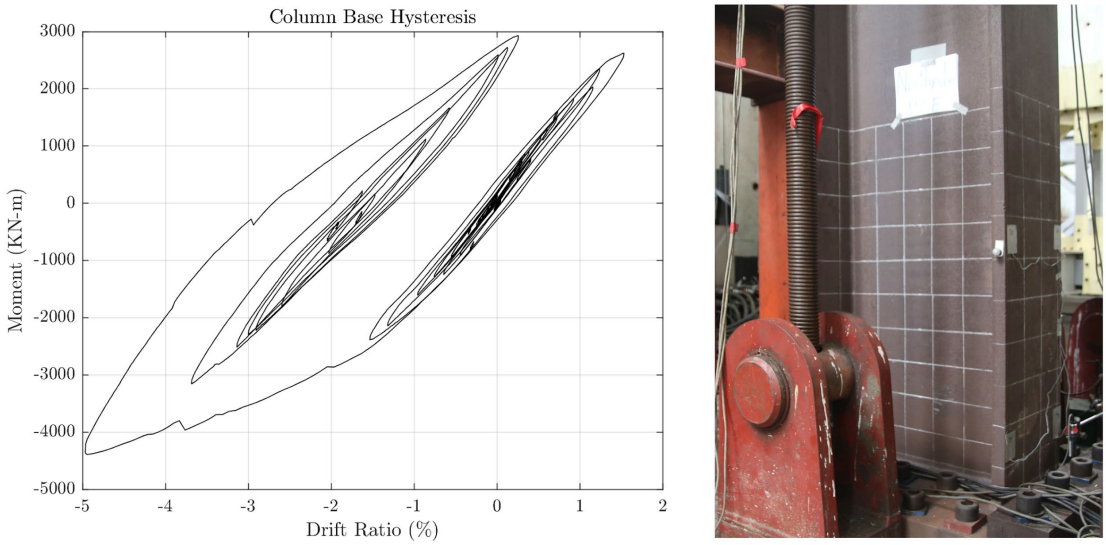

Figure 4. Measured response at column base and photo after testing.

The performance of the mixed displacement and force control method is shown in Figure 5. The axial force obtained from the numerical model is used to command the loading jacks on top of the specimen. The measured vertical displacement is imposed as the target for the numerical substructure using an equivalent force. The achieved displacement committed at each integration time step in the numerical model verifies the compatibility between the experimental and numerical substructure. The axial shortening during MCE ground motion produced a decrease in the axial force due to the redistribution of vertical loads, showing the force/displacement coupling in the vertical direction. More results including column buckling can be found in Sepulveda et al (2023).

The beams exhibited nonlinear response prior to the columns as expected during DBE loading and maintained a stable response through MCE loading. The beam hysteretic behavior in Figure 6 does not indicate strength degradation and no localized buckling was observed in the beam. The OMU algorithm successfully tracked the measured response through the fitted Bouc-Wen model as shown in Figure 6. More in depth preliminary studies of the performance of the hybrid simulation indicate that the numerical model with model updating more closely resembles the experimental response and improves the agreement in compatibility between the numerical and experimental substructures using the simplified substructuring strategy with overlapping domains.

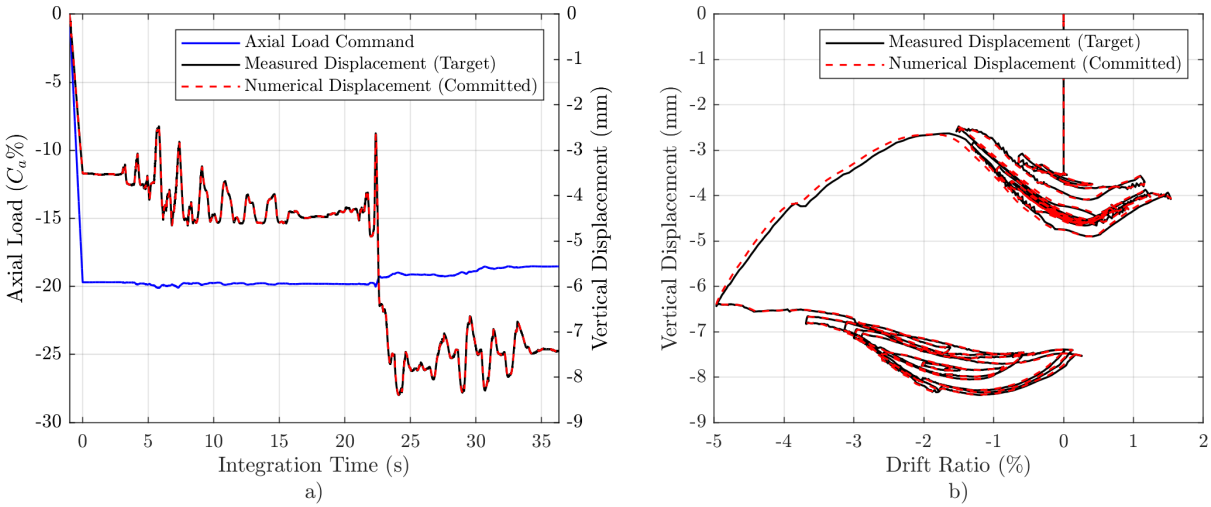

Figure 5. Axial load and shortening of column during DBE and MCE tests.

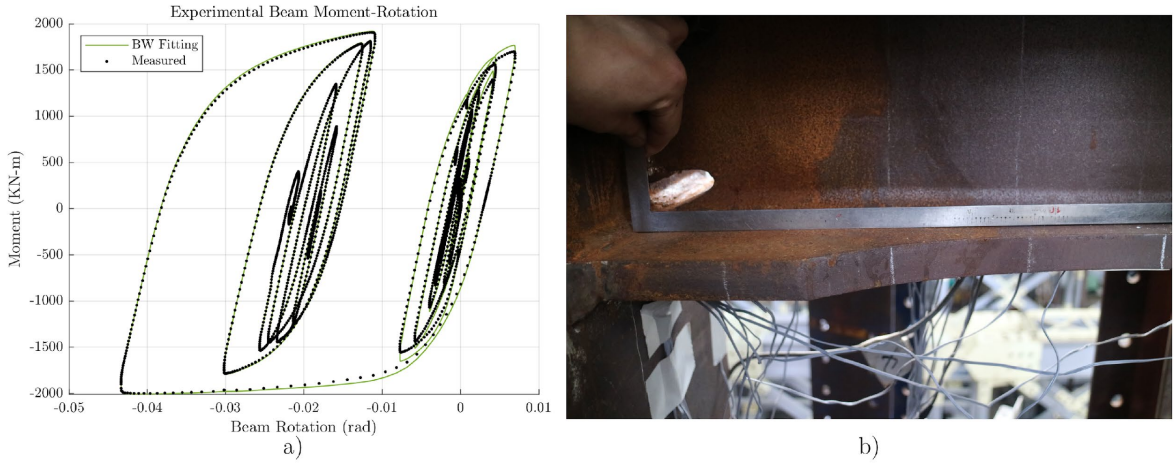

Figure 6. Hysteretic response and fitted model; b) Photo after MCE.

CONCLUSIONS

Hybrid simulations were conducted using full-scale beam and column subassemblies to study the complex behavior of steel moment frames with deep and slender columns beams with reduced beam sections (RBS) under different seismic intensities. The system behavior of the structure was captured through the interaction of the specimen with a full nonlinear numerical model. Column buckling was not observed for the test presented, though notable axial shortening was measured. The vertical deformation was successfully applied within the numerical substructure to comply with force equilibrium and displacement compatibility for the force-controlled direction. An online model updating (OMU) algorithm was implemented to improve the numerical model of RBS hinges and have better agreement with the measured response of the experimental substructure. The algorithm was stable without compromising the stability of the hybrid simulation. Additional analysis of the data is ongoing and future studies will compare the seismic demand obtained from the hybrid tests with observations with conventional quasi-static tests and tests of individual columns.

ACKNOWLEDGMENTS

This collaborative project was funded by NIST under Award 70NANB171TZ91 to University of Michigan and UC San Diego and by the National Center for Research on Earthquake Engineering (NCREE) supported by the Ministry of Science and Technology (MOST 110-2625-M-002-015), Taiwan.

REFERENCES

Ozkula G, Uang C-M, Harris J. (2021). "Development of Enhanced Seismic Compactness Requirements for Webs in Wide-Flange Steel Columns. *Journal of Structural Engineering*. 2021;147(7):04021100.

Elkady A, Asce AM, Lignos DG. (2017). Full-Scale Testing of Deep Wide-Flange Steel Columns under Multiaxis Cyclic Loading: Loading Sequence, Boundary Effects, and Lateral Stability Bracing Force Demands. *Journal of Structural Engineering*.;144(2).

Chansuk P, Ozkula G, Uang C-M, Harris III JL. (2021). Seismic Behavior and Design of Deep, Slender Wide-Flange Structural Steel Beam-Columns. *NIST.TN.2169*.

Chou C, Lai Y, Xiong H, Lin T, Uang C, Mosqueda G, Ozkula G, El-Tawil S, McCormick JP. (2022) Effect of boundary condition on the cyclic response of I-shaped steel columns: Two-story subassemblage versus isolated column tests. *Earthquake Engineering & Structural Dynamics*. doi:10.1002/EQE.3730

Wu T-Y, El-Tawil S, McCormick J. (2018). Seismic Collapse Response of Steel Moment Frames with Deep Columns. *Journal of Structural Engineering*;144(9).

Del Carpio, M., Mosqueda, G. and Hashemi, M.J. (2015) Large-Scale Hybrid Simulation of a Steel Moment Frame Building Structure through Collapse. *Journal of Structural Engineering,* 142(1):04015086.

Gupta A, Krawinkler H. (1999). Seismic Demands for Performance Evaluation Of Steel Moment Resisting Frame Structures. Blume Earthquake Engineering Center; 1999.

Ibarra LF, Medina RA, Krawinkler H.(2005). Hysteretic models that incorporate strength and stiffness deterioration. *Earthquake Engineering & Structural Dynamics*. 2005;34(12):1489–1511.

Hashemi MJ, Mosqueda G. (2014). Innovative substructuring technique for hybrid simulation of multistory buildings through collapse. *Earthquake Engineering & Structural Dynamics*. 43(14):2059–2074.

Cheng, M. and T. C. Becker. (2021). "Performance of unscented Kalman filter for model updating with experimental data," *Earthquake Engineering & Structural Dynamics.*, 50(7):1948–1966.

Sepulveda C, Mosqueda G, Wang K-J, Huang B-C, Huang C-W, Uang C-M, Chou C-C. Hybrid Simulation Framework with Mixed Displacement and Force Control for Fully Compatible Displacements. (2023). *Earthquake Engineering and Structural Dynamics*. (in review)

Day3 (Wednesday, Sep. 27th, 2023) 11:05~11:40

Multi-Degree of Freedom Hybrid Testing with Model Updating of an Isolated Bridge

Tracy Becker

Associate Professor, University of California, Berkeley, California, USA

Tracy Becker is an associate professor and the Ed & Diane Wilson Presidential Chair in Structural Engineering at University of California, Berkeley. She has expertise in performance-based design and the design, modeling, and experimental testing of high-performance structural systems used for limiting structural and component losses in seismic events. Her research has focused on expanding the use of seismic isolation to a broader category of structures, understanding ultimate failure mechanisms of isolated buildings to ensure robust designs, and improving existing control systems to further minimize structural responses in seismic events. As part of this work, she conducted the first bidirectional tests of triple friction pendulum bearings, the first dynamic failure tests of double concave bearings, as well as multiple other experimental programs. The data from her work has been used to develop new models and propose new design guidance for these systems.

MULTI-DEGREE OF FREEDOM HYBRID TESTING WITH MODEL UPDATING OF AN ISOLATED BRIDGE

Tracy Becker[1] Camila Lopez-Ruiz[2] and Mao Cheng[2]
1. Associate Professor, University of California, Berkeley, California, USA
2. PhD Candidate, University of California, Berkeley, California, USA
Email: tcbecker@berkeley.edu

ABSTRACT

Seismic solation bearings are widely considered an effective solution to protect bridges against earthquake damage. The traditional design of isolation assumes that the upper and lower framing components are stiff and, as such, bearing end-plates remain parallel during loading bearings for bridge applications neglects rotations at the bearings. However, for many bridges the piers are tall, creating flexible supports, and the deck is relatively flexible. Previous research has shown that the bearing end conditions can significantly affect the lateral stiffness of bearings. Thus, these assumptions should be investigated. This study uses hybrid simulation with model updating to explore the design and its limitations. The test was off a major toll bridge with piers of varying heights and lead rubber bearings (LRB). One LRB was physically tested considering axial, shear, and rotational loading, while the remainder of the bearings are simulated and updated with a phenomenological model within the numerical substructure. A weighted adaptive constrained unscented Kalman filter was applied as the online model updating algorithm. The bridge was analyzed to determine the seismic demands on the isolation bearings under these end conditions and quantify any effects on bridge or bearing demands due to the consideration of rotations.

Keywords: Isolated bridges, bearing rotation, hybrid simulation, model updating

INTRODUCTION

Isolation bearings are commonly used in bridges in regions with mid to high seismicity. Their local behavior and its effect on bridge performance is well understood under typical design applications and loading. However, when applied in bridges with tall, flexible piers, rotation can be introduced in the bearings. This behavior and its coupling with the shear, is not well understood for rubber bearings. A limited number of experiments have explored this behavior. For example, He *et al.* (2012) and Ishii *et al*. (2017) investigated the moment-rotational behavior by applying cyclic rotations at pre-applied constant shear strains. Both found that bearing rotational stiffness increases with increasing vertical load but decreases with increasing shear strain. Crowder and Becker (2017) and Darlington and Becker (2021) tested rubber bearings with combined simultaneous translation and rotation. The tests found that rotation of the bearing end-plates leads to a reduction in the horizontal stiffness of isolation bearings. While these tests applied demands closer to those seen in the field, they were still cyclical. No tests have explored seismic input representing the combinations of demands that would arise from flexible framing bounding the bearing.

To investigate (1) the change in the behavior of the rubber bearings when placed on tall, flexible piers and (2) any potential resulting changes in the behavior of the bridge, the system level performance is best evaluated. As such a hybrid simulation with model updating was selected for the test. Hybrid simulation is a testing methodology that combines numerically modeled and physically tested subassemblies of a structure (Nakashima *et al*., 1992). Model updating is used to enhance hybrid simulation by learning from the physical experimental data to update the numerical substructure elements of similar characteristics, improving the overall accuracy, while reducing the extent of the experimental setup (Kwon and Kammula, 2013).

The test is based on a major California toll bridge which features seismic isolation above half of its piers. The experimental substructure is the isolation bearing located on the tallest pier. The design of the isolation bearings at each pier is identical. However, as the height of piers increases, the demand for each bearing varies from one to the next. This combination makes the bridge a good candidate for model updating. During the hybrid simulation tests, three representative site-specific ground motions were used to evaluate the performance of the bearing, bridge, and overall testing methodology. The model updating was used to learn both the shear and rotational behavior of the bearing, making the application unique as there are very limited applications of multi degree of freedom model updating.

HYBRID SIMULATION SETUP

The outline of the hybrid simulation with model updating is shown in Fig. 1. The bridge model is based on the San Diego Coronado bridge, but for the purpose of the test, it the bridge is modeled in-plane. Piers 2 through 14, ranging in height from 10.7 m to 48.7 m, are isolated. The bearings have the same design at each pier. The bridge is modeled in OpenSees. The deck is modeled as elastic while nonlinear behavior is modeled in the columns using the concrete02 material model.

For the experimental setup, the LRB bearing is controlled in the three in-plane DOFs through one horizontal actuator located above the loading beam and two vertical actuators on either side of the bearing. The physical test has a 1/3 scale LRB to fit the capacity of the lab. The diameter of the tested bearing is 381 mm, and the lead diameter is 76 mm. The total rubber thickness is 127 mm with 20 rubber layers, and the resulting shape factor is 12. The shear modulus of the rubber is 0.4 MPa.

The hybrid simulation follows a traditional three-loop hardware architecture as shown in Fig. 2; the inner servo-control loop, operated by an MTS controller, dispenses target commands to the actuators and logs measured feedback. The outer integrator loop conducts numerical simulation and model updating analysis, utilizing OpenSees, OpenFresco, and Python-based model updating. The middle predictor-corrector loop receives target commands and generates continuous displacement commands to the MTS control system. Data is transmitted through SCRAMNet and a local web socket.

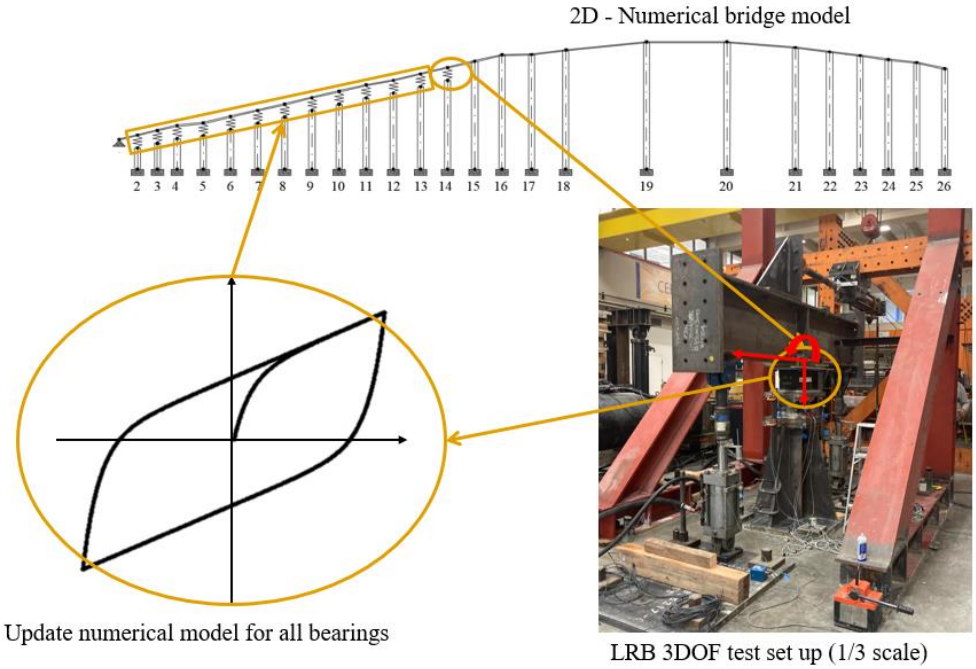

Figure 1. Overview of the hybrid simulation with model updating for the bridge with bearings on tall piers.

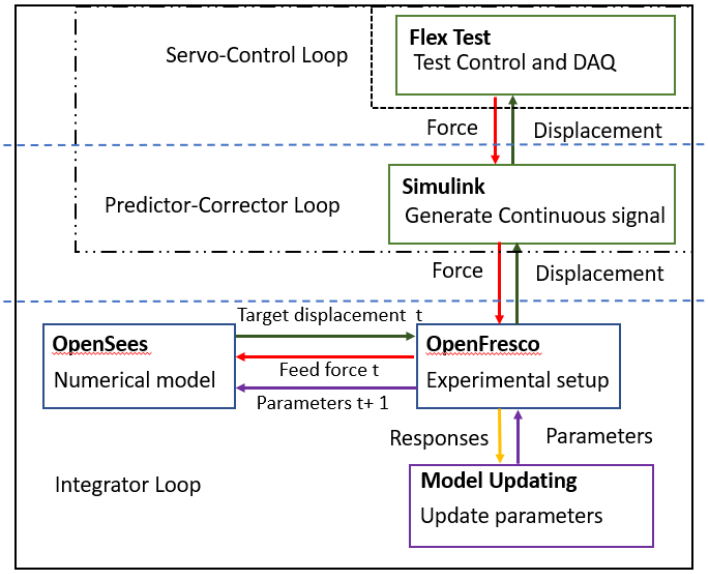

Figure 2. Hybrid simulation software and hardware overview.

Model Updating

The model updating uses a weighted adaptive constrained unscented Kalman filter (WACUKF) based on the unscented Kalman filter with the addition of the constrained unscented transformation, weighting functions, and adaptive calculation of the noise matrices (Cheng and Becker (2021). Adding the constraints in the unscented transformation eliminates the possibility of model parameters exceeding physically meaningful boundaries. The weighting function is applied to leverage the learning rate by the loading condition (e.g. displacement demand); a higher weight puts more emphasis on learning at larger loading while preserving the features learned under smaller loadings. Adding an adaptive noise matrix calculation improves the robustness and stability of the UKF.

As the bearings are expected to have both translational and rotational demands, the model used for representing and updating the numerical bearings must capture this behavior. Multiple numerical models have been proposed to simulate this behavior, many requiring many parameters. For model updating, it is important to balance simplicity and complexity in the model so that the number of parameters to be learned is limited while all behavior can be captured. To balance these, a Bouc Wen model (Park et al., 1986) in the shear DOF and a bilinear model in the rotational DOF with two separate influence terms was used. Both the shear and rotational behavior are dependent on the axial load. The axial behavior itself was modeled as a linear spring.

The displacement, velocity, and forces measured from the experiments serve as inputs for the model. The model parameters and calculated states are subject to continuous updating during the updating process. For each updating step, the recorded displacement and velocity are fed into the numerical model, yielding predicted forces. These predictions are then compared with the measured forces from the experiments, and the discrepancy between these values informs the parameter updating. Over sequential of time steps, this procedure facilitates the progressive honing of the model parameters, driving the numerical model towards convergence with the experimental data.

RESULTS

Two representative ground motions were used for the experimental test. Both ground motions were scaled to the local 2475-year earthquake hazard spectrum and then the amplitude was scaled again by 2. The experimental bearing shear and rotation hysteresis for ground motion 1 (GM1) and ground motion 2 (GM2) are shown in Fig. 3. GM1 had shear and rotational demands of around ±0.4 m and ±0.01 rad, respectively. GM2 had larger shear and rotational demands of around ±0.7 m and ±0.02 rad, respectively.

It can be seen that at larger rotations the moment-rotation hysteresis begins to exhibit a softening behavior and, due to the interaction with shear and axial loads, exhibits negative stiffness. However, the experiments remained stable throughout.

Table 1 compares the parameters of the bearing from analytical predictions to the values found through the model updating in the hybrid simulation. The analytical values are found assuming a linear rotational spring and considering only manufacturer provided bearing properties without any experimental data. The testing found reduced characteristic strength, initial stiffness, and rotational stiffness. The model also found non-negligible hysteretic behavior in the rotational degree of freedom. As these changes are significant, there are clear benefits to using the model updating in the hybrid simulation.

A comparison of the bridge pier and bearing demands under GM1 between numerical simulations of the bridge using the initial analytical bearing values and the hybrid simulation results is shown in Fig. 4. The hybrid simulation with model updating found larger pier drift and bearing strain demands for the taller piers. The changes in demand were on the order of 5%. As such, incorporating the rotational behavior of the bearing and its coupling with the shear behavior may not be of major concern.

CONCLUSIONS

To assess the performance of an isolated bridge with isolators located on the tops of tall flexible piers, subjecting them to rotation, a series of hybrid simulation experiments were run utilizing model updating to learn the bearing performance. The tests were run successfully with the model updating performing well even when predicting unknown behavior including coupling in multiple degrees of freedom. When compared to predicted responses when using a purely linear rotational spring with analytically derived stiffness, the hybrid simulation found displacement demands on the other of 5% larger for both piers and bearings. As such, the rotational demands will likely not have significant implications on bridge damage but should be considered for displacement capacity limits in design.

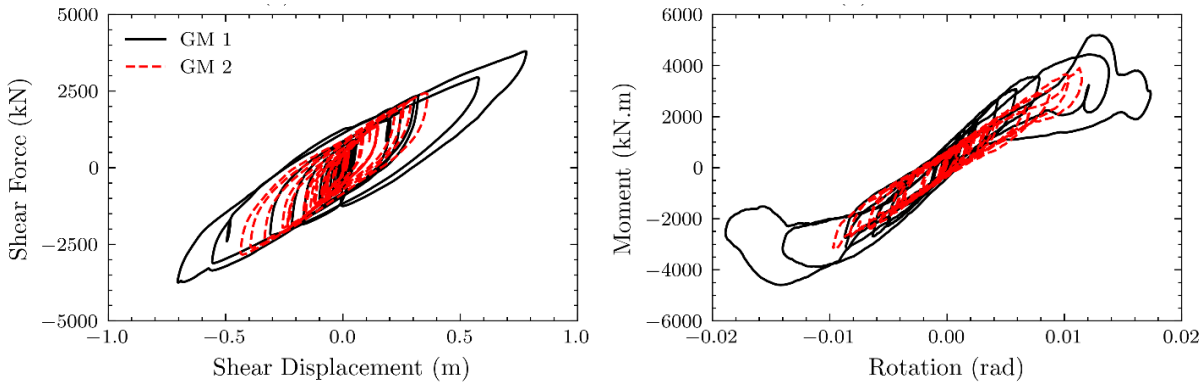

Figure 3. Experimental shear and rotational hysteresis.

Table 1. Updated bearing parameters

Bearing Parameter	Analytical Values	Updated Values	Change (%)
Shear initial stiffness, $\boldsymbol{K_1}$ (kN/mm)	8.97	5.61	-37.5%
Post-yield stiffness ratio, $\boldsymbol{\alpha}$	0.119	0.172	+44.7%
Characteristic strength, $\boldsymbol{Q_d}$ (kN)	390	282	-27.83%
Rotational initial stiffness, $\boldsymbol{K_{\theta 1}}$ (kNm/rad)	1,089,000	740,000	-32%
Rotational post-yield stiffness ratio, $\boldsymbol{\alpha_\theta}$	n/a	0.08	

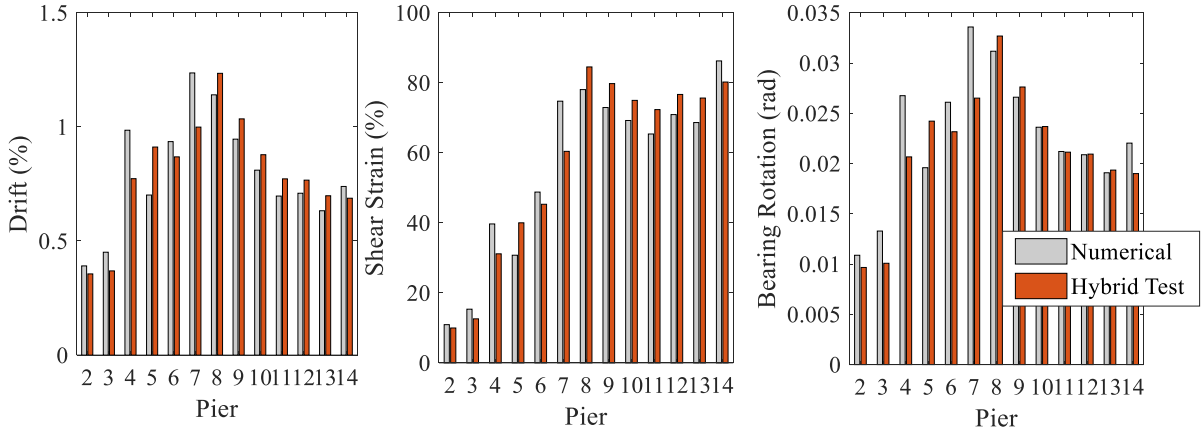

Figure 4. Pier drift demands and bearing shear and rotational demands for GM1 predicted from a purely numerical simulation with a linear spring compared with the results from the hybrid test.

REFERENCES

Cheng, M. and T.C. Becker (2021). "Performance of Unscented Kalman filter for Model Updating with Experimental Data," *Earthq. Eng. Struct. Dyn.*, **50**(7), 1948-1966.

Crowder, A.P. and T.C. Becker (2017). "Experimental Investigation of Elastomeric Isolation Bearings with Flexible Supporting Columns." *J. Struct. Eng.*, **143**(7): 04017057.

Darlington R. and T.C. Becker (2021). Stiffness of Rubber Bearings Considering Nonstandard Top and Bottom Boundary Conditions," *J. Struct. Eng.*, **147**(7): 04021101.

He, W.F., W.G. Liu, Q.R. Yang and D.M. Feng. (2012). "Nonlinear Rotation and Shear Stiffness Theory and Experiment Research on Rubber Isolators." *J. Eng. Mech.*, **138** (5):441-449.

Ishii, K., M. Kikuchi, T. Nishimura and C.J. Black (2017). "Coupling Behavior of Shear Deformation and End Rotation of Elastomeric Seismic Isolation Bearings." *Earthq. Eng. Struct. Dyn.*, **46**(4): 677-694.

Kwon, O. and V. Kammula (2013). "Model Updating Method for Substructure Pseudo-Dynamic Hybrid Simulation." *Earthq. Eng. Struct. Dyn.*, **42**(13), 1971-1984.

Nakashima, M., H. Kato and E. Takaoka (1992). "Development of real-time pseudo dynamic testing," *Earthq. Eng. Struct. Dyn.*, **21**(1), 79-92.

no presentation

Floor Acceleration Spectra Based on Structural Dynamics

Peter Fajfar

Emeritus Professor, Faculty of Civil and Geodetic Engineering, University of Ljubljana, Slovenia.

Peter Fajfar is Professor Emeritus at the University of Ljubljana, Slovenia. His main research interest is seismic analysis and design of structures. He was a visiting professor at several renowned universities, including Stanford University. In the period 2003-2015 he was one of three Editors of the journal Earthquake Engineering and Structural Dynamics. He served on the Board of Directors of the International Association of Earthquake Engineering and was a member of the Executive Committee of the European Association of Earthquake Engineering. In both associations he was elected an Honorary Member. He has been involved in the development of the European standard Eurocode 8. As a designer, consultant and/or reviewer, he has participated in a large number of projects for industry. He received several awards, among them the highest award for the scientific work in Slovenia and Prof. Nicholas Ambraseys Distinguished Lecture Award. Fajfar is a member of the Slovenian Academy of Sciences and Arts, of the Slovenian Academy of Engineering, of the European Academy of Sciences (Belgium), and of the National Academy of Engineering (USA).

FLOOR ACCELERATION SPECTRA BASED ON STRUCTURAL DYNAMICS

Peter Fajfar[1] and Vladimir Vukobratović[2]
1. Emeritus Professor, Faculty of Civil and Geodetic Engineering, University of Ljubljana, Slovenia.
2. Associate Professor, Faculty of Technical Sciences, University of Novi Sad, Serbia.
Email: peter.fajfar@fgg.uni-lj.si, vladavuk@uns.ac.rs

ABSTRACT

Seismic design and evaluation of acceleration-sensitive nonstructural components is usually performed by using floor acceleration spectra. In this paper, a direct code-oriented method for the determination of the floor acceleration spectra is summarized and applied in a test example. In the proposed method, floor acceleration spectra are, to a great extent, based on the theory of the dynamics of structures, and are partly combined with empirical values and well established approaches for considering nonlinear effects. Floor acceleration spectra explicitly take into account ground motion spectra and dynamic characteristics of buildings and components. The advantage of such an approach is its general applicability which allows diverse design options.

Keywords: floor acceleration spectra, nonstructural components, dynamics of structures, seismic analysis

INTRODUCTION

Floor response spectra in terms of acceleration are used for the seismic design and evaluation of acceleration-sensitive nonstructural components. In everyday design practice usually an approximate "direct" approach is used, where the floor spectra are determined directly from the ground motion spectra taking into account the characteristics of both the primary structure and the nonstructural components. Several direct methods of different complexity and with different limitations exist. In this paper, a direct code-oriented method for the determination of the floor acceleration spectra, proposed by the authors (Vukobratović and Fajfar, 2017), is summarized and applied in a test example. The method was, with some modifications, adopted in the final draft of the second generation of the European seismic code Eurocode 8 (CEN, 2022).

THE DIRECT METHOD

Floor acceleration spectra depend on the ground motion characteristics (represented by the ground motion spectrum), the characteristics of the primary structure (periods and mode shapes, damping, ductility, strength), and the characteristics of the nonstructural component (period, damping, ductility, strength, location within the primary structure). Using the basic structural dynamics, Yasui *et al*. (1993) derived a closed form expression for spectral floor accelerations as a function of ground motion spectrum and the dynamic characteristics of the structure and the component. The formula is limited to linear elastic behaviour of both the structure and the component. The authors (Vukobratović and Fajfar, 2017) extended the Yasui *et al*. formula to nonlinear primary structures by using strength reduction factor. In the resonance an empirical formula for the amplification factor, proposed by Sullivan *et al*. (2013) is used. The influence of the component nonlinearity is taken into account through equivalent damping. In the following text the authors' method is summarized.

The floor acceleration spectrum represents the acceleration of the secondary system, S_s, as a function of its period T_s. Floor acceleration spectra are determined separately for each considered mode of the primary structure, and are then combined by using the standard SRSS (Square Root of Sum of Squares) or CQC (Complete Quadratic Combination) modal combination, with the exception of the post-resonance region of the fundamental mode, where the algebraic sum (ALGSUM) is used. In this way,

the relevant signs of individual modes are taken into account in order to obtain the resulting floor response spectrum.

For mode 'i' and floor 'j', the value of the floor acceleration spectrum, $S_{s,ij}$, is determined as (for a more detailed description see Vukobratović and Fajfar, 2017):

$$S_{s,ij} = \frac{\Gamma_i \phi_{ij}}{\left| \left(T_s / T_{p,i} \right)^2 - 1 \right|} \sqrt{\left(\frac{S_{ep,i}}{R_p} \right)^2 + \left\{ \left(T_s / T_{p,i} \right)^2 S_{es} \right\}^2} \tag{1}$$

$$\left| S_{s,ij} \right| \le AMP_i \times \left| PFA_{ij} \right| \tag{2}$$

$$PFA_{ij} = \Gamma_i \phi_{ij} \frac{S_{ep,i}}{R_p} \tag{3}$$

$$AMP_i = \begin{cases} 2.5\sqrt{10/(5+\xi_s)}, & T_{p,i}/T_C = 0 \\ \text{linear between } AMP_i\left(T_{p,i}/T_C = 0\right) \text{ and } AMP_i\left(T_{p,i}/T_C = 0.2\right), & 0 \le T_{p,i}/T_C \le 0.2 \\ 10/\sqrt{\xi_s}, & T_{p,i}/T_C \ge 0.2 \end{cases} \tag{4}$$

Along the bottom 1/3 of the building height, the lower limit of the floor response spectrum is represented by the ground motion acceleration spectrum corresponding to the component damping and ductility.

The indices 'p' and 's' correspond to the primary (building) structure and the secondary element (i.e., nonstructural component), respectively. S_{ep} is a value in the elastic acceleration spectrum. $S_{ep,i} = S_e(T_{p,i}, \xi_{p,i})$ applies to the ith mode of the primary structure, whereas $S_{es} = S_e(T_s, \xi_s)$ applies to the component. $T_{p,i}$ and T_s are the natural periods of the ith mode of the structure and component, respectively, and $\xi_{p,i}$ and ξ_s are the damping values of the structure (for the ith mode) and of the component, respectively, expressed as the percentage of critical damping. T_C is the characteristic period of the ground motion. Γ_i is the modal participation factor for the ith mode, whereas ϕ_{ij} represents the ith mode shape value at the jth floor. AMP_i is the amplification factor (for the ith mode, it applies to all floors j), defined as the ratio between the peak value in the floor acceleration spectrum (the value in the plateau of the ith mode for any floor j), $S_{s,ij}$, and the corresponding peak floor acceleration PFA_{ij}. The equation in the third line of Eq. 4 was proposed by Sullivan *et al.* (2013).

The nonlinear behaviour of the primary structure is taken into account by the ductility and period dependent strength reduction factor R_p. The term ($S_{ep,i}/R_p$) represents the value in the inelastic acceleration spectrum for the primary structure. It is assumed that the nonlinear behaviour is related only to the fundamental mode, whereas all higher modes are treated as elastic. Thus, for all higher modes (i > 1), R_p amounts to 1. As an approximation, implemented also in the draft new Eurocode 8 (CEN, 2022), the part of the force modification factor corresponding to the energy dissipation capacity of the building structure can be used as R_p. The fundamental mode shape ϕ_1 is, in the case of an inelastic structure, approximated with the deformation shape determined in pushover analysis.

Nonlinear behaviour of ductile nonstructural components can be approximately taken into account by increasing the component damping. Our studies (Vukobratović and Fajfar, 2017) indicated that floor acceleration spectra for elastic components with 10% and 20% damping approximately correspond to the spectra for inelastic components in the case of a ductility demand μ_s equal to 1.5 and 2.0, respectively, and the actual damping of the component equal to 1%. It was also found that, with increasing nonlinear behaviour of the component, the influence of its damping rapidly decreases. Based on these observations

we proposed to use ξ_s = 10% and ξ_s = 20%, independently of the actual damping of component, as a preliminary conservative approach for taking into account the nonlinear behaviour of ductile components with ductilities 1.5 and 2, respectively.

The described direct method is based on the principles of structural dynamics. Empirical values obtained in a parametric study are used only in the resonance region in order to improve the accuracy of the peak values of floor acceleration spectra. Inertial forces on nonstructural components depend on the characteristics of the ground motion (intensity and frequency content), of the building (period, damping, ductility), and of the component itself (period, damping, ductility and vertical location in the building). Eqs. 1 to 4 take into account all above parameters. The ground motion characteristics are represented by ground response spectra. Periods and damping values of the building and the component are explicitly included in the equations. Nonlinear effects due to the possible ductile response of the primary structure and nonstructural components are approximately taken into account by using well established concepts (inelastic spectra, equivalent damping).

Eq. 1 indicates that the acceleration of a component depends both on the dynamic characteristics of the building and of the component. In the case of rigid components (relative to building), the vibration of the building prevails, whereas the vibration of the component is decisive in the case of flexible components. When T_s is much smaller than T_p, the response of the component is almost identical to the response of the building. In the opposite case, where T_s is much larger than T_p, the component response is almost the same as it was attached to the ground.

TEST EXAMPLE

As demonstrated in Fig. 1 (and elsewhere), the floor spectra obtained by Eqs. 1 to 4 match well with the floor spectra obtained by the more accurate approach based on nonlinear dynamic analysis.

In Fig. 1, floor acceleration spectra at the roof and at the first floor of a three-storey reinforced concrete frame building, known as the “SPEAR building”, are shown. A variant of the building re-designed in compliance with Eurocode 8 (2004) as a high ductility class structure (see Rozman and Fajfar, 2009, variant EC8 H) was used. The ground motion (peak ground acceleration PGA = 0.35 g) is described in (Vukobratović and Fajfar, 2015), whereas the most important properties of the model and its analysis are described in (Vukobratović and Fajfar, 2017). The first three natural periods of the building in the considered direction are 0.56 s, 0.19 s, and 0.12 s. The global ductility demand of the structure subjected to the applied ground motion amounts to 2.4, resulting in the same value of the first mode strength reduction factor. Floor spectra are shown for linear elastic (μ_s = 1) and nonlinear (μ_s = 2) components with ξ_s = 2%. In the case of the direct approach, 20% component damping is used to simulate the nonlinear component response. A fair agreement of the results obtained by response history analysis and by the proposed direct approach can be observed. In the case of the linear elastic component a large influence of the second mode of the structure is visible both at the first floor and at the roof. At the first floor the lower limit (equal to the ground motion acceleration spectrum corresponding to the component damping and ductility) applies in a limited period range. A large reduction of the spectral accelerations due to the component nonlinearity is obvious in the whole period range, with the exception of very stiff nonstructural components. The reduction is especially pronounced in the resonance regions.

CONCLUSIONS

A reliable prediction of floor response spectra is possible only by considering the basic structural characteristics of the primary structure and the nonstructural component. The proposed direct method fulfills this requirement. It is, to a great extent, based on the theory of the dynamics of structures, partly combined with empirical values and well established approaches for considering nonlinear effects. Comparisons of floor acceleration spectra determined with the proposed method and more accurate spectra obtained by nonlinear response history analysis presented in this paper and elsewhere demonstrate a fair correlation of results. The advantage of the proposed approach is its general

applicability, both in research and practice. The closed form equations can be applied for different structural systems and different components, provided that the main characteristics of the primary structure and nonstructural components (period, strength, damping, ductility) are known with a sufficient accuracy.

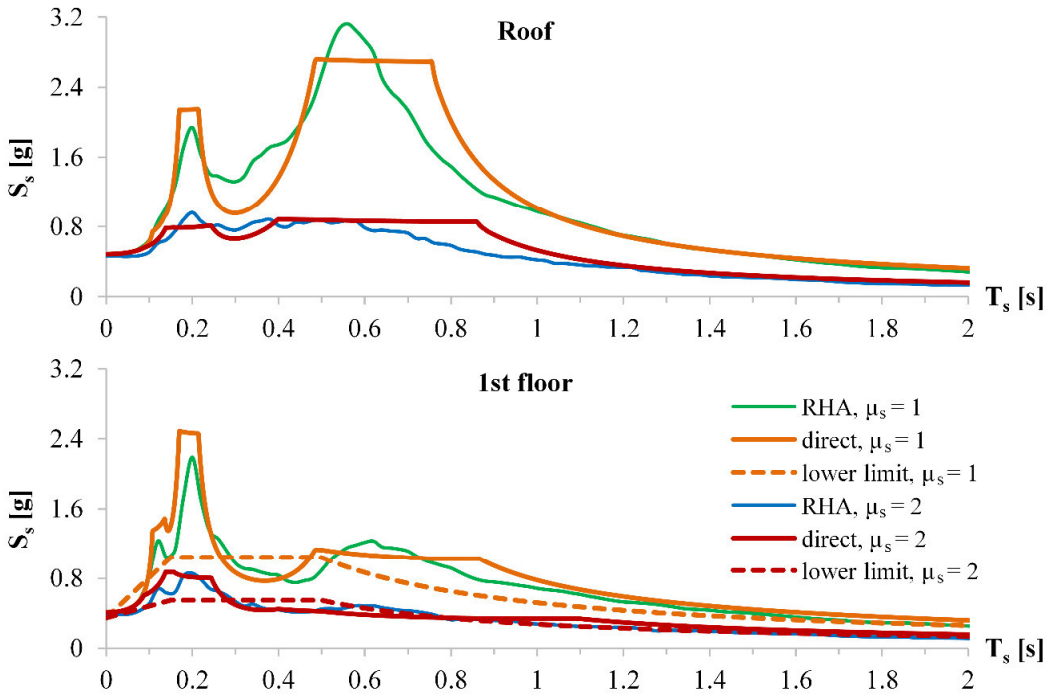

Figure 1. Floor acceleration spectra for linear elastic ($\mu_s = 1$) and nonlinear ($\mu_s = 2$) components with $\xi_s = 2\%$ in SPEAR building.

ACKNOWLEDGMENT

The research of the second author has been supported by the Ministry of Science, Technological Development and Innovation through project no. 451-03-47/2023-01/200156 "Innovative scientific and artistic research from the FTS domain".

REFERENCES

CEN (2022). "prEN 1998–1–2, Eurocode 8: Design of structures for earthquake resistance. Part 1-2: Buildings", Draft, CEN, Brussels.

Rozman, M., P. Fajfar (2009). Seismic response of a RC frame building designed according to old and modern practices. *Bull Earthq Eng* **7**(3), 779–799. https://doi.org/10.1007/s10518-009-9119-4

Sullivan, T.J., P.M. Calvi, R. Nascimbene (2013). "Towards improved floor spectra estimates for seismic design", *Earthquakes and Structures* **4**(1), 109–132. https://doi.org/10.12989/eas.2013.4.1.109

Vukobratović, V., P. Fajfar (2015). "A method for the direct determination of approximate floor response spectra for SDOF inelastic structures", *Bull Earthq Eng* **13**(5), 1405–1424. https://doi.org/10.1007/s10518-014-9667-0

Vukobratović, V., P. Fajfar (2017). "Code-oriented floor acceleration spectra for building structures", *Bull Earthq Eng* **15**(7), 3013–3026. https://doi.org/10.1007/s10518-016-0076-4

Yasui, Y., J. Yoshihara, T. Takeda, A. Miyamoto (1993). "Direct generation method for floor response spectra", Kussmaul K (ed.), *Transactions of the 12th International Conference on Structural Mechanics in Reactor Technology (SMiRT 12)*, Elsevier Science Publishers B.V.: Stuttgart, Germany: Paper K13/4, pp. 367–372.

SPONSORS

- JJ HUANG INTERNATIONAL CO., LTD.
  捷懷有限公司
- P-WAVER Inc.
  衛波科技股份有限公司
- Sinodynamics Corporation
  國科企業股份有限公司
- Ton Yuan Technology & Engineering Co.,Ltd.
  東源科技工程有限公司
- WELL LINK INDUSTRY CO., LTD.
  劦承精密股份有限公司
- CECI Engineering Consultants, Inc., Taiwan
  台灣世曦工程顧問股份有限公司
- CONN-TEK VIBRATION CONTROL INC.
  富堡瓏國際實業股份有限公司
- Sinotech Engineering Consultants, LTD.
  中興工程顧問股份有限公司
- T.Y.Lin Taiwan Consulting Engineers, Inc.
  林同棪工程顧問股份有限公司
- Sinotech Engineering Consultants, Inc.
  財團法人中興工程顧問社
- Taipei Professional Civil Engineers Assoociation
  社團法人台北市土木技師公會
- Taiwan Professional Geotechnical Engineers Association
  社團法人中華民國大地工程技師公會

捷懷有限公司

聯絡請洽 0921880951 jayhuang0730@hotmail.com

美國 ITT ENIDINE 黏滯液阻尼器

短衝程

- 速度指數 α = 0.1~2.0
- 出力噸數可達 2000kN 以上
- 衝程長度可達 2000mm 以上
- 可適用於隔震、制震及調諧質量阻尼器 TMD
- 可因應各種需求客制化

長衝程

加拿大 RWDI / Motioneering 調諧液態質量阻尼器TSD

- 基本原理、用途與 TMD 相同。
- 利用攪動流體吸收及消散結構振動的能量。
- 調整液體頻率，與結構頻率做匹配。

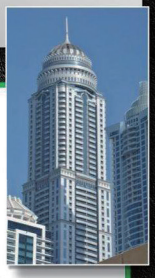

調諧質量阻尼器TMD

- 利用次結構之質量、阻尼、勁度系統來改變主結構之動態特性。
- 主要用途為增加超高樓層居住舒適性。
- 採用美國 ITT ENIDINE 消能阻尼器。

震前地震預警、平時rFDD 、震後結構安全監測平台

中央氣象局 + NCREE 國家地震中心

複合式地震速報

頂樓地震儀

2樓地震儀

1樓地震儀

地震記錄主機

警報自動控制器

結構安全監測主機

・於地震四級以上前停妥電梯

・收到地震速報後2秒內啟動連動服務

喇叭

避難點投射燈

地震警報燈

・電梯運轉至就近樓層自動停車開門

・電梯自動關門並停止運轉

・直至地震終了，維護人員重啟電梯

P.S.
1.電梯本身有自動停梯功能
2.連動部分須由系統整合商或電梯廠

電梯自動停梯

震後10分鐘

自動產出結構安全分析報告

① Line快速通報

② 結構安全分析平台

③ 結構安全評估報告

平時rFDD

溫度越高，頻率越高

風速越高，頻率越低

頻率與阻尼等模態參數，是評估建築物在地震後是否損壞的指數，日漸廣泛運用於結構健康監測上

掌握全台｜震後建築結構安全分析

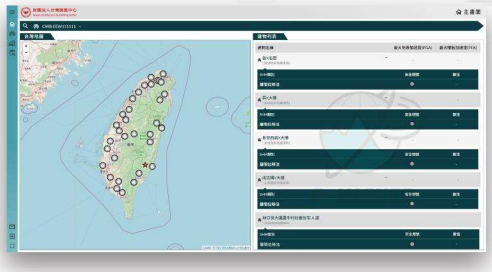

全台建築結構安全，瞬間掌握！

建築結構安全分析結果
燈號顯示，一目瞭然

安全	0%~0.2%
輕損	0.2%~0.5%
中損	0.5%~1.5%
重損	1.5% ↑

衛波科技股份有限公司 90772077
地址：台北市中山區松江路82號6樓
電話：02-2522-1580
EMail：hello@pwaver.com
網址：www.pwaver.com

MTS®

來自美國
材料測試第一品牌

311系列 液壓軸向動態土木結構材料測試機

適用於測試土木工程材料 、次結構件以及大型結構物，
特別適用於需要大力量或大位移的材料測試 。
此款大型結構材料測試系統，採用精確的油壓伺服控制
技術， 可滿足靜態和動態測試需求。

MAST™六自由度震動模擬實驗平台

可依試驗需求， 針對建築結構之關鍵零組件、
中控系統機箱、安全系統， 模擬測試其餘地震
載重下之安全等級、強度與結構完整性。
亦可應用於車輛總成、零組件或精密設備於振
動負載條件下之運作狀態。

國科企業股份有限公司
SINODYNAMICS CORPORATION
共創價值
TEL 02-2792-2440 | FAX 02-2790-4564
臺北市內湖區成功路4段168號4樓

SEISMIC ENGINEERING

- Earthquake Monitoring
- Earthquake Engineering Professional Instruments
- Geodetic Monitoring Projects

SPC-52 Portable Ambient Vibration Monitoring System

- **Building Vacillation**
- **Microtremor Monitoring**
- **Moving observation for earthquake**
- **Ambient Vibration Monitoring**

1. Two in one system, with recorder system and built-in PC.
2. Operate with velocity sensor VSE-15D6, acceleration and displacement data can be obtained in phase.
3. 24 Bit AD convert and GPS sync.
4. Expansive application with Max 18 channels(or 9 CH), including measurement of acceleration, velocity and displacement.
5. Real Time Waveform Display in Time and Freq. domain.

SPC-52

CV-375 Strong Motion Recorder

- **Structure Health monitoring**
- **Performance evaluation of seismic isolated structure**
- **Health monitoring of high-rise building**

1. Variable with continuous data and trigger data setting.
2. 24 Bit AD convert and support GPS or NTP sync.
3. Expansive application with Max 6 CH. (internal or external sensors).
4. Network interface functions: far-end monitoring, transmission,setting, and data download.
5. More choices about sampling rate: 20, 50, 100, 200, 500, 1000 Hz.
6. Excellent International Protection level IP67 for various on-site situation.

CV-375

VSE-15D

Servo Velocity Seismometer

- **Survey of an underground structure**
- **Microtremor observation**
- **Micro-earthquake**
- **Any of vibration Experiment**
- Small size, Light weight
- Low frequency range
- High resolution
- Servo Velocity Sensor

AS-301 series

Servo Accelerometer

- **Strong Earthquake Observation**
- **Accelerometer for Seismic Measurement**
- High Resolution
- Waterproof

SAMTAC-850

Portable Vibration Recorder

- **Microtremor array**
- **Temporary survey**
- **Microtremor observation**
- **Volcano monitoring**
- Hight resolution
- Portabla 6 CH Recorder
- Long-time recording
- Supports USB memory storage

DPT-800

Upright Type Long Stroke Displacement Meter

- **Measures displacement in 2 orthogonal directions**
- Space saving for installation
- Saves time-series date of displacement on the internal recording medium
- Real time date transfer to external PC
- Correction of internal clock by connecting NTP server

TON YUAN TECHNOLOGY & ENGINEERING CO.,LTD.
http://www.tonyuan.com.tw/
TEL：886-2-2708-3019

TOKYO SOKUSHIN CO., LTD.
http://www.tosoku.co.jp/index.html
TEL：81-3-3855-5911

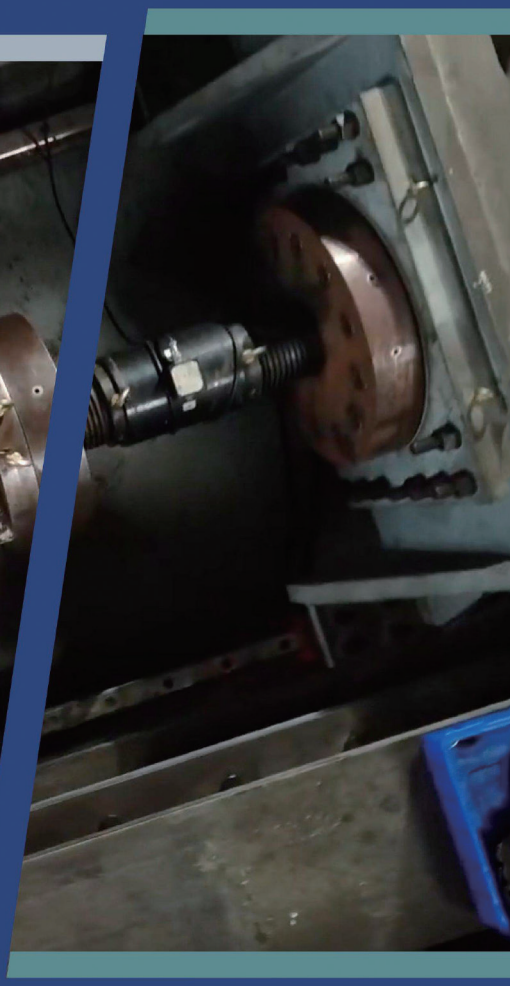

ANTI-SEISMIC DEVICES

WELL LINK®
INDUSTRY CO., LTD.

STRUCTURAL BEARINGS

EQUIPMENT PROTECTION

SERVICES

www.welllink.com.tw

Dreams and Happiness

Closing the Gap

Technology standing before the test of uncompromising professionalism,
Bringing a castle of dreams, a happy home closer into view,
CECI joins hands with you in building up dreams with attentive care,
And providing a world of hope for all of our collaborative efforts in all that we do.

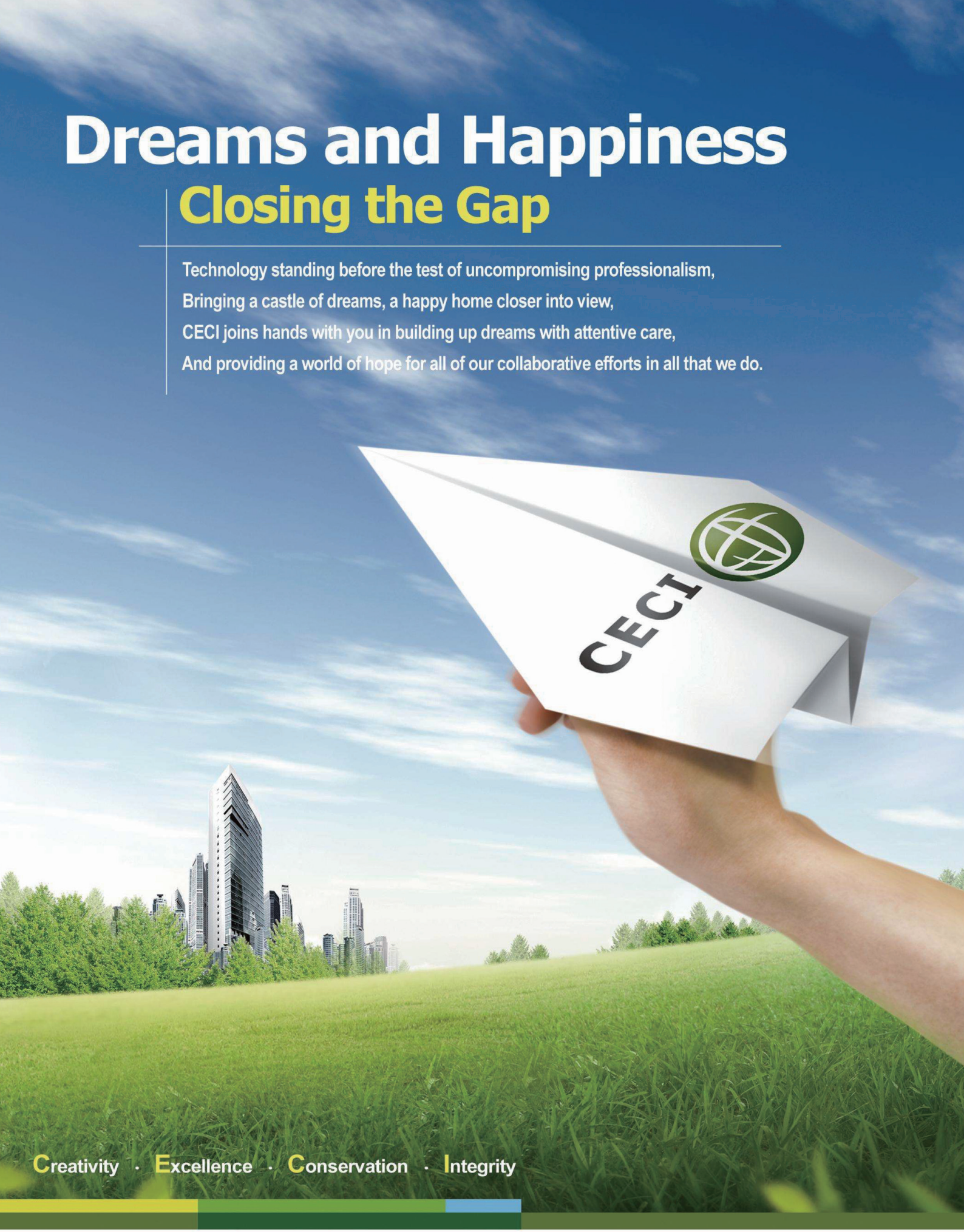

Creativity · Excellence · Conservation · Integrity

CECI CECI Engineering Consultants, Inc., Taiwan

No. 323 Yangguang Street, Neihu District, Taipei City 11491, TAIWAN
Tel:+886 2 8797 3567 Fax:+886 2 8797 3568
http://www.ceci.com.tw E-mail:pr@ceci.com.tw

日本免制震系統

JFE シビル 株式会社 耐震・制震デバイス

住友ゴム工業株式会社 SUMITOMO RUBBER INDUSTRIES, LTD.

三菱重工機械

SENQCIA Chains & Building Solutions

BRIDGESTONE

DAMTEC®

速度型系統

《住友 - 制震壁》

住友ゴム工業株式会社 SUMITOMO RUBBER INDUSTRIES, LTD.

- 日本第一制震品牌
- 免除維修的困擾

《森科 - 油壓阻尼器》

SENQCIA Chains & Building Solutions

- 日本阻尼器權威
- 30年以上實績鑑驗

位移型系統

《二重鋼挫屈束制斜撐》

JFE シビル 株式会社 耐震・制震デバイス

- 世界前十大鋼鐵廠
- 全鋼式業界最新技術

《制震間柱》

JFE シビル 株式会社 耐震・制震デバイス

- 世界前十大鋼鐵廠
- 日本間柱領導品牌

免震系統

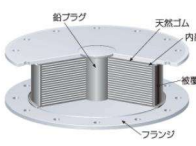

《免震系統》

BRIDGESTONE

- 日本免震第一品牌
- 高專業性(30多年經驗)

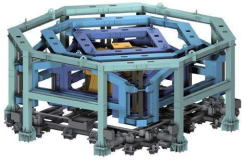

《超高層 AMD》

三菱重工機械

- 日本實績第一
- 抗風阻尼權威

CEI CONN-TEK 富堡瓏國際實業股份有限公司

電話：+886-2-2798-7200　　傳真：+886-2-2798-7238

地址：台北市11492內湖區瑞光路302號10樓(亞洲科技大樓)

正派經營　品質保證　追求卓越　創新突破

中興工程顧問股份有限公司
SINOTECH ENGINEERING CONSULTANTS, LTD.

Safety,Economy,and Aesthetics
Creation and Evolution for the best

TYLin

About Us :

After Taiwan's 921 Earthquake, most authorities are actively involved in the inspection and retrofit works for bridge repair. TYLIN TW has good reputation on both bridge designand retrofit for a long time, maintains a good relationship and cooperation with domestic research institutes,and also timely introduces the latest seismic design from international practices. The company has currently performed over 1000 major bridges retrofit projects over the nation.

- Taipei City Bridge Safety Inspection Program
- National Freeway Bridge Seismic Analysis Evaluation and Retrofit Program
- Taiwan High Speed Railway - Seismic Capacity Performance Evaluation (SCPE)
- Safety Inspection on Changhua fault for affecting the structure of HSR, Lot CI-14-003
- New Taipei City bridge safety inspection and system information upgrade
- Provincial Highway 88 Wanda Bridge Bridge abutment Reinforcement reconstruction

Structural Engineering / Civil Engineering / Hydraulic Engineering / City Planning / Landscaping Engineering / Geotechnical Engineering / Transportation Engineering / Environmental Engineering / Water and Soil Conservation / Drainage Engineering / Industrial Engineering / Applied Geology / Electrical Engineering / Mechanical Engineering / Construction Management

Tel : 02-2784-0988

Fax : 02-2707-1430

Email : tylintw@tylin.com.tw

Address : Suite 1202, 12F NO. 136, Sec.3 Jen Ai Rd. Taipei, 106 Taiwan

TYLin

社團法人中華民國大地工程技師公會
Taiwan Professional Geotechnical Engineers Association





1. 提供政府與民間機構各類建築、土木、水利、道路、隧道、海洋、環境、下水道等工程中有關大地工程(含土壤工程、岩石工程及工程地質)與地質法、水土保持法及其他法令規定得由大地工程科技師辦理工程之研究、評估、審查及鑑定等相關服務。
2. 參與相關之災害防治與勘災工作。
3. 辦理水土保持、地下構造及設施等業務相關講習會。
4. 辦理大地工程薪傳講座及各項專業技術研討會。
5. 協助辦理鄰高鐵(或捷運)近接施工之安全影響評估審查作業。
6. 土壤液化潛能評估分析及諮詢顧問服務。

社團法人
中華民國大地工程技師公會

(115) 台北市南港區成功路一段 32 號 4 樓之 8
電話：02-2782-0022 傳真：02-2782-0272
E-MAIL: pgea@pgea.org.tw
網址：www.pgea.org.tw

桃竹辦事處
(330) 桃園市桃園區正光路 423-6 號 12 樓
電話：03-3230975 傳真：03-3605752

中部辦事處
(427) 台中市潭子區中山路二段 135 號 15 樓之 1
電話：04-25346986 傳真：04-25340823

雲嘉南辦事處
(711) 台南市仁德區中山路 758 巷 2 弄 68 號
電話：06-2493720 傳真：06-2495365

高屏辦事處
(804) 高雄市鼓山區中華一路 350 號 2 樓之 2
電話：07-5537936 傳真：07-5530290

基隆辦公室
(200) 基隆市仁愛區愛九路 1 號 6 樓
電話：02-24294812 傳真：02-24251970

花東辦公室
(971) 花蓮縣新城鄉嘉里三街 113 巷 3 之 16 號
電話：03-8267159 傳真：03-8237499

網址:acccs.ncree.org.tw

Advised by

NSTC 國家科學及技術委員會
National Science and Technology Council

Co-organized by

Chinese Taiwan Society for Earthquake Engineering (CTSEE)

Chinese Society of Structural Engineering (CSSE)

Chinese Institute of Civil and Hydraulic Engineering (CICHE)

Taiwan Earthquake Research Center (TEC)